PERFORMANCE ANALYSIS OF SPATIALLY CODED OFDM WIRELESS SYSTEMS USING CHANNEL STATE INFORMATION

A THESIS

SUBMITTED IN FULFILLMENT OF THE REQUIREMENT

FOR THE AWARD OF DEGREE OF

DOCTOR OF PHILOSOPHY

IN

ELECTRONICS AND COMMUNICATION ENGINEERING

SUBMITTED BY

DIVNEET SINGH KAPOOR

SUPERVISOR

DR. AMIT KUMAR KOHLI

ASSOCIATE PROFESSOR, ECED, TIET

ELECTRONICS AND COMMUNICATION ENGINEERING DEPARTMENT

THAPAR INSTITUTE OF ENGINEERING AND TECHNOLOGY, PATIALA, PUNJAB, INDIA

2020

CERTIFICATE

I, **Divneet Singh Kapoor**, hereby declare that the thesis entitled, "**Performance Analysis of Spatially Coded OFDM Wireless Systems using Channel State Information,**" submitted to Thapar Institute of Engineering and Technology, Patiala, in fulfilment of the requirement for the award of the Degree of **Doctor of Philosophy** in **Electronics and Communication Engineering** is a record of original and independent research work done by me during 2014-2020. This thesis has been conducted under the guidance and supervision of **Dr. Amit Kumar Kohli**, Associate Professor, Electronics and Communication Engineering Department, Thapar Institute of Engineering and Technology. It has not formed the basis for the reward of any Degree/ Diploma/ Associate-ship/ Fellowship or other similar title to any candidate of any university.

Divneet Singh Kapoor

Date: 23/12/2020

This is to certify that above statement made by the candidate is correct to the best of my knowledge.

Dr. Amit Kumar Kohli

Associate Professor

Electronics and Communication Engineering Department,

Thapar Institute of Engineering and Technology, Patiala, Punjab, India

ABSTRACT

With the dawn of next-generation technologies, the current as well as future wireless communication systems are driven by applications that are mostly multimedia-based. And, it requires a humongous exchange of data in terms of audio/video content, which poses a challenge to enable the high data-rate capable communication networks. The combination of spatial-coding techniques and multicarrier transmission has been found as an appropriate choice for supporting the high data-rate/capacity without compromising the performance of wireless systems. The orthogonal-frequency-division-multiplexing (OFDM) has been recognized as a promising candidate for the multicarrier communication technique. The exclusive feature of OFDM is its capability to divide the allocated bandwidth into a number of orthogonal narrowband subchannels (overlapping) that transforms a frequency-selective channel into a set of frequency-nonselective flat-fading subchannels. In addition, the deployment of multi-antennas for wireless transmission and reception introduces subchannels in the spatial-domain, by which, a set of subchannels are established over the same time and frequency parallely. Therefore, the high data-rate services can be catered to the wireless communication users by utilizing the spatially-coded OFDM systems without the requirement of extra bandwidth, by enhancing signal-to-noise-ratio (SNR) at the receiving end. Due to a crucial need for channel-state-information (CSI) in the spatially-coded OFDM systems, the channel estimation/prediction has emerged as an integral part of such systems, which provides an opportunity to combat the adverse effects of fading, interference and noise/disturbances. It also enhances the information symbol-detection rate at the wireless receiver. Therefore, the spatially-coded OFDM strategies stand as a promising choice also for the future high data-rate communication techniques.

In order to enhance the spectral efficiency of the system, the incorporation of adaptive modulation techniques in OFDM systems (based on SNR criterion) has appeared as a lucrative option. It is beneficial to employ higher-order modulation modes on the subcarriers exhibiting relatively higher values of SNR, in the adaptive-orthogonal-frequency-division-multiplexing (AOFDM) systems. In uniform case, each subcarrier carries equal number of bits with equal power, but the order of modulation (on all subcarriers) can be switched according to the received SNR. Therefore, the AOFDM system relies on accurate channel-state-information (CSI) estimated/predicted at the receiver for its efficient working. We first present the channel estimation and long-range prediction technique for the AOFDM system. The efficient channel loading is accomplished by feeding the accurately predicted CSI back to the transmitter. The frequency-selective wireless fading channel is modelled as a tapped-delay-line-filter governed by a first-order

autoregressive (AR1) process; and an adaptive channel estimator based on the generalized-variable-step-size least-mean-square (GVSS-LMS) algorithm is employed to track the AR1 correlation coefficient. To compensate for the signal fading due to channel state variations, a modified-Kalman-filter (MKF)-based channel estimator is utilized. In addition, channel tracking is also performed for predicting the future CSI at receiver, based on the numeric-variable-forgetting-factor recursive-least-squares (NVFF-RLS) algorithm. Subsequently, adaptive bit-allocation for AOFDM system is employed by using predicted CSI at transmitter. Here, the proposed combination of GVSS-LMS and MKF algorithms for robust channel estimation and the NVFF-RLS algorithm for efficient channel prediction is incorporated, which is validated by using different channel realizations through simulation, and also by comparing it with the fixed step-size LMS, MKF and fixed forgetting-factor RLS algorithm based conventional techniques. For appropriate prediction of CSI at the receiver, the wireless fading channel modelling plays a vital role. We also suggest an alternate approach for the simulation of basis-expansion-model (BEM) for channel fading, in which each time-varying BEM coefficient is considered to be governed by an AR1 process. To introduce a high degree of uncorrelation among the BEM coefficients, the Markov parameter of each AR1 process is also assumed to be time-varying according to another independent stationary ergodic AR1 process, which forms the base of BEM–AR1–AR1 paradigm. The simulation results manifest that the proposed BEM–AR1–AR1 scheme is in close agreement with the ideal BEM for slow as well as fast channel fading. However, the first-order Markov-model (AR1-based) and second-order Markov-model (AR2-based), representing the wireless fading channels, have an edge due to their mathematical simplicity; and these models are the close approximation of Jakes' model. Therefore, these paradigms may find applications in the time-varying channel estimation due to its compatibility with model based adaptive algorithms.

However, the utilization of training data (in terms of information symbol-blocks) in adaptive algorithms deployed for the channel estimation/prediction impose burden on the wireless OFDM communication system, which in turn leads to reduction in the bandwidth efficiency. Therefore to reduce this training data overhead, we present adaptive channel prediction techniques for wireless OFDM systems using cyclic-prefix (CP). The CP not only combats intersymbol-interference, but it also precludes requirement of additional training symbols. The proposed adaptive algorithms exploit the channel-state-information contained in CP of received OFDM symbol, under the time-invariant and time-variant wireless multipath Rayleigh fading channels. For channel prediction, the convergence and tracking characteristics of conventional RLS algorithm, NVFF-RLS algorithm, Kalman-filtering (KF) algorithm and reduced Kalman least mean squares (RK-LMS) algorithm are compared. The simulation results are presented to demonstrate that KF algorithm is

the best available technique as compared to RK-LMS, RLS and NVFF-RLS algorithms by providing low mean squared channel prediction error. But, RK-LMS and NVFF-RLS algorithms exhibit lower computational complexity than KF algorithm. Under typical conditions, the tracking performance of RK-LMS is comparable to RLS algorithm. However, RK-LMS algorithm fails to perform well in convergence-mode. For time-variant multipath fading channel prediction, the presented NVFF-RLS algorithm supersedes RLS algorithm in the channel tracking-mode under moderately high fade-rate conditions. This technique is further extended to the multiple transmitter-antenna systems along with spatial block-coding. The usage of CP can be helpful for both the space-time-block-coded OFDM (STBC-OFDM) systems as well as for the efficient channel estimation/prediction (when utilized as the training data). Under appropriate parameter setting in 2×1 STBC-OFDM system, the NVFF-RLS algorithm bestows enhanced channel tracking performance than RLS algorithm under the static as well as dynamic environment, which leads to significant reduction in the symbol-error-rate (SER).

Moreover in frequency-domain, the multiple transmitter-antenna systems can also be employed with space-frequency-clock-codes (SFBC), in which the adjacent subcarriers are mapped onto the orthogonal/quasi-orthogonal codes, and that is analogous to STBC scheme in time-domain. But these have a common motive to improve the overall SNR. Therefore, we next present bit-error-rate (BER) performance analysis of the space-frequency-block-coded OFDM (SFBC–OFDM) communication systems, working over wireless fading channels under the impulsive environment. The effects of imperfect channel-state-information on the BER performance are also investigated, while using the *M*-ary phase-shift keying and *M*-ary quadrature amplitude modulation for the digital data transmission over the fading channels corrupted by the impulse-noise and additive-white-Gaussian-noise (AWGN). The imperfect CSI usually arises due to the noisy channel estimates at wireless receiver. The major focus is on the description of closed-form expressions for the BER performance of underlying SFBC–OFDM systems impaired by the impulse-noise, in which the noise bucket concept helps in quantifying its performance under the Rayleigh fading scenario. Simulation results are presented to connote the deterioration of BER performance of SFBC–OFDM systems due to the presence of impulse-noise, AWGN and noisy channel estimates at the receiver, under the different channel fading conditions exhibiting Rayleigh and Nakagami-*m* probability distributions. For lower values of m in the range $0.5 \leq m < 1$, the adverse impact of impulse-noise can be reduced by increasing the number of subcarriers in an OFDM symbol-block period.

With the advent of machine learning techniques, the CSI-estimation/prediction using artificial-neural-network (ANN) based architectures have emerged as a viable strategy in the intelligence-

based advanced wireless communication systems. Therefore, we further present an adaptive-slope squashing-function (ASF) based ANN for the efficient estimation of smoothly time-varying multipath fading channels, in a 4×1 SFBC-OFDM system using 64 subcarriers. The CSI estimated at the first-stage is further used for OFDM information symbol-detection (through minimum mean square error criterion based detection) at the second-stage. To combat the impact of smoothly time-varying environment, we emphasize on the utilization of ASF-ANN using backpropagation (BP) algorithm for the estimation of channel tap-coefficients in the frequency-domain. The underlying ANN is modelled as feedforward multi-layered perceptron that updates the network weights. The major focus is on the gradient-descent algorithm based adaptation of the slope of squashing-function (SF) along with other ANN parameters, which enhances the training efficiency of ASF-ANN in terms of the lower mean squared channel estimation error in comparison to the traditional fixed-slope squashing-function (FSF) ANN technique. Simulation results corresponding to the underlying 4×1 SFBC-OFDM system are presented to depict that the ASF-ANN based approach outperforms the FSF-ANN technique by providing lower symbol error rate due to the usage of well-estimated CSI. At 15dB SNR and fade-rate = 0.001, the average BER reduces to 2.85×10^{-4} for the ASF-ANN based approach, due to improved CSI-estimation; which accounts for approximately 5% improvement in the detection success-rate as compared to the FSF-ANN based approach. Furthermore, it has been observed that the squashing-function used for ANN deployment in many real-world applications is hyperbolic-tangent function. The usage of softsign squashing-function in an ANN based channel estimation (in the frequency-domain) for SFBC-OFDM system is also considered. The softsign based approach outperforms the hyperbolic-tangent squashing-function by providing smoother asymptotes, while using feedforward neural networks for the estimation of slowly varying fading channels. By exploiting the lower saturation tendency of softsign-function, the efficiency of channel estimator can be enhanced, which in turn improves SER performance of SFBC-OFDM system.

The intelligence-based signal processing using the ANN approach provides us an opportunity to recover/detect information symbols directly precluding the requirement of CSI at the receiver. Therefore, an intelligent receiver based on ANN for a 4×1 SFBC-OFDM system, working under slow time-varying frequency-selective fading channels, is also proposed that directly recovers the transmitted symbols from the received signal, without the explicit requirement of channel estimation. The ANN based equalizer is modelled by using the feedforward as well as the recurrent neural-network architectures, and is trained using the error backpropagation algorithms. The major focus is on efficiency and efficacy of three different strategies; namely, the gradient-descent with momentum (GDM), resilient-propagation (RProp), and Levenberg-Marquardt (LM) algorithms.

The recurrent neural-network architecture based SFBC-OFDM system is found to be an appropriate choice in terms of the low bit-error-rate performance, while using the different quasi-orthogonal space-time block-codes.

Based on the aforementioned research work, which mainly addresses the spatially-coded OFDM systems (working under wireless fading environment) using CSI, it is apparent that channel estimation/prediction is the backbone of STBC-/SFBC-OFDM systems, which plays a pivotal role in the information symbol recovery. The upcoming advanced wireless communication systems are likely to utilize the STBC-/SFBC-OFDM system architectures along with the intelligent signal processing based channel estimation techniques, to combat the interference and noise. The future work includes the implementation of machine learning techniques to further improve the channel estimation/prediction and to enhance the symbol-detection/recovery in the spatially-coded OFDM systems.

LIST OF PUBLICATIONS

1. Divneet Singh Kapoor and A. K. Kohli, "Adaptive-slope squashing-function based ANN for CSI estimation and symbol detection in SFBC-OFDM system," *Arabian Journal of Science and Engineering, Springer,* In Press. (SCI Indexed; Impact Factor = 1.711)
2. Divneet Singh Kapoor and A. K. Kohli, "Spatially-coded OFDM wireless systems employable in 5G communication networks – A review", *International Journal of Advanced Science and Technology*, vol. 29, no. 04, pp. 10965-11003, November 2020.
3. Divneet Singh Kapoor and A. K. Kohli, "Impact of squashing function's slope on ANN based channel estimation in SFBC-OFDM system," *Proc. IEEE 12th International Conference on Computational Intelligence and Communication Networks*, Bhimtal, India, pp. 258-260, September 2020.
4. Divneet Singh Kapoor and A. K. Kohli, "Intelligence-based channel equalization for 4x1 SFBC-OFDM receiver," *Intelligent Automation & Soft Computing, Tech Science Press*, vol. 26, no. 3, pp. 439-446, July 2020. (SCI Indexed; Impact Factor = 1.276)
5. A. K. Kohli and Divneet Singh Kapoor, "BER performance of SFBC–OFDM systems working over fading channels under impulsive environment," *Arabian Journal of Science and Engineering, Springer,* vol. 45, no. 3, pp. 1749-1763, March 2020. (SCI Indexed; Impact Factor = 1.711)
6. Divneet Singh Kapoor and A. K. Kohli, "Channel estimation and long-range prediction of fast fading channels for adaptive OFDM system," *International Journal of Electronics, Taylor & Francis*, vol. 105, no. 9, pp. 1451-1466, September 2018. (SCI Indexed; Impact Factor = 1.004)
7. A. K. Kohli and Divneet Singh Kapoor, "Adaptive filtering techniques using cyclic prefix in OFDM systems for multipath fading channel prediction," *Circuits, Systems and Signal Processing, Springer*, vol. 35, no. 10, pp. 3595-3618, October 2016. (SCI Indexed; Impact Factor = 1.681)
8. Divneet Singh Kapoor and A. K. Kohli, "Simulation of basis expansion model for channel fading using AR1 process," *Wireless Personal Communications, Springer*, vol. 85, no. 3, pp. 791-798, December 2015. (SCI Indexed; Impact Factor = 1.061)

CONFLICT OF INTEREST STATEMENT

I (Divneet Singh Kapoor) hereby declare that I have no conflict of interest in relation to the research work presented in the aforementioned publications.

ACKNOWLEDGMENT

The real spirit of achieving a goal is through the way of excellence and austere discipline. I would have never succeeded in completing my task without the cooperation, encouragement and help provided to me by various personalities.

First of all, I would like to render my gratitude to the Almighty, and I bow before Him for His umpteen blessings and bestowing in me the grit and confidence to carry out my thesis research work successfully.

It is my privilege to express my sincere thanks to our Hon'ble Director **Prof. (Dr.) Prakash Gopalan** and Esteemed Dean RSP **Prof. (Dr.) Rafat Siddique**, for giving me this opportunity to undertake the Ph.D. With deep sense of gratitude, I express my sincere thanks to my esteemed and worthy supervisor, **Dr. Amit Kumar Kohli**, Associate Professor, Electronics & Communication Engineering Department, Thapar Institute of Engineering & Technology, Patiala, for his valuable guidance in carrying out the research work under his effective supervision, encouragement, enlightenment and cooperation. Most of the novel ideas and solutions found in this thesis are the result of our numerous stimulating discussions. His feedback and editorial comments were also extremely valuable for writing this thesis.

I would also like to acknowledge **Dr. Alpana Agarwal**, Professor and Head of Department, **Dr. Hem Dutt Joshi**, Associate Professor, **Dr. Vinay Kumar**, Associate Professor, Electronics & Communication Engineering Department, and **Dr. Mandeep Singh**, Professor, Electrical and Instrumentation Engineering Department, who have been a constant source of inspiration for me throughout this dissertation.

I also thank the management of Chandigarh University, Mohali, Punjab, India for countenancing me to pursue Ph.D. at Thapar Institute of Engineering & Technology, Patiala.

I am greatly indebted to all my friends especially **Mr. Kiran Jot Singh**, **Mr. Anshul Sharma** and **Mr. Khushal Thakur**, who constantly supported and encouraged me all the time. I also express my sincere gratitude, deep love, and fondness to my wife **Ms. Manveen Kaur** and my son **Jivansh Singh** for enduring a seemingly endless ordeal, for sacrificing some of their best years. Their love, patience and persistent encouragement enabled me to finally finish this research work.

At last, but not the least, I express my gratitude towards my parents, **Mr. Kanwaljit Singh Kapoor** and **Ms. Ujinder Kaur**, who have always supported me in doing the things my way and whose everlasting desires, selfless sacrifices, encouragement, affectionate blessings and help, made it possible for me to complete my thesis in time.

Place: PATIALA **Divneet Singh Kapoor**

Date:

TABLE OF CONTENTS

LIST OF FIGURES

LIST OF TABLES

ACRONYMS AND ABBREVIATIONS

ASF-ANN	:	Adaptive-slope Squashing Function Artificial Neural Network
ANN	:	Artificial Neural Network
AOFDM	:	Adaptive Orthogonal Frequency Division Multiplexing
AR	:	Autoregressive Process
AR1	:	First-Order Autoregressive Process/First-Order Markov Model
AR2	:	Second-Order Autoregressive Process/Second-Order Markov Model
ARMA	:	Autoregressive Moving-Average
ASF	:	Adaptive-slope Squashing Function
AWGN	:	Additive White Gaussian Noise
BEM	:	Basis Expansion Model
BER	:	Bit Error Rate
BLUE	:	Best Linear Unbiased Estimator
BP	:	Backpropagation
BPNN	:	Backpropagation Neural Network
CDF	:	Cumulative Distribution Function
CDMA	:	Code-Division Multiple Access
CE	:	Channel Estimation
CFO	:	Carrier Frequency Offset
CP	:	Cyclic Prefix
CSI	:	Channel State Information
DAB	:	Digital Audio Broadcasting
DAB-T	:	Terrestrial Digital Audio Broadcasting
dB	:	Decibel
DF	:	Decision Feedback
DFT	:	Discrete Fourier Transform
DMT	:	Discrete Mutiple Tone
DNN	:	Deep Neural Network
DSL	:	Digital Subscriber Loop
DVB	:	Digital Video Broadcasting
DVB-T	:	Terrestrial Digital Video Broadcasting
EM	:	Expectation Maximization
EVD	:	Eigen Value Decomposition

EW-RLS	:	Exponentially-Windowed Recursive Least Squares
FDM	:	Frequency Division Multiplexing
FEC	:	Forward Error Correction
FFF	:	Fixed Forgetting Factor
FFNN	:	Feedforward Neural Network
FFT	:	Fast Fourier Transform
FIR	:	Finite Impulse Response
FSF	:	Fixed-slope Squashing Function
FSS	:	Fixed Step Size
GDM	:	Gradient Descent with Momentum
GSM	:	Global System for Mobile Communications
GVSS	:	Generalized Variable Step Size
GVSS-LMS	:	Generalized Variable Step Size Least Mean Square Algorithm
IBI	:	Interblock Interference
ICE	:	Intelligent Channel Estimator
ICI	:	Intercarrier Interference
IDMA	:	Interleave Division Multiple Access
IFFT	:	Inverse Fast Fourier Transform
ISI	:	Intersymbol Interference
JML	:	Joint Maximum Likelihood
KF	:	Kalman Filtering
LM	:	Levenberg-Marquardt algorithm
LMMSE	:	Linear Minimum Mean Square Error
LMS	:	Least Mean Square
LRP	:	Long Range Prediction
LS	:	Least Squares
LTE	:	Long Term Evolution
LTE-A	:	LTE-Advanced
MBWA	:	Mobile Broadband Wireless Access
MC	:	Multicarrier
MCM	:	Multicarrier Modulation
MIMO	:	Multiple Input Multiple Output
MKF	:	Modified Kalman Filter
MKF-FSS-LMS	:	Modified Kalman Filter Fixed Step-Size Least Mean Square

MKF-GVSS-LMS	:	Modified Kalman Filter Generalized Variable Step-Size Least Mean Square
ML	:	Maximum Likelihood
MLP	:	Multi-layered Perceptron
MMSE	:	Minimum Mean Square Error
MPSK	:	M-ary Phase Shift Keying
MQAM	:	M-ary Quadrature Amplitude Modulation
MRC	:	Maximal Ratio Combiner
MSE	:	Mean Squared Error
MSK	:	Minimum Shift Keying
NN	:	Neural Network
NVFF	:	Numeric Variable Forgetting Factor
NVFF-RLS	:	Numeric Variable Forgetting Factor Recursive Least Squares
OFDM	:	Orthogonal Frequency Division Multiplexing
OOB	:	Out of Band
OSTBC	:	Orthogonal STBC
PAPR	:	Peak to Average Power Ratio
PSK	:	Phase Shift Keying
QAM	:	Quadrature Amplitude Modulation
QO	:	Quasi-Orthogonal
QoS	:	Quality of Service
RBF	:	Radial Basis Function
ReLU	:	Rectified Linear Unit
RK-LMS	:	Reduced Kalman Least Mean Square
RLS	:	Recursive Least Squares
RNN	:	Recurrent Neural Network
RProp	:	Resilient-Propagation
RV	:	Random Variable
S/P	:	Serial to Parallel
SD	:	Symbol Detection
SDRQR	:	Square-root and Division-free Recursive QR decomposition
SER	:	Symbol Error Rate
SF	:	Squashing Function
SFBC	:	Space Frequency Block Code

SFBC-OFDM	:	Space Frequency Block Code OFDM
SIC	:	Successive Interference Cancellation
SNR	:	Signal to Noise Ratio
SS	:	Softsign Function
ST	:	Space-Time
STBC	:	Space-Time Block Code
STBC-OFDM	:	Space-Time Block Code OFDM
STF	:	Space-Time-Frequency
STTC	:	Space-Time Trellis Code
SVD	:	Singular Value Decomposition
Tanh	:	Hyperbolic Tangent Function
TBH	:	Tirkkonen–Boariu–Hottinen Code
TDMA	:	Time-Division Multiple Access
TS	:	Training Symbols
TSK	:	Takagi-Sugeno-Kang Fuzzy System
TWDP	:	Two-Wave with Diffuse Power
VFF	:	Variable Forgetting Factor
VSS	:	Variable Step Size
W-CDMA	:	Wideband CDMA
WiMax	:	Worldwide Interoperability for Microwave Access
WLAN	:	Wireless Local Area Network
WMAN	:	Wireless Metropolitan Area Network
WWAN	:	Wireless Wide Area Network
ZF	:	Zero-Forcing

CHAPTER 1

INTRODUCTION BASED ON LITERATURE REVIEW

1.1 Conventional OFDM Communication Systems

The world has seen an upgradation in the technologies driven by the multimedia based applications, which makes the requirement of high data-rate capable technologies to be more prominent over wireless/mobile channels. However, due to enhancement in the data-rate, the duration of transmitted symbol decreases, which leads to severe degradation of the received symbols because of the intersymbol-interference (ISI), due to the dispersive-fading in wireless environment. This phenomenon can be observed in the single-carrier modulation techniques, like in time-division-multiple-access (TDMA) and Global-System-for-Mobile-Communications (GSM) [1]. Orthogonal-frequency-division-multiplexing (OFDM) with the combination of multiple-input-multiple-output (MIMO) system has appeared as a promising choice to compensate the current high data-rate requirements [2], [3]. Broadly, OFDM can be viewed as an extension to frequency-division-multiplexing (FDM), in which the subchannels/ subcarriers overlap without interfering, since those are orthogonal to each other over one symbol-period [4]. The data in OFDM is transmitted, in parallel over different frequencies, which leads to an increase in the information symbol-block duration as compared to a serial data-transmission system. The increased information symbol-block duration gives rise to deleterious effects of ISI at the most for one symbol-block, which in turn simplifies the equalization of an OFDM information symbol-block. Moreover, extending the OFDM symbol with a small part of its head/tail (in the form of prefix/suffix), as a guard interval known as cyclic-prefix (CP), can be utilized to eliminate any residual ISI [6]. Exclusive benefit of OFDM techniques is that the signal/symbol processing takes place in digital-domain, rather than in analog-domain. A small phase variation at the receiver can be amended approximately at no cost by using digital parts of the system, in contrast to the performance degradation due to the precise design of analog filters in serial-modulation systems [5]. While the main idea of OFDM is relatively easy to understand, but the details of OFDM based communication techniques appear to be much complex [7]–[10]. The orthogonality of different subcarriers is incorporated by multiplexing (at the transmitter) the symbols digitally via inverse-fast-Fourier-transform (IFFT), which is a precise and computationally efficient method [11]. The demultiplexing of the symbols is conducted by utilizing the fast-Fourier-transform (FFT) at receiver. The bandwidth of individual subcarriers in this orthogonal-FDM system overlaps with each other taking the form of $\left|\sin(x)/x\right|^2$. And due to the inherent orthogonality property of

discrete-time Fourier-transform, the subcarriers can be demodulated without any hindrance. The spectra of OFDM and FDM are illustrated in Fig. 1.1. It may be observed from Fig. 1.1 that OFDM subcarriers span the frequency range, which includes the domain of other subcarriers as well, which makes it much responsive to the frequency-offset as well as phase-disturbance. In general sense, the merits/advantages of OFDM system can be summed up as follows [12]:

- With the usage of IFFT/FFT in OFDM technology, the whole system is easier to implement in digital-domain.
- Because of orthogonal subcarriers, the OFDM is bandwidth efficient.
- The usage of CP makes the OFDM robust to multipath fading.
- Since the transmission of symbols is in parallel-mode in OFDM, it is also immune to impulse-noise.
- The power and data-rate can be dynamically allocated to the different subcarriers; this makes OFDM more flexible in terms of resource allocation.

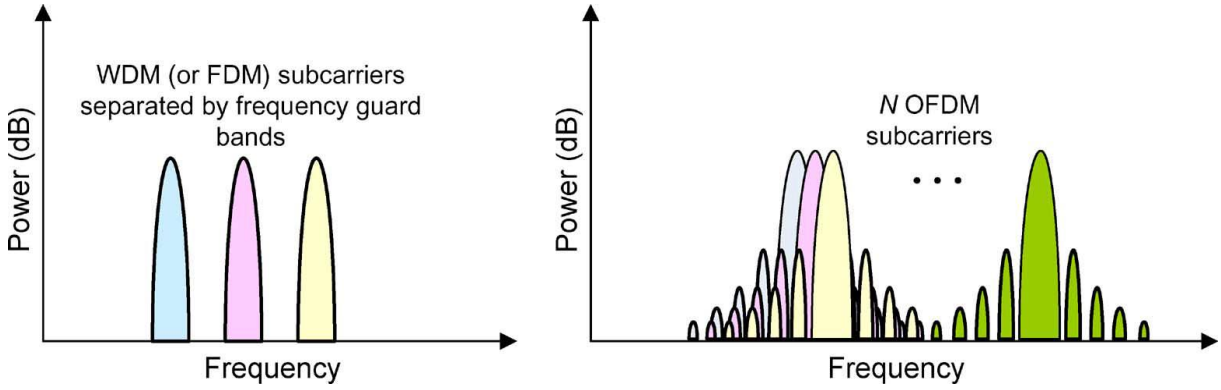

Fig. 1.1: Spectra of (a) WDM or FDM signals (b) orthogonal-FDM signals [5].

Considering these imperative advantages, orthogonal-FDM has been extensively utilized/adopted in different wireless technologies as well as standards like DAB, DVB, WLAN, and WMAN [13, 14]. Some of the other OFDM-enabled networks that are prevalent nowadays are IEEE 802.20 Mobile-Broadband-Wireless-Access (MBWA) [15], [16], Worldwide-interoperability-for-Microwave-Access (WiMAX) [17], 3GPP Long-Term-Evolution (LTE) [18] and next-generation Wireless-Wide-Area-Network (WWAN) [19]. On the contrary, some of the demerits of OFDM systems are its higher peak-to-average-power-ratio (PAPR) and its responsivity towards time-domain as well as frequency-domain synchronization errors, as compared to the single-carrier modulation schemes.

1.1.1 Basic OFDM Paradigm

OFDM can be termed as a particular type of multicarrier (MC) technique, which was pioneered in late 1960s. The basic idea of MC scheme has been coined in 1966 by Chang at Bell Labs [20] for the fading channels, which is also detailed in [21] and [22]. The implementation of MC system for the application of single-sideband voice channel was demonstrated in 1957 by Doelz *et al.* [23]. In the year 1971, Weinstein and Ebert came up with an idea of time-limited MC system based on discrete-time Fourier-transform, which has become the foundation stone of OFDM systems used today [11]. The equalization of MC systems has been examined by Horosaki *et al.* in [24], [25]; and Peled and Ruiz [26] in 1980 introduced CP in a practical implementation of OFDM systems to combat ISI. The earliest implementation of MC system in the high-frequency radio was reported in 1967 by Zimmerman and Kirsch [27], which has been extended in [28]. However, the bandwidth efficiency of OFDM system has been explored in [29] and [30]. The OFDM has been chosen for real-time wireless communication services during mid 1980s. The OFDM has been applied in mobile wireless communication system by Cimini at Bell Labs in the year 1985 [3]. In 1987, Lassalle and Alard utilized OFDM for the radio broadcasting, and observed the performance of the combination of forward-error-correction (FEC) with orthogonal-FDM (sometimes referred to as Coded-OFDM) [31]. Further, the application of MC modulation over mobile FM radio channels have also been discussed by Casas and Leung in [32]. Also, the complexity and performance of MC modulation system has been studied by Bingham in [7], which spearheaded the usage of MC schemes. For an MC system, Shannon in 1948 proposed that the utilization of infinitely dense set of subchannels along with adaptive data-rate and transmission power (in accordance with the variation in the values of SNR) could be beneficial in achieving highest data-rate under frequency-selective fading scenarios [33]. In case of wired communication systems, the application of OFDM as a successful modulation scheme for the digital-subscriber-loop (DSL) technology was invented by Cioffi *et al.* at Stanford University, which has become the basis for most of the DSL standards and is often known as discrete-multiple-tone (DMT) system [34]. The significant findings pertaining to different real-time loading procedures for orthogonal-FDM or DMT technologies are discussed in [35]. The various milestones in the establishment of OFDM based systems have been outlined in Fig. 1.2.

The OFDM based wireless communication system has significantly resolved the problems caused by multipath fading channel, but OFDM system has inherent shortcomings in terms of large PAPR value, time- and frequency-synchronization errors under the mobile multipath fading environment. The OFDM signal is the superposition of modulated complex-valued sinusoidal signals mapped onto various subcarriers, which may exhibit higher instantaneous signal power as

compared to the average signal power. This leads to elevated out-of-band (OOB) harmonic distortion power, as the power-amplifier at the transmitter is not perfectly linear always across the whole range of signal power level [36]. This causes interference in the adjacent channels, which in turn alleviates the overall system performance. The remedy to this problem lies in the reduction of PAPR and/or enhancing the transmitter's amplification stage. One of the methods is to employ certain coding techniques (before modulation) that can minimize the peak power of the OFDM signal [37]–[39]. The block-codes serve this purpose by exhibiting lower PAPR or reduced signal power envelope fluctuations. Also, the time-domain OFDM signal can be processed using different algorithms to suppress the peak power prior to amplification by the transmitter [40]. Further, the quality-of-service (QoS) of orthogonal-FDM communication systems is also dependent on time-domain and frequency-domain synchronization between the transmission device and reception equipment. It is necessary to efficiently estimate and correct the timing as well as carrier frequency-offsets that come into picture at the OFDM receiver, to successfully decode/demodulate the transmitted symbols [41].

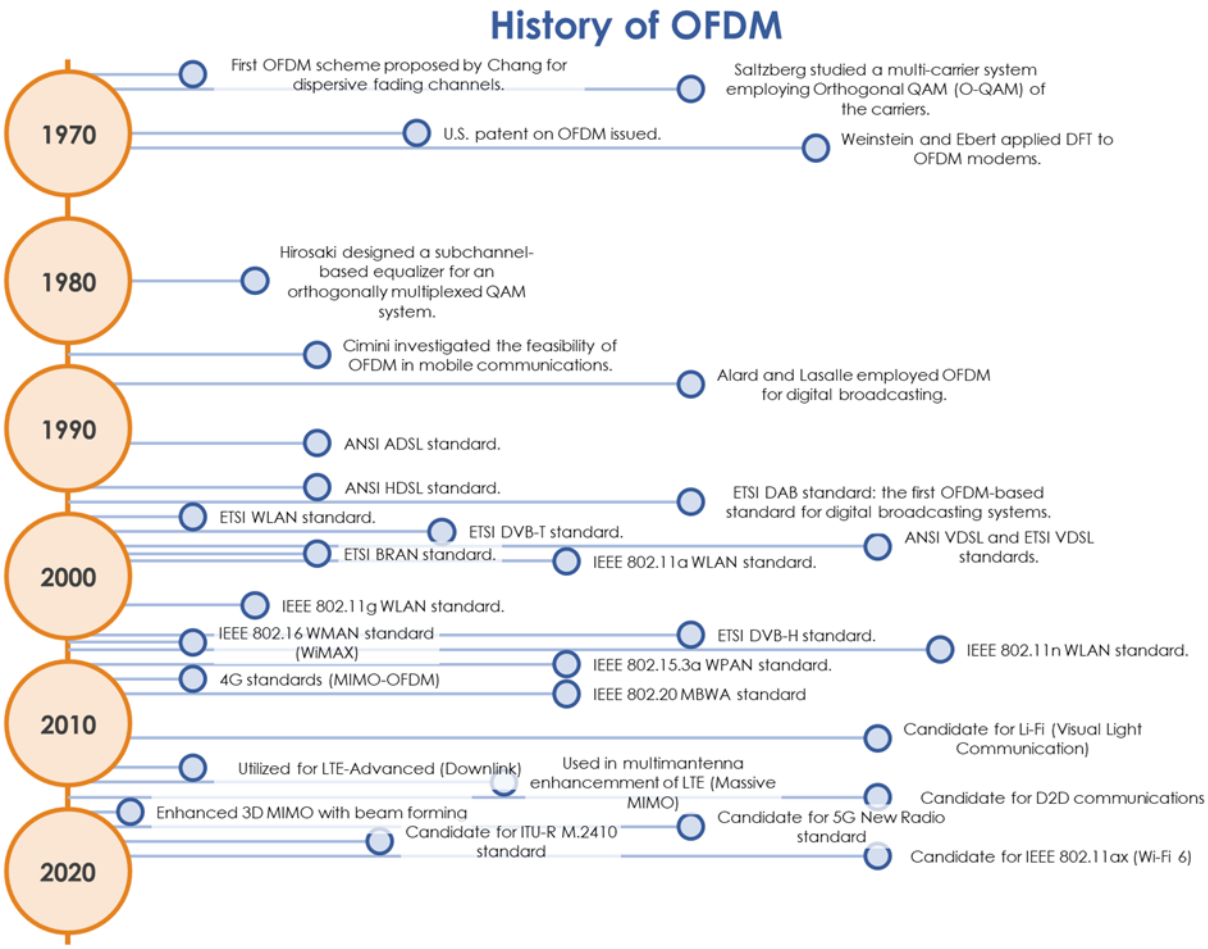

Fig. 1.2: Milestones in the history of OFDM [36].

In wireless communication systems, the high QoS is achieved when the underlying system exhibits higher data-rates and enhanced performance in terms of detection success-rate. However, the multipath signal transmission (as caused by reflections or diffractions and fading effects, which escalates the turbulent behaviour of wireless channels) makes it more difficult to achieve better QoS. Evidently, there is always a tradeoff between high data-rate (which accounts for bandwidth efficiency) and small error-rate (which accounts for power efficiency) for a fixed bandwidth of the channel. In order to resolve the aforementioned problems, the combination of MIMO and OFDM has appeared as one of the most promising solutions for broadband wireless systems. A MIMO system may be viewed as a wireless technique, in which transmitter and receiver need to be equipped with multiple number of antennas separated in space. The vital advantages of incorporating multiple antennas lie in attaining superior as well as reliable QoS by using diversity, and in attaining better data-rate by using spatial-multiplexing [42]. The signals at the transmitter and receiver are combined in such a way that QoS of the wireless link improves, making its reception performance superior as compared to single-antenna systems [43]. It is quite fascinating to know that the MIMO systems are beneficial in the same multipath fading channel, which is considered disruptive for the single-antenna systems. Further, a MIMO system improves the capacity of a wireless system by a factor of $\min\left(N_{Tx}, N_{Rx}\right)$, where $\min(.)$ is the choose-minimum operator, N_{Tx} is number of transmitter-antennas, and N_{Rx} is number of receiver-antennas [44]. Sometimes, the channel's multipath characteristics make the MIMO channel frequency-selective, which can be converted to parallel frequency flat-fading channels using the OFDM technique, that can in turn decrease the complexity of receiver [45]. Hence, the combination of MIMO (which boosts capacity and diversity) and OFDM (which mitigates the channel's detrimental effects) has been adopted in various applications and standards. It can be perceived that the future wireless systems will be enabled with the MIMO-OFDM architectures, as it provides diversification options in the domain of space, time, as well as frequency. Also, the combination of these attributes can be utilized to avail the benefits of diversity from MIMO channels with space-time-frequency (STF), space-frequency (SF), and space-time (ST) coding [45] techniques.

1.1.2 STBC-OFDM Paradigm

In multiple antenna systems, the effects of multipath channel fading may be combated by transmitting same information from a number of antennas and also receiving signal through a number of antennas concurrently. This is due to the assumption of each link of transmitter-antenna and receiver-antenna to be independent in terms of the channel fading. In addition to the spatial (or space-related) diversity, MIMO systems can achieve a significant level of diversity by

transmitting same information from various antennas at different time-slots, which is called Space-Time Block-Codes (STBC) [46]. This is an orthogonal-code design for 2 transmitter-antennas, in which, the information symbols are transmitted from different antennas in a different order. Rather than sending the same information symbols over different antennas, Alamouti [46] suggested to transmit information symbols and their complex-conjugate counterparts to achieve full-diversity at code-rate of 1. Since the coding matrix is orthogonal, this code inherited a simple and fast decoding strategy using a single-symbol maximum-likelihood (ML) detection. Moreover, this code strategy is also generalized for multiple antennas (more than 2) by utilizing the same concept and idea. But, the highest code-rate that could be achieved with this orthogonal STBC code for more than 2 transmitter-antennas is 3/4 with full-diversity [47], [48]. Another form of space-time coding is Space-Time Trellis-Code (STTC), in which, the information symbols are encoded using convolutional encoders to obtain simultaneous multiple transmitter-antenna streams of information symbols for transmission. STTC exploits delay-diversity in its functionary, in which the delayed version of information symbols' streams are sent over the multiple antennas. However, complexity of the system increases manifold with the increase in diversity level and transmission rate [49]. Due to the enhanced computational complexity of STTC in terms of its decoding, STBC technique proposed by Alamouti in the wireless communication system design (which utilizes only two transmitting-antennas and multiple receiving-antennas with the achievable diversity order of $2N_{Rx}$) is considered appropriate for deployment. Taking into consideration the simplicity and structure of the basic STBC, it can be readily deployed as advantageous diversity schemes in W-CDMA and CDMA-2000 both [50]. The orthogonal class of space-time codes is usually preferred, owing to its relatively lower decoding complexity along with the capability for the efficient mitigation of channel distortions, which provides full transmit-diversity. In [51], full-rate OSTBCs (orthogonal-STBCs) for multiple antennas (two to eight) are presented, which connotes that for the multiple number of transmitter-antennas, the full-rate orthogonal-code designs only exist for real constellations of modulation schemes for two, four and eight transmitter-antennas and for complex constellations based two-transmitter antenna system. If the number of transmitter-antennas are more than two, then it results in half-rate OSTBCs for modulation schemes that are complex-valued. Further, for arbitrary number of transmitter-antennas and complex-valued modulation schemes, a systematic design method has been presented to achieve the high-rate orthogonal-codes, which enjoy the benefit of a simplistic decoder [52]. The different forms of OSTBCs can be found in [53] and [54]; and the performance analysis of which are presented in [55] based on channel capacity; and the inference about average symbol-error-rate (SER) is presented in [56]. Considering the implementation of space-time codes, which are in the form of

matrices, the decoding of these orthogonal-codes can be highly complex due to the increased size of the codebook, when higher number of transmitter-antennas are utilized to achieve higher code-rate. It has been suggested that a reasonable effective space-time code must have the properties of full-diversity and relatively fast decoding.

The orthogonal design of STBCs have the ability to realize full-diversity and fast decoding at the receiver. Although, the increase in complexity with respect to the code size is linear for OSTBCs; however, the maximum code-rate achievable from these codes for multiple antennas greater than two is 3/4 (which is 1/2 for more than four transmitter-antennas) [51], [57], [58]. In order to achieve higher code-rates for multiple antennas in a MIMO system, the complex orthogonal design has been transformed to the quasi-orthogonal structure, in which the codes transmitted from various/multiple antennas are orthogonal to each other, but the transmission codes are made up of groups that are not orthogonal to each other. Rather than utilization of single transmitted symbol for decoding, the quasi-orthogonal codes utilize pairs of transmitted symbols to efficiently decode itself at the receiver [59]. The quasi-orthogonal space-time-block-code (QO-STBC) design for multiple antennas help in achieving higher code-rate, but alleviates the diversity order of the underlying wireless communication system. It has been depicted that QO-STBCs are useful for the communication systems working under low SNR scenario, and the codes with full-diversity orders are more beneficial for elevated SNR values, as the performance of a MIMO system depends on its diversity order. Further, QO-STBCs are designed as mentioned in [60] and [61], in which authors discuss the effects of interference caused by the symbols due to non-orthogonal structures of QO-STBCs. For slow-fading scenario, Tirkonnen *et al.* [60] have found that the multiple transmitter-receiver channels are approximately the same for a relatively longer period of time, which makes the decoding matrix singular and makes decoding more difficult, as the receiver is not able to differentiate between transmitted and interfering symbols. Hence, it is required for a QO-STBC to have full-diversity to achieve better performance at higher SNR values. This can be implemented by carefully choosing the signal constellations for different symbols to be transmitted through multiple antennas. One of the methods is to employ different constellations (differentiated by a small phase angle rotation) for different sets of symbols in QO-STBC structure. This method results in full-diversity order and faster decoding; and the computational complexity of which is similar to the other QO-STBC schemes [62]. The major disadvantage of QO-STBC is the elevated complexity while decoding the transmitted symbols, because of non-orthogonality of the codes. Since the ML decoder at the receiver processes pairs of transmitted symbols (for higher-order modulation schemes), the decoding complexity increases significantly. In order to mitigate this problem, the sphere-decoding algorithm can be used to decode the QO-STBC transmitted

symbols that substantially simplifies the decoding complexity, but it is quite susceptible to variations in SNR values [63], [64]. A low-complexity ML detector [65] and a low-complexity minimum-mean-square-error (MMSE) with QR-decomposition based ML decoding procedure [66] are presented to reduce the decoding complexity; however, these are also sensitive to the SNR values. The conventional linear decoding algorithms, such as zero-forcing (ZF) and MMSE, can also be utilized for QO-STBC decoding in communication systems [67], [68]. Another low-complexity ML detector that utilized real-valued lattice representation is proposed in [69] for quadrature-amplitude-modulation (QAM) schemes only. Further, the QR-decomposition is used to reduce the decoding complexity at the receiver, but it is not able to modify bit-error-rate (BER) performance of underlying QO-STBC based communication system [70]. An efficient strategy to reduce the interference caused by other symbols in QO-STBC scheme utilizes Givens rotation to efficiently eliminate the interference terms for simple linear decoding and full-rate encoding matrix [71]. Also, a similar method using the eigen-value-decomposition (EVD) has been introduced for three and four transmitter-antenna QO-STBC based systems in [72].

The spatial-diversity at the receiver leads to additional burden on the overall physical size and power consumption that hampers the portability advantage of wireless equipment. However, the diversity at the transmission side may be viewed as an opportunity to provide reliable data transmission to mobile users from the base-stations. The space-time coding techniques discussed above are quite susceptible to wireless fading channels that easily inhibit the orthogonality of the codes, which is alarming for these techniques. Hence, these coding techniques work efficiently in channels having flat-fading impulse response, which limits its usage to applications where the delay-spreads are nominal or small. OFDM has the inherent property to convert the frequency-selective wireless fading channel to the multiple flat-fading subchannels without ISI due to the usage of FFT and CP. The combination of STBC with OFDM can be utilized for improving the overall wireless system performance working under fading channels with large delay-spreads [73]. The STBC-OFDM technique presented in [73] utilized the Alamouti's coding scheme for the two transmitter-antennas, which is capable to achieve the diversity-gain approximately equal to maximal-ratio-combiner (MRC) receiver under the slow-fading environment. The Alamouti scheme decouples the transmitted symbols from different antennas that reduces the complexity of the receiver by employing ML decoding algorithm. Further, the space-time codes have been utilized in OFDM systems for two transmitter-antenna systems (with one and two receiver-antennas) in [74] and [75] to mitigate adverse effects of frequency-selective fading of the encountered wireless channel. The second-order diversity provided by Alamouti code used in these schemes is not sufficient for wireless communication systems providing adequate reliability under

fading environment. Therefore, ST codes that are capable to yield fourth-order diversity-gain by employing the four transmitter-antennas, have been considered as an opportunity for the implementation of STBC-OFDM systems [76]. The orthogonal space-time codes for four antennas with 1/2 code-rate and quasi-orthogonal codes with 3/4 code-rate have also been employed for STBC-OFDM systems in [77], [78]. However, these conventional coding schemes are utilized in the spatially correlated channels without taking into consideration the randomness and independence constraint due to the transmitter-antenna based correlation function. This results in BER deterioration for STBC-OFDM systems employing fourth-order diversity-gain [79]. An STBC-OFDM scheme, which utilizes the frequency-diversity, is also presented in [80] that enhances the performance of system in spatially correlated environment, in comparison to traditional STBC-OFDM techniques, by improving the determinant of channel correlation matrix. The orthogonal-coding of data symbols as provided by Alamouti coding scheme yields the advantage of lower decoding complexity only when underlying channel appears to be invariant for the period of orthogonal-FDM codeword transmission [81]. That is, a quasi-static block-fading environment is assumed for this STBC-OFDM system, which is a rare condition in practical scenario. Hence, it is necessary to consider and analyse the effects of time-varying channels on STBC-OFDM system, as a relatively longer symbol duration can deteriorate the system performance [82]. Also in fast time-varying fading environment, the performance gets degraded further because of the introduction of inter-carrier-interference (ICI) for demodulated subcarriers when channel variations within one OFDM symbol-block are significant [83]. The performance degradation of STBC-OFDM system working under the time-varying fading channel (modelled using first-order autoregressive (AR1) process) is also studied, for different types of receivers. It has been demonstrated that degradation occurs in all the receivers, but the receiver with decoupling capability performs similar to ML decoding receiver with a reduced diversity-order [84]. The detectors, namely zero-forcing (ZF), decision-feedback (DF) and joint ML (JML) detectors, are also utilized to improve performance of two-branch STBC-OFDM systems working under time-variant spatially uncorrelated multipath fading scenarios (which are modelled using Rayleigh distribution). Assuming sufficient CP to avoid ISI in the underlying system, JML detector has been found to alleviate crosstalk and noise simultaneously, whereas ZF detection procedure impels the crosstalk to null and DF detection procedure suppresses the crosstalk through the usage of whitened-matched filtering [85].

Conventionally, wireless channel is usually considered to be of flat-fading nature and known at receiver (for analytical simplicity) for the STBC-OFDM systems, which is not a practical approach in the wireless communication systems. This assumption leads to elevated BER due to ISI in time-

varying channel, which makes the channel estimation and equalization necessary for better performance. A channel estimation technique that utilizes training symbols for efficient estimation of channel fading conditions is presented in [86], [87], which utilizes relatively larger bandwidth and reduces throughput, as training symbols are also sent along with data symbols. Since, the ML detection requires channel-state-information (CSI) at the receiving end for proper detection (which is relatively computationally complex); therefore blind and semi-blind linear methods for equalization have also been used extensively. The blind equalization algorithm implementation (as discussed in [88]), utilizes a block channel encoder for redundancy that is placed before the space-time encoder in STBC system. Also, a semi-blind equalization algorithm for channel estimation has been developed in [89] for the zero-padded MIMO-OFDM system and it is not applicable to CP based OFDM systems. Also, different kinds of equalizers for spatially-coded systems working under the frequency-selective channels, which assume the availability of CSI at the receiver, have been detailed in [90]. A unified framework that encompasses basic STBC system, STBC-OFDM system and STBC-CDMA system, with a semi-blind equalization procedure for channel approximation that doesn't rely on the precisely available CSI, has been addressed in [91]. In order to eliminate ISI at the receiver, the information available as redundancy in space-time codes and training symbols have been exploited to develop a direct equalization technique for the generalized and hybrid STBC systems as well [91]. For STBC based MIMO-OFDM systems utilized in various practical applications, the signal identification that includes STBC identification, MIMO modulation identification and number of transmitter-antennas detection is deemed important for military as well as civilian applications in wireless communication. The signal identification in MIMO systems poses a larger difficulty, as along with the estimation of signal parameters and channel coefficients, there is a need to estimate the number of transmitter-antennas and the type of coding/configuration used at the transmitter. In order to efficiently perform the STBC identification, the feature-based approaches have been utilized that exploit the correlations in time-domain (induced by space-time coding) in transmitted signalling waveform. The schemes that use second-order zero-conjugate cross-correlation between signals transmitted from the different antennas have been introduced for MIMO-OFDM techniques utilizing more than 2 receiver-antennas in [92], [93]. These techniques assume Alamouti coding at the transmitter, and observe the cross-correlation function between the signals received at different antennas, which exhibit significant peaks corresponding to the number of transmitter-antennas. The sensitivity towards carrier frequency-offset is the major drawback of these techniques along with relatively longer observation time. The received signals can also be rearranged to induce correlation among all subcarriers, which can be utilized to differentiate the

peaks for different STBC schemes [94], [95]. Similarly, a technique that utilizes cyclic cross-correlation function of second-order and zero-conjugate type has been demonstrated to perform STBC signal identification, which has an advantage of shorter observation time for similar performance at a given SNR [96]. The techniques for modulation identification in STBC-OFDM systems is still lacking, as this requires the knowledge of incorporated coding scheme. Also, the joint identification of STBC and modulation scheme can be suggested based on the cyclic nature of OFDM signals transmitted using iterative processing techniques [97]. These strategies can trigger the utilization of STBC-OFDM methodology in the emerging wireless technologies to enable the fifth-generation (5G) of wireless communication systems.

1.1.3 SFBC-OFDM Paradigm

For a wireless communication system, different types of diversities that can be exploited by coding and transmission schemes are temporal-diversity, frequency-diversity and spatial-diversity. The space-time coding introduces redundancy across space as well as time to comprehend the diversity-gain in spatial-domain. In multipath fading MIMO channels, it is important to exploit frequency as well as spatial-diversity concomitantly. It is rather straightforward to employ space-frequency diversity with forward-error-correction (FEC) coding and interleaving across tones/subcarriers, which are deployed practically as bit-interleaved coded modulation [98]. A more systematic approach for obtaining the spatial diversity-gain is to utilize the space-time codes for the coding across space as well as frequency (in place of time), to form space-frequency codes [99]. Here, the desired symbols are encoded in spatial-domain (antennas) and frequency-domain (subcarriers), which makes the coding applicable in one OFDM symbol only, rather than different OFDM symbols, as in STBC-OFDM system. That is, in order to realize space-frequency coding for the two transmitter-antenna system, the Alamouti-code is applied on two consecutive subcarriers in single orthogonal-FDM symbol-block (through spreading) [100]. The space-time codes that has replaced the time-domain with frequency-domain achieved only spatial-diversity, but it could not guarantee full frequency-diversity. The performance criteria for SFBC-OFDM are discussed in [99], [101]. It is found that the maximum attainable diversity-order is the product of number of transmitting-antennas, number of receiving-antennas, and number of resolvable paths of a multipath fading channel ($N_{Tx}N_{Rx}L$). The existing space-time codes are not able to efficiently utilize frequency-diversity in a frequency-selective environment, therefore a different code design strategy has to be followed in case of SFBC-OFDM technology [99]. Further, a method for space-frequency code generation has utilized multiplication of a portion of discrete-Fourier-transform (DFT) matrix with transmitted symbol-vectors [102]. These codes attain full spatial as well as

frequency-diversity at the cost of reduced capacity. Also, this is assumed while designing these codes that power is spread uniformly across all multipaths; and multipath delays precisely fall on the sampling points at the receiving end. For arbitrary power delay-profile as well as for any number of transmitter-antennas, a systematic procedure for designing space-frequency codes is suggested in [103]. It has been demonstrated that a full-diversity space-frequency code can be constructed using a simple mapping from any STBC achieving the full spatial-diversity, working under a quasi-static flat-fading channel. These coding schemes are not able to achieve the full-rate (single information symbol per subcarrier). Eventually, a full-rate and full-diversity code design procedure is coined in [104] for any number of transmitter-antennas, memory-less modulation methods, and power delay-profiles.

The performance of STBC scheme gets degraded severely in the fast-fading wireless environment because of relatively longer duration of successive OFDM symbol-blocks. This disadvantage of STBC is resolved by the utilization of SFBC scheme, as the orthogonal design is structured with the utilization of neighbouring subcarriers of same OFDM symbol-block. Hence, SFBC scheme is less sensitive towards the Doppler-effect, which makes it a strong candidate for the IEEE 802.16e standard, which also takes user mobility into account [105]. It has also been presented that the orthogonal designs of STBC scheme are effective for the design of SFBC scheme in OFDM systems for achieving the maximum diversity-order, along with its effectiveness over fast-fading and frequency-selective wireless fading channels [106]. The SFBC scheme is also beneficial when the channel is slow varying in frequency-domain (with small delay-spread of fading channel), as compared to the STBC scheme that works well in slow varying environment in the time-domain. The utilization of orthogonal-codes for SFBC in OFDM systems have been shown to yield full-diversity-order under the multipath fading channel scenario in [107]. The assumption in the design of orthogonal-codes for SFBC is the constant channel gain across the whole duration of information symbol-block. However, this assumption fails to meet in many practical scenarios, where the channel is frequency-selective with higher delay-spreads. However, usage of traditional linear processing decoders (mentioned in [46], [51]) exhibit degraded performance, as ICI is induced due to the varying channel frequency response over the adjacent subcarriers. The induced ICI may be suppressed by introducing more subcarriers in each OFDM information symbol-block. This, in turn, leads to reduction in the bandwidth efficiency of SFBC-OFDM system, and it makes the system more prone to the frequency-offset related problems and phase-noise impairments. In order to minimize the errors caused due to the varied response of adjacent subcarriers, it is rendered important to perform interference cancellation in the frequency-domain. A low complexity successive-interference-cancellation (SIC) strategy has been proposed

in [108], which uses QR decomposition algorithm (that is square-root as well as division free) based on scaled Givens rotation matrices. The presented algorithm is relatively computationally simplified, as the conventional receivers utilizing square-root and divisions are computationally rigorous (because of high-bit precision needs), and therefore it emerges to be appropriate candidate in deployment of SFBC-OFDM receivers.

The block-codes (in time-domain or frequency-domain) require to be configured to achieve full-diversity-order while working under frequency-selective fading environment. However, the usage of algebraic theory for design of SFBC for frequency-selective fading scenario has been explored in [109], [110]. Also, a full-rate full-diversity code has been suggested in [111] that utilizes complex field decoding [112]. However, these techniques assume the uniform power delay-profile and equally spaced channel path-delays for a multipath fading channel. Further, a SFBC criterion has been derived in [103] that illustrates the relationship between SFBC code matrix and fading channel parameters (path-delays and power delay-profile). It is noteworthy that if any full-diversity STBC code is utilized as an SFBC code in MIMO-OFDM system, the diversity-order designed for time-domain is at least achieved, which emphasises on usability of space-time codes as well as space-frequency codes [103]. The utilization of SFBC has proven to be a useful method for combating ISI effects also [113]. The reported SFBCs are normally based on the complex-valued orthogonal STBCs, as suggested in [77]. It has been observed that the performance of these orthogonal STBCs gets degraded significantly under the time-varying environment that changes from one OFDM information symbol-block to another. A higher code-rate SFBCs have been designed in [114], that is proportional to number of transmitter-antennas used in underlying system. In [104], SFBCs with rate-one have been explored that has a benefit of maximum coding advantage, which are further optimized using the linear transformations [115]. Akin to the case of STBC, the orthogonal SFBCs also fail to exhibit full code-rate for more than two transmitter-antennas. Hence, for large number of transmitter-antennas, the SFBCs either have lower code-rates or are quasi-orthogonal with diminished diversity-gain. In QO-SFBC technique, the loss of diversity-gain is primarily because of the coupling between adjacent subcarriers due to the codeword design. The non-orthogonality of the QO-SFBC technique can be mitigated by its combination with the ML decoder, but that significantly increases the computational complexity of the wireless receiver [116]. Also, the diversity-gain can be improved by incorporating schemes like constellation expansion and symbol-rotation [62]. The data-rate can be further increased with higher diversity-gain by employing beamforming schemes with asymmetric antenna configuration. However, these schemes require full CSI at the transmitter [117] or rely on the intensive feedback from the receiver for steering vectors [118]. Also, the feedback received at the

transmitter may become obsolete in case of the time-varying channels that poses a significant burden on the throughput of wireless systems. The usage of multiple streams in SFBC methodology with or without partial CSI feedback has been observed as a promising technique. The interference between different streams (that are Alamouti encoded) has been suppressed by the utilization of ZF [119] or MMSE [120] receiver. The interference can also be mitigated by using the combination of beamforming (with SFBCs) and partial CSI available at the wireless transmitter [121], [122]. These techniques impose an extra burden of more than 16-bits for appropriate feedback in order to achieve the substantial performance, and is also prone to quantization noise [118]. An SFBC codeword with angle rotation has been discussed in [123], which utilizes only 1-bit feedback to improve the channel characteristics by choosing smaller residual interference power between 0^o and 180^o symbol rotation. This scheme proves to be a better performer as compared to the open-loop SFBC system counterpart. Furthermore, a novel class of SFBCs has been addressed in [124] that utilizes the linear combination of symbols using the Vandermonde matrices in the orthogonal-codes. This code design attains full-diversity and unity code-rate for the two transmitter-antennas, and full-diversity for more than three transmitter-antennas with reduced code-rate. This scheme is able to achieve the maximum coding advantage, when partial CSI is available at the transmitter.

The SFBC-OFDM systems mainly rely on the assumption of quasi-static (flat-fading for one OFDM information symbol-block) channels, for alleviating the computational complexity of the optimal ML decoding receiver. However for fast-fading channels, severe delay-spreads and Doppler-effects tend to degrade the performance of decoding algorithm due to the interference caused by the intermingling of signals from the different transmitter-antennas [125]. It has been observed that the receiver's decoding complexity gets increased exponentially with increase in the modulation size (constellation-size), which can give rise to a difficulty in the implementation of decoding algorithm for SFBC-OFDM systems. Furthermore, generalized simplified ML decoder has been detailed in [126] that cancels interference completely, while keeping the decoding complexity as given by Alamouti in [46]. Also, a concatenated ML decoder is investigated in [127] for SFBC-OFDM equipment working over frequency-selective fading scenario, in which authors have delineated a relationship between the degradation of channel decoders and the channel variations within the time-frame of one OFDM symbol-block. The decoding algorithms for the wireless receivers employing expectation-maximization (EM) [128], MMSE [129], MRC [46], ML [130] and low-complexity ZF [131] have been utilized for the flat-fading channels, which also tend to degrade their performances under the high mobility scenarios. Several attempts towards combining the spatially-coded symbol decoding and ICI cancellation in the SFBC-OFDM systems

have been mentioned in [132] and [133], which utilize the schemes based on correlative coding and linear interference cancellation. Recently, the performance of OFDM systems utilizing SFBC schemes has been studied using the numerical analysis method. A novel algorithm to identify spatial-codes through the analysis of discriminating features for different SFBCs is detailed in [134]. Also, the SFBC identification procedure for multiple transmitter-antennas in an OFDM system is analysed in [135]. For a SFBC system, the integer carrier-frequency-offset (CFO) estimation procedure is also proposed in [136]. Further, a distributed QO-SFBC is constructed for single-carrier transmission scheme in [137]. In order to mitigate the effects of PAPR in SFBC based MIMO-OFDM systems, several techniques have been discussed in [138] and [139]. A vector based OFDM system has been designed for STBC as well as SFBC schemes in [140]. However, a new iterative channel estimation scheme for SFBC based MIMO-OFDM systems that utilizes pilot symbols has been suggested in [141]. The SFBC-OFDM systems working over various fading channels have been analysed for BER performance in literature [142]–[146]. The outage-probability and frame-error-rate for BPSK and QPSK modulation schemes in STBC- as well as SFBC-OFDM systems have been addressed in [142]. The closed-form BER expressions for SFBC-OFDM systems utilizing MQAM as well as MPSK schemes are showcased in [143]. A detailed study of the BER performance of SFBC-OFDM receivers that are working in different fading environments has been presented in [144]–[146]. The performance of this system is also limited by nonlinear distortion caused due to power-amplifiers (at transmitter as well as receiver) [147]. Moreover, the practical performance analysis of SFBC based MIMO-OFDM receivers has been given in [148], which indicates/ highlights the deteriorating effects of nonlinear noise caused by power-amplifier working in TWDP (two-wave with diffuse power) fading environment. Here, closed-form expressions quantified the detrimental effects of nonlinearity on its BER performance [148], which can be quite useful while utilizing adaptive channel estimation and equalization techniques.

1.2 Channel-State-Information (CSI) Estimation in OFDM Systems

The transmitted information symbols reach the receiver after passing through a radio channel in the wireless communication systems. In order to efficiently retrieve the desired information in the presence of detrimental effects of channel, it is necessary to estimate the same for the case of conventional coherent receivers [149]. The accurate recovery of the transmitted signal is directly proportional to the efficiency in tracking of the channel variations. The utilization of differential modulation schemes and CSI-estimation at the transmitter helps to reduce the need of CSI-estimation at the receiver. However for the systems handling large data-rate, the CSI-estimation

becomes a crucial part of communication system. Since, wireless fading channel is highly dynamic in nature, the channel estimation becomes a challenging problem. The performance of channel estimation directly depends upon the statistics like scattering, spreading, mobility of transmitters and receivers, etc., which are exploited by different techniques to achieve better CSI estimates in the OFDM based multicarrier systems [150]. Usually, the channel is modelled as an unknown time-variant filter (with finite-impulse-response), and the coefficients of which are estimated by different algorithms and techniques [149]. In the case of OFDM system, the information symbols are mapped onto the orthogonal frequency-domain subcarriers, which makes the estimation of channel frequency response an important aspect for coherent detection of transmitted information symbols. The techniques for efficient CSI-estimation in OFDM based communication systems may be broadly categorized into blind as well as non-blind techniques. Blind CSI-estimation approaches require huge amount of statistical data of the received signals [151], which makes it unfavourable in the fast-fading environment [152]. However, in the case of non-blind channel estimation techniques, some amount of transmitted information symbols or previous channel estimates are available at the receiver for an improved CSI-estimation. Furthermore, non-blind techniques for CSI-estimation may be divided into two broad categories: data-aided as well as decision-directed. The data-aided approach (or commonly, pilot symbol-aided) makes use of the transmitted symbol information (that is known at the receiving end) for effective CSI-estimation by simply demodulating the received symbols. The deployment of pilot-symbols in frequency-domain for channel estimation is analogous in new generation IEEE 802.11a and HYPERLAN2 standards for WLAN [153]. It has been observed that accuracy of CSI-estimation increases with increase in number of pilot-symbols added; but that also elevates the transmission overhead and alleviates the spectral efficiency of underlying system. For slow time-varying environment, where channel is considered to be constant over a group of transmitted information symbol-blocks, the pilot-symbols are inserted over all subcarriers at the beginning of the information symbol-block group [154]. This type of pilot-symbol arrangement is known as block-type pilot arrangement, and is commonly used in WLAN and WiMAX systems [155]. For the case of fast-fading environment, the channel changes in between consecutive orthogonal-FDM information symbol-blocks, therefore pilot-symbols are inserted within OFDM symbol-block (on certain subcarriers), which is known as comb-type pilot arrangement. Also, in order to boost receiver performance, underlying channel can be tracked in decision-directed-mode, in which, current OFDM symbol demodulation is performed with the utilization of channel estimates obtained previously. The channel coefficients related to current decoded symbols are then estimated, which can be marginally reliable, as the channel is varying after each symbol [156], [157]. Therefore, the channel coding,

interleaving and periodic pilot-symbols are added to enhance the performance of decision-directed techniques in the time-varying environment.

The literature has suggested a number of techniques (using time- as well as frequency-domain samples) to estimate channel coefficients in OFDM based communication technology. Hence, basic channel estimation techniques utilize *a priori* information, which may be subcarriers' correlation in the frequency-domain [158], or in time-domain [159], or even in spatial-domain [160], and it can also be the length of channel impulse response [161]. In general, the better estimates may be retrieved by the utilization of *a priori* information at receiver [162]. The MSE is usually considered as a performance metric for indicating the efficiency of channel estimation techniques. Apart from MSE, the BER performance can also be used for measuring the system performance [163], [164], which is mostly utilized when the performance of OFDM system is evaluated along with the channel estimation errors [165], [166]. The common strategies for data-aided channel estimation are either transmitting known training-data over one or more orthogonal-FDM information symbol-blocks, or transmitting known training-data along with continuous stream of information symbols (pilot-symbol aided channel estimation). The spacing of pilot-symbols in the OFDM symbol-block depends upon the delay-spread of channel (that relates to channel's frequency response). The spacing between consecutive pilot-symbols should be small enough; such that channel variations in frequency-domain may be captured effectively. However, if this condition fails to meet, the aliasing of impulse response in the time-domain leads to an irreducible error floor (according to Nyquist sampling theorem) [167]. For a set number of pilot-symbols to be inserted, optimum locations in time-frequency grid are decided based on the Nyquist rate [168]. Moreover, the optimization of pilot-symbol allocation is a trade-off between the excessive energy utilized for pilot-symbols, insufficient fading channel sampling, accuracy of channel estimation technique and overall spectral efficiency of system [169]. Also, the optimum pilot allocation cannot be generalized for the different fading channels, as the fading process is quite different. It has been observed that pilot-symbols in frequency-domain need to be equipowered (same power as for data-symbols) and equispaced (same spacing between consecutive pilot-symbols). Here, number of pilot-symbols in each orthogonal-FDM symbol-block has to be at least equal to the length of channel impulse response. As the utilization of pilot-symbols for effective channel estimation is a trade-off, the adaptive allocation of pilot-symbols based on channel length estimation may provide another alternative [170]. Since the transmitter employs IFFT block, the OFDM suffers from high PAPR that can be different for different training symbols [171]. Further, different pilot-symbol allocation procedures may lead to different PAPR, when transmitted along with information-symbols. This leads to varying pilot-symbol allocation

for random data, in order to minimize PAPR [172], which in turn requires the information to be communicated to receiver that alleviates spectral efficiency of underlying OFDM system. The information related to channel statistics becomes a crucial part for designing an optimal pilot-symbol allocation strategy. The information related to delay-spread estimation is required for the frequency-domain pilot allocation, and Doppler-spread is required for pilot allocation over full OFDM symbol-blocks. The availability of these estimates results in acceptable performance of the system with right amount of pilot-symbols. Also, a scheme can be designed while taking worst channel conditions into consideration, if proper channel estimates are not available [172].

The commonly used simplistic CSI-estimation method for orthogonal-FDM systems is the least-squares (LS) estimation, which is utilized by many methods to obtain an initial channel estimation at pilot subcarriers for further enhancement in estimation performance [173]. With the knowledge about the number of channel tap-coefficients, the performance of LS estimation gets boosted due to the reduction in noise, as the dimensions of LS matrices get reduced [174], [175]. However, it increases the computational complexity, but the performance enhancement due to exploitation of subcarrier correlation amounts to the merit of LS estimation. The maximum-likelihood (ML) estimation is a similar technique to LS estimation that is utilized for efficient channel estimation [176]. Both of the techniques (LS and ML) rely on the pilot-symbols for the effective channel tap-coefficient estimation. However, when the number of pilot-symbols inserted in a single orthogonal-FDM symbol-block is more than channel length, the performance of both techniques is at par with each other [176], [177]. In training phase, all subcarriers of two OFDM symbol-blocks are reserved for known pilot-symbols (like in WLAN or WiMAX). For the system working under slow time-varying environment, the channel can be assumed as same for the subcarriers across OFDM symbol-blocks, which can be further utilized for the additive noise reduction [173]. The Kalman-filtering technique can be used, if different OFDM symbol-blocks experience different noise variances, provided the noise statistics are exploited as weighting parameters for the filtering process [178]. The CSI estimated from the training symbols may be further utilized for CSI-estimation in between training symbols (for the span, in which data symbols are transmitted). Usually, it is considered that channel is constant between orthogonal-FDM training symbols, and the channel tap-coefficients do not change until fresh training data is received [155], [179]. But, this technique impose a constant error floor for varying channels in practical scenarios. Also, it has been observed that the performance gets degraded significantly for the information symbols, which are transmitted farthest from the training symbols. Hence, it is beneficial to send the critical information over the symbols that are closer to training symbols [155], [180]. On the contrary, only few subcarriers in an OFDM symbol-block are utilized for the

training symbols in pilot-mode of channel estimation process. The channel response in frequency-domain is first estimated (via LS estimation) over pilot subcarriers, which are then interpolated/ extrapolated over non-pilot subcarriers. The most common method for interpolation is utilization of piecewise constant (where the channel response between consecutive pilots are assumed to be constant) [181], or linear interpolation (where the non-pilot channel response is approximated from a straight line between the consecutive pilot subcarriers) [182]. The piecewise linear interpolation technique needs more number of pilot subcarriers for achieving an acceptable level of performance under frequency-selective environment [181]. The performance of the systems can be enhanced by using the higher-order polynomials for channel frequency response fitting, provided that, *a priori* knowledge about frequency-/time-selectivity is available. Commonly used higher-order interpolation schemes are spline interpolation [183], Gaussian interpolation [184], and polynomial fitting [185]. However, if the OFDM systems are working under channels with lower selectivity, then the complicated estimation techniques can be replaced with simple interpolators.

An optimum method for minimization of MSE of estimated channel tap-coefficients in the presence of AWGN is the linear-minimum-mean-square-error (LMMSE) technique, which is widely used as one of the CSI-estimation strategies. LMMSE is an interpolator/ extrapolator/ smoother for the orthogonal-FDM based communication systems with pilot subcarriers, which utilizes additional information like channel statistics and SNR for the effective estimation. This leads to an increase in computational complexity (in terms of multiplication operations) of the LMMSE receiver as mentioned in [158], [176], and [184], that makes it relatively hard to deploy in the practical applications, although it is optimum. Hence, the computationally efficient techniques for LMMSE are realized for the CSI-estimation in orthogonal-FDM transmission. In [158], singular-value-decomposition (SVD) method is exploited for reducing number of multiplications needed for estimating CSI for single subcarrier. A pre-defined channel length is assumed in [186] that reduces the complexity of LMMSE substantially. However, when number of channel taps are less than actual channel length (sparse channel), this technique leads to unnecessary computations. SVD results in as many significant values as the number of channel taps, when channel length is quite smaller than number of subcarriers in an orthogonal-FDM symbol-block. Since, SVD transforms the information to a subspace-domain, the noise is also transformed that can be eliminated in the subspace-domain, which results in overall noise reduction at the receiver [187]. It has been observed that the utilization of SVD of auto-covariance matrices alleviates number of multiplications, but calculations of SVD of these matrices involve high computational complexity [188]. The robust channel estimation methods utilize assumed power delay-profile of fading channel, which is further used to pre-calculate auto-covariance

matrix and SVD values, in order to minimize the computational load [189], [190]. The reason behind significant performance of the robust LMMSE estimation is the available knowledge of channel statistics and SNR; without which, the desired improvement cannot be expected for a given computational complexity. In training based systems, the decision-directed channel estimation has been widely applied for OFDM based communication systems. The main motive of decision-directed technique is to utilize the previously estimated CSI for the current data detection, which is used to further improve the current CSI-estimation [191], [192]. If data at different subcarriers is identified, the aforementioned schemes can be employed for CSI-estimation. The decision-directed strategy inherently introduces two basic problems, that are related to the outdated (or previous) CSI estimates and about the consideration of correct (current) data detection. Decision-directed approach can be beneficial over the slow varying channels, but poses a problem when channel varies, that makes previously estimated CSI outdated for the current data detection. Therefore, the channel estimation and data detection errors get accumulated and make the overall system performance unacceptable for practical scenarios [193]. This accumulated error propagates with the increasing number of decisions (while performing data detection), which becomes critical for the system performance in the low SNR regions [194], [195]. The transmission of the training symbols (or pilots) can be seen as a potential strategy for overcoming the inherent problems of decision-directed technique. The time-period for sending training symbols can be pre-determined for a given system [195], or can also be adaptive based on the degree of variation in the estimated CSI [196]. The use of prediction algorithms can be considered as an alternative approach for the channel estimation. The previously estimated CSI can be utilized to predict the CSI for the next OFDM information symbol-block [197]. The prediction strategies may also be incorporated in time-domain (on channel tap-coefficients) [198] or in frequency-domain (on the CSI at the subcarriers) [197]. Further, it has been showcased that the utilization of ARMA modelling and Kalman-filtering leads to substantial enhancement in the performance of decision-directed estimation methods with prediction, in [198]–[200].

The expectation-maximization (EM) algorithm is one of the most promising technique for decision-directed channel estimation method. The EM procedure uses error probabilities utilized by the decoders (as provided by maximum-a-posteriori (MAP) decoder in turbo decoding), which is required for effective CSI-estimation [201]–[203]. This reduces the computational complexity of EM procedure, and makes it a viable choice for OFDM CSI-estimation. It has been shown in [204] that EM procedure may also be integrated with a QRD-M algorithm by utilizing the correlative coding, in the turbo-coded OFDM systems. It has been observed that EM procedure converges to ML procedure with a sufficient number of iterations, without the need of channel

statistics [205]. However, the performance relies on the initially assumed/ estimated values for the algorithm to converge rapidly. This iterative scheme may also be generalized as joint and iterative CSI-estimation techniques, which are useful in the fast-fading environment. Here, a reduced number of pilot-symbols are sent while taking non-linear distortions into account [206], [207]. The combinations of coherent detection, channel estimation as well as decoding schemes are used in OFDM based systems. In [208], the time-domain CSI-estimation is performed using Kalman-filtering, and the data is detected using QRD-M algorithm. Since, RLS is also an iterative method, it is combined with decision-directed estimation schemes to provide accurate estimates in the time-domain (as the number of parameters to track are less) [209], [210]. The CSI-estimation techniques offer a trade-off between performance and computational complexity. It has been demonstrated that LMMSE offers the best performance, but it has the highest computational complexity. Hence, it becomes important that the estimation techniques are unified to cater to the aforementioned trade-off [150]. The performance of CSI-estimation techniques gets degraded in the fast-fading environment (that forces the channel to change within an OFDM symbol-block), which makes the channel matrix non-circulant resulting in off-diagonal elements in the decoding matrix (commonly known as ICI) [211]. The frequency-offset (because of the transmitter/ receiver oscillator mismatching), phase-noise and non-linear distortions also degrade CSI-estimation performance [212]. Usually as a part of preamble, two OFDM symbol-blocks are transmitted for the synchronization purposes, in which, the synchronization errors can cause the significant performance degradation of LMMSE based channel estimation techniques [213]. The channel tap-coefficients vary at each sampling instance under the fast-fading scenario, which makes the time-domain estimation of each tap-coefficient necessary for obtaining better channel estimates in the frequency-domain. This increases the number of unknown parameters to be estimated that makes the solution as under-determined, as the number of equations are less than the number of variables. By correlating the channel-taps at each time-domain sample via certain basis functions can reduce the required number of equations. The most commonly used method for channel-tap evolution over time is the assumption of linear variation over the time [214], [215]. The lowpass filtering may also be incorporated for interpolation to achieve improved CSI estimates in the time-selective environment, as discussed in [211]. If the actual channel follows Jakes' channel model, the channel-tap variations are assumed to follow the zeroth-order Bessel-function of first-kind [214], in which, parameters are found by locating the zero-crossings over the time. Further, the channel-taps can also be modelled using an autoregressive (AR) process as specified in [216], the parameters of which can be obtained from the underlying channel statistics.

Furthermore, the artificial-neural-networks (ANNs) have also been incorporated in the problem of CSI-estimation in the communication systems. The ANNs have an inherent advantage of learnability from the environment under supervised and unsupervised conditions, which mimics the human brain with a network of interconnected neurons [217]. The massively parallel and highly distributed structure makes it appropriate for finding solution for the complex nonlinear problems that covers the applications of image processing [218], signal processing [219], computer vision [220], robotics [221]–[224], etc. A type of neural network based on radial basis function has been presented in [225]–[227], for effectively mitigating the channel effects in the pilot-symbol aided OFDM systems. In [228], the CSI-estimation technique based on ANNs has been showcased for OFDM systems working over Rayleigh fading environment without the assistance of pilot-symbols, which has led to an increase in the bandwidth efficiency as compared to the conventional techniques. Apart from SISO-OFDM, ANN based channel estimators have also been deployed for MIMO-OFDM systems that estimate channel effects by utilizing the comb-type pilot-symbol arrangement in [229], and are trained regularly by providing the feedback over communication channels [230]. In order to effectively approximate channel parameters as well as coefficients, the backpropagation-neural-network (BPNN) is the most commonly used architecture in OFDM based systems [231]–[234]. The BPNN architecture has also been employed in STBC based OFDM systems, as presented in [235]–[238], and in OFDM-IDMA (-interleave-division-multiple-access) systems for approximating the channel coefficients. Further, soft computing techniques like genetic algorithm optimization have been combined with BPNN to modify estimation performance as well as convergence speed of the channel estimator [239]. Since the aforementioned neural networks are real-valued, their utilization in complex-valued communication systems cause significant deterioration in the estimation performance due to inherent complications. The deep-neural-network (DNN) that contains more number of layers as well as neurons can be considered as a promising choice, as DNN paradigms are more flexible with greater number of attributes to have stronger generalization capability, as compared to the BPNN models. DNN approaches have been utilized for fingerprinting-based indoor localization with commodity 5G WiFi networks in [240] and [241]. Also, a new signal detection scheme for OFDM systems, that is based on DNN model, is presented in [242]. An efficient online technique that employs DNN for CSI prediction in 5G wireless communication systems has been discussed in [243]. The PAPR problem in OFDM systems has also been addressed using autoencoder architecture of DNN [244]. Further, for combating the large Doppler-shifts, a new DNN architecture has been suggested for orthogonal-FDM symbol identification in [245]. In [246], DNN based architectures and techniques have been deployed for orthogonal-FDM receivers under the constraint of one-bit complex quantization. In

order to retrieve information transmitted in orthogonal-FDM systems with the linear as well as nonlinear distortions, a model-driven strategy that combines DNN with expert knowledge has been discussed in [247]. Moreover in [248], a five-layer DNN architecture is trained with offline simulated information set for CSI approximation and symbol identification in orthogonal-FDM systems. A joint channel-equalization and decoding technique utilizes a six-layer DNN in [249]. In [250], a five-layer DNN based receiver is proposed to retrieve the transmitted signal directly after appropriate training. The training of such models can be done using the real wireless channel sample-data to further fine-tune the model to achieve higher degree of performance.

1.3 STBC-OFDM Systems using CSI

STBC wireless communication systems are based on the MIMO technology, which exhibit an ability to convert the multipath propagation phenomenon, conventionally a pitfall of the wireless signal transmission and reception, into an advantage for wireless mobile customer. The MIMO efficiently makes use of the random fading [2], [44], [251] as well as the multipath delay-spread by multiplying wireless data transmission rates [252], [253]. Here, the fundamental phenomenon is the space-time signal processing, in which time (the natural dimension of digital communication data) is complemented with the spatial dimension inherent in the utilization of multiple spatially distributed antennas. Though severe attenuation under multipath wireless scenario makes it highly tedious for wireless receiver to approximate the transmitted signaling waveform [77], but the deployment of multiple transmitter as well as the receiver antennas improves the SNR to enhance the data detection process. In addition, the underlying mathematical characteristics of the MIMO wireless systems (where data is communicated through a matrix-channel rather than a vector-channel) generate novel and ample alternatives beyond just the added transmitter as well as receiver antenna diversities or array gain benefits [44]. Two major problems encountered in the implementation of wireless transmitter-diversity are: a) unlike receiver antenna diversity, the transmitter antenna diversity does not exhibit instantaneous knowledge regarding wireless fading channels; and b) the transmitted signaling waveforms get mixed spatially before these arrive at wireless receiving equipment. The main wireless transmitter antenna diversity schemes may be categorized into two types: the open-loop [254]–[256], and the closed-loop [257]–[259]. The difference between the open-loop and the closed-loop techniques is that the former doesn't need the CSI at the wireless transmitting equipment, while the latter depends on CSI at the wireless transmitter (which is obtained through wireless feedback paths). Such feedback channels are there in almost all of the wireless paradigms for the power control changes as well. However, the mobility of wireless equipment can lead to fast channel changes. Consequently, the wireless

transmitter can't acquire and track the wireless channel variations. Therefore, the utilization of open-loop transmitter-antenna diversity techniques are well inspired for the future broadband communication technologies, that are capable of handling the high mobility of wireless user. The transmitter diversity can be classified into the following three categories based on the availability of CSI at the wireless transmitter and receiver: i) the schemes with feedback and feedforward information (giving complete CSI to both the wireless transmitter as well as receiver); ii) the techniques with feedforward data but with no feedback (receiver has CSI, but the transmitter does not have any information; and iii) the schemes without any CSI at the transmitter or at the wireless receiver. The aforementioned category (i) uses the implicit or explicit feedback of the information from the receiving equipment to wireless transmitting equipment to configure transmitter. However, in time-division duplex paradigms [260], similar antenna weights are utilized for the wireless reception as well as transmission, such that feedback reflects the channel symmetry implicitly. Here, weights are optimized during the wireless reception to maximize SNR. However, the mobile wireless equipment movements and/or interference cause a mismatch between CSI perceived by the wireless transmitting equipment and that perceived by the wireless receiving equipment. The aforementioned category (ii) is with feedforward scheme without the feedback technique. This scheme uses linear processing at wireless transmitting equipment to spread information across antennas. At wireless receiving equipment, the information is attained by either using the linear processing or using the maximum likelihood decoding scheme. The feedforward information is needed to estimate CSI from the wireless transmitting equipment to receiving equipment, and these estimates are utilized to compensate for channel response at the wireless receiving equipment [261]. The aforementioned category (iii) doesn't need feedback or feedforward knowledge. Instead, it utilizes multiple transmitter antennas in combination with the channel coding to give the diversity [262].

The STBC codes are used because of their simple decoding algorithm, which need information about channel-state-information at wireless receiving equipment. However, the CSI may be acquired at the wireless receiving end by sending the pilot symbols from each of the transmitter antennas to the wireless receiving antenna. Thus, the channel estimation or channel prediction is the backbone of STBC wireless systems, and it is necessary to use the excellent, efficient and unbiased channel estimation/prediction algorithms to enhance the efficiency of the STBC wireless systems working over time-varying (under mobility constraint) fading channels. For many advanced wireless communication systems, the channel fading is comparatively slow in comparison to frame-rate, and therefore the symbol-by-symbol channel estimation is much needed to attain an appropriate frame-error-rate (FER) performance [263]. Such technique is based on the

consideration that channel coefficients are not going to change substantially within one frame period/duration. The slow fading channel is particularly approximated by least-mean-squares (LMS) or by exponentially-windowed recursive-least-squares (EW-RLS) procedures [264]. When the channel fading is very slow (approximately under stationary conditions), the channel variations within an information symbol-block is low, and LMS or EW-RLS adaptive procedures may track channel variations quite effectively. On the contrary, when channel fading is fast, such adaptive procedures fail to track the changes in channel effectively [265]. An adaptive filter operating under the nonstationary scenario requires to be capable of tracking changes in the input statistics. An adaptive filter has four sources of misadjustment error [266], if it is implemented with infinite precision arithmetic operations [267]: i) this error originates from the noise i.e., measurement noise, ii) this error comes into picture due to finite data, which exhibits zero-bias and a variance that gets alleviated with increasing window-size, iii) this error arises due to the variance of nonstationarity, that gets elevated with the window-size, and iv) the model error may be there in terms of prediction error. The optimum adaptive algorithm for the nonstationary environment is the Kalman-filtering algorithm. An exclusive characteristic of Kalman-filter is that its mathematical modelling is detailed in terms of state-space concepts [268], [269], which is suitable for both stationary and nonstationary wireless channels. The computation burden and need about the information of system paradigm may usually preclude the aforementioned Kalman-filter based strategies. However, the tracking performance of RLS algorithm lies between the LMS algorithm and Kalman-filtering algorithm i.e., it has less complexity than Kalman-filtering algorithm and it performs better than LMS algorithm under the wireless time-variant channels. Therefore, RLS adaptive algorithm with some improvements is considered in [264] to track the wireless channels in the nonstationary environment. In RLS adaptive algorithm, the usage of weighting factor is intended to make certain that the input information about the distant past are “forgotten” in order to afford the possibility of following the statistical changes in the observable data, when the adaptive filter is operational under the slow or smoothly time-varying wireless channels. The STBCs are utilized in conjunction with OFDM technology to enhance SNR. In addition to the spatial- as well as temporal-diversity, the merger of MIMO-OFDM furnishes a third-dimension of coding that attains the frequency-diversity. However in STBC-OFDM systems, the channel statistics are required to be known at wireless receiving equipment to detect the transmitted symbols. Hence, the channel estimation with admissible level of accuracy as well as hardware complexity has emerged as an important research topic for the MIMO-OFDM wireless technology. The decoding procedure in STBC wireless systems requires the information about underlying channel at receiving end. This knowledge of channel may be attained at wireless receiving

equipment by conveying the pilot symbols from each of the transmitter antennas to the receiver antenna (and thus CSI can be estimated). However, better estimation of CSI improves the performance of the STBC wireless systems working under time-variant environment. The longer OFDM symbol duration gives a benefit, because the impulse-noise energy gets spread over concurrently transmitted orthogonal-FDM subcarriers [5]. This benefit turns in to loss, if impulse-noise energy exceeds a typical threshold level [270]. Therefore, the impulse-noise in addition to AWGN appears to be a serious problem in 4G mobile wireless communication systems.

It has also been observed that the signaling waveforms transmitted concurrently from the different transmitter-antennas appear as interference for one another, while performing the channel estimation procedure in STBC-OFDM based systems. Since, the channel estimation relies on the predetermined signaling waveforms transmitted as training and/or pilots, the decision-directed and pilot-symbol aided estimators have a major difference in their performance. This difference becomes significant when the signals start interfering with each other during estimation and decoding process in the multiple-antenna systems. With the employment of properly designed orthogonal training symbols (or pilots), such interference can be minimized for decision-directed as well as pilot-symbol aided systems [86], [271]. However, during the data transmission (other than training symbols or pilots), the interference from adjacent antennas poses a bigger hindrance in the efficient decoding of the symbols. Hence, the best estimate amidst the interfering signals is given by the MMSE channel estimator for decision-directed scheme [86]. The MMSE channel estimator presented in [86] has high computational complexity, which may be reduced by a low complexity channel approximation technique for STBC-OFDM system, as illustrated in [272]. Moreover, for pilot-symbol aided techniques, these types of interference are not of a concern, as the channel estimation for multiple antenna system is done by transmitting pilot symbols from only one transmitter-antenna at a single instant [46]. This requires a large number of pilot symbols as compared to the single-antenna system, which alleviates the data throughput and bandwidth efficiency. So, it is required that pilot signaling waveforms transmitted from various transmitter-antennas should engage different frequency subcarriers, for an efficient channel estimation [272]. The aforementioned techniques for channel approximation in STBC-OFDM systems assume the availability of channel statistics/ data at the wireless transmitting- and/or receiving-equipment, that puts an extra burden on the transmission overhead. The blind channel estimation techniques can avoid the penalty in overall spectral efficiency and SNR of the system. The blind channel estimation techniques relying on second-order statistics are the most preferred techniques, because of their lower computation burden and independence regarding a typical signal constellation [273]–[275]. The blind channel approximation or equalization techniques in frequency-selective

environment is looked from two different viewpoints. Firstly, the standard blind estimation techniques are applied that do not exploit the STBC structure, but these require relatively higher number of accessible blocks at the receiving end [276], [277]. In addition, subspace-based blind techniques are used that require long channel coherence times [278], [279]. These techniques also impose certain constraints on the signal constellations that might be impossible for linearly precoded systems. It has been depicted in [280] that the large number of STBC-based latest technologies (including STBC-OFDM) can be addressed regarding the blind estimation of frequency- as well as time-selective channels. In [280], the frequency- or time-variant MIMO channel is modelled by using basis-expansion-model (BEM) to alleviate number of parameters to be approximated, which are further estimated using subspace-based blind channel estimation scheme. Other than channel estimation, the information symbol identification also plays a significant role in different practical applications, like software-defined radio and spectrum awareness in cognitive radio [281], [282]. The signal identification includes identification of modulation format, identification of single- or multi-carrier transmission, identification of channel encoders, and also blind parameter estimation [283]. Specifically for STBC-OFDM systems, the blind signal identification caters to the techniques used for identification of number of transmitter-antennas, modulation identification and identification of STBC used [283].

Akin to the case of single-antenna conventional OFDM systems, ANNs in various forms and structures have also been utilized for channel approximation in STBC-OFDM systems. ANNs may be effectively used for decoding of symbols through multiple antennas under different fading scenarios, as ANNs have the inherent nonlinearity. The task of channel-equalization can be considered as a classification task for reliable deployment of ANNs [284]. ANNs are capable to form arbitrarily shaped decision boundaries because of its property of universal approximation [285]. For MIMO-OFDM systems employing STBCs, the channel estimation scheme based on ANNs is presented in [286], which carries out CSI-estimation and compensation. The CSI estimates are calculated in the terms of synaptic weights of the neural network; and comparative analysis of different training algorithms have also been illustrated in [286]. It has been concluded in [229], that the neural network based on Levenberg-Marquardt (LM) algorithm provides better performance in terms of SER, in comparison to the conventional LS estimator. In [286], the combination of ANNs with pilot symbols has been utilized as an estimation technique for MIMO-OFDM technologies, which exploits pilot symbols as references to efficiently estimate the CSI in frequency-domain. A channel estimation technique based on ANNs with feedback has been illustrated in [230], which utilizes feedback signals to train ANNs that precludes the usage of pilot symbols and knowledge availability of channel statistics at the receiver. Further, the radial basis

function network based channel estimation scheme is proposed in [287], which employs gradient-descent algorithm for training of the neural network for MIMO-OFDM systems working under Rayleigh fading environment. For STBC-OFDM systems, a multi-layered perceptron model based ANN has been presented in [236] that uses LM algorithm as training algorithm. It has been depicted that, after proper training, these ANN structures can outperform the conventional LS and LMS based channel estimators. In addition to the usage of ANN for channel estimation in STBC-OFDM systems, a Takagi-Sugeno-Kang (TSK) fuzzy approach has been applied to track the dynamic variations of the underlying channel [288].

1.4 SFBC-OFDM Systems using CSI

The STBC-OFDM as well as SFBC-OFDM techniques have been known to demonstrate similar performances under the slow fading environment, with the assumption of the availability of known CSI at the wireless receiver. However, SFBC-OFDM outperforms STBC-OFDM in the practical scenarios where the wireless information signal propagation experiences large Doppler-shifts [100], [289]. Moreover, the performance advantage of SFBC may be enhanced by the usage of large number of subcarriers for a given transmission bandwidth. Also, SFBC-OFDM systems require comparatively reduced decoder memory, as the decoding is performed within the same OFDM information symbol-block [289]. In order to achieve better performance for MIMO-OFDM systems, the CSI-estimation (or CSI availability) plays a pivotal role, which has been pioneered in [86] and has been extended to SFBC-OFDM systems in [289]–[308]. In [290], the impact of real propagation environment (modelled by considering the Rician K-factor, transmitting as well as receiving angle-spread, along with antenna spacing) on SFBC-OFDM system has been studied. In hostile environments, due to the presence of multipath fading, some subcarriers experience higher attenuation and lower SNR leading to degraded system performance. This problem can be mitigated by utilization of adaptive modulation, in which different signal constellations can be employed for different subcarriers depending on the channel effects. In [291], the transmitter-antenna selection and adaptive modulation have been jointly utilized to increase the efficiency of the underlying SFBC-OFDM system. Furthermore, the usage of adaptive modulation in SFBC-OFDM systems has been presented to combat the fast-fading environment, and also to overcome the frequency-selective fading with the adjustment of coding-size and subcarrier-bandwidth [292]. The conventional decoders assume that the channel-taps are static over adjacent subcarriers for efficient decoding. But, in frequency-selective environment with high delay-spreads, this quasi-static assumption cannot be considered true, which leads to degraded output of decoders. In order to tackle this problem, the quasi-ML strategy is incorporated in the SFBC-OFDM system [293].

In [294], an efficient decoder that uses square-root as well as division-free recursive QR (SDRQR) detection based on scaled Givens rotations has been presented for the SFBC-OFDM system using four transmitter-antennas. It has been observed that the SDRQR detector outperforms conventional ZF receiver for orthogonal as well as quasi-orthogonal (QO) codes, with the CSI available at the receiver [294]. Since, the channel response varies across adjacent subcarriers under the frequency-selective fading environment, therefore orthogonality of the SFBC code matrix gets destroyed, which leads to the consideration of alternative receivers. It becomes necessary to exploit both spatial- as well as frequency-diversities for the efficient decoding, while keeping the receiver's computational complexity low. A concatenated coding strategy that uses FEC in the combination with SFBC has been illustrated in [295], which has also presented a simple method for theoretical BER approximation of an optimal ML detector. Also, a multi-stage iterative QR-decomposition dependent interference cancellation detector has been demonstrated in [295], for SFBC-OFDM system utilizing the knowledge of available CSI at the receiver for efficient decoding of the transmitted symbols. It has been observed that for high mobility of either transmitter or receiver, ICI becomes the limiting factor in overall performance of the SFBC-OFDM systems. A novel SFBC-OFDM scheme that integrates with the FIR based ICI mitigating equalization has been presented in [296]. The fast time-varying channel matrix is also efficiently estimated by exploiting the sparse and banded structure of the matrix in time- as well as frequency-domain [296]. An efficient channel estimation and symbol decoding method, that takes into account the channel variations along adjacent subcarriers, has been discussed in [297]. This technique can be used for more than two transmitter-antenna systems with a little increase in the system complexity, which can achieve full-diversity with partial CSI feedback. A new technique of channel matrix shaping has been presented in [298], which guarantees identical channel responses over two adjacent subcarriers. This technique is based on 2×2 Walsh-Hadamard-Transforms, and makes the channel piecewise flat that allows the usage of conventional ML decoder even for the frequency-selective environment.

In order to efficiently conduct coherent detection as well as to attain higher transmission reliability, the accurate CSI knowledge becomes a necessity for SFBC-OFDM systems. The most common methods for reliable CSI-estimation are the LS [150], [299], [300] and the MMSE [299], [301], [302] based schemes. Another class of CSI estimators, which have been utilized are dependent on EM procedure. In [300], authors have presented different EM-based algorithms for CSI-estimation under both frequency-flat as well as frequency-selective MIMO channels. An iterative EM-based maximum *a posteriori* scheme has been illustrated in [303], which employs truncated Karhunen–Loeve expansion for the efficient channel approximation in SFBC-OFDM

systems working over doubly-selective environment. The *a posteriori* probabilities of transmitted symbols are first calculated by utilizing estimates from previous iteration. Then, these probabilities are utilized to refine CSI estimates, which leads to convergence. This scheme assumes quasi-static channel frequency response that makes it unsuitable for fast-fading environment [303]. Furthermore, the DFT-based channel estimation scheme with ML decoding that utilizes CP sequence has been depicted in [304]. The aforementioned techniques involve high computational complexity due to matrix inversions. Hence, lower computational complexity methods have been presented in [305], [306] that tends to degrade the performance when Doppler-shift is greater than 40 Hz. A low-complexity decision-directed estimator for SFBC-OFDM system has been demonstrated in [307], which utilizes a square-root-free inverse-QR-decomposition-based group-wise recursive CSI approximation technique. It has been depicted that this technique is useful for SFBC-OFDM applications that requires relatively lower computational complexity and better estimation of the channel response. Also, a robust iterative CSI-estimation procedure has been suggested in [308] for SFBC-OFDM systems working under fast-fading scenarios, that is based on ML decoding. The scheme presented in [308] does not involve any matrix inversion, which leads to lower computational complexity, even in highly mobile scenarios. Further, the effect of channel estimation error on the coding gain has also been investigated that makes it acceptable for arbitrary number of transmitter- or receiver-antennas along with arbitrary type of modulation for pilot and data subcarriers [308]. The closed-loop techniques can mitigate the effects of ill-conditioning of channel matrix and enhance the overall system output. It is usually required that the complete knowledge about CSI is available at transmitting equipment to perform precoding. The CSI can be made available to transmitter by sending a feedback signal from the receiver [118]. However, the availability of full CSI is quite difficult to obtain at the transmitter, which leads to the design of reliable limited-feedback signals and linear precoders, in order to reduce the volume of feedback [309]. The closed-loop OFDM systems utilizing partial or complete CSI at the transmitter have been used for mitigating the effects of interference [310]. A nonlinear Tomlinson-Harashima precoding technique to mitigate ICI with partial CSI availability has been presented in [311] for MIMO-OFDM techniques with frequency-offsets. The limited-feedback precoding reduces the number of bits to be transmitted back, which alleviates the overall system error rate and enhances system's capacity. Also, the closed-loop algorithm has been illustrated in [312] for SFBC-OFDM systems, which is able to achieve full transmit-diversity with only one-bit feedback per subcarrier for obtaining satisfactory performance. The feedback overhead is reduced by exploiting the feedback correlation among OFDM subcarriers that results in a group-based quantization technique.

In wireless transmission, estimated/predicted channel response can be noisy as well as outdated due to the delay in getting CSI to transmitting equipment [313]. Imperfect CSI comes into picture because of noisy as well as time-variant characteristics of fading environment. The Nakagami-*m* fading model covers a wide range of multipath fading channel models (by varying its parameter *m*) and offers greater flexibility than Rayleigh or Rician fading models [314]. The efficiency of SFBC-OFDM systems working under Nakagami-*m* fading-channels have been investigated in [315]. The authors have also analysed the impact of ICI caused due to frequency-offset and phase-noise on the underlying system under Nakagami-*m* fading environment. In order to investigate the impact of imperfect channel approximation over SFBC-OFDM systems, the closed-form expressions to calculate the BER have been presented in [143]. The researchers have derived the closed-form expressions (including exact expressions and approximate formulae) for average BER analysis regarding SFBC-OFDM techniques employed under frequency-selective fading environment. Also, the effects of CSI-estimation errors resulting from imperfect channel knowledge have been considered for evaluating BER degradation [143]. The BER analysis of SFBC-OFDM technique employing MSK as well as Gaussian-MSK has been discussed in [316]. The performance of orthogonal SFBC-OFDM systems in terms of average spectral efficiency and average BER has been analyzed, which considers the system working under α-μ fading [317] and η–μ fading environments [318]. Further, the impact of frequency-selectivity and CSI-estimation errors on the SFBC-OFDM scheme for 3GPP LTE system has been described in [319]. It has been suggested that the channel variation across two consecutive subcarriers leads to performance degradation, which can be mitigated by the utilization of interpolation method for the estimated CSI, that results in 3 dB BER improvement at high SNR values. The appropriate desired data communication over available transmission link, while considering manmade noise/interference, is one of the most challenging problems. These interferences originate due to powerlines, heavy current switching systems, electrical-furnaces and domestic equipment (microwave ovens), etc. [320], which become the sources of impulse-noise generation. The combination of spatial-diversity with OFDM boosts the total SNR to suppress the effects of impulse-noise [321]–[323]. The impact of impulsive noise as well as imperfect channel-state-information on SFBC-OFDM system has been detailed in [324], with the mathematical expressions for its average BER.

1.5 Statement of Problem

The presented work includes a detailed study of spatially-coded OFDM wireless communication systems using the channel-state-information, in which CSI is estimated/predicted using the adaptive techniques. However, the information symbol signal transmission in the conventional OFDM, adaptive-OFDM, STBC-OFDM, and SFBC-OFDM systems encounter the frequency-selective multipath fading channels, which leads to unavoidable symbol-error-rate (or bit-error-rate) performance degradation in terms of increased SER, due to the fading process. This problem appears to be more severe, when the wireless channel is time-varying (categorized as quasi-static channel, when the fade-rate is low, i.e., smoothly time-varying; and dynamic channel, when the fade-rate is high, i.e., fast time-varying; (See Appendix-A)). It particularly adversely affects the performance of AOFDM systems, which needs to be resolved.

In STBC-OFDM systems, the usage of cyclic-prefix to combat intersymbol-interference and the utilization of training symbols for channel estimation/prediction using the adaptive algorithms result in high overhead burden on communication system. Therefore, the high-speed and efficient adaptive channel predictors/estimators appear as a dire requirement for the STBC-OFDM systems, typically under the time-varying multipath fading environment. The accurate knowledge of CSI at the STBC-OFDM and SFBC-OFDM receivers is undoubtedly desired for the SER reduction. But, the symbol-detection process becomes difficult in the SFBC-OFDM systems, while working over fading channels under the impulsive environment, as both the impulse-noise and AWGN adversely affect the information symbol-detection success-rate. For smoothly time-varying channel estimation/prediction, the traditional fixed-slope squashing-function based ANN techniques fail to perform well. And the resulting channel estimation/prediction errors lead to elevated SER in SFBC-OFDM systems, which must be controlled for the efficient symbol-detection using CSI. However, ANN based configurations can be directly incorporated to recover/detect the desired information symbols in an SFBC-OFDM system from the received wireless signal, using the intelligent signal processing approaches.

And the problem (P), as treated in this research work, may be broken into five foremost sections; which are as follows:

P1.) Analysis and design of channel estimation and long-range prediction of fast-fading channels for the adaptive-OFDM system
It is based on the combination of GVSS-LMS and MKF algorithms for the robust channel estimation at transmitter and the NVFF-RLS algorithm for efficient channel prediction at receiver.

P2.) Analysis and design of adaptive filtering techniques using cyclic-prefix in STBC-OFDM systems for multipath fading channel prediction
It is based on the utilization of NVFF-RLS and KF algorithms for the cyclic-prefix based channel prediction to track the fast time-varying wireless fading channels.

P3.) Analysis of BER performance of SFBC–OFDM systems working over fading channels under the impulsive environment
It is based on the analysis of closed-form expressions for the BER of SFBC-OFDM systems working under Nakagami-m fading environment in the presence of impulse-noise.

P4.) Analysis and design of the adaptive-slope squashing-function based ANN for CSI-estimation and symbol-detection in the SFBC-OFDM system
It is based on the utilization of adaptive-slope squashing-function based ANNs for the effective CSI-estimation in the SFBC-OFDM systems.

P5.) Analysis and design of the intelligence-based channel-equalization for 4×1 SFBC-OFDM receiver
It is based on the usage of ANNs for directly estimating/detecting the transmitted desired information symbols from the received signals under slowly time-varying fading channels.

1.6 Organization of Thesis

Chapter 1:- "Introduction Based on Literature Review"

Chapter 2:- "Channel Estimation and Long-Range Prediction of Fast-Fading Channels for Adaptive-OFDM System"

In this chapter, the details about the adaptive-OFDM based communication system working under the time-varying multipath channel conditions are given. Then, the MKF-GVSS-LMS algorithm based channel estimation scheme for the time-variant frequency-selective channels is described. The estimated channel-state-information is then fed to a long-range-predictor based on NVFF-RLS algorithm, which has been further discussed for predicting the channel-state-information, and then feeding this information back to the transmitter for invoking the adaptive-bit-allocation algorithm. Subsequently, the performance of algorithms used for the channel estimation and prediction are validated and compared with the conventional techniques with the aid of computer simulation. Finally, summary of the chapter is provided to illustrate the substantial contributions in presented research work.

Chapter 3:- "Adaptive Filtering Techniques Using Cyclic-Prefix in STBC-OFDM Systems for Multipath Fading Channel Prediction"

In this chapter, we first give details about a wireless OFDM communication system model working under the time-invariant and time-variant multipath fading channels, which comprises of the channel prediction and equalization procedures at the wireless receiver. We next describe the Kalman-filtering and RK-LMS algorithm-based channel predictors using the cyclic-prefix of OFDM signals. Subsequently, the details of conventional RLS and NVFF-RLS algorithms for the multipath fading channel estimation is described. Further, simulation results are presented to compare the channel tracking performances of KF, RK-LMS, RLS and NVFF-RLS adaptive algorithms under the static and dynamic environment, which are appraised on the basis of MMSE criterion. The presented channel estimation/prediction algorithms are incorporated in 2×1 STBC-OFDM system for the symbol error rate (SER) performance analysis. Eventually, summary of the chapter is given to depict the important contributions in presented research work.

Chapter 4:- "BER Performance of SFBC–OFDM Systems Working over Fading Channels Under Impulsive Environment"

In this chapter, we first give details about the system model for uncoded-OFDM system working under the impulsive environment. The main focus is on the impact of impulse-noise and imperfect

CSI on the performance of OFDM systems working over fading channels. Then, the system model for SFBC–OFDM system working under impulsive environment is described. The mathematical expressions for the average BER and the effective/normalized instantaneous SNR per subchannel are presented for the SFBC–OFDM wireless systems, while utilizing the M-ary QAM and M-ary PSK digital modulation techniques under Rayleigh fading environment in the presence of impulse-noise and imperfect CSI (i.e., using noisy channel estimates) at the receiver. Further, simulation results are presented, and finally, summary of the chapter is highlighted.

Chapter 5:- "Adaptive-Slope Squashing-Function Based ANN for CSI-Estimation and Symbol-Detection in SFBC-OFDM System"

In this chapter, we first describe the transceiver paradigm for the underlying 4×1 SFBC-OFDM system with two-stage receiver configuration working under the slow time-variant environment. Subsequently, the channel estimation using ASF-ANN at the CE-stage of underlying system is detailed. Simulation results to depict the efficiency and efficacy of addressed intelligent estimator in terms of the mean-squared-channel-estimation-error are further presented, which in turn makes a substantial impact on the SER of underlying system. In the end, summary of the chapter is provided to demonstrate the significant findings in presented research work.

Chapter 6:- "Intelligence-Based Channel-Equalization for 4×1 SFBC-OFDM Receiver"

This chapter addresses an ANN based receiver for the 4×1 SFBC-OFDM system using the backpropagation algorithm for the network training, which directly recovers the transmitted symbols from the received signal. Further, the feedforward-neural-network (FFNN) as well as the recurrent-neural-network (RNN) architectures are explored as the intelligent receivers for underlying system, while utilizing various learning algorithms for the intended equalization. The bit-error-rate (BER) performance evaluation of the underlying SFBC-OFDM system is then analyzed (through Monte-Carlo simulation) using distinct QO-STBC schemes. At last, summary of the chapter illustrates the imperative outcomes and contributions of the presented work.

Chapter 7:- "Concluding Remarks and Future Scope"

We conclude the thesis with a summary of the important results, observations and suggestions for future work.

CHAPTER 2

CHANNEL ESTIMATION AND LONG-RANGE PREDICTION OF FAST-FADING CHANNELS FOR ADAPTIVE-OFDM SYSTEM

2.1 Introduction

The high data-rate wireless communication systems use the orthogonal-frequency-division-multiplexing (OFDM), a multi-carrier-modulation (MCM) technique, which makes use of closely spaced subcarriers for the data symbol transmission on several parallel subchannels. The inherent advantage of MCM or OFDM is their ability to counter the frequency-selectivity of channel fading by altering the same into the flat-fading [159]. Also, the usage of cyclic-prefix (CP), of length greater than or equal to the maximum delay-spread of channel, reduces the inter-symbol-interference (ISI) [6]. Moreover, one-tap equaliser can recover the received data, when channel is assumed to be stationary or constant over the extended symbol-period including CP [3]. With these vital benefits, OFDM has been adopted by many wireless standards such as digital-audio-broadcasting (DAB), digital-video-broadcasting (DVB), WLAN, and WMAN [13], [14]. The OFDM systems are quite prone to the time-varying fading, and these systems appear to be vulnerable to the time-selective fading. Moreover, the frequency-offset and phase-noise adversely affect the orthogonality of subcarriers, which in turn introduces inter-carrier-interference (ICI). Hence, the estimation of channel and its equalization at the receiver are considered more important to mitigate the effects of channel fading, for the proper decoding of the received symbols [325].

The adaptive-OFDM (AOFDM) optimises the modulation level and the transmission power over the frequency band in order to maximize the spectral efficiency, akin to the single-carrier adaptive modulation schemes [326]–[330]. The subcarriers experience different channel conditions operating under the frequency-selective fading channel. In order to improve the spectral efficiency, more bits are allocated to the subcarriers, which experience less fading as compared to the ones with the deeper fading conditions [326], [331]. Hence for the proper allocation of bits and power optimization, highly accurate channel-state-information (CSI) is much needed at the wireless transmitter. The channel estimation of OFDM systems has been employed through various techniques. In Ref. [325], a minimum-mean-square-error (MMSE) channel estimator, that utilises the correlation functions in both time-domain as well as frequency-domain, has been reported. A low-rank approximation to the frequency-domain linear MMSE estimator is also suggested in literature [158]. These techniques alleviate the computational complexity of MMSE procedure with the help of singular-value-decomposition (SVD). However, the OFDM systems

utilising these estimators suffer from ICI, when operated under the time-varying channel conditions. Moreover, these techniques require the channel statistics' knowledge for the high quality estimation. However in order to mitigate the effects of ICI, the time-domain channel estimators are described in [332], [333], which exploit the time-variant nature of the channel by assuming that the CSI varies linearly, and these utilize SVD to reduce the computational complexity. As these techniques depend on the initial CSI assumption, therefore the system performance can vary significantly, if the difference between initial state assumption and true value of channel state is high. A generalized autoregressive (AR) process can be used to exploit the time progression of multipath fading channels [334]. Using the first-order autoregressive (AR1) process model [335], a modified Kalman-filter based fast-fading channel estimation in OFDM systems is explored in [336]. This algorithm estimates the AR1 model parameters by minimizing the mean-squared-error (MSE), and the estimated parameters are then subsequently fed to the Kalman-filter for the efficient channel tracking. Also, the low density parity check codes with the aid of Kalman equalization for better channel tracking can be utilized under the slow fading environment [337]. Recently, the estimation of long delay channels by utilizing the complex interpolators in the frequency-domain has been introduced in [338].

In order to fully exploit the potential of AOFDM, a highly reliable predicted CSI is required at the transmitter [326]. A multivariate adaptive regression splines model, proposed in [339], has used the dynamics for predicting parameters of the fading channels for fast vehicle speeds. Different prediction techniques (like subspace-based [268], root-MUSIC method [340] and ESPRIT algorithm [341]) estimate the power spectrum of fading process, and then extrapolate it to predict the future samples. An adaptive long-range-prediction (LRP) method [326] utilizes the AR process model of any order to portray fading channel, and it predicts the future channel fading coefficients based on some past observations, while minimising the MSE. Since LRP may be implemented adaptively, it is less complex and more robust than the other fading channel prediction algorithms. In this work, we utilise the variable step-size adaptive algorithm in LRP for better convergence characteristics and tracking speeds.

The dynamic step-size is an efficient solution for better convergence characteristics of the adaptive algorithms. A variable-step-size (VSS) least-mean-square (LMS) algorithm is presented in [342] to track the channels modelled by AR1 process, in which the prediction error controls the step-size update. The step-size updating can be controlled by the correlation of estimation error over a time period taking into account its present and past values [343], or by adjusting it in accordance with the stochastic gradient to reduce the estimation error [344]. The combination of generalized-VSS (GVSS) and least-mean-p^{th}-power (LMP) algorithm helps to enhance the

convergence-rate under the noisy and time-varying environment [345]. The recursive-least-squares (RLS) algorithm utilizes information contained in the underlying system model statistics, which results in the enhanced convergence-rate in comparison to the fixed-step-size (FSS) LMS algorithm [268]. As compared to the fixed-forgetting-factor (FFF) RLS algorithm, the numeric-variable-forgetting-factor (NVFF) RLS algorithm performs better in terms of MSE, as it accounts for the nonstationarity of the signal [346]. The variable-forgetting-factor (VFF) is adjusted according to the channel variations, which results in better convergence and lower MSE in estimation/prediction process.

In this chapter, the wireless channel is considered to be time-varying and exhibiting variable fade-rate, and its estimation is improved by introducing GVSS-LMS algorithm [347] while estimating the correlation coefficient of AR1 process/fading parameter of the channel coefficient in the modified Kalman-filter [336], which is denoted as MKF-GVSS-LMS. The performance of this proposed combination is compared with the combination of FSS-LMS [268] and modified Kalman-filtering algorithm [336], which is indicated as MKF-FSS-LMS. The estimated channel tap-coefficients are then fed to the NVFF-RLS [346] algorithm based channel predictor, which predicts CSI in advance by providing better performance than the conventional FFF-RLS algorithm [326]. It is subsequently fed to the transmitter (through a feedback strategy), for adaptation to the channel conditions and, to change the modulation level for achieving the maximum throughput. Hence, in this research work, we focus on the AOFDM system using the MKF-GVSS-LMS algorithm for channel estimation and the NVFF-RLS algorithm for channel prediction to mitigate the adverse effects of time-varying wireless fading channels, for the adaptive bit-allocation.

This chapter is organised as follows. In Section 2.2, the details about the adaptive-OFDM based communication system working under the time-varying multipath channel conditions are given. Section 2.3 describes the MKF-GVSS-LMS algorithm based channel estimation scheme for the time-varying frequency-selective channels. The estimated channel-state-information is then fed to a long-range-predictor based on NVFF-RLS algorithm, which is described in Section 2.4 for predicting the channel-state-information, and then feeding this information back to the transmitter for invoking the adaptive bit-allocation algorithm. The performance of algorithms used for the channel estimation and prediction are validated and compared with conventional techniques with the aid of computer simulation in Section 2.5. Finally, summary of this chapter is provided in Section 2.6.

2.2 System Paradigm

An OFDM-based communication system for tracking the channel variations is considered, as shown in Fig. 2.1. The binary data is first mapped to the M-ary quadrature-amplitude-modulation (M-QAM) [347] to generate the symbol constellation points depending upon the adaptive binary data allocation based on the feedback received from the wireless receiver. The M-QAM modulated symbols are then mapped on to N subcarriers via inverse-fast-Fourier-transform (IFFT), which are concatenated to form a useful OFDM symbol of duration $T = NT_s$, where T_s is the M-QAM information symbol duration, which is also equal to the sampling interval.

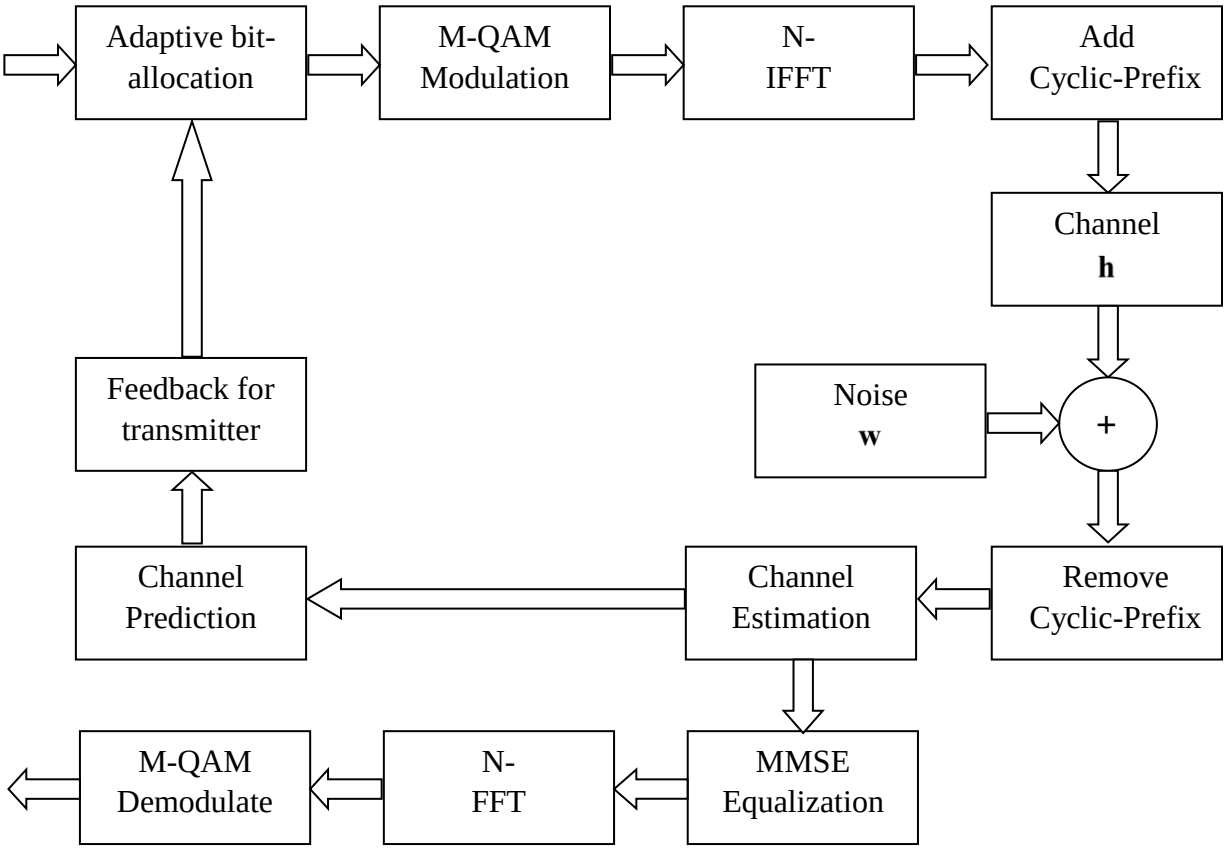

Fig. 2.1: Adaptive-OFDM system paradigm for wireless multipath fading environment using feedback and long-range prediction strategies.

In the time-domain, the OFDM information symbol of the p^{th} block at n^{th} instant is given as

$$x_n(p) = \frac{1}{\sqrt{N}} \sum_{k=0}^{N-1} X_k(p) e^{\frac{j2\pi kn}{N}} \qquad \text{(normalised)} \qquad (2.1)$$

for $n = 0,1,...N-1$, where $X_k(p)$ is the k^{th} M-QAM symbol of p^{th} block in the frequency-domain. The useful OFDM symbol-block is expressed as

$$\mathbf{x}(p) = \left[x_0(p), \quad x_1(p), \quad ..., \quad x_{N-1}(p) \right]^T_{N\times 1} \qquad (2.2)$$

where, $[.]^T$ and $[.]^H$ represent the simple transposition and Hermitian transposition of vector/matrix respectively. The CP of length *G* is constructed from the last *G* samples of the OFDM symbol-block, and it is appended in front of the OFDM symbol-block, which is transmitted as

$$\mathbf{x}_t(p) = \left[x_{N-G}(p), \quad ..., \quad x_{N-1}(p), \quad x_0(p), \quad ..., \quad x_{N-1}(p) \right]^T_{(N+G)\times 1} \qquad (2.3)$$

with a duration of $T_1 = (N+G)T_s$. The OFDM symbol-block with appended CP is transmitted over a Rayleigh distributed time-varying multipath channel of length *L* with independent and identically distributed (i.i.d.) tap-coefficients. The channel is assumed to be time-varying with the channel tap-coefficients that remain static for one CP-OFDM information symbol-block period. The channel tap-coefficient vector is denoted as

$$\mathbf{h}(p) = \left[h_0(p) \quad h_1(p) \quad ... \quad h_{L-1}(p) \right]^T_{L\times 1} \qquad (2.4)$$

where, $h_l(p)$ is the channel tap-coefficient for l^{th} tap encountered while the transmission of p^{th} block. Assuming the tapped-delay-line model for the multipath fading channel, the received signal is expressed as

$$y_n(p) = \sum_{l=0}^{L-1} h_l(p) x_{n-l}(p) + w_n(p) \qquad (2.5)$$

where, $w_n(p)$ is the additive-white-Gaussian-noise possessing zero-mean and σ_w^2 variance. Assuming the length of channel, $G \geq L-1$, the received symbol does not encounter any interference from the previously transmitted block. After the removal of CP, the same can be expressed in vector/matrix form as

$$\mathbf{y}(p) = \tilde{\mathbf{x}}(p)\mathbf{h}(p) + \mathbf{w}(p) \qquad (2.6)$$

or it can be simply represented in the form as

$$\begin{bmatrix} y_0(p) \\ y_1(p) \\ \vdots \\ y_{N-1}(p) \end{bmatrix}_{N\times 1} = \begin{bmatrix} x_0(p) & x_{N-1}(p) & \cdots & x_{N-L+1}(p) \\ x_1(p) & x_0(p) & \cdots & x_{N-L+2}(p) \\ \vdots & & \ddots & \vdots \\ x_{N-1}(p) & x_{N-2}(p) & \cdots & x_{N-L}(p) \end{bmatrix}_{N\times L} \begin{bmatrix} h_0(p) \\ h_1(p) \\ \vdots \\ h_{L-1}(p) \end{bmatrix}_{L\times 1} + \begin{bmatrix} w_0(p) \\ w_1(p) \\ \vdots \\ w_{N-1}(p) \end{bmatrix}_{N\times 1} \qquad (2.7)$$

The time-varying channel tap-coefficients are assumed to be governed by the first-order autoregressive (AR1) process, which is a tractable mathematical paradigm for the Rayleigh fading environment [348] i.e.,

$$h_l(p) = Ah_l(p-1) + v_l(p), \qquad l = 0,1,...,L-1 \tag{2.8}$$

which can be represented in the matrix form as

$$\mathbf{h}(p) = A\mathbf{h}(p-1) + \mathbf{v}(p) \tag{2.9}$$

where, $A = J_0(2\pi f_D T_1)$ is the correlation coefficient/fading parameter, $J_0(.)$ is the zeroth-order Bessel-function of first-kind, f_D is the maximum Doppler-shift, and $f_D T_1$ is the fade-rate. Here, $\mathbf{v}(p) = \left[v_0(p), \;\; v_1(p), \;\; \ldots, \;\; v_{L-1}(p)\right]_{L\times 1}^T$ is the process-noise, which is assumed to follow Gaussian-distribution with zero-mean and variance $\sigma_v^2 = \sigma_h^2\left(1-|A|^2\right)$ with $1 > |A| \geq 0$ [349].

The estimated and predicted channel-state-information, as discussed in the subsequent sections, is then fed to the linear block MMSE equalizer to obtain the transmitted OFDM information symbol-block. Here, the MMSE estimate of information symbol vector [350] is expressed as

$$\hat{\mathbf{x}}(p) = \bar{\mathbf{h}}^H(p)\left(\bar{\mathbf{h}}(p)\bar{\mathbf{h}}^H(p) + \sigma_w^2\mathbf{I}_N\right)^{-1}\mathbf{y}(p) \tag{2.10}$$

where, $\bar{\mathbf{h}}(p) = \begin{bmatrix} \hat{h}_0(p) & 0 & \cdots & 0 & \hat{h}_{L-1}(p) & \cdots & \hat{h}_1(p) \\ \hat{h}_1(p) & \hat{h}_0(p) & 0 & \cdots & 0 & \hat{h}_{L-1}(p)\cdots & \hat{h}_2(p) \\ \vdots & \vdots & \ddots & & & & \vdots \\ \hat{h}_{L-1}(p) & \cdots & \hat{h}_1(p) & \hat{h}_0(p) & 0 & \cdots & 0 \\ 0 & \hat{h}_{L-1}(p) & \cdots & \hat{h}_1(p) & \hat{h}_0(p) & 0\cdots & 0 \\ \vdots & & & & & \ddots & \\ 0 & \cdots & 0 & \hat{h}_{L-1}(p) & \cdots & \hat{h}_1(p) & \hat{h}_0(p) \end{bmatrix}_{N\times N}$

is the estimated channel matrix formed from the estimated channel coefficients $\hat{h}_l(p)$, and $\mathbf{I}_N$ is the identity-matrix with dimension $N \times N$. The equalized received symbol-block is then processed for *N*-point FFT to obtain the OFDM information symbol-block in the frequency-domain as $\hat{\mathbf{X}}(p) = \left[\hat{X}_0(p) \;\; \hat{X}_1(p) \;\; \ldots \;\; \hat{X}_{N-1}(p)\right]_{N\times 1}^T$. Subsequently, the M-QAM demodulation operation of the information symbols takes place to generate the decoded information symbols and bit stream.

The predicted CSI, fed back to the transmitter for adaptive modulation, is imperfect or noisy due to the channel estimation error and inherent delays [313], [351]. The actual / true channel fading gain is denoted as c, and the predicted channel gain is indicated as $\tilde{c}$. The bit-error-rate

(BER) constraint (under the imperfect predicted CSI $\tilde{c}$ with the transmitted power Ω scenario) can be obtained as [352],

$$BER_{\tilde{c}} = \int_0^{\infty} BER_{M(i)}\left(SNR_{M(i)}u^2\right) p_{c|\tilde{c}}\left(u\right) du \tag{2.11}$$

where, $BER_{M(i)}$ is the bit-error-rate for $M(i)$-QAM modulation, where $M(1)=0, M(i)=2^{i-1}$ for $i=2,...,6$, on the AWGN channel, and $p_{c|\tilde{c}}$ is the conditional probability density function of c for the given $\tilde{c}$, which is considered to be [352]

$$p\left(c\,|\,\tilde{c}\right) = \frac{2c}{(1-\rho)\Omega} I_0\left(\frac{2\sqrt{\rho}c\tilde{c}}{(1-\rho)\sqrt{\Omega\tilde{\Omega}}}\right)\exp\left(-\frac{1}{(1-\rho)}\left(\frac{c^2}{\Omega}+\rho\frac{\tilde{c}^2}{\tilde{\Omega}}\right)\right) \tag{2.12}$$

where, the parameter ρ is the correlation coefficient, which is obtained by using

$$\rho = \frac{Cov\left(c^2,\tilde{c}^2\right)}{\sqrt{Var(c^2)\times Var(\tilde{c}^2)}} \tag{2.13}$$

and $\Omega = E\left[c^2\right]$, $\tilde{\Omega} = E\left[\tilde{c}^2\right]$; and here $I_0(.)$ is the zeroth-order Bessel-function of first-kind. The thresholds for the imperfectly predicted CSI can be attained as in [352],

$$T(i) = \left\{\tilde{c}\,|\,BER_{\tilde{c}} = BER_T\right\} \tag{2.14}$$

where, BER_T is the target BER. The modulation level for the predicted CSI is considered as $M = M(i)$ if $T_{i+1} > \tilde{c} > T_i$. The selected modulation level is now utilized to modulate the next symbol-block to be transmitted over the multipath fading wireless channel.

2.3 Adaptive Channel Estimation Technique

The OFDM symbol-block consists of a preamble of training-symbols (TS), which are utilized for the channel estimation and tuning of estimator parameters. The data equalized is to be used thereafter. As the data can be uncertain and may cause error propagation, therefore the insertion of pilots is also necessary. The symbol-block structure considered for the above mentioned system paradigm, is shown below.

TS	TS	Data	...	Data	Pilot	Data	...	Data
0	1			...	...			N–1

Considering the state-space paradigm described in Eqs.(2.6) and (2.9), the correlation coefficient/fading parameter A and the channel state vector $\mathbf{h}(p)$ are estimated based on the

GVSS-LMS algorithm and the MKF algorithm respectively, as described by Han et al. [336]. The cost function is defined in terms of the mean-squared-error (MSE) as

$$J(p) = \frac{1}{2} E\left[\mathbf{e}^H(p)\mathbf{e}(p)\right] \tag{2.15}$$

where, $\mathbf{e}(p) = \mathbf{y}(p) - \tilde{\mathbf{x}}(p)\hat{\mathbf{h}}(p)$ with $\hat{\mathbf{h}}(p)$ denoted as the estimate of $\mathbf{h}(p)$, and $E[.]$ is the expectation/ensemble average operator. In order to estimate the correlation coefficient (fading parameter), we need to calculate the gradient of cost function with respect to A, which minimises the MSE. Upon differentiation of the cost function $J(p)$ with respect to A, the estimate of A [336] can be computed recursively as

$$\hat{A}(p) = \left[\hat{A}(p-1) + \mu \,\mathrm{Re}\left\{\mathbf{q}^H(p)\tilde{\mathbf{x}}^H(p)\mathbf{e}(p)\right\}\right]_{A-}^{A+} \tag{2.16}$$

where, $\mathbf{q}(p) = \dfrac{\partial \hat{\mathbf{h}}(p)}{\partial A}$, which can also be computed recursively as suggested in [336], μ is the fixed-step-size (FSS) parameter that controls the convergence characteristics, and $\hat{A}(p)$ is bounded with upper limit $A+$ and lower limit $A-$.

The nonstationarity/variable Doppler-spread of the time-varying channel that changes the fade-rate of the channel, necessitates the usage of variable-step-size (VSS). Under this scenario, the combination of GVSS-LMS algorithm and modified Kalman-filter also helps to improve the convergence-rate. The VSS algorithm tracks the changes in underlying system by varying the step-size as the MSE gets elevated or alleviated. The VSS has the capability to provide small misadjustment without compromising on the speed of tracking. Therefore, VSS criterion is introduced to adjust the step-size under the time-varying environment. Since the channel parameters are not known, the optimum value of step-size cannot be determined *a priori*. Therefore, the generalized-VSS algorithm (GVSS-LMS) has been proposed in [345] to update the step-size under nonstationary channel conditions, which is as follows

$$\mu(p) = \alpha_G \mu(p-1) + \gamma_G J_1(p-1) + \beta_G J_2(p) \tag{2.17}$$

where, $\mu_{Min} \le \mu(p) \le \mu_{Max}$ (bounded)

$$J_1(p) = \sum_{r=0}^{R} \lambda_1^r \mathbf{e}^H(p)\mathbf{e}(p-r) \qquad \text{with } 0 \le \lambda_1 < 1$$

$$J_2(p) = \left[\sum_{q=0}^{Q} \lambda_2^q \mathbf{e}^H(p-q)\tilde{\mathbf{x}}(p-q)\right]\tilde{\mathbf{x}}^H(p)\mathbf{e}(p) \qquad \text{with } 0 \le \lambda_2 < 1$$

where, the convergence parameters $0 < \alpha_G \leq 1$, $0 \leq \gamma_G < 1$, and $0 \leq \beta_G < 1$ control the behaviour of the adaptive algorithm to improve the convergence-rate. The recursive updating equation for the fading parameter (i.e., AR1 parameter) can now be rewritten as

$$\hat{A}(p) = \left[\hat{A}(p-1) + \mu(p)\,\mathrm{Re}\left\{ \mathbf{q}^H(p)\tilde{\mathbf{x}}^H(p)\mathbf{e}(p) \right\} \right]_{A-}^{A+} \tag{2.18}$$

The GVSS-LMS algorithm can track the dynamic channel variations more efficiently, resulting in the lower channel estimation error, which leads to low symbol error rate at the receiver. The modified Kalman-filter in combination with the GVSS-LMS (MKF-GVSS-LMS) is incorporated for the channel tracking, which can be summarized as follows

$$\mathbf{e}(p) = \mathbf{y}(p) - \tilde{\mathbf{x}}(p)\hat{\mathbf{h}}(p) \tag{2.19}$$

$$\mathbf{r}(p) = \tilde{\mathbf{x}}(p)\mathbf{P}(p)\tilde{\mathbf{x}}^H(p) + \sigma_w^2\mathbf{I}_N \tag{2.20}$$

$$\hat{A}(p) = \left[\hat{A}(p-1) + \mu(p)\,\mathrm{Re}\left\{ \mathbf{q}^H(p)\tilde{\mathbf{x}}^H(p)\mathbf{e}(p) \right\} \right]_{A-}^{A+} \tag{2.21}$$

$$\mathbf{K}(p) = \hat{A}(p)\mathbf{P}(p)\tilde{\mathbf{x}}^H(p)\mathbf{r}^{-1}(p) \tag{2.22}$$

$$\mathbf{C}(p) = \hat{A}(p)\mathbf{I}_L - \mathbf{K}(p)\tilde{\mathbf{x}}(p) \tag{2.23}$$

The above equation can also be approximated into a diagonal matrix, as given in [336].

$$\mathbf{M}(p) = \hat{A}^{-1}(p)\mathbf{K}(p) + \mathbf{C}(p)\mathbf{S}(p)\tilde{\mathbf{x}}^H(p)\mathbf{r}^{-1}(p) \tag{2.24}$$

$$\mathbf{q}(p+1) = \mathbf{C}(p)\mathbf{q}(p) + \hat{\mathbf{h}}(p) + \mathbf{M}(p)\mathbf{e}(p) \tag{2.25}$$

$$\mathbf{S}(p+1) = \mathbf{C}(p)\mathbf{S}(p)\mathbf{C}^H(p) - \frac{2\hat{A}(p)}{L}\mathbf{I}_L + 2\mathbf{C}(p)\mathbf{P}(p) \tag{2.26}$$

$$\hat{\mathbf{h}}(p+1) = \hat{A}(p)\hat{\mathbf{h}}(p) + \mathbf{K}(p)\mathbf{e}(p) \tag{2.27}$$

$$\mathbf{P}(p+1) = \hat{A}(p)\mathbf{C}(p)\mathbf{P}(p) + \mathbf{Q}_v(p+1) \tag{2.28}$$

where, $\mathbf{Q}_v(p+1) = \dfrac{1-\hat{A}^2(p)}{L}\mathbf{I}_L$ is the process-noise covariance-matrix obtained through the Yule-Walker equation, which is based on the assumption that there is equal power at each tap-coefficient of the channel, i.e., $\sigma_h^2 = 1/L$, $\mathbf{M}(p) = \dfrac{\partial \mathbf{K}(p)}{\partial A}$, $\mathbf{S}(p) = \dfrac{\partial \mathbf{P}(p)}{\partial A}$, $\mathbf{I}_L$ is the identity-matrix of dimension $L \times L$, and $\mathbf{P}(p) = E\left[\left(\mathbf{h}(p) - \hat{\mathbf{h}}(p) \right)\left(\mathbf{h}(p) - \hat{\mathbf{h}}(p) \right)^H \right]$ is the estimation error-covariance matrix, with $\mathbf{h}(p)$ and $\hat{\mathbf{h}}(p)$ exhibiting zero-mean.

2.4 Adaptive Channel Prediction

During the transmission of an OFDM symbol-block over a fast-fading time-varying channel, the estimated CSI cannot be fed back perfectly to the transmitter without delay. This results in the degraded performance of an AOFDM system. Therefore to exploit the potential of an AOFDM system, a highly reliable predicted CSI is required in advance at the transmitter [326], which is fed back from receiver to the transmitter for appropriate adaptive bit-allocation. The channel prediction by utilising the estimated channel state at the l^{th} tap and p^{th} block based on P_o previously observed samples for the L taps can be obtained by using

$$\tilde{h}_l(p) = \sum_{j=1}^{P_o} \sum_{l=0}^{L-1} d^*_{j,l}(p) \hat{h}_l(p-j) \tag{2.29}$$

The optimum prediction filter coefficients $d_{j,l}(p)$ that minimize the MSE $E\left[\left|h_l(p) - \tilde{h}_l(p)\right|^2\right]$ can be obtained by applying the orthogonality principle [326]. The optimum MMSE is computed by taking into account the previous channel tap-coefficients. But, this method is quite complex. However, it has been observed that if the signal-to-noise-ratio (SNR) of received signal is relatively high, then the prediction accuracy can be achieved while considering only the desired tap-coefficients and neglecting the adjacent tap-coefficients, since the channel tap-coefficients are independent to each other. Thus, the equation (2.29) is simplified to give

$$\tilde{h}_l(p) = \sum_{j=1}^{P_o} d^*_j(p) \hat{h}_l(p-j) \tag{2.30}$$

with $\mathbf{d}(p) = \left[d_1(p),\ \ d_2(p),\ \ \ldots,\ \ d_{P_o}(p)\right]^T_{P_o \times 1}$ as the filter tap-coefficients, which can be employed for each channel tap. The *a priori* knowledge of time- and frequency-domain correlation functions is required for the optimum MMSE channel prediction, which is usually unknown. The filter tap-coefficients are adaptively computed with the aid of adaptive algorithms, as these do not need the knowledge of correlation functions of channel. The adaptive algorithms update the filter tap-coefficients to reduce the error between the actual/true channel tap-coefficient and the predicted channel tap-coefficient, such that

$$\xi_l(p) = h_l(p) - \tilde{h}_l(p) = h_l(p) - \sum_{j=1}^{P_o} d^*_j(p) \hat{h}_l(p-j) \qquad (\textit{a posteriori} \text{ error}) \tag{2.31}$$

Here, the prediction error $\xi_l(p)$ is assumed to possess zero-mean and variance σ^2_ξ. The average mean squared error utilised for updating the filter tap-coefficients of the adaptive algorithms is expressed as

$$J_{\xi}(p) = \frac{1}{L}\sum_{l=0}^{L-1}\left|\xi_l(p)\right|^2 \tag{2.32}$$

Taking ensemble average on both sides of Eq.(2.32), we get $\tilde{J}_{\xi}^{+} = E\left[J_{\xi}(p)\right] = \sigma_{\xi}^2$. Here, the RLS algorithm is incorporated to obtain the predictor coefficients in order to minimise the following cost function [268], such that

$$J_{\xi,RLS}(p) = \sum_{i=1}^{p}\sum_{l=0}^{L-1}\lambda_{RLS}^{p-i}(p)\left|\xi_l(i)\right|^2 \tag{2.33}$$

where, $\lambda_{RLS}(p) \in (0,1]$ is the variable-forgetting-factor (VFF) [353]. When $\lambda_{RLS}(p) = \lambda_{RLS}$, the forgetting-factor is said to be the fixed-forgetting-factor (FFF) [268]. The predictor coefficient vector is updated using the following recursive equations subject to the condition that the true channel tap-coefficients are replaced by their estimated values $\hat{h}_l(p)$, while implementing the RLS algorithm [326].

$$\mathbf{K}_{RLS}(p) = \frac{\lambda_{RLS}^{-1}(p)\mathbf{P}_{RLS}(p-1)\tilde{\mathbf{h}}(p)}{\mathbf{I}_L + \lambda_{RLS}^{-1}(p)\tilde{\mathbf{h}}^H(p)\mathbf{P}_{RLS}(p-1)\tilde{\mathbf{h}}(p)} \tag{2.34}$$

$$\boldsymbol{\xi}_{RLS}(p) = \tilde{\mathbf{h}}_d(p) - \mathbf{d}_{RLS}^H(p-1)\tilde{\mathbf{h}}(p) \qquad (\textit{a priori} \text{ error}) \tag{2.35}$$

$$\mathbf{d}_{RLS}(p) = \mathbf{d}_{RLS}(p-1) + \mathbf{K}_{RLS}(p)\boldsymbol{\xi}_{RLS}^H(p) \tag{2.36}$$

$$\mathbf{P}_{RLS}(p) = \lambda_{RLS}^{-1}(p)\mathbf{P}_{RLS}(p-1) - \lambda_{RLS}^{-1}(p)\mathbf{K}_{RLS}(p)\tilde{\mathbf{h}}^H(p)\mathbf{P}_{RLS}(p-1) \tag{2.37}$$

where, $\mathbf{K}_{RLS}$ is the gain matrix, and $\mathbf{P}_{RLS}$ is the inverse correlation matrix. The convergence of the RLS algorithm is dependent upon the initial setting of this algorithm, which is performed as $\mathbf{d}_{RLS}(0) = \mathbf{0}_{P_o \times 1}$ (the filter tap-coefficient vector in case of RLS algorithm, which is assumed as the null vector in beginning) and $\mathbf{P}_{RLS}(0) = \left(\tilde{\mathbf{h}}(1)\tilde{\mathbf{h}}^H(1) + \delta\mathbf{I}_{P_o}\right)^{-1}$ with $\delta = 0.01$. Here, $\tilde{\mathbf{h}}_d(p)$ is the desired response, that is the estimated channel response vector at p^{th} block, which is given as $\tilde{\mathbf{h}}_d(p) = \left[\hat{h}_0(p),\ \hat{h}_1(p),\ \ldots,\ \hat{h}_{L-1}(p)\right]_{1\times L}$, and the corresponding estimated tap-coefficient matrix (input to predictor) $\tilde{\mathbf{h}}(p)$ is represented as

$$\tilde{\mathbf{h}}(p) = \begin{bmatrix} \hat{h}_0(p-1) & \hat{h}_1(p-1) & \ldots & \hat{h}_{L-1}(p-1) \\ \hat{h}_0(p-2) & \ddots & & \vdots \\ \vdots & & \ddots & \vdots \\ \hat{h}_0(p-P_o) & \ldots & \ldots & \hat{h}_{L-1}(p-P_o) \end{bmatrix}_{P_o \times L} \tag{2.38}$$

provided that the first P_o samples of all the channel tap-coefficients are available for computation. The convergence characteristics and tracking performance of the RLS algorithm can be improved

by implementing the numeric-variable-forgetting-factor (NVFF) [346]. The NVFF accounts for the nonstationarity of signal, as it is based on the extended estimation error criterion. The NVFF value adapts to the global trend quickly, by reducing the value $(\lambda_{RLS}(p) = \lambda_{NVFF}(p) \geq \lambda_{\min})$ in the case of nonstationary scenario and, by increasing the value $(\lambda_{RLS}(p) = \lambda_{NVFF}(p) \leq \lambda_{\max})$ under the stationary conditions. The speed of adaptation is dependent on the memory length given as $\tilde{N}(p) = \frac{1}{1-\lambda_{NVFF}(p)}$. The NVFF can be incorporated in the conventional RLS algorithm [354], and it is calculated based on the similar strategy as used in the extended estimation error criterion [355],

$$\tilde{J}_{\xi}^{-}(p) = \frac{1}{Z}\sum_{z=0}^{Z-1}\left[\xi_{RLS}(p-z)\xi_{RLS}^{H}(p-z)\right] \tag{2.39}$$

where, Z is kept smaller than the minimum memory length. It is assumed that the maximum variance of prediction error $\tilde{J}_{\xi}^{+} = \sigma_{\xi}^{2}$ is approximately equal to the variance of encountered AWGN, i.e.,

$$\sigma_{\xi}^{2} \approx \sigma_{w}^{2} \tag{2.40}$$

It follows that

$$\tilde{N}(p) = \frac{\sigma_{\xi}^{2}\tilde{N}_{\max}}{\tilde{J}_{\xi}^{-}(p)} \approx \frac{\sigma_{w}^{2}\tilde{N}_{\max}}{\tilde{J}_{\xi}^{-}(p)} \tag{2.41}$$

where, $\tilde{N}_{\max}$ is the maximum memory length corresponding to $\lambda_{\max}$. Hence, the NVFF is calculated as [345]

$$\lambda_{NVFF}(p) = \left[1 - \frac{1}{\tilde{N}(p)}\right]_{\lambda_{\min}}^{\lambda_{\max}} \tag{2.42}$$

where, $\lambda_{NVFF}(p)$ is bounded as $\lambda_{\max} \geq \lambda_{NVFF}(p) \geq \lambda_{\min}$. The RLS algorithm for LRP utilises the NVFF obtained from Eq.(2.42) in place of $\lambda_{RLS}(p)$ to update the predictor coefficients recursively at each iteration, as depicted in Eqs.(2.34) to (2.37). The predicted channel-state-information is then fed back to the wireless transmitter for the adaptive modulation to achieve higher throughput and also for the mitigation of channel fading as well as noise.

2.5 Simulation Results

The performance characteristics of presented channel estimation and prediction algorithms are investigated corresponding to the system paradigm given in Section 2.2, with the help of computer simulation. The adaptive channel estimator and the long-range-predictor are utilised to enhance the prediction accuracy for the improved performance of adaptive modulation based OFDM systems. In order to conduct the simulation, the number of subcarriers for the underlying AOFDM system is considered to be $N = 64$, with cyclic-prefix symbols as $G = 16$. The length of channel impulse response is fixed at $L = 6$. The nonstationary environment is generated by assuming the time-varying channel following Rayleigh distribution, which is simulated by using AR1 process as in Eq.(2.9). The transmitted power is kept same for all the underlying subcarriers. The presented outcomes are based on the ensemble average of 1000 independent Monte-Carlo simulation trials using different channel fading realisations at the various values of SNR.

The convergence characteristics and tracking capability of MKF-GVSS-LMS are explored for the OFDM wireless systems under the time-varying channel conditions. The channel is assumed to have dynamic characteristics with the variable fade-rate $f_D T_1$ that changes between 0.0001 and 0.1 at the constant intervals after the transmission of 100 blocks, as depicted in Fig. 2.2. The performance of channel estimation algorithms is compared on the basis of mean squared channel estimation error. The channel tap-coefficients are estimated using the MKF-GVSS-LMS algorithm, in which the initial values of the parameters used in the algorithm are as follows: $\hat{\mathbf{h}}(0) = \mathbf{0}_{L\times 1}$, $\mathbf{P}(0) = 100\mathbf{I}_L$, $\mathbf{S}(0) = \mathbf{0}_{L\times L}$, $\mathbf{q}(0) = \mathbf{0}_{L\times 1}$, and $\hat{A}(0) = 1$. The fixed-step-size (FSS) is kept $\mu = 5\times 10^{-5}$, and the limits for fading parameter are chosen to be $A- = 0.98$ and $A+ = 1$ (as in [336]). However, the parameters for MKF-GVSS-LMS algorithm for controlling the behaviour of convergence-mode characteristics are chosen as follows: $\alpha_G = 1$, $\gamma_G = 2.5\times 10^{-5}$, $\beta_G = 5\times 10^{-15}$, $R = 3$, $Q = 3$, $\lambda_1 = 0.98$ and $\lambda_2 = 0.95$. Here, the initial value of step-size is considered to be same as mentioned above, i.e., μ (at the starting point of GVSS updating). However, μ_{Min} is kept 5×10^{-6}, and μ_{Max} is set based on the eigenvalue criterion given in [356].

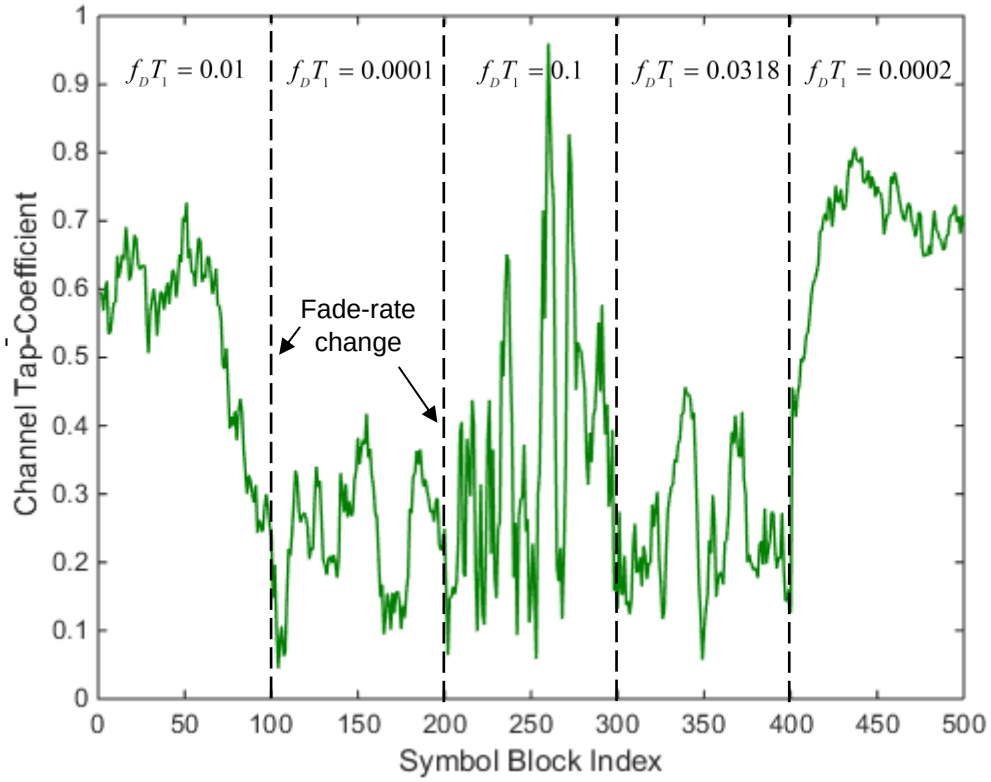

Fig. 2.2: Time-variations of the fading channel tap-coefficient (a typical sample).

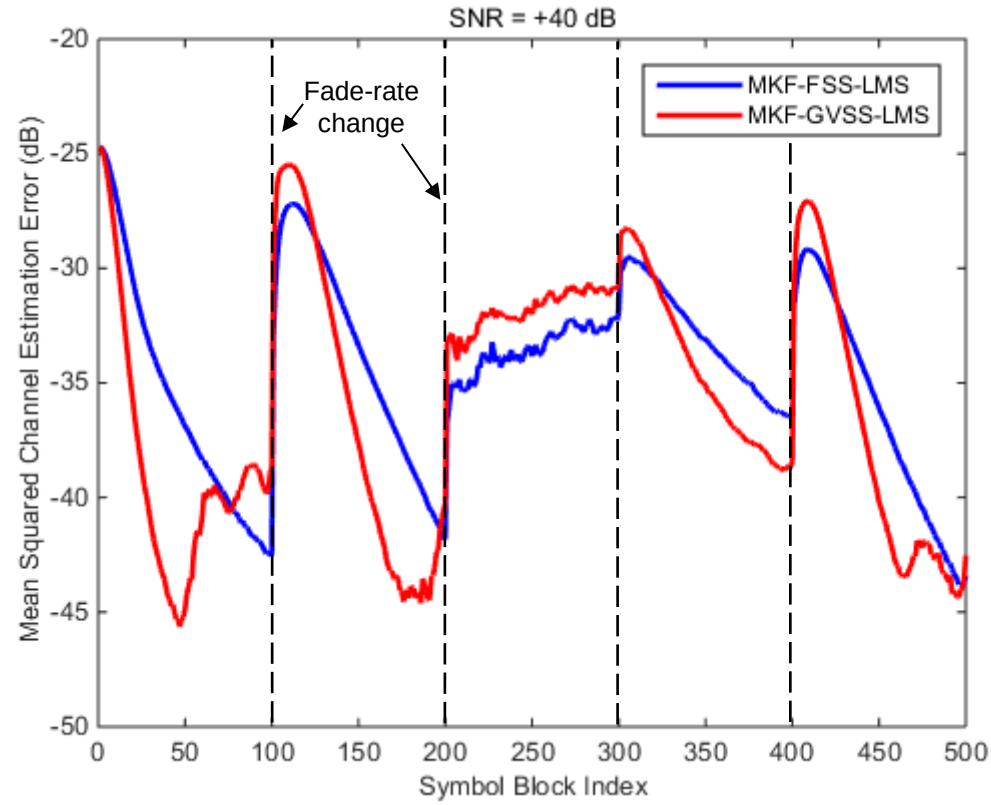

Fig. 2.3: Fading channel tap-coefficient tracking performance in terms of mean squared estimation error.

The mean squared channel estimation error for a single fading channel tap-coefficient is shown in Fig. 2.3 at +40dB, which illustrates that the MKF-GVSS-LMS algorithm performs better than the MKF-FSS-LMS algorithm for the variable fade-rate channel conditions, in the convergence-mode as well as tracking-mode [336], [345]. The MKF-GVSS-LMS algorithm tracks the channel variations more efficiently, and it converges more swiftly than the MKF-FSS-LMS algorithm. The MKF-GVSS-LMS algorithm is quite sensitive to the parameter setting and initialization conditions, which depends on the nature of frequency-selective time-varying wireless fading channel characteristics. Here, the multipath channel fade-rate $f_D T_1$ is abruptly varied after every 100 OFDM symbol-block period in simulation, as demonstrated in Fig. 2.2. It is quite evident from the results presented in Fig. 2.3 that the MKF-GVSS-LMS algorithm provides improvement in terms of the lower mean squared channel estimation error, as compared to the MKF-FSS-LMS algorithm, while working under similar conditions at the different values of fade-rate. However, it is observed that the performance of MKF-GVSS-LMS algorithm based channel estimator gets deteriorated, when the fade-rate $f_D T_1$ is abruptly increased from 0.0001 to 0.1 at the 201th OFDM symbol-block (i.e., a large sudden increase in the fade-rate), as shown in Fig. 2.2. Here, the MKF-GVSS-LMS algorithm fails to perform well due to its sensitivity regarding the initial parameter setting, while responding to a large abrupt change in the values of channel tap-coefficients. However, it outperforms the MKF-FSS-LMS algorithm based approach, when the fade-rate changes smoothly. The MKF-GVSS-LMS algorithm not only provides the higher convergence-rate, but also accounts for the lower tracking-error under the time-varying environment.

The estimated channel tap-coefficients are then fed to the long-range-predictor at receiver, which predicts the fading channel impulse response tap-coefficients at the next symbol-block in advance, which is fed back to the transmitter to adjust the modulation parameters to enhance the throughput of the underlying AOFDM system. The order of prediction filter is chosen to be $P_o = 20$. The average MSE, as mentioned in Eq.(2.32), is considered as the performance metric for the comparison of different algorithms for the prediction accuracy, as illustrated in subsequent figures. It is clear from Fig. 2.4 that the NVFF-RLS algorithm with parameters $Z = 3$, $\lambda_{\max} = 0.1$ and $\lambda_{\min} = 0.05$ supersedes the FFF-RLS algorithm with the forgetting-factor $\lambda = 0.1$ in terms of the prediction accuracy. The predicted channel tap-coefficients are then fed back to the transmitter to adaptively modulate the information symbol stream for the next OFDM symbol-block.

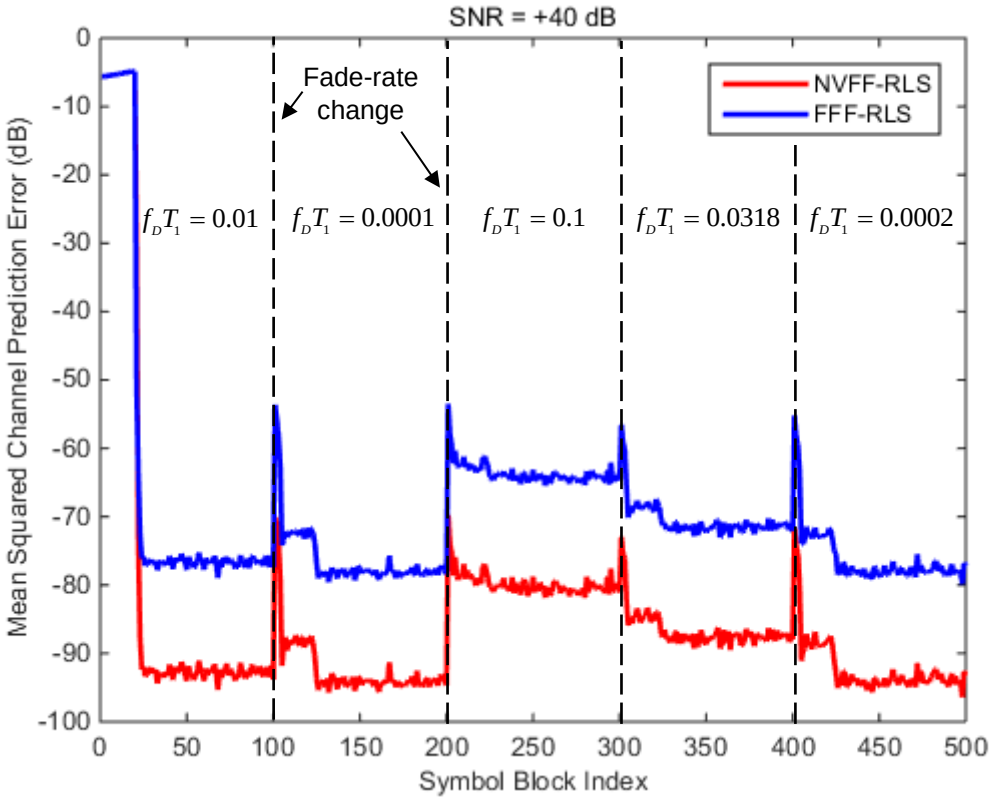

Fig. 2.4: Average mean squared prediction error for the different prediction algorithms at varying fade-rate.

The symbol-error-rate (SER) for the different fade-rate values ($f_DT_1 = 0.01$ and $f_DT_1 = 0.1$) are compared and depicted in Fig. 2.5 and Fig. 2.6 respectively. It can be inferred from the simulation results that the proposed combination of MKF-GVSS-LMS estimation algorithm and the NVFF-RLS prediction algorithm leads to the lower SER in comparison to that of the combination of MKF-FSS-LMS and FFF-RLS algorithm, and the SER performance difference is observed to be more profound at the higher SNR values. It is apparent from the results shown in Fig. 2.5 at $f_DT_1 = 0.01$ that the proposed combination provides approximately +1.5dB performance advantage in terms of the SNR at $SER = 10^{-4}$, which tends to increase with the increasing value of SNR. However from Fig. 2.6, it is also clear that this performance advantage in terms of the SNR increases to about +17dB for the presented combination of the MKF-GVSS-LMS algorithm based channel estimator and the NVFF-RLS algorithm based channel predictor at the $SER = 2\times10^{-4}$ and $f_DT_1 = 0.1$; and its performance advantage over the combination of MKF-FSS-LMS algorithm (channel estimation) and FFF-RLS algorithm (channel prediction) increases substantially at the higher SNR values. Here, the substantial benefit of NVFF-RLS algorithm implementation is noteworthy under the fast-fading scenario for the underlying AOFDM system.

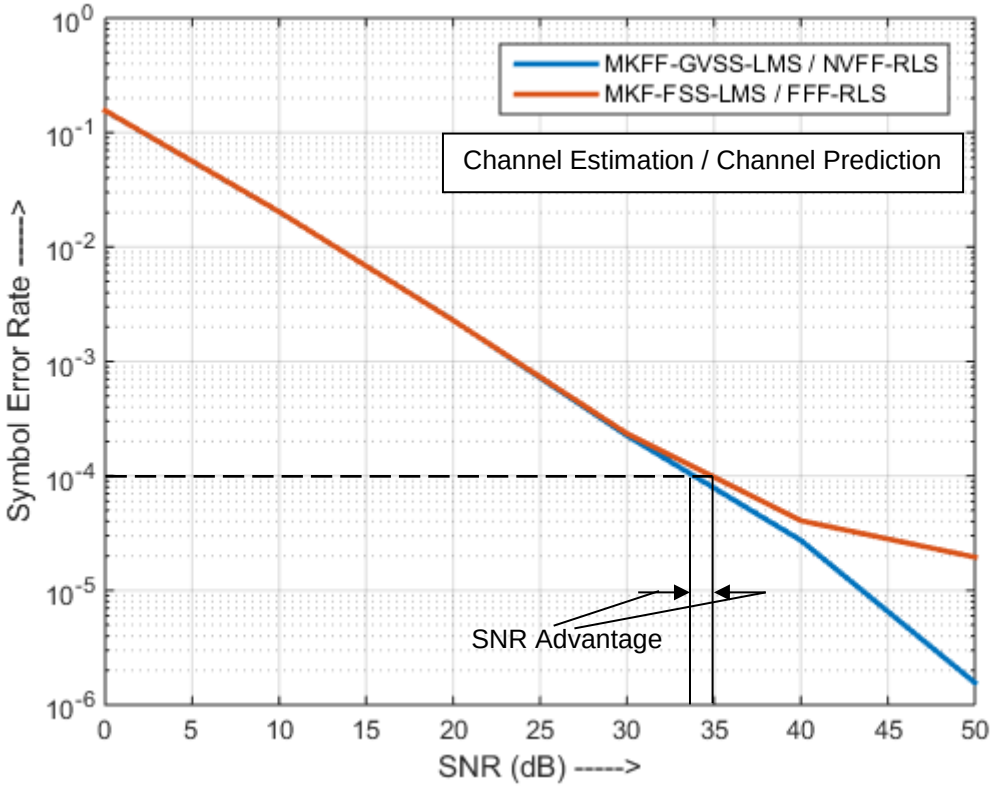

Fig. 2.5: Symbol error rate performance comparison at the fade-rate $f_D T_1 = 0.01$.

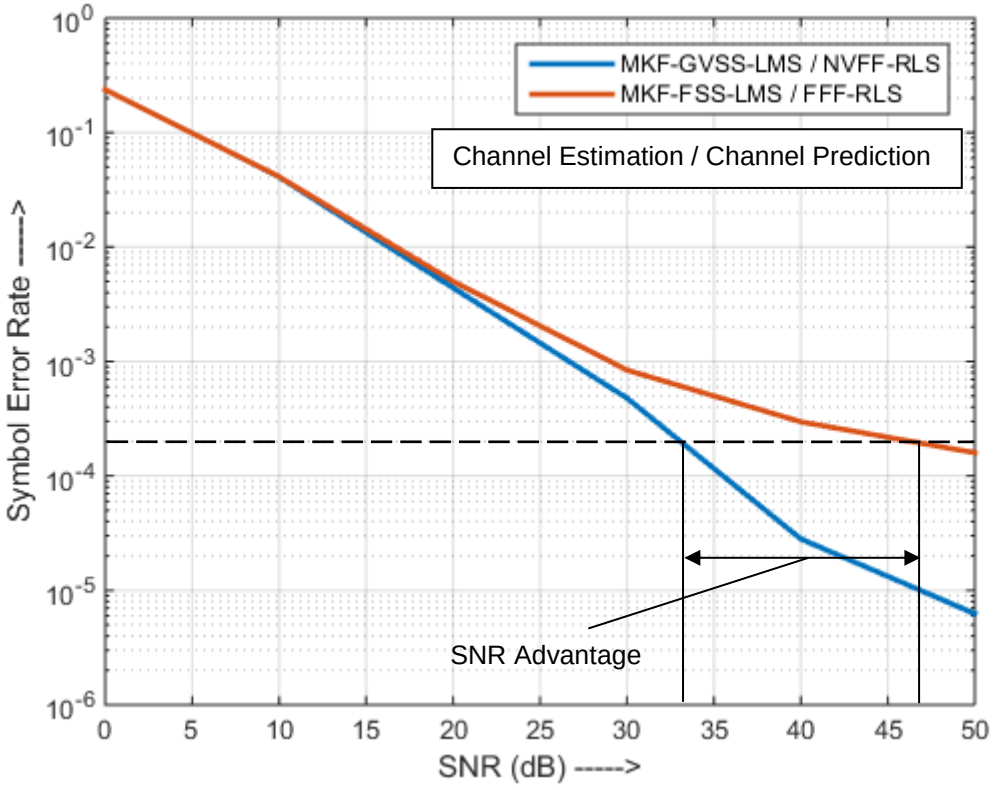

Fig. 2.6: Symbol error rate performance comparison at the fade-rate $f_D T_1 = 0.1$.

2.6 Summary of Chapter

A channel estimation and long-range prediction based technique for the AOFDM system has been investigated, while working under the time-varying multipath environment. The “combination of GVSS-LMS and MKF algorithms for robust channel estimation” and the “NVFF-RLS algorithm for efficient channel prediction” has been utilized. The efficient channel loading has been accomplished by feeding the accurately predicted CSI back to the wireless transmitter (i.e., for the adaptive bit-allocation algorithms). We have replaced MKF-FSS-LMS algorithm with the MKF-GVSS-LMS algorithm to enhance the performance of adaptive channel estimator, and we have also replaced FFF-RLS algorithm with the NVFF-RLS algorithm to obtain improved performance of the long-range predictor, under the time-varying multipath fading channel. Eventually, these two major changes result in the appropriate adaptive bit-allocation, which in turn boosts the overall performance of the underlying AOFDM system in terms of symbol-detection success-rate at the wireless receiver.

The future work includes extension of presented research work to the STBC-AOFDM based wireless communication systems [326]. Moreover, the reduced Kalman/LMS algorithm may also be incorporated to reduce the computational complexity of the channel estimator. However, the performance evaluation of STBC/SFBC-AOFDM communication systems working over the wireless channels under the impulsive environment needs to be investigated further.

CHAPTER 3

ADAPTIVE FILTERING TECHNIQUES USING CYCLIC-PREFIX IN STBC-OFDM SYSTEMS FOR MULTIPATH FADING CHANNEL PREDICTION

3.1 Introduction

To fulfill the ever-increasing demand for high data-rate transmission under wireless fading environment, the interest has peaked in orthogonal frequency division multiplexing (OFDM) systems [357]. This technology exploits the frequency-selective channels by partitioning the available channel bandwidth into subchannels in frequency domain, which eventually results in flat fading subchannels for wireless transmission [6], [7]. In time domain, the high data-rate symbol stream is partitioned into low data-rate symbol streams, which are used to modulate carriers of aforementioned subchannels, respectively. It facilitates the channel estimation as well as equalization schemes for varying symbol transmission rates of subchannels [6], [358]–[367]. However, longer symbol duration exhibits innate immunity to impulse-noise [34], [323] and channel nonstationarities arising due to the fast-fading, which in turn enhances channel capacity usage by improving the signal-to-noise ratio (SNR).

The knowledge of channel-state-information (CSI) is the backbone of multicarrier communication (MCM) as well as OFDM systems. For time-invariant channels, an initial training symbol sequence is used to estimate the channel tap-coefficients [34]. However, for time-variant channels, a training symbol sequence is transmitted periodically to train the channel estimator [368], at the cost of increased overhead of OFDM systems. The convergence and training-mode characteristics of adaptive channel estimator play an important role in the determination of CSI, using a training symbol sequence [268], [369], [370]. The cyclic-prefix (CP) is an inevitable part of OFDM systems, which is incorporated in the underlying system to combat intersymbol-interference (ISI), by keeping the length of CP more than the number of multipaths in wireless fading channels [371], [372]. Though CP is usually discarded at the receiver prior to main OFDM signal processing and detection, it can also be viewed as a training symbol sequence for adaptive channel estimation [373]. This innovative technique precludes the requirement of training symbols, which in turn alleviates the overhead data transmission [374].

In order to eliminate the need for pilot symbols [375] to track channel variations, we can utilize the repeated part of transmitted data, i.e., CP for the adaptive CSI-estimation, which is aided by output symbols obtained in the decision-directed-mode [374]. The decision error and channel

estimation error affect each other, because the closed feedback loop constituted by OFDM symbol-detection, channel estimation and equalization controls the average output symbol error rate (SER), which significantly influences the tracking performance of adaptive channel estimator [373]. In this chapter, the main goal is to develop adaptive channel prediction techniques using CP in wireless OFDM systems working under static and dynamic environment (as shown in Fig. 3.1), which is motivated by the research work presented by Wang and Liu [373], [374] using recursive least squares (RLS) algorithm. Under static environment, we propose the Kalman filtering algorithm-based channel estimator [376], [377], which is also known as a best linear unbiased estimator (BLUE). Moreover, RLS algorithm is reported to be a special case of KF under typical parameter setting [377], and KF produces relatively lower misadjustment [268]. However, the computational complexity and the need of knowledge about system paradigm often avert KF schemes. Therefore, to avoid the online Riccati updating in ordinary Kalman adaptation laws [378], Kohli *et al*. have proposed the reduced Kalman least mean squares (RK-LMS) algorithm for improved convergence and tracking performance relative to conventional LMS algorithm [379], [380]. It does not require any prior information about time-variations of a true system, and it also reduces lag misadjustment and gradient misadjustment [369]. The computational complexity of RK-LMS algorithm is substantially lower than that of KF and RLS algorithms. But in this case, the tracking performance of adaptive channel estimator is compromised to reduce the computational burden.

Under fast-fading mobile environment, we present the Kalman-filtering and numeric variable forgetting factor RLS (NVFF-RLS) algorithm-based channel estimation/prediction techniques using CP. The unknown channel tap-coefficients are often considered to follow the first-order autoregressive AR(1) process for the tracking performance analysis of adaptive algorithms [269], [370], [379], [381]. The analytical analysis as well as simulation results presented in [348] connotes that first-order Markov channel provides a mathematically tractable paradigm for the time-variant Rayleigh fading channels [335], [382]. However, under this nonstationary environment, the value of NVFF decreases automatically to estimate the channel rapidly using the extended estimation error criterion [267], [383]. But under stationary environment, the value of NVFF increases by increasing the memory for accurate channel estimation [267], [346], [353], [354], [383]. The NVFF-RLS algorithm undoubtedly outperforms VFF-RLS and conventional RLS algorithm by yielding minimum mean square error (MMSE) in CSI-estimation, in the field of linear and nonlinear filtering [346]. However, the tracking performance of LMS algorithm-based channel estimators severely suffer due to the lag noise and gradient noise under time-varying

channels [268], [369], [370]. Therefore, in this chapter, we focus on the NVFF-RLS and KF algorithms for CP-based channel prediction to track the fast time-varying wireless fading channels.

This chapter is organized as follows. In Section 3.2, we first give details about a wireless OFDM communication system model working under the time-invariant and time-variant multipath fading channels, which comprises of the channel prediction and equalization procedures at receiver (as shown in Fig. 3.1). The multipath fading channels are modeled as the tapped-delay-line filter with time-variant Rayleigh-distributed tap-coefficients. We next describe the Kalman-filtering and RK-LMS algorithm-based channel predictors using the cyclic-prefix of OFDM signals, in Section 3.3. Subsequently, this section also includes details of conventional RLS and NVFF-RLS algorithms for the multipath fading channel estimation. The presented channel estimation/prediction algorithms are incorporated in 2×1 STBC-OFDM system for the symbol error rate (SER) performance analysis in Section 3.4. However, in Section 3.5, simulation results are presented to compare the channel tracking performances of KF, RK-LMS, RLS and NVFF-RLS adaptive algorithms under static and dynamic environment, which are appraised on the basis of MMSE criterion. Finally, summary of the chapter is provided in Section 3.6.

3.2 Basic Wireless OFDM System Model

Let us consider an OFDM wireless communication system, which is a block-oriented modulation scheme. The processed data bit stream is first buffered to blocks. Each block of data is then divided into $N/2$ parallel bit streams, and subsequently mapped to the complex M-ary QAM constellation points $X_{n,k}$ using a QAM modulator (as shown in Fig. 3.1) for the k^{th} OFDM symbol-block, such that $n = 0,\ 1,\ .....,\ (N/2)-1$.

$$\vec{\mathbf{X}}_{\mathbf{k}} = \Big[\underbrace{X_{0,k}\ .....\ X_{(N/2)-1,k}}\ \underbrace{X_{N/2,k}\ .....\ X_{N-1,k}} \Big]^{T}_{N\times 1} \tag{3.1}$$

To generate a real OFDM signal $x_{n,k}$ in time-domain by using IFFT operation, last $N/2$ samples are just the conjugates of first $N/2$ samples in the k^{th} OFDM symbol-block in frequency-domain (3.1). It follows that

$$\vec{\mathbf{x}}_{\mathbf{k}} = \Big[x_{0,k}\ x_{1,k}\ .....\ x_{p,k}\ .....\ x_{N-1,k} \Big]^{T}_{N\times 1} \tag{3.2}$$

where, $x_{p,k} = \dfrac{1}{\sqrt{N}} \sum_{n=0}^{N-1} X_{n,k} \exp\left(j \dfrac{2\pi pn}{N} \right)$ for $p = 0,\ 1,\ .....,\ N-1$, $[.]^{T}$ and $[.]^{H}$ represent the matrix transposition operator and Hermitian transposition operator respectively, and N is the number of subcarriers in OFDM signal.

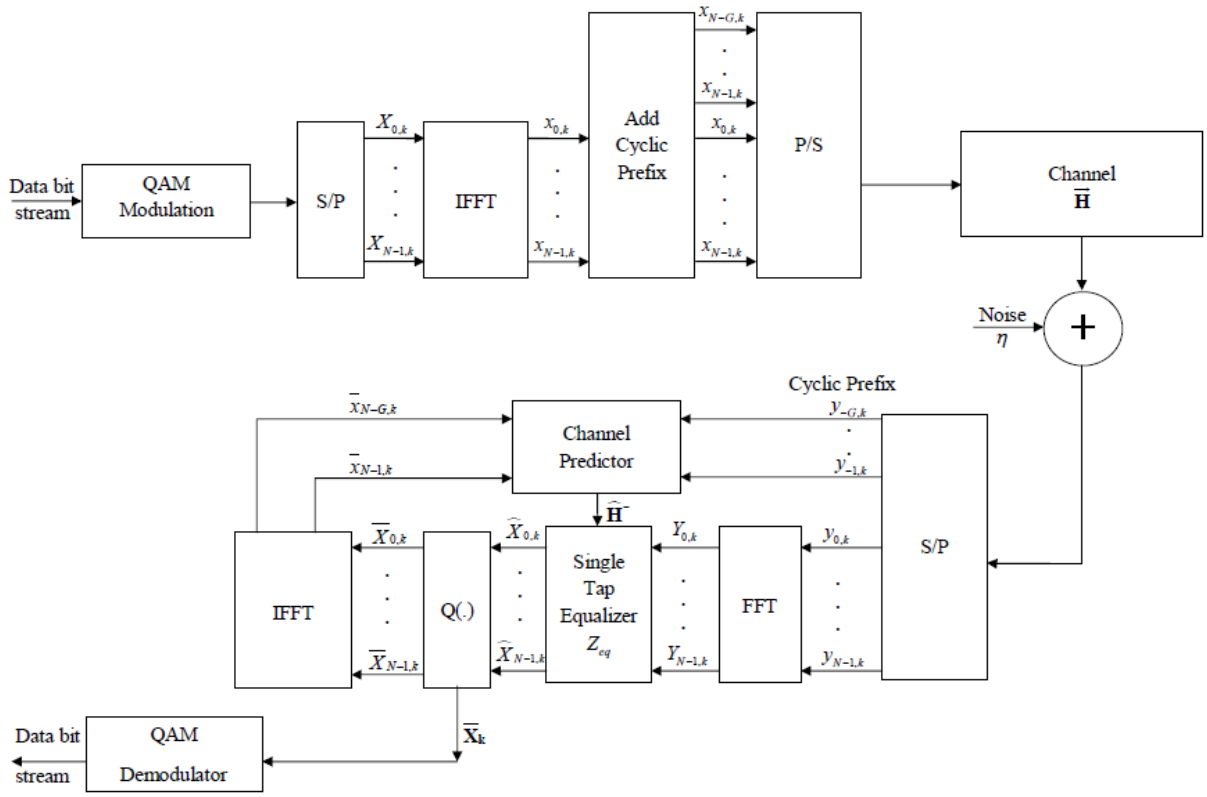

Fig. 3.1: CP-OFDM system paradigm for wireless multipath fading environment using channel prediction strategy.

The wireless multipath fading channel is modelled as a tapped-delay-line filter [331], in which the impulse response is expressed in terms of the following time-domain $L\times 1$ dimensional tap-coefficient vector as

$$\vec{\mathbf{h}}_{\mathbf{k}} = \left[h_{0,k} \; h_{1,k} \; ..... \; h_{l,k} \; ..... \; h_{L-1,k} \right]^{T}_{L\times 1} \tag{3.3}$$

where, $h_{l,k}$ is the l^{th} channel tap-coefficient during the k^{th} OFDM symbol-block. To circumvent problems arising due to the intersymbol-interference and interblock interference, cyclic-prefix of length $G \geq L-1$ is appended in the beginning of OFDM symbol-block, which is transmitted as

$$\vec{\mathbf{x}}_{\mathbf{co,k}} = \left[\vec{\mathbf{x}}^{\mathbf{T}}_{\mathbf{cp,k}} \;\; \vec{\mathbf{x}}^{\mathbf{T}}_{\mathbf{k}} \right]^{T}_{(N+G)\times 1} \tag{3.4}$$

where, $G\times 1$ dimensional cyclic-prefix vector is given as

$$\vec{\mathbf{x}}_{\mathbf{cp,k}} = \left[x_{N-G,k} \; ..... \; x_{N-g,k} \; ..... \; x_{N-1,k} \right]^{T}_{G\times 1} \tag{3.5}$$

in which, $x_{-t,k} = x_{N-t,k}$.

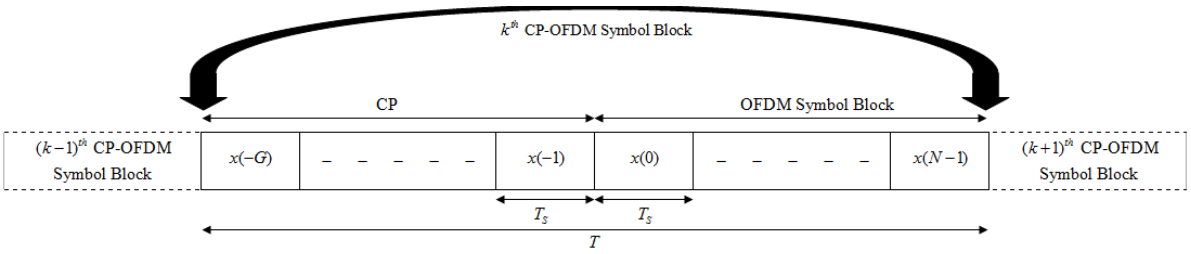

Fig. 3.2: CP-OFDM symbol-blocks for wireless transmission under static environment.

Invoking the linear convolution property for underlying multipath fading transmission channel, it can be shown that the received signal is $y_{p,k} = x_{p,k} * h_{p,k} + \eta_{p,k}$ (with convolution operator $*$). It results in

$$\vec{\mathbf{y}}_{\mathbf{co,k}} = \left[\vec{\mathbf{y}}_{\mathbf{cp,k}}^{\mathbf{T}} \;\; \vec{\mathbf{y}}_{\mathbf{k}}^{\mathbf{T}}\right]^{T}_{(N+G)\times 1} \tag{3.6}$$

where, $\vec{\mathbf{y}}_{\mathbf{cp,k}} = \left[y_{-G,k} \;\; ..... \;\; y_{-g,k} \;\; ..... \;\; y_{-1,k}\right]^{T}_{G\times 1}$ (3.7)

and $\vec{\mathbf{y}}_{\mathbf{k}} = \left[y_{0,k} \;\; y_{1,k} \;\; ..... \;\; y_{p,k} \;\; ..... \;\; y_{N-1,k}\right]^{T}_{N\times 1}$ (3.8)

At OFDM receiver, FFT operation is performed to obtain the frequency-domain signal as

$$\vec{\mathbf{Y}}_{\mathbf{k}} = \left[Y_{0,k} \;\; ..... \;\; Y_{(N/2)-1,k} \;\; Y_{N/2,k} \;\; ..... \;\; Y_{N-1,k}\right]^{T}_{N\times 1} \tag{3.9}$$

where, $Y_{n,k} = \frac{1}{\sqrt{N}} \sum_{p=0}^{N-1} y_{p,k} \exp\left(-j\frac{2\pi pn}{N}\right)$ for $n = 0,\ 1,\ ..... ,\ N-1$.

In the presented research work, the length of CP is kept $G \geq L-1$ for channel estimation of time-invariant (static) channels (as shown in Fig. 3.2). In the present scenario,

$$y_{p,k} = \begin{cases} \sum_{l=0}^{L-1} h_l x_{p-l,k} + \eta_{p,k} & for\ p = -(G-L)-1,\ ..... ,-1,0,1,\ ..... ,N-1 \\ \sum_{l=0}^{G+p} h_l x_{p-l,k} + \sum_{l=G+p+1}^{L-1} h_l x_{N-l,k-1} + \eta_{p,k} & for\ p = -G,-G+1,\ ..... ,-(G-L)-2 \end{cases} \tag{3.10}$$

in which, the channel coefficients ..... $h_{l,k-1} = h_{l,k} = h_{l,k+1} ..... = h_l$ remain unchanged with time. Here, the uncorrelated complex additive-white-Gaussian-noise (AWGN) component $\eta_{p,k}$ is assumed to possess zero-mean and σ_η^2 variance [384].

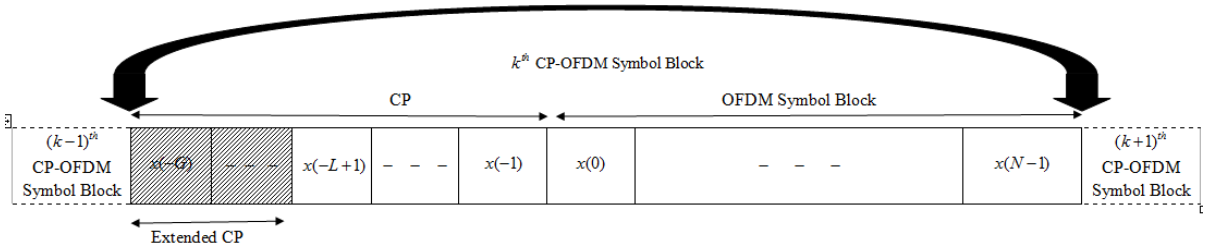

Fig. 3.3: CP-OFDM symbol-blocks for wireless transmission under dynamic environment.

However, the length of CP is kept $G = 2L-2$ for channel estimation of time-variant (dynamic) channels (as shown in Fig. 3.3). It leads to

$$y_{p,k} = \left[\sum_{l=0}^{L-1} h_{l,k} x_{p-l,k} + \eta_{p,k} \qquad for\ p = -L+1,\ \ldots..\ , -1, 0, 1,\ \ldots..\ N-1 \right. \tag{3.11}$$

It is noteworthy that if $G \geq 2L-2$ is kept in dynamic environment, then the useful sample points are $p = -(G-L+1),\ \ldots..\ , -1, 0, 1,\ \ldots..\ N-1$ in Eq.(3.11). The extended length of CP helps the adaptive channel estimator/predictor to track time-varying channels in OFDM systems, when it is assumed that the channel coefficients change after each CP-OFDM symbol-block i.e., after duration $T = (N+G)T_s$ with sampling interval T_s. The l^{th} channel tap-coefficient (complex) is time-varying as per an AR(1) process [348], [379], i.e.,

$$h_{l,k} = \alpha_l h_{l,k-1} + w_{l,k} \tag{3.12}$$

where, $\alpha = \alpha_l$ is an AR(1) state transition coefficient/Markovian parameter in Eq.(3.12), $w_{l,k}$ is the zero-mean complex process-noise with variance σ_w^2 for all values of l, and therefore $h_{l,k}$ is considered to be zero-mean and unit variance complex Gaussian process [125], [385]. The simplification of Eq.(3.12) leads to $\sigma_w^2 = 1 - |\alpha|^2$ and $\alpha = \alpha_l = E\{h_{l,k} h_{l,k-1}^*\} = J_0\{2\pi f_D T\}$, in which f_D is the maximum Doppler-spread/shift, $f_D T$ is the fade-rate [335], and $J_0(.)$ is the Bessel-function of zeroth-order and first-kind. However under this multipath fading situation, $\bar{\mathbf{y}}_\mathbf{k}$ is not affected by ISI due to the presence of cyclic-prefix. From n^{th} independent subchannel, it is clear that

$$Y_{n,k} = X_{n,k} H_{n,k} + N_{n,k} \tag{3.13}$$

where, channel frequency response of the n^{th} independent subchannel is $H_{n,k} = \frac{1}{\sqrt{N}} \sum_{l=0}^{L-1} h_{l,k} \exp\left(-j \frac{2\pi l n}{N}\right)$, and $N_{n,k} = \frac{1}{\sqrt{N}} \sum_{p=0}^{N-1} \eta_{p,k} \exp\left(-j \frac{2\pi p n}{N}\right)$ is the complex additive-white-Gaussian-noise with zero-mean and variance σ_η^2 [323] for $n = 0,\ 1,\ \ldots..\ ,\ N-1$. For n^{th}

subchannel, one-tap equalizer with frequency response $Zeq_{n,k} = \left(1/H_{n,k}\right)$ is used to obtain coarse estimate of a transmitted symbol as

$$\hat{X}_{n,k} = Y_{n,k} \times Zeq_{n,k} \tag{3.14}$$

Using this coarse estimated symbol (as shown in Fig. 3.1), the final decision $\bar{X}_{n,k}$ is made using an appropriate quantization function $Q(.)$. The estimated OFDM symbol-block $\bar{\mathbf{X}}_{\mathbf{k}} = \left[\underline{\bar{X}_{0,k} \ \ldots\ldots \ \bar{X}_{(N/2)-1,k}} \ \ \underline{\bar{X}_{N/2,k} \ \ldots\ldots \ \bar{X}_{N-1,k}}\right]^T_{N\times 1}$ is further processed using a QAM demodulator to generate the data bit stream. Now at this stage, well-estimated cyclic-prefix vector $\bar{\mathbf{X}}_{\mathbf{CP,k}} = \left[\bar{X}_{N-G,k} \ \ldots\ldots \ \bar{X}_{N-g,k} \ \ldots\ldots \ \bar{X}_{N-1,k}\right]^T_{G\times 1}$ is fed back to the channel predictor module for next iteration.

3.2.1 Basic System Equations Under Time-Invariant Multipath Fading Channels

In OFDM systems, $\vec{\mathbf{y}}_{\mathbf{cp,k}}$ is conventionally discarded at the wireless receiver. The pioneering work of Wang and Liu in [373], [374] manifests that if all the prefix parts are concatenated together as a pair of sequences $\vec{\mathbf{x}}_{\mathbf{cpc}} = \left[\ldots\ldots \ x_{-G,k-1} \ \ldots\ldots \ x_{-1,k-1} \ x_{-G,k} \ \ldots\ldots \ x_{-1,k} \ \ldots\ldots\right]$ and $\vec{\mathbf{Y}}_{\mathbf{cpc}} = \left[\ldots\ldots \ y_{-G,k-1} \ \ldots\ldots \ y_{-1,k-1} \ y_{-G,k} \ \ldots\ldots \ y_{-1,k} \ \ldots\ldots\right]$, then the concatenated received cyclic-prefix vector $\vec{\mathbf{Y}}_{\mathbf{cpc}}$ and the concatenated transmitted cyclic-prefix vector $\vec{\mathbf{x}}_{\mathbf{cpc}}$ are found to be related through linear convolution between $\vec{\mathbf{x}}_{\mathbf{cpc}}$ and $\vec{\mathbf{h}}$. For $G = L-1$, well estimated cyclic-prefix can be used as a training sequence in the decision-directed-mode. But, an initial training sequence is stringently required. If the channel changes after a long duration of time, then a training sequence needs to be transmitted again [373], [374]. The cyclic-prefix of received CP-OFDM symbol signal $\vec{\mathbf{y}}_{\mathbf{CP,k}}$ can be represented in matrix form as

$$\vec{\mathbf{y}}_{\mathbf{CP,k}} = \vec{\mathbf{d}}_{\mathbf{k}}\vec{\mathbf{h}}_{\mathbf{k}} + \vec{\mathbf{n}}_{\mathbf{k}} \tag{3.15}$$

where, $\vec{\mathbf{d}}_{\mathbf{k}} = \begin{bmatrix} x_{-L+1,k} & x_{N-1,k-1} & \ldots\ldots\ldots\ldots & x_{N-L+1,k-1} \\ \ldots\ldots & \ldots\ldots & \ldots\ldots\ldots\ldots & \ldots\ldots\ldots \\ \ldots\ldots & \ldots\ldots & \ldots\ldots\ldots\ldots & \ldots\ldots\ldots \\ x_{-1,k} & \ldots\ldots\ldots & \ldots\ldots & x_{-L+1,k} \ x_{N-1,k-1} \end{bmatrix}_{L-1\times L}$ (3.16)

The covariance-matrix of zero-mean stationary data matrix $\vec{\mathbf{d}}_{\mathbf{k}}$ is $\vec{\mathbf{R}} = E\left[\vec{\mathbf{d}}_k^H \vec{\mathbf{d}}_{\mathbf{k}}\right]$, where $E[.]$ is the expectation/ensemble average operator. The lower triangular part of matrix $\vec{\mathbf{d}}_{\mathbf{k}}$ is composed of

the elements of $\vec{\mathbf{x}}_{\mathbf{CP,k}}$, while the upper triangular part of this matrix is consisting of elements of $\vec{\mathbf{x}}_{\mathbf{CP,k-1}}$. However, AWGN sample vector in Eq.(3.15) is

$$\vec{\mathbf{n}}_{\mathbf{k}} = \left[\eta_{-L+1,k}\ \eta_{-L+2,k}\ .....\ \eta_{-2,k}\ \eta_{-1,k}\right]^{T}_{L-1\times 1} \tag{3.17}$$

with $(L-1)\times(L-1)$ dimensional covariance-matrix $\sigma_{\eta}^{2}\vec{\mathbf{I}}_{L-1\times L-1}$. However under static/stationary conditions, we assume that the parameter $\alpha = \alpha_l = 1$ and $\sigma_w^2 \to 0$ in Eq.(3.12) for the modeling of l^{th} channel tap-coefficient.

3.2.2 Basic System Equations Under Time-Variant Multipath Fading Channels

On the contrary, under dynamic channel conditions, we consider different scheme to preclude the usage of x_{k-1} in (3.16). Therefore, the length of cyclic-prefix is kept $G \geq 2L-2$. Consequently for $G = 2L-2$, it can be shown that

$$\vec{\mathbf{d}}_{\mathbf{k}} = \begin{bmatrix} x_{-L+1,k} & x_{-L,k} & x_{-L-1,k} & ..... & x_{-2L+2,k} \\ ..... & ..... & ..... & ..... & \\ ..... & ..... & ..... & ..... & \\ x_{-1,k} & x_{-2,k} & ..... & ..... & x_{-L+1,k}\ \ x_{-L,k} \end{bmatrix}_{L-1\times L} \tag{3.18}$$

The time-varying channel tap-vector (3.3) is assumed to be excited by the first-order Markov processes using Eq.(3.12), which can be represented in matrix form as

$$\vec{\mathbf{h}}_{\mathbf{k}} = \vec{\mathbf{A}}\vec{\mathbf{h}}_{\mathbf{k-1}} + \vec{\mathbf{w}}_{\mathbf{k}} \tag{3.19}$$

where, $\vec{\mathbf{A}} = \alpha\vec{\mathbf{I}}_{L\times L}$ is the channel state transition matrix with $L\times L$ dimensional identity-matrix $\vec{\mathbf{I}}$. The above paradigm is applicable to a fading channel only if the channel coherence time is large enough to estimate/predict the channel response. The process-noise vector with covariance-matrix $\sigma_w^2\vec{\mathbf{I}}_{L\times L}$ is given as

$$\vec{\mathbf{w}}_{\mathbf{k}} = \left[w_{0,k}\ .....\ w_{l,k}\ .....w_{L-1,k}\right]^{T} \tag{3.20}$$

which results in uncorrelated tap-coefficients of multipath fading channel i.e., wide sense stationary uncorrelated scattering channel. Hence, the extended CP helps in adaptive channel estimation/prediction of underlying CSI. After the transmission of a small number of CP-OFDM training symbols, the presented system works under the decision-directed-mode.

3.3 Adaptive Channel Estimation/Prediction Techniques for Multipath Fading Channels

3.3.1 Kalman-Filtering Algorithm-Based Channel Estimation

Using the measurement equation (3.15) for CP and the process equation (3.19) for underlying channel, the coarse prediction/ *a priori* estimates are represented as

$$\hat{\mathbf{y}}_{\mathbf{CP,k}}^{-} = \vec{\mathbf{d}}_{\mathbf{k}} \hat{\mathbf{h}}_{\mathbf{k}}^{-} \qquad \text{(Coarse measurement of received CP)} \qquad (3.21)$$

$$\hat{\mathbf{h}}_{\mathbf{k}}^{-} = \vec{\mathbf{A}} \hat{\mathbf{h}}_{\mathbf{k-1}}^{+} \qquad \text{(Coarse channel prediction)} \qquad (3.22)$$

where, $\hat{\mathbf{h}}_{\mathbf{k}}^{-}$ and $\hat{\mathbf{h}}_{\mathbf{k}}^{+}$ are *a priori* and *a posteriori* channel estimates respectively. If $\hat{\mathbf{e}}_{\mathbf{k}}^{-} = \mathbf{h}_{\mathbf{k}} - \hat{\mathbf{h}}_{\mathbf{k}}^{-}$ and $\hat{\mathbf{e}}_{\mathbf{k}}^{+} = \mathbf{h}_{\mathbf{k}} - \hat{\mathbf{h}}_{\mathbf{k}}^{+}$ are *a priori* and *a posteriori* zero-mean channel estimation errors with covariance-matrices $\hat{\mathbf{P}}_{\mathbf{k}}^{-} = E\left[\hat{\mathbf{e}}_{\mathbf{k}}^{-}\, \hat{\mathbf{e}}_{\mathbf{k}}^{-\mathbf{H}}\right]_{L\times L}$ and $\hat{\mathbf{P}}_{\mathbf{k}}^{+} = E\left[\hat{\mathbf{e}}_{\mathbf{k}}^{+}\, \hat{\mathbf{e}}_{\mathbf{k}}^{+\mathbf{H}}\right]_{L\times L}$ respectively. In the present scenario, basic Kalman-filtering equations are

$$\hat{\mathbf{P}}_{\mathbf{k}}^{-} = \vec{\mathbf{A}} \hat{\mathbf{P}}_{\mathbf{k-1}}^{+} \vec{\mathbf{A}}^{\mathbf{H}} + \boldsymbol{\sigma}_{\mathbf{w}}^{2} \vec{\mathbf{I}}_{\mathbf{L\times L}} \qquad (3.23)$$

Based on an innovation vector $\left\{\vec{\mathbf{y}}_{\mathbf{CP,k}} - \hat{\mathbf{y}}_{\mathbf{CP,k}}^{-}\right\}$, *a posteriori* channel estimate is

$$\hat{\mathbf{h}}_{\mathbf{k}}^{+} = \hat{\mathbf{h}}_{\mathbf{k}}^{-} + \hat{\mathbf{K}}_{\mathbf{k}} \left[\vec{\mathbf{y}}_{\mathbf{CP,k}} - \hat{\mathbf{y}}_{\mathbf{CP,k}}^{-}\right] \qquad (3.24)$$

where, $\hat{\mathbf{K}}$ is the $L\times(L-1)$ dimensional Kalman gain / blending factor, which is calculated by minimizing $\hat{\mathbf{P}}_{\mathbf{k}}^{+}$ to give

$$\hat{\mathbf{K}}_{\mathbf{k}} = \hat{\mathbf{P}}_{\mathbf{k}}^{-} \vec{\mathbf{d}}_{\mathbf{k}}^{\mathbf{H}} \left[\vec{\mathbf{d}}_{\mathbf{k}} \hat{\mathbf{P}}_{\mathbf{k}}^{-} \vec{\mathbf{d}}_{\mathbf{k}}^{\mathbf{H}} + \boldsymbol{\sigma}_{\boldsymbol{\eta}}^{2} \vec{\mathbf{I}}_{L-1\times L-1}\right]^{-1} \qquad (3.25)$$

$$\hat{\mathbf{P}}_{\mathbf{k}}^{+} = \left[\vec{\mathbf{I}}_{L\times L} - \hat{\mathbf{K}}_{\mathbf{k}} \hat{\mathbf{d}}_{\mathbf{k}}\right] \hat{\mathbf{P}}_{\mathbf{k}}^{-} \qquad (3.26)$$

Using abovementioned Eqs.(3.21)–(3.26), the coarse predicted values of channel coefficients are determined using Eq.(3.22) as $\hat{\mathbf{h}}_{\mathbf{k+1}}^{-} = \vec{\mathbf{A}} \hat{\mathbf{h}}_{\mathbf{k}}^{+}$. Subsequently, FFT operation is performed on $\hat{\mathbf{h}}_{\mathbf{k+1}}^{-}$ to obtain the coarse channel prediction $\hat{\mathbf{H}}_{\mathbf{k+1}}^{-}$ (as shown in Fig. 3.1), which is further used in one-tap equalizer for the OFDM symbol-detection at $(k+1)^{th}$ iteration.

3.3.2 Reduced Kalman-LMS Algorithm-based Channel Estimation

Based on aforementioned KF algorithm and the pioneering work of Gazor in [381], the following RK-LMS [379] algorithm can be used for the cyclic-prefix based channel estimation/coarse prediction in wireless OFDM systems.

$$\hat{\mathbf{h}}_{\mathbf{k}}^{+} = \hat{\mathbf{h}}_{\mathbf{k}}^{-} + \mu \vec{\mathbf{d}}_{\mathbf{k}}^{\mathbf{H}} \left[\vec{\mathbf{y}}_{\mathbf{CP,k}} - \hat{\mathbf{y}}_{\mathbf{CP,k}}^{-}\right] \qquad (3.27)$$

The Kalman gain $\hat{\mathbf{K}}_{\mathbf{k}}$ is replaced by $\mu\vec{\mathbf{d}}_{\mathbf{k}}^{\mathbf{H}}$ in Eq.(3.24). Akin to [379], [381], a first-order weight increment vector $\dot{\hat{\mathbf{h}}}^{+}$ is used to determine

$$\hat{\mathbf{h}}_{\mathbf{k}}^{-} = \hat{\mathbf{h}}_{\mathbf{k-1}}^{+} + \hat{\beta}\dot{\hat{\mathbf{h}}}_{\mathbf{k-1}}^{+} \tag{3.28}$$

Using the conventional LMS algorithm [268] to update a first-order weight increment vector [369], [379], [381], it can be shown that

$$\dot{\hat{\mathbf{h}}}_{\mathbf{k}}^{+} = \dot{\hat{\mathbf{h}}}_{\mathbf{k}-1}^{+} + \hat{\alpha}\mu\vec{\mathbf{d}}_{\mathbf{k}}^{\mathbf{H}}\left[\vec{\mathbf{y}}_{\mathbf{CP,k}} - \hat{\mathbf{y}}_{\mathbf{CP,k}}^{-}\right] \tag{3.29}$$

where, the scalar parameter μ is step-size, which controls stability as well as convergence of LMS algorithm, $0 \le \hat{\alpha} \le 1$ is the smoothing parameter, which controls lag-misadjustment in adaptive weights while tracking the time-varying system. The estimated first-order weight increment vector is scaled with a real valued control parameter $0 \le \hat{\beta} < 1$ [369], which controls the oscillatory behavior of adaptive algorithm. Hence, KF is reduced to provide a computationally efficient two-step RK-LMS algorithm, which is not including the matrix inversion operation in Riccati update equation. Finally, channel coarse prediction $\hat{\mathbf{h}}_{\mathbf{k}+1}^{-} = \vec{\mathbf{A}}\hat{\mathbf{h}}_{\mathbf{k}}^{+}$ is achieved using Eq.(3.27).

3.3.3 RLS and NVFF-RLS Algorithm-Based Channel Estimation

In recursive least squares algorithm based channel estimation [268], [353], $L-1\times 1$ dimensional *a priori* estimation error vector is defined as

$$\vec{\boldsymbol{\varepsilon}}_{\mathbf{k}} = \vec{\mathbf{y}}_{\mathbf{CP,k}} - \vec{\mathbf{d}}_{\mathbf{k}}\hat{\mathbf{h}}\left(k-1\middle|k-1\right) \tag{3.30}$$

where, $\hat{\mathbf{h}}\left(k-1\middle|k-1\right)$ is an estimated channel tap-coefficient vector at $\left(k-1\right)^{th}$ iteration. Subsequently,

$$\hat{\mathbf{h}}\left(k\middle|k\right) = \hat{\mathbf{h}}\left(k-1\middle|k-1\right) + \bar{\mathbf{K}}_{\mathbf{k}}\vec{\boldsymbol{\varepsilon}}_{\mathbf{k}} \tag{3.31}$$

where, $\bar{\mathbf{K}}_{\mathbf{k}}$ is the $L\times\left(L-1\right)$ dimensional gain matrix, which is determined as

$$\bar{\mathbf{K}}_{\mathbf{k}} = \bar{\mathbf{P}}_{\mathbf{k-1}}\vec{\mathbf{d}}_{\mathbf{k}}^{\mathbf{H}}\left[\lambda_k\sigma_\eta^2\vec{\mathbf{I}}_{L-1\times L-1} + \vec{\mathbf{d}}_{\mathbf{k}}\bar{\mathbf{P}}_{\mathbf{k-1}}\vec{\mathbf{d}}_{\mathbf{k}}^{\mathbf{H}}\right]^{-1} \tag{3.32}$$

where, $\lambda_k = \lambda = \textit{fixed}$ is the forgetting factor in conventional RLS algorithm, and $L\times L$ dimensional inverse correlation matrix is

$$\bar{\mathbf{P}}_{\mathbf{k}} = \lambda_k^{-1}\left[\bar{\mathbf{P}}_{\mathbf{k-1}} - \bar{\mathbf{K}}_{\mathbf{k}}\vec{\mathbf{d}}_{\mathbf{k}}\bar{\mathbf{P}}_{\mathbf{k-1}}\right] \tag{3.33}$$

To execute this conventional RLS algorithm, $\hat{\mathbf{h}}\left(0\right) = \textit{null}$ at initial point and $\bar{\mathbf{P}}_{\mathbf{0}} = \bar{\delta}^{-1}\vec{\mathbf{I}}_{L\times L}$. The value of $\bar{\delta}$ is kept small positive constant under the high SNR conditions and large positive constant under the low SNR conditions. For time-varying multipath channel estimation using RLS

algorithm, the lag-error variance due to time-variations and the AWGN variance in channel estimation error have tradeoff relation with each other [264], [353].

Further, the convergence as well as tracking performances of RLS algorithm based channel estimation /prediction using CP can be improved by incorporating the numeric-variable-forgetting-factor [346], [353]. The NVFF reckoning is based on the extended estimation error criterion [267], [383], which accounts for the nonstationarity of signal. The value of NVFF decreases adaptively to estimate a global trend quickly, when the underlying signal experiences nonstationarity i.e., $\lambda_k \to \lambda_{Min}$. However, it increases under stationary conditions by increasing the memory for efficient estimation i.e., $\lambda_k \to \lambda_{Max}$. In conventional RLS algorithm, the speed of adaptation is proportional to the asymptotic memory length $\bar{N} = (1-\lambda)^{-1}$ [268], [354], in which memories related to λ_{Max} and λ_{Min} are denoted by $\bar{N}_{Max}$ and $\bar{N}_{Min}$ respectively for the parameter setting. Therefore, we next focus on the calculation of NVFF λ_k, which can be incorporated in conventional RLS algorithm to formulate NVFF-RLS algorithm using the extended estimation error criterion. From RLS algorithm perspective [268], *a posteriori* estimation error is written as

$$\bar{\mathbf{e}}_{\mathbf{k}} = \vec{\mathbf{y}}_{\mathbf{CP,k}} - \vec{\mathbf{d}}_{\mathbf{k}} \hat{\mathbf{h}}(k|k) \tag{3.34}$$

However, $\vec{\boldsymbol{\varepsilon}}_{\mathbf{k}}$ in Eq.(3.30) is viewed as a tentative value of $\bar{\mathbf{e}}_{\mathbf{k}}$ before updating the tap-weight vector. Using Eq.(3.15), the above equation (3.34) can be simplified as

$$\bar{\mathbf{e}}_{\mathbf{k}} = \vec{\mathbf{d}}_{\mathbf{k}} \left[\vec{\mathbf{h}}_{\mathbf{k}} - \hat{\mathbf{h}}(k|k) \right] + \vec{\mathbf{n}}_{\mathbf{k}} \tag{3.35}$$

Substitution of Eq.(3.19) in equation (3.35) results in

$$\bar{\mathbf{e}}_{\mathbf{k}} = \vec{\mathbf{d}}_{\mathbf{k}} \left[\vec{\mathbf{A}}\vec{\mathbf{h}}_{k-1} + \vec{\mathbf{w}}_k - \hat{\mathbf{h}}(k|k) \right] + \vec{\mathbf{n}}_{\mathbf{k}} \tag{3.36}$$

Subsequently, it is assumed that $\hat{\mathbf{h}}(k|k) \approx \vec{\mathbf{A}}\vec{\mathbf{h}}_{k-1}$ under the optimum tracking conditions. The above equation can be simplified as

$$\bar{\mathbf{e}}_{\mathbf{k}} = \vec{\mathbf{d}}_{\mathbf{k}} \vec{\mathbf{w}}_k + \vec{\mathbf{n}}_{\mathbf{k}} \tag{3.37}$$

By statistical analysis [384], it is apparent that the zero-mean $\bar{\mathbf{e}}_{\mathbf{k}}$ exhibits

$$\sigma_{\bar{e}}^2 = \sigma_\eta^2 \left(1 + \sigma_w^2 / \sigma_\eta^2\right) \tag{3.38}$$

However, $\sigma_{\bar{e}}^2 \simeq \sigma_\eta^2 \qquad for\ \sigma_w^2/\sigma_\eta^2 << 1$ (3.39)

The extended estimation error is determined by

$$\Gamma_k = \frac{1}{M} \sum_{m=0}^{M-1} \left\{ \vec{\boldsymbol{\varepsilon}}_{\mathbf{k-m}}^{\mathbf{H}} \vec{\boldsymbol{\varepsilon}}_{\mathbf{k-m}} \right\} \tag{3.40}$$

To ensure the appropriate averaging in Eq.(3.40) under nonstationary environment, the parameter $M << \bar{N}_{Min}$.

$$\bar{N}_k = \frac{\sigma_{\bar{e}}^2 \bar{N}_{Max}}{\Gamma_k} \simeq \frac{\sigma_{\eta}^2 \bar{N}_{Max}}{\Gamma_k} \tag{3.41}$$

which is further used to calculate NVFF as

$$\lambda_k = 1 - \bar{N}_k^{-1} \tag{3.42}$$

To ensure a positive non-zero value of NVFF, the stringent condition/bound is $\lambda_{Max} \geq \lambda_k \geq \lambda_{Min}$.

The research work presented by Sayed and Kailath in [377] delineated a relationship between KF and RLS algorithm, which manifests that $\hat{\mathbf{h}}_{\mathbf{k}}^{+} = \hat{\mathbf{h}}\left(k|k\right)$ (estimation) and $\hat{\mathbf{h}}_{\mathbf{k+1}}^{-} = \hat{\mathbf{h}}\left(k+1|k\right)$ (prediction). Therefore, the coarse predicted value of channel tap-coefficient vector is $\hat{\mathbf{h}}_{\mathbf{k}+1}^{-} = \vec{\mathbf{A}}\hat{\mathbf{h}}\left(k|k\right)$. The above discussed NVFF scheme is reported to outperform the LMS based VFF computation procedure, in combination with conventional RLS algorithm [353]. In this section, we have discussed the NVFF-RLS adaptive algorithm for channel estimation/prediction using CP in wireless OFDM systems.

The computational complexity of conventional Kalman-filtering algorithm is reported to be $O\left(\bar{N}^3\right)$, where $\bar{N}$ is the filter length. However, some special cases like covariance KF, square-root KF and extended square-root KF exhibit $O\left(\bar{N}^2\right)$ computational burden, subject to different mathematical decompositions of the covariance-matrices (Toeplitz) [386], which is equivalent to that of conventional RLS algorithms and its types [377]. The NVFF-RLS algorithm involves an additional calculation procedure to obtain the NVFF update continuously, which slightly increases its computational complexity in comparison with traditional RLS algorithm. Similarly, RK-LMS possess approximately double computational complexity (i.e., $2O\left(\bar{N}\right)$) than conventional LMS algorithm.

3.4 Description of 2×1 STBC-OFDM System Model

Let us consider 2×1 STBC-OFDM system with two transmitters (TX1 and TX2) and one receiver (RX1) antennas (as in [387]), in which the k^{th} and $(k+1)^{th}$ OFDM symbol-blocks are denoted as $\vec{\mathbf{X}}_{\mathbf{o}} = \left[\, X_{0,k} \quad X_{1,k} \quad \ldots \quad X_{N-1,k} \,\right]_{N\times1}^{T}$ and $\vec{\mathbf{X}}_{\mathbf{e}} = \left[\, X_{0,k+1} \quad X_{1,k+1} \quad \ldots \quad X_{N-1,k+1} \,\right]_{N\times1}^{T}$, respectively. By performing IFFT operation, the $\vec{\mathbf{X}}_{\mathbf{o}}$ *and* $\vec{\mathbf{X}}_{\mathbf{e}}$ can be expressed in time-domain as

$\vec{\mathbf{x}}_{\mathbf{o}} = \begin{bmatrix} x_{0,k} & x_{1,k} & \cdots & x_{N-1,k} \end{bmatrix}^T_{N\times 1}$ and $\vec{\mathbf{x}}_{\mathbf{e}} = \begin{bmatrix} x_{0,k+1} & x_{1,k+1} & \cdots & x_{N-1,k+1} \end{bmatrix}^T_{N\times 1}$ respectively.

Subsequently by incorporating CP, these two OFDM symbol-blocks are represented as

$$\vec{\mathbf{x}}_{\mathbf{co,o}} = \begin{bmatrix} \vec{\mathbf{x}}^T_{\mathbf{cp,o}} & \vec{\mathbf{x}}^T_{\mathbf{o}} \end{bmatrix}^T_{(N+G)\times 1} \quad \text{and} \quad \vec{\mathbf{x}}_{\mathbf{co,e}} = \begin{bmatrix} \vec{\mathbf{x}}^T_{\mathbf{cp,e}} & \vec{\mathbf{x}}^T_{\mathbf{e}} \end{bmatrix}^T_{(N+G)\times 1} \tag{3.43}$$

Applying the space-time block-coding scheme using these two OFDM symbol-blocks with CP [387], it can be shown that

$$\vec{\mathbf{x}}_{\mathbf{STBC}} = \begin{bmatrix} +\vec{\mathbf{x}}_{\mathbf{co,o}} & +\vec{\mathbf{x}}_{\mathbf{co,e}} \\ -\vec{\mathbf{x}}^*_{\mathbf{co,e}} & +\vec{\mathbf{x}}^*_{\mathbf{co,o}} \end{bmatrix} \tag{3.44}$$

The transmitted wireless OFDM signals encounter multipath fading with L channel tap-coefficients, which leads to $G \geq 2L-2$ in the present scenario. The two independent wireless channel tap-coefficient vectors are $\vec{\mathbf{h}}_{\mathbf{1,k}}$ (from TX1 to RX1) and $\vec{\mathbf{h}}_{\mathbf{2,k}}$ (from TX2 to RX1) respectively. The wireless channel tap-coefficient vectors are assumed to be constant for two OFDM symbol-blocks, such that

$$\vec{\mathbf{h}}_{\mathbf{1,k}} = \vec{\mathbf{h}}_{\mathbf{1,k+1}} \quad \text{and} \quad \vec{\mathbf{h}}_{\mathbf{2,k}} = \vec{\mathbf{h}}_{\mathbf{2,k+1}} \quad \text{for period } T_{STBC} = 2\left(N+G\right)T_s \tag{3.45}$$

The received composite wireless signals at the receiver are

$$\vec{\mathbf{y}}_{\mathbf{co,k}} = \begin{bmatrix} \vec{\mathbf{y}}^T_{\mathbf{cp,k}} & \vec{\mathbf{y}}^T_{\mathbf{k}} \end{bmatrix}^T_{(N+G)\times 1} \quad \text{and} \quad \vec{\mathbf{y}}_{\mathbf{co,k+1}} = \begin{bmatrix} \vec{\mathbf{y}}^T_{\mathbf{cp,k+1}} & \vec{\mathbf{y}}^T_{\mathbf{k+1}} \end{bmatrix}^T_{(N+G)\times 1} \tag{3.46}$$

The cyclic-prefix part is extracted at the receiver considering $G = 2L-2$ (as in subsection 3.2.2) to provide

$$\vec{\mathbf{y}}_{\mathbf{cp,k}} = \vec{\mathbf{d}}_{\mathbf{o}}\vec{\mathbf{h}}_{\mathbf{1,k}} + \vec{\mathbf{d}}_{\mathbf{e}}\vec{\mathbf{h}}_{\mathbf{2,k}} + \vec{\mathbf{n}}_{\mathbf{cp,k}} \quad \text{in } k^{th} \text{ OFDM symbol-block period} \tag{3.47}$$

$$\vec{\mathbf{y}}_{\mathbf{cp,k+1}} = -\vec{\mathbf{d}}^*_{\mathbf{e}}\vec{\mathbf{h}}_{\mathbf{1,k+1}} + \vec{\mathbf{d}}^*_{\mathbf{o}}\vec{\mathbf{h}}_{\mathbf{2,k+1}} + \vec{\mathbf{n}}_{\mathbf{cp,k+1}} \quad \text{in } \left(k+1\right)^{th} \text{ OFDM symbol-block period} \tag{3.48}$$

where,

$$\vec{\mathbf{d}}_{\mathbf{o}} = \begin{bmatrix} x_{-L+1,k} & x_{-L,k} & \cdots & x_{-2L+2,k} \\ \vdots & \ddots & & \vdots \\ \vdots & & \ddots & \vdots \\ x_{-1,k} & x_{-2,k} & \cdots & x_{-L,k} \end{bmatrix}_{(L-1)\times L} \tag{3.49}$$

$$\vec{\mathbf{d}}_{\mathbf{e}} = \begin{bmatrix} x_{-L+1,k+1} & x_{-L,k+1} & \cdots & x_{-2L+2,k+1} \\ \vdots & \ddots & & \vdots \\ \vdots & & \ddots & \vdots \\ x_{-1,k+1} & x_{-2,k+1} & \cdots & x_{-L,k+1} \end{bmatrix}_{(L-1)\times L} \tag{3.50}$$

In matrix form, Eqs.(3.47) and (3.48) can be rearranged by invoking (3.45) to give

$$\vec{\mathbf{y}}_{\mathbf{CP}} = \vec{\mathbf{d}}_{\mathbf{CP}}\vec{\mathbf{h}}_{\mathbf{CP}} + \vec{\mathbf{n}}_{\mathbf{CP}} \tag{3.51}$$

where, $\vec{\mathbf{y}}_{\mathbf{CP}} = \begin{bmatrix} \vec{\mathbf{y}}_{\mathbf{cp,k}} \\ \vec{\mathbf{y}}_{\mathbf{cp,k+1}} \end{bmatrix}_{2(L-1)\times 1}$, $\vec{\mathbf{d}}_{\mathbf{CP}} = \begin{bmatrix} +\vec{\mathbf{d}}_{\mathbf{o}} & +\vec{\mathbf{d}}_{\mathbf{e}} \\ -\vec{\mathbf{d}}_{\mathbf{e}}^{*} & +\vec{\mathbf{d}}_{\mathbf{o}}^{*} \end{bmatrix}_{2(L-1)\times 2L}$,

$\vec{\mathbf{h}}_{\mathbf{CP}} = \begin{bmatrix} \vec{\mathbf{h}}_{\mathbf{1,k}} \\ \vec{\mathbf{h}}_{\mathbf{2,k}} \end{bmatrix}_{2L\times 1} = \begin{bmatrix} \vec{\mathbf{h}}_{\mathbf{1,k+1}} \\ \vec{\mathbf{h}}_{\mathbf{2,k+1}} \end{bmatrix}_{2L\times 1}$ and $\vec{\mathbf{n}}_{\mathbf{CP}} = \begin{bmatrix} \vec{\mathbf{n}}_{\mathbf{cp,k}} \\ \vec{\mathbf{n}}_{\mathbf{cp,k+1}} \end{bmatrix}_{2(L-1)\times 1}$

Analogous to Eq.(3.19), if the channel is assumed to be constant for two consecutive OFDM symbol-blocks, then

$$\begin{bmatrix} \vec{\mathbf{h}}_{\mathbf{1,2q}} \\ \vec{\mathbf{h}}_{\mathbf{2,2q}} \end{bmatrix} = \vec{\mathbf{A}}_{\mathbf{2}} \begin{bmatrix} \vec{\mathbf{h}}_{\mathbf{1,2q-2}} \\ \vec{\mathbf{h}}_{\mathbf{2,2q-2}} \end{bmatrix} + \begin{bmatrix} \vec{\mathbf{w}}_{\mathbf{1,2q}} \\ \vec{\mathbf{w}}_{\mathbf{2,2q}} \end{bmatrix} \qquad for\ q = 1,2,3,..... \tag{3.52}$$

where, $\vec{\mathbf{A}}_{\mathbf{2}} = \alpha \vec{\mathbf{I}}_{2L\times 2L}$ is the channel state transition matrix with $2L \times 2L$ dimensional identity-matrix $\vec{\mathbf{I}}$. Using the aforementioned equation (3.51), the presented channel estimation schemes are used to obtain $\hat{\mathbf{h}}_{\mathbf{1,k}} = \hat{\mathbf{h}}_{\mathbf{1,k+1}}$ and $\hat{\mathbf{h}}_{\mathbf{2,k}} = \hat{\mathbf{h}}_{\mathbf{2,k+1}}$. Further, this estimated/predicted channel-state-information is used to decode the STBC-OFDM symbols, as in [46], [74], [387].

3.5 Simulation Results

We shall investigate the behavior of presented adaptive filtering techniques in the convergence and tracking-modes, using cyclic-prefix in OFDM systems for the multipath fading channel prediction. The CP used in OFDM systems is actually designed to reduce ISI, which is a repeated part of the transmitted data (that is used for the channel estimation/prediction). For simulation, the number of subcarriers is considered to be $N = 512$, the length of CP is $G = 64$, the length of channel impulse response is fixed at $L = G + 1$, the number of initial training blocks is 100, and the system is switched to decision-directed-mode afterwards. The transmitted power of all the used subchannels is kept equal with bit-allocation keeping the subchannels with same preset error probability, as in [373]. To generate nonstationary environment, the channel tap-coefficient vector $\vec{\mathbf{h}}_{\mathbf{k}}$ is assumed to be a fast-fading mobile communication channel (Rayleigh). The Jakes' paradigm is widely accepted as the realistic fading channel model, which is simulated by using an AR(1) process (3.12). We shall compare the performance of KF, RK-LMS, RLS and NVFF-RLS algorithms in terms of the minimum mean square channel prediction error. The presented results are based on the ensemble average of 100 independent simulation runs using the different fading channel realizations and 64-QAM constellations, as in [374]. It follows that

$$\vec{\mathbf{J}}_{\mathbf{k}} = E\left[\left| \vec{\mathbf{h}}_{\mathbf{k}} - \hat{\mathbf{h}}_{\mathbf{k}}^{-} \right|^2 \right] \tag{3.53}$$

$$\vec{\mathbf{J}}_{\mathbf{k}} \simeq \frac{1}{100} \sum_{j=1}^{100} \left| \vec{\mathbf{h}}_{\mathbf{k},j} - \hat{\mathbf{h}}_{\mathbf{k},j}^{-} \right|^2 \tag{3.54}$$

Case 1:- In first case, the channel tap-coefficient vector $\vec{\mathbf{h}}_{\mathbf{k}} = \vec{\mathbf{h}}$ is kept constant by considering the state transition matrix $\vec{\mathbf{A}} = \vec{\mathbf{I}}_{\mathbf{L\times L}}$ and process-noise variance $\sigma_w^2 = 0$ in Eq.(3.19). The adaptation parameters are set as $\mu = 0.001$, $\hat{\alpha} = 0.0001$ and $\hat{\beta} = 0.5$ in Eqs.(3.27)–(3.29) for the simulation of RK-LMS algorithm for channel estimation/prediction. The forgetting factor is fixed at $\lambda = 0.9$ in Eqs.(3.30)–(3.33) in case of conventional RLS algorithm. In NVFF-RLS algorithm, the parameters are kept at $\lambda_{Max} = 0.99$, $\lambda_{Min} = 0.9$ and $M = 5$ in Eqs.(3.40)–(3.42). For guaranteed numerical stability of RLS algorithm under stationary environment and for the positive definiteness of finite-precision inverse data covariance-matrix, the stringent condition to be fulfilled is $\bar{\mathbf{P}}_{\mathbf{k}}\vec{\mathbf{R}}_{\mathbf{k\text{-}1}} \approx \mathbf{I}_{\mathbf{L\times L}}$ [388]. When an input data matrix $\vec{\mathbf{d}}_{\mathbf{k}}$ is stationary and the value of λ_{Max} is close to unity, this approximation is often used under steady-state/stationary conditions. Here, the recursive equation $\vec{\mathbf{R}}_{\mathbf{k}} = \lambda_{Max}\vec{\mathbf{R}}_{\mathbf{k}-1} + \vec{\mathbf{d}}_k^H\vec{\mathbf{d}}_{\mathbf{k}}$ is updated continuously. Under the above scenario, simulation results are presented in Fig. 3.4 and Fig. 3.5 at $SNR = +25dB$.

It may be inferred that KF based channel predictor outperforms other adaptive algorithms in the convergence as well as training-mode. However as the value of λ increases, the tracking performance of RLS algorithm improves in training-mode. The convergence of RK-LMS algorithm is observed to be inferior to the RLS, NVFF-RLS and KF algorithms. In decision-directed-mode, the tracking performance of RK-LMS algorithm is comparable to RLS algorithm with $\lambda = 0.9$. However, the NVFF-RLS scheme performs marginally better than the RLS and RK-LMS algorithm based channel predictors. It is apparent from the results depicted in Fig. 3.4 that channel estimation/prediction error appears at the decision point as an additional noise component, which in turn accounts for the higher mean square channel prediction error in all the simulated algorithms. Further, the value of SNR is reduced to +15dB, and the corresponding results in Fig. 3.6 manifest that overall mean square channel prediction error increases in all the underlying adaptive algorithms due to an increase in the measurement noise and decision errors. However, the existence of decision errors results in biased channel prediction due to the feedback loop (as shown in Fig. 3.1). But, adaptive algorithms converge at the same rate as that without the decision errors [373], [374]. The elevated mean square channel prediction error in the decision-directed-mode (as shown in Fig. 3.4 and Fig. 3.6) clearly illustrates that the decision error and channel prediction error affect each other adversely.

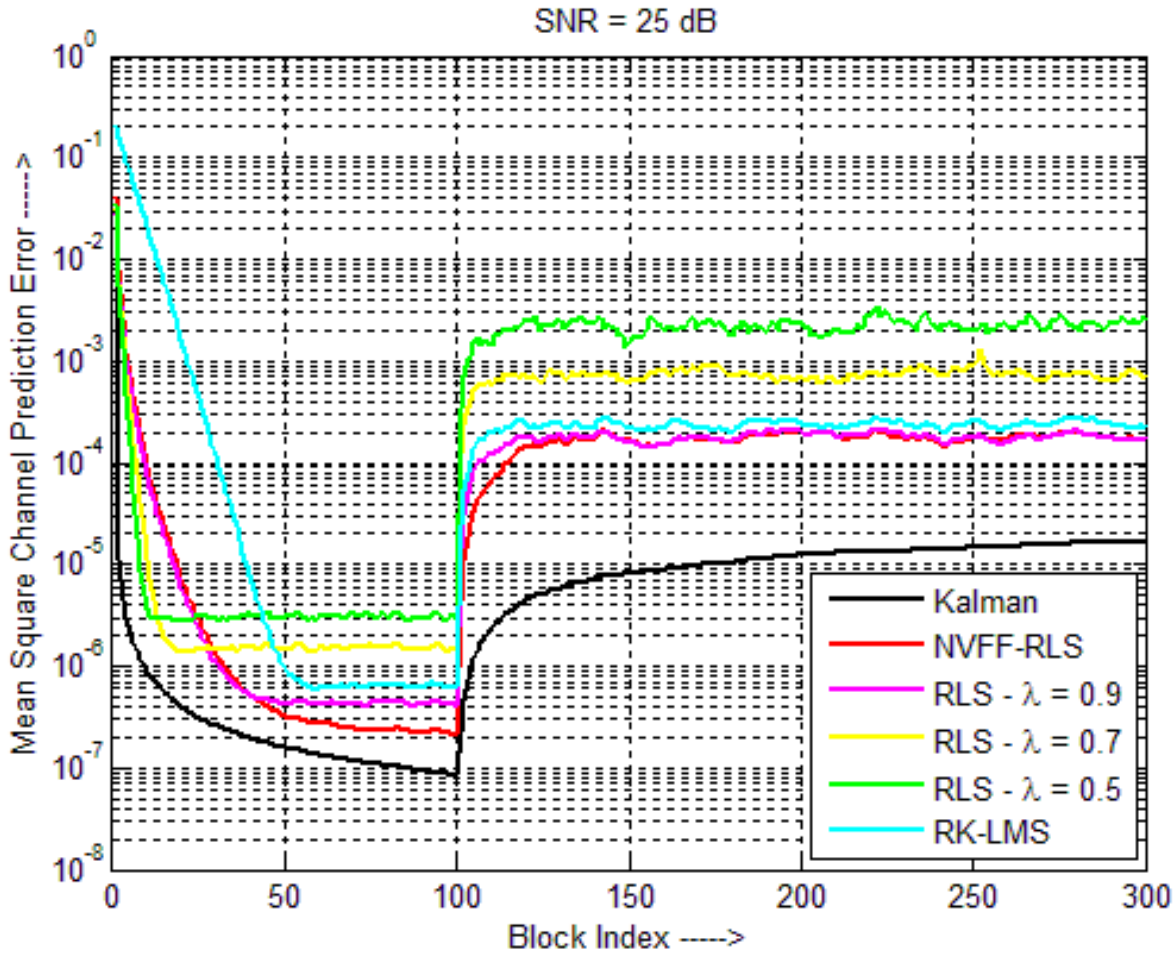

Fig. 3.4: Channel prediction error vs. block index for different adaptive algorithms at SNR = 25dB, under static environment.

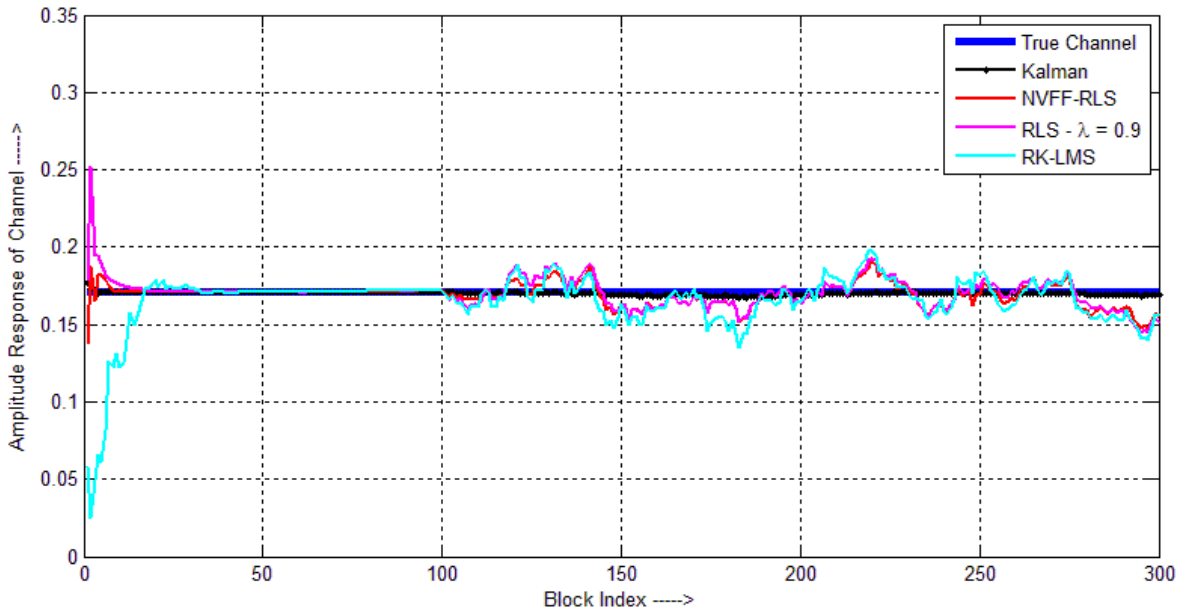

Fig. 3.5: Amplitude response of predicted channel tap-coefficient vs. block index for different adaptive algorithms under static environment.

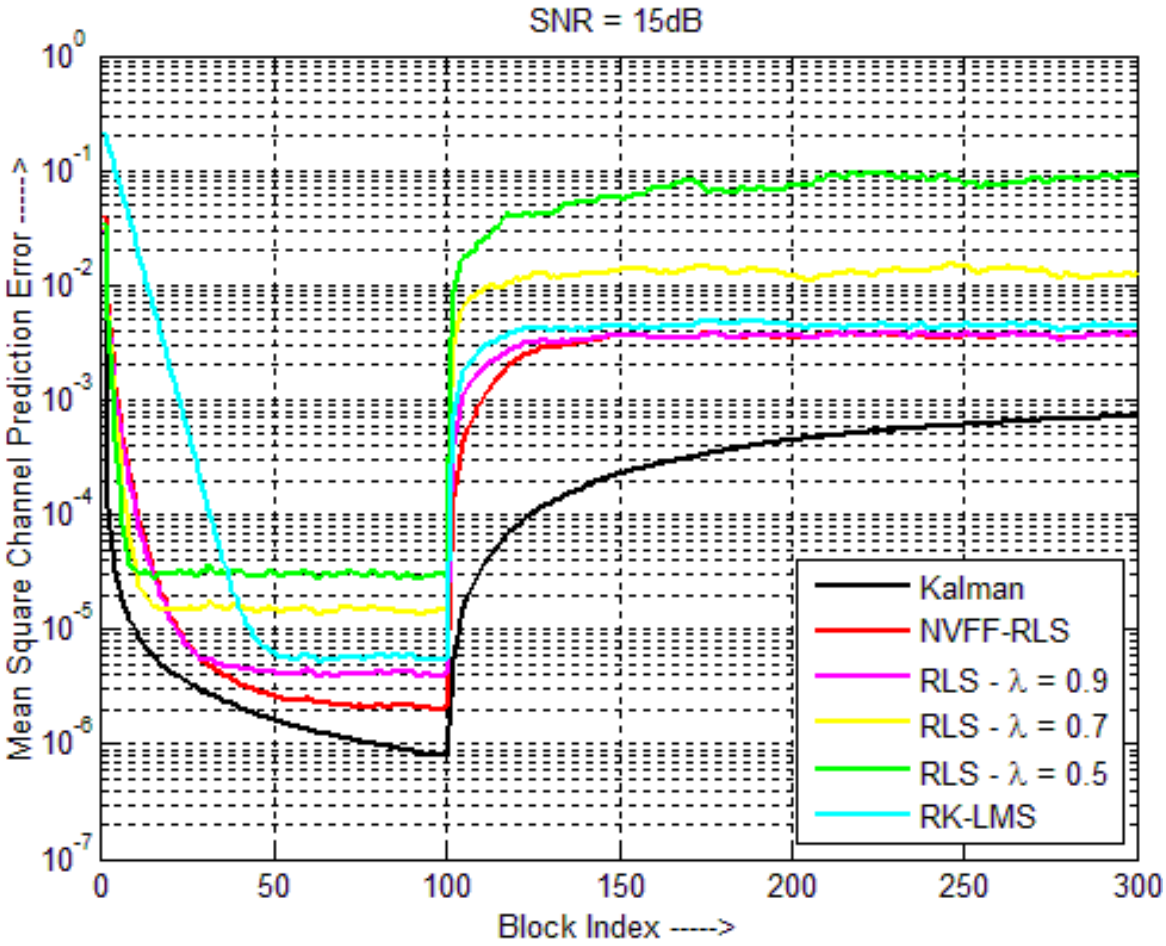

Fig. 3.6: Channel prediction error vs. block index for different adaptive algorithms at SNR = +15dB, under static environment.

***Case 2*:-** In second case, the channel tap-coefficient vector $\vec{\mathbf{h}}_{\mathbf{k}}$ is considered to be time-variant with the state transition matrix $\vec{\mathbf{A}} = \alpha \vec{\mathbf{I}}_{\mathbf{L}\times\mathbf{L}}$ and process-noise variance $\sigma_w^2 = 1 - |\alpha|^2$ in Eq.(3.19); where Markovian parameter is $\alpha = J_0\{2\pi f_D T\}$ with the maximum Doppler-spread/shift f_D and $T = (N+G)T_s$ with sampling interval T_s. To generate time-variant frequency-selective multipath fading channels, the fade-rate is kept $f_D T = 0.01$. The adaptation parameters are set as $\mu = 0.01$, $\hat{\alpha} = 0.001$ and $\hat{\beta} = 0.25$ in Eqs.(3.27)–(3.29) for the simulation of RK-LMS algorithm for channel estimation/prediction. The forgetting factor is fixed at $\lambda = 0.5$ in conventional RLS algorithm (3.30)–(3.33). In NVFF-RLS algorithm, the parameters are kept at $\lambda_{Max} = 0.5$, $\lambda_{Min} = 0.2$ and $M = 5$ in Eqs.(3.40)–(3.42). Under the above scenario, simulation results are demonstrated in Fig. 3.7 and Fig. 3.8 at $SNR = +20dB$. It may be inferred that KF based channel predictor outperforms other adaptive algorithms in the convergence as well as training-mode. However as the value of λ decreases under time-varying nonstationary environment, the tracking performance of RLS

algorithm improves in training-mode. The convergence-rate of RK-LMS algorithm is found to be lower in comparison to the RLS, NVFF-RLS and KF algorithms.

In decision-directed-mode, the tracking performance of RK-LMS algorithm is approximately equivalent to the RLS algorithm with $\lambda = 0.7$. It is evident from simulation results shown in Fig. 3.8 that the RLS algorithm with $\lambda = 0.9$ experiences lag-misadjustment due to the presence of high level of lag-noise, which can be suppressed by using the variable forgetting factor. However for time-varying wireless multipath fading channels, the NVFF-RLS scheme supersedes the RLS ($\lambda = 0.9$) and RK-LMS algorithm based channel predictors not only in the convergence-mode, but also in the training-mode.

Based on the extended estimation error criterion, the value of NVFF decreases adaptively to track the fast time-variations in channel response, and it increases for the tracking under slow time-varying environment. In training-mode, NVFF-RLS algorithm performs approximately $2.5dB$ better than traditional RLS algorithm with $\lambda = 0.5$, which reduces to approximately $1.35dB$ in the decision-directed-mode, as shown Fig. 3.7. It is noteworthy that the tracking performance of KF algorithm degrades due to the adverse effects of decision feedback errors in decision-directed-mode.

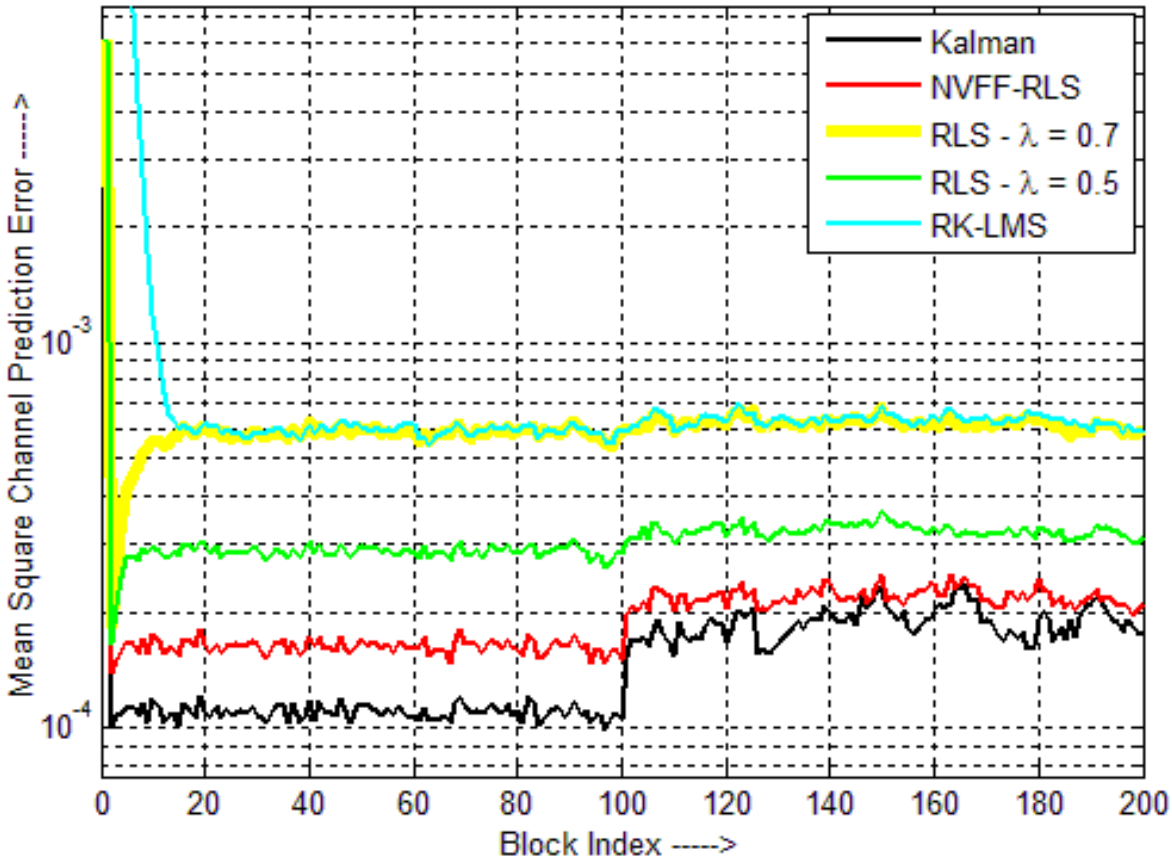

Fig. 3.7: Channel prediction error vs. block index for different adaptive algorithms at SNR = +20dB, under dynamic environment.

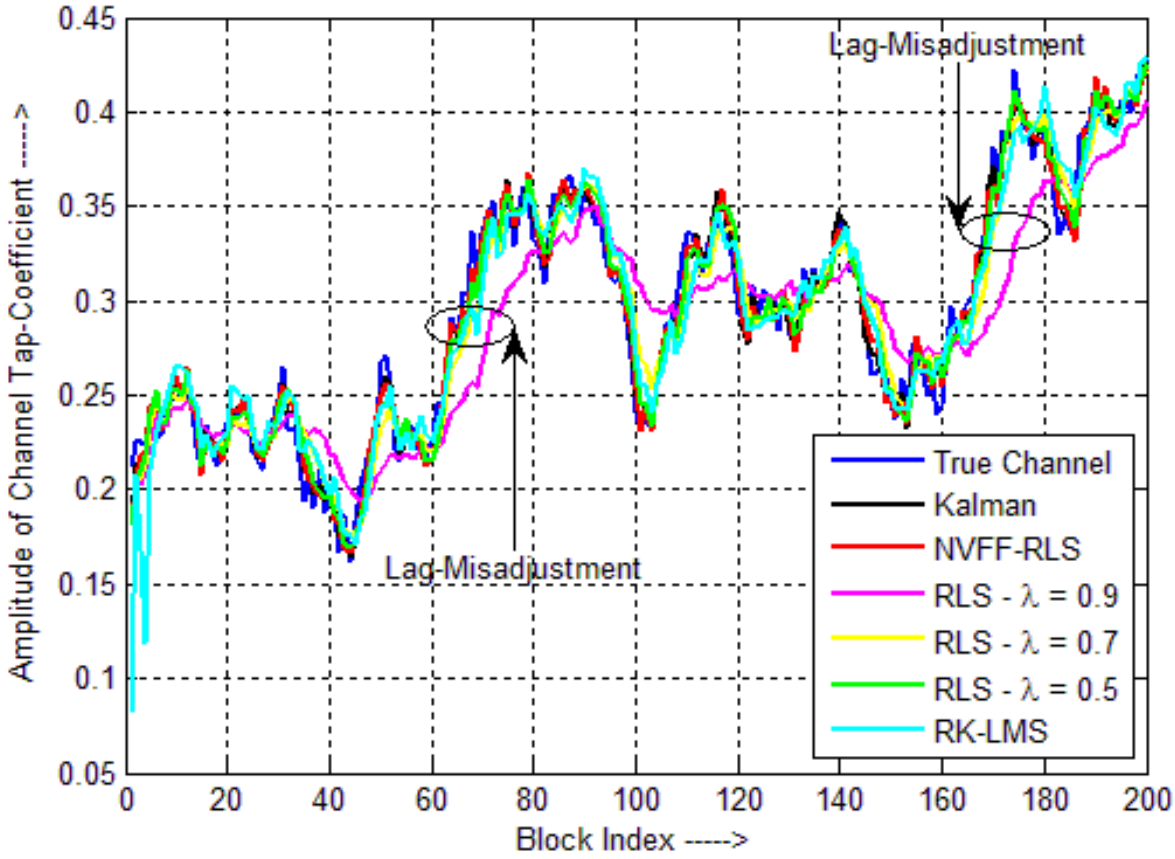

Fig. 3.8: Amplitude response of predicted channel tap-coefficient vs. block index for different adaptive algorithms, under dynamic environment.

***Case 3*:-** In third case, the aforementioned channel estimation/prediction techniques are incorporated in 2×1 STBC-OFDM system (as described in Section 3.4). For similar parameter setting as in Case 1 under the static environment (at $SNR = +30dB$), NVFF-RLS algorithm based channel estimator performs approximately $3.5dB$ better than traditional RLS $(\lambda = 0.9)$ algorithm in the decision-directed-mode, in terms of mean square channel estimation error, as shown in Fig. 3.9. However for similar parameter setting as in Case 2 under the dynamic environment (at $SNR = +40dB$), the wireless channel coefficients are assumed to change after two OFDM symbol-blocks. The NVFF-RLS algorithm performs approximately $4.2dB$ better than conventional RLS ($\lambda = 0.5$) in the tracking-mode. However, this performance advantage in terms of the mean square channel estimation error reduces to approximately $3dB$ in the decision-directed-mode, as shown in Fig. 3.10. The significantly improved channel estimation performance in Fig. 3.9 and Fig. 3.10 is because of the substantially enhanced signal-to-noise ratio due to the usage of 2×1 STBC scheme in combination with OFDM system. But, simulation results clearly manifest that decision feedback errors and channel prediction errors adversely affect each other in the decision-directed-mode.

The symbol error rate performances of conventional OFDM system and 2×1 STBC-OFDM system are demonstrated (using estimated channel-state-information) in Fig. 3.11 and Fig. 3.12 respectively, which are considered to be working under dynamic environment. In OFDM system at 0.01 SER, the NVFF-RLS algorithm based channel estimator provides approximately $2.75dB$ performance advantage over conventional RLS ($\lambda = 0.5$) algorithm in the decision-directed-mode (as shown in Fig. 3.11). However in STBC-OFDM system at 0.001 SER, the NVFF-RLS algorithm based channel estimator provides approximately $3dB$ performance advantage over conventional RLS ($\lambda = 0.5$) algorithm in the decision-directed-mode (as shown in Fig. 3.12). The space-time block-coding scheme undoubtedly improves SNR, which in turn reduces SER in the STBC-OFDM system in comparison with conventional OFDM system.

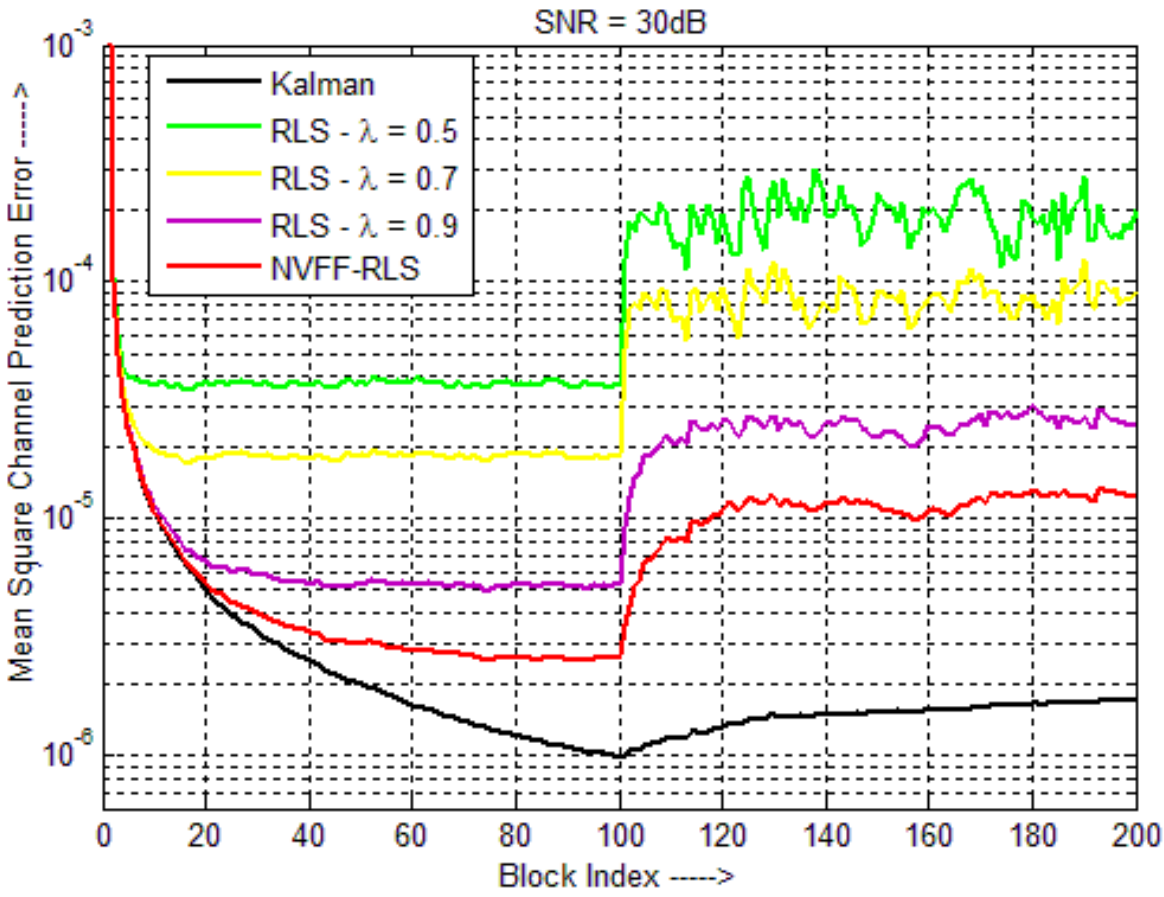

Fig. 3.9: Channel prediction error vs. block index for different algorithms working in STBC-OFDM system, under static environment.

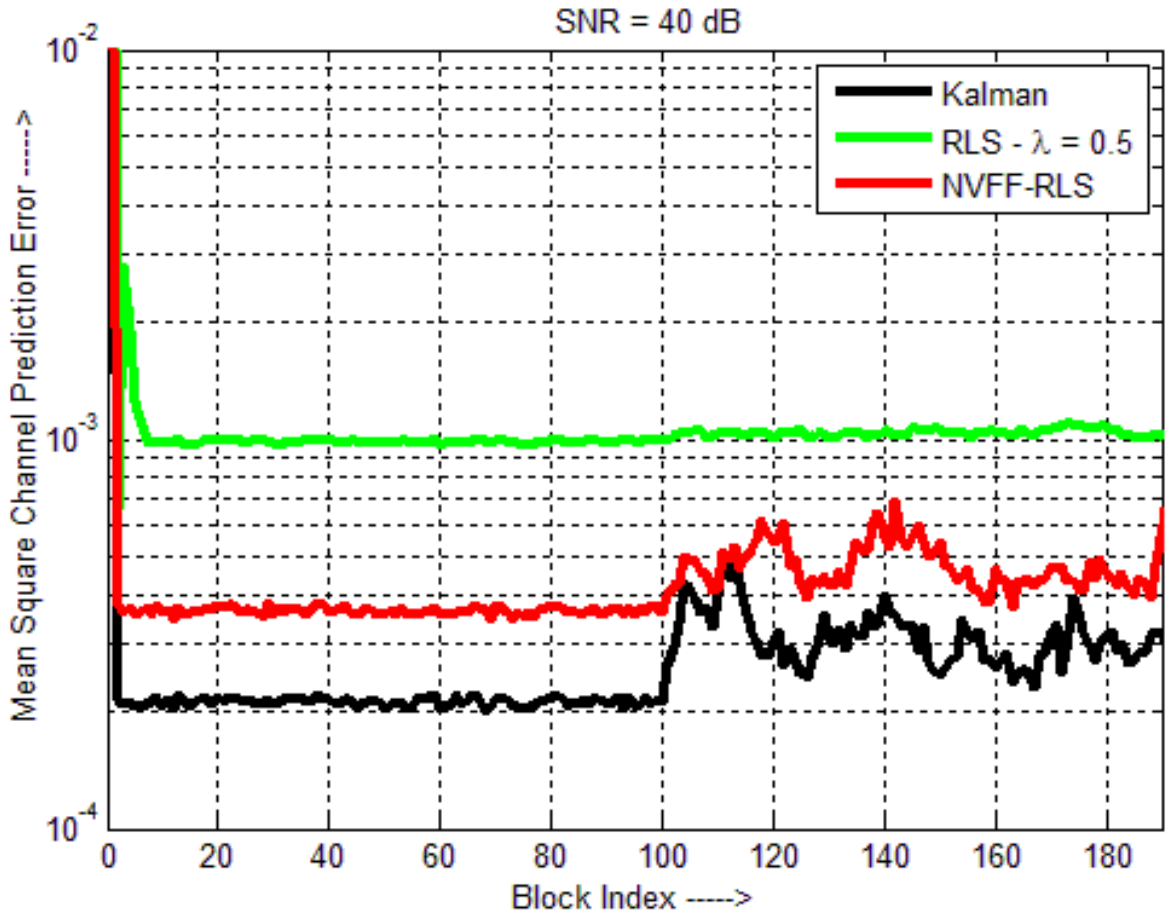

Fig. 3.10: Channel prediction error vs. block index for different algorithms working in STBC-OFDM system, under dynamic environment with $f_D T = 0.01$.

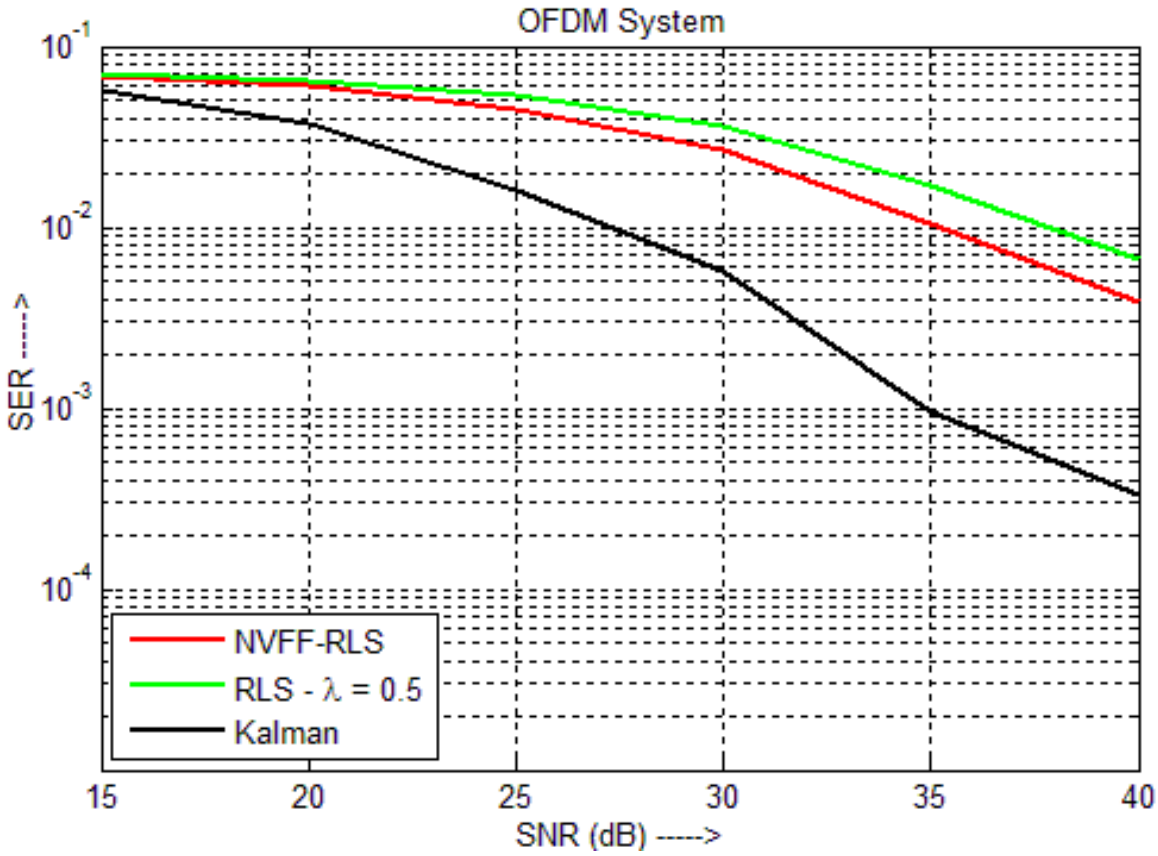

Fig. 3.11: Symbol error rate vs. block index for different algorithms working in OFDM system, under dynamic environment with $f_D T = 0.01$**.**

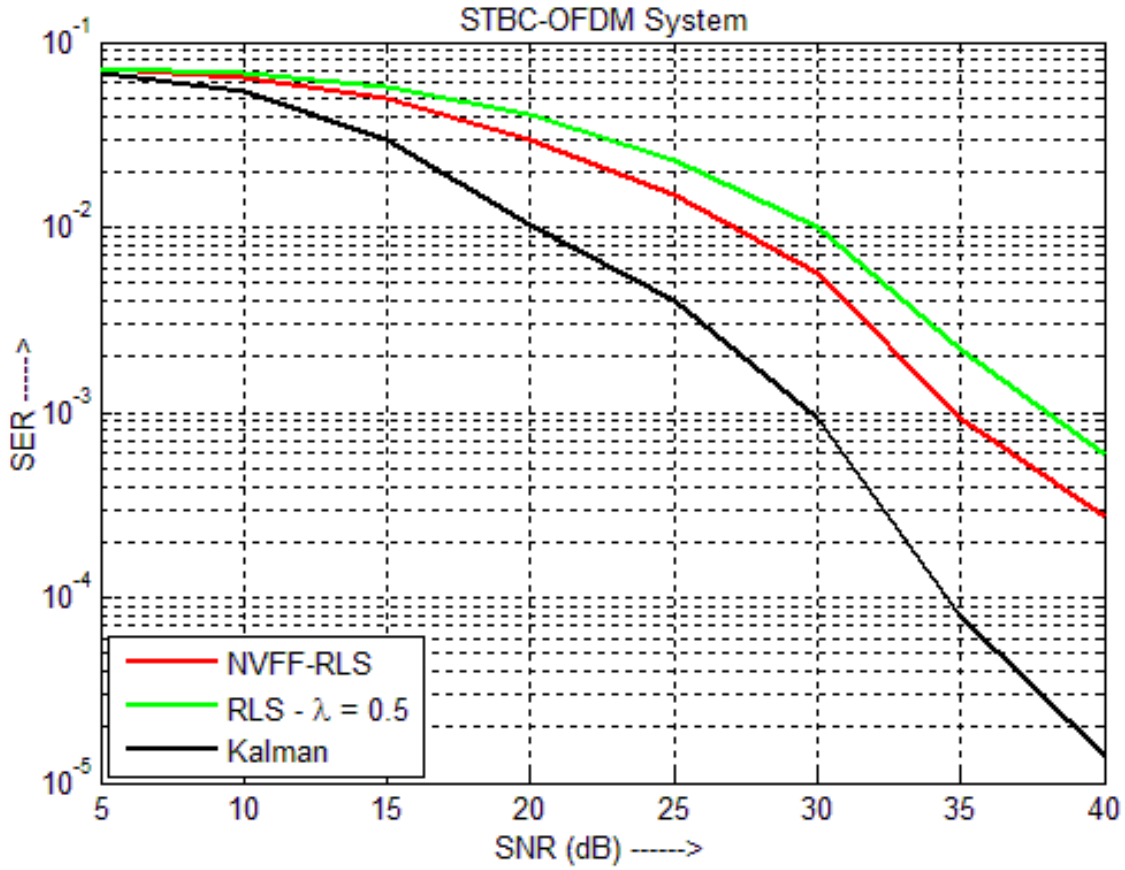

Fig. 3.12: Symbol error rate vs. block index for different algorithms working in STBC-OFDM system, under dynamic environment with $f_D T = 0.01$.

3.6 Summary of Chapter

In this chapter, the adaptive channel prediction techniques for CP-OFDM systems have been presented, in which the cyclic-prefix plays an important role by replacing the training symbols, in addition to its utility in combating the intersymbol-interference. Here, the NVFF-RLS algorithm outperforms the conventional RLS algorithm based channel prediction, under the moderately high fade-rate conditions. Eventually, the predicted channel-state-information has been utilized for the information symbol-detection in 2×1 space-time block-coded OFDM system. It is quite evident that the NVFF-RLS algorithm performs well under the static as well as dynamic environment by providing the low channel prediction error, which in turn results in the substantial alleviation in symbol error rate in 2×1 STBC-OFDM systems, in comparison with the conventional RLS algorithm based approach.

Future scope includes the application of presented NVFF-RLS algorithm for time-varying multipath fading channels and the low complexity RK-LMS algorithm for time-invariant frequency-selective fading channels for the channel estimation/prediction in high data-rate space-time/frequency block-coded OFDM wireless communication systems [296], as these adaptive algorithms are emerging as an economical choice in terms of computational complexity.

CHAPTER 4

BER PERFORMANCE OF SFBC–OFDM SYSTEMS WORKING OVER FADING CHANNELS UNDER IMPULSIVE ENVIRONMENT

4.1 Introduction

Orthogonal-frequency-division-multiplexing (OFDM) is an efficient modulation technique for the broadband communications [3], [7], [20], [26], which has found commercial applications in the domain of wireless local area networks (IEEE 802.11a and HIPERLAN/2), terrestrial digital-audio-broadcasting (DAB-T), terrestrial digital-video-broadcasting (DVB-T) and in other broadband access systems belonging to the IEEE 802.16 workgroup. In addition, two transmitter-antenna diversity schemes pioneered to combat the detrimental effects of frequency-selective fading are the space-frequency-block-coded (SFBC) OFDM [100] and space-time-block-coded (STBC) OFDM [73]. In STBC-OFDM systems, the information symbols are transmitted over the multiple adjacent OFDM symbol-blocks; but in SFBC-OFDM systems, the information symbols are transmitted across a single OFDM symbol-block by utilizing the adjacent subcarrier groups. However, one of the most challenging problems in such practical applications is the reliable information transmission over communication links in the presence of man-made noise/interference, which originates from powerlines, heavy current switches, electrical furnaces and domestic appliances [320] like microwave ovens, etc. Due to different types of sources of impulse-noise generation, it is tedious to model the statistical details of impulsive noise accurately. But, the degradation caused by impulse-noise in DVB systems is dependent on the total energy of noise within one OFDM symbol-block period, irrespective of its probabilistic distribution. This fact has been explored and justified in [270], [389]–[391], by utilizing the concept of noise bucket effect, while considering that the impulse-noise can be precisely modelled as the gated Gaussian-noise.

In practice, SFBC based communication systems are observed to outperform the STBC based transmission systems under fast-fading channels [392], [393]. Therefore, SFBC-OFDM is quite suitable technique for the wireless systems working under the time-selective fading channels; and STBC-OFDM is much reliable scheme for the communication systems working under the frequency-selective fading channels [357]. But, both transmitter diversity techniques require availability of the channel-state-information (CSI) at receiver for the appropriate demodulation and decoding of information symbols. In wireless communication, the estimated/predicted channel response may be noisy and outdated because of the delay in getting CSI to the transmitter [313].

Imperfect CSI comes into picture due to the noisy and time-varying nature of fading channels. Torabi *et al.* [143] have proposed the closed-form expressions for the average bit-error-rate (BER) of SFBC-OFDM system working under the Rayleigh fading environment, which take the channel estimation error into consideration. Moreover, the BER performance deterioration that results from imperfect CSI at the receiver has also been quantified, in the presence of additive-white-Gaussian-noise (AWGN) [143], [313].

The combination of OFDM and antenna-diversity/spatial-diversity boosts the total signal-to-noise-ratio (SNR) to suppress the impulse-noise effects [321]–[323]. The weak impulse-noise can be tackled by utilizing the cyclic-prefix (CP) based long OFDM symbol-block of length $(G+N)$ with fixed time-period $\left(T=(G+N)T_s\right)$, in which, the total noise energy gets spread over the simultaneously transmitted N subcarriers, irrespective of the impulse-noise energy distribution [323]. Here, N also indicates the length of basic OFDM symbol-block without CP, T_s is the sampling interval (which is also equal to the duration of one digitally modulated information symbol, such that the corresponding symbol transmission bandwidth is $B_s \simeq 1/T_s$ Hz), $G \geq L-1$ is the length of CP, and L is the number of multipaths. If number of subcarriers is increased for the long OFDM symbol-block, then impulse energy per subcarrier gets reduced due to the discrete-Fourier-transform (DFT) operation at receiver. The probability distribution of output noise is observed to be approximately Gaussian due to the impulse-noise energy spreading caused by DFT operation, based on the noise bucket effect [389]. Therefore in this chapter, we focus on

- *average BER performance analysis of the SFBC-OFDM systems using M-ary PSK (MPSK) and M-ary QAM (MQAM) schemes, working over the Rayleigh fading multipath channels under the impulsive environment (an extension of the research work presented in [143], [394]).*
- *simulation results to investigate the BER performance of SFBC – OFDM system for the Rayleigh as well as Nakagami-m fading channels. (Nakagami-m fading channel modelling and its simulation procedure are also detailed).*

Nakagami-*m* distribution has gained widespread applications in the modelling of physical fading radio channels, in which, the magnitude of tap-coefficients of the channel impulse response can be modelled as Nakagami-*m* random-variables (RVs) with the fading parameter m and mean power Ω [395]. The magnitude of the DFT of channel impulse response can be modelled as Nakagami-*m* RVs with same fading parameter m [396], [397]. While dealing with OFDM systems, its analysis has been facilitated by the circular symmetry of complex Nakagami-*m* RVs due to the uniform phase distribution assumptions [398], which is quite different from [399]. Here, the parameter m controls the severity of amplitude fading. The value $m<1$ corresponds to the

fading more severe than the Rayleigh fading, and $m>1$ corresponds to relatively less severe fading [314]. However, the value $m=1$ leads to the well-known Rayleigh fading paradigm. The proposed research work is motivated by the BER approximations reported by Chung *et al.* [394] and Torabi *et al.* [143], [400] for OFDM systems working under rapidly fading channels.

This chapter is organized as follows. In Section 4.2, we first give details about the system model for uncoded OFDM system working under impulsive environment. The main focus is on the impact of impulse-noise and imperfect CSI on the performance of OFDM systems working over fading channels. Section 4.3 describes the system model for SFBC–OFDM system working under impulsive environment. The mathematical expressions for the average BER and the effective/normalized instantaneous SNR per subchannel are presented for the SFBC–OFDM wireless systems, while utilizing M-ary QAM and M-ary PSK digital modulation techniques [46], [401]–[405] under Rayleigh fading environment in the presence of impulse-noise and imperfect CSI (*i.e.,* using noisy channel estimates) at the receiver. Simulation outcomes are presented in Section 4.4. Finally, summary of the chapter is provided in Section 4.5.

4.2 System Model for Uncoded OFDM System Working Under Impulsive Environment

Let us consider an uncoded cyclic-prefix (CP) based OFDM system [270], [320]–[323], [389], [402], in which, the received time-domain OFDM signal sample is expressed as

$$r(n)=h(n)*s(n)+w(n)+imp(n) \tag{4.1}$$

where, $s(n)$ is the time-domain OFDM signal sample at the nth instant of time, which is assumed to exhibit zero-mean and variance σ_s^2 (such that its energy is represented as $E_s=\sigma_s^2 T_s \simeq \sigma_s^2/B_s$), $h(n)$ is the channel impulse response with "L" zero-mean complex tap-coefficients $h_l(n)=h_l$ exhibiting variance $\sigma_{hl}^2=(1/2)E\left[h_l h_l^*\right]=(1/L)$ (total number of resolvable significant multipaths is L), "*" is the linear convolution sum operator in Eq.(4.1), $w(n)$ is the inevitable zero-mean equivalent lowpass AWGN with variance $\sigma_w^2=(1/2)E\left[w(n)w^*(n)\right]$. Here, the autocorrelation function of AWGN samples is $R_{ww}(\tau)=N_o B_s\ sinc(B_s\tau)$, in which, N_o is the power spectral density of equivalent lowpass complex AWGN (where, $N_o/2$ is the variance of real/imaginary part of AWGN per unit bandwidth) [331], [357]. Its limiting form is viewed as $R_{ww}(\tau)\big|_{B_s\to\infty}=N_o\delta(\tau)$, where δ is the Dirac delta function. The impulse-noise $imp(n)$ is considered to exhibit zero-mean and variance $\hat{\sigma}_i^2=(1/2)E\left[imp(n)imp^*(n)\right]$ with unknown

distribution function [389]; where, $E[.]$ is the expectation or ensemble average operator [384], and $(.)^*$ is the conjugate operator. Based on the OFDM technology concepts of CP removal and normalized N-point DFT processing [357], [401], the received frequency-domain signal sample is represented as

$$R\{k\} = H\{k\}\,S\{k\} + W\{k\} + Imp\{k\} \qquad \text{with } k = 0,1,2,.....,N-1 \qquad (4.2)$$

where, $R\{k\} = \frac{1}{\sqrt{N}}\sum_{n=0}^{N-1} r(n)\exp\left(\frac{-j2\pi kn}{N}\right)$, $S\{k\} = \frac{1}{\sqrt{N}}\sum_{n=0}^{N-1} s(n)\exp\left(\frac{-j2\pi kn}{N}\right)$,

$H\{k\} = \sum_{l=0}^{L-1} h_l \exp\left(\frac{-j2\pi kl}{N}\right)$ with $k = 0,1,2,.....,N-1$,

$W\{k\} = \frac{1}{\sqrt{N}}\sum_{n=0}^{N-1} w(n)\exp\left(\frac{-j2\pi kn}{N}\right)$ with zero-mean and variance $\sigma_w^2 = \sigma_W^2$,

$Imp\{k\} = \frac{1}{\sqrt{N}}\sum_{n=0}^{N-1} imp(n)\exp\left(\frac{-j2\pi kn}{N}\right)$ with zero-mean and variance

$\sigma_{Imp}^2 = (1/2)E\left[Imp\{k\}\,Imp^*\{k\}\right] = (1/2N)\sum_{n=0}^{N-1} E\left[imp(n)\,imp^*(n)\right] = (N_i/N)\hat{\sigma}_i^2$ with

$\mu = (N_i/N)$

Here, N_i is the average number of impulses occurring randomly in a single OFDM symbol-block period. This impulse-noise component is found to reveal Gaussian-distribution at the output of DFT operator block, due to the noise bucket effect [323], [389]. In matrix form, Eq.(4.2) can be rewritten as

$$\vec{R} = \vec{H}\vec{S} + \vec{W} + \vec{Imp} \qquad (4.3)$$

where, $\vec{R} = \left[R\{0\}, R\{1\}, ..., R\{N-1\}\right]^T$, $\vec{S} = \left[S\{0\}, S\{1\}, ..., S\{N-1\}\right]^T$,

$\vec{H} = diag\left[H\{0\}, H\{1\}, ..., H\{N-1\}\right]_{N\times N}$, $\vec{W} = \left[W\{0\}, W\{1\}, ..., W\{N-1\}\right]^T$,

$\vec{Imp} = \left[Imp\{0\}, Imp\{1\}, ..., Imp\{N-1\}\right]^T$ with $[.]^T$ as the matrix transpose operator.

Invoking the concept of imperfect channel-state-information at the receiver [313], [402], [403], it is considered that $\Delta\vec{H} = \vec{H} - \hat{H}$, where $\Delta\vec{H}$ is the channel estimation error/noise matrix, and $\hat{H}$ is the estimated channel impulse response coefficient matrix. It is apparent that $E\left[\left(\vec{H} - \hat{H}\right)\left(\vec{H} - \hat{H}\right)^H \Big/ \hat{H}\right] = \sigma_\varepsilon^2 \vec{I}$ with identity-matrix $\vec{I}$ and $E\left[H/\hat{H}\right] = \hat{H}$. Here, σ_ε^2 is the variance of zero-mean channel estimation error/noise [143]. Therefore, Eq.(4.3) can be rearranged as

$$\vec{R} = \hat{H}\vec{S} + \left\{\Delta\vec{H}\vec{S} + \vec{W} + \vec{I}mp\right\} \qquad \text{with } \vec{H} = \hat{H} + \Delta\vec{H} \tag{4.4}$$

Here, total noise component is described as

$$\vec{\eta} = \Delta\vec{H}\vec{S} + \vec{W}Imp \qquad \text{with } \vec{W}Imp = \vec{W} + \vec{I}mp \tag{4.5}$$

$$\vec{\eta} = \left[\eta\{0\}, \eta\{1\}, ..., \eta\{k\}, ..., \eta\{N-1\}\right]^T$$

If signal-to-noise-ratio is defined as $\hat{\gamma}_s = E_s / \hat{N}_o = \sigma_s^2 / \left(\hat{N}_o B_s\right)$, then it can be statistically demonstrated in frequency-domain that total noise component possesses the Gaussian-distribution [389], [402], [406] with zero-mean and variance per unit bandwidth $\sigma_\eta^2 = \hat{N}_o \left\{1 + \sigma_\varepsilon^2 \hat{\gamma}_s\right\}$ (See Appendix-B); where $\hat{N}_o = N_o + \mu\sigma_i^2$, in which the "effective impulse-noise variance" is $\sigma_i^2 = \hat{\sigma}_i^2 / B_s$.

The total noise component statistics can be utilized in deriving the average bit error rate expression for the SFBC-OFDM systems working under impulsive environment (as illustrated in Fig. 4.1), in subsequent section. The real and imaginary independent components of total complex noise $\eta\{k\}$ in Eq.(4.5) exhibit $\mathbb{N}\left(mean = 0; variance = \left(\hat{N}_o/2\right)\left(1 + \sigma_\varepsilon^2 \hat{\gamma}_s\right)\right)$ per unit bandwidth, which are substantially dependent on the statistics/characteristics of unintended impulse-noise.

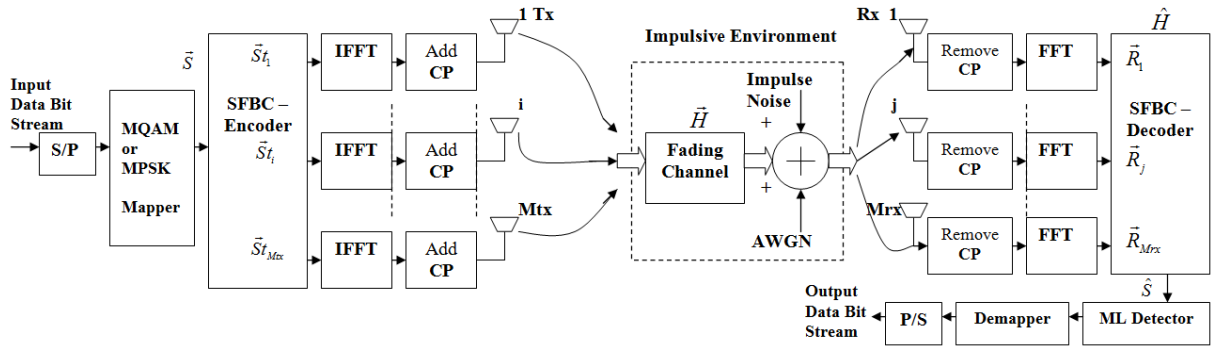

Fig. 4.1: $Mtx \times Mrx$ **SFBC-OFDM system working over wireless fading channels in impulsive environment utilizing imperfect CSI matrix** $\hat{H}$ **.**

4.3 System Model for SFBC–OFDM System Working Under Impulsive Environment

Let us consider an SFBC-OFDM system with $Mtx = 2$ transmitter-antennas (Tx) and Mrx receiver-antennas (Rx). The data bit stream is first mapped by using the MQAM or MPSK digital modulation technique based constellations. The resultant information symbol stream is then converted from serial-to-parallel (S/P), and subsequently, these are fed to an SFBC encoder. For exploiting the space-frequency diversity, the input blocks are encoded as

$$\vec{St}_1 = \left[+S\{0\} \;\; -S^*\{1\}, \;\; +S\{2\} \;\; -S^*\{3\}, \;\; ..... \;\; , +S\{N-2\} \;\; -S^*\{N-1\} \right]^T$$

$$\vec{St}_2 = \left[+S\{1\} \;\; +S^*\{0\}, \;\; +S\{3\} \;\; +S^*\{2\}, \;\; ..... \;\; , +S\{N-1\} \;\; +S^*\{N-2\} \right]^T$$

These two encoded blocks of length N are processed using a normalized N -point IFFT operation, and then the cyclic-prefix (CP) of length $G \geq L-1$ is appended in the beginning of resultant time-domain OFDM symbol-blocks before transmitting them from the transmitter antennas $Tx1$ and $Tx2$ respectively (here, L is the number of multipaths encountered in the wireless channel). The CP helps in mitigating problems arising due to the intersymbol-interference (ISI) and interblock-interference (IBI).

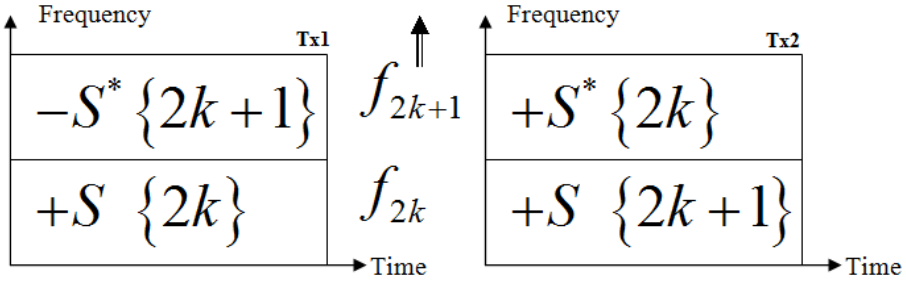

Fig. 4.2: Illustration of SFBC-OFDM with $(Mtx=2)\times Mrx$ antenna system.

At the receiving end, the CP is removed first to convert the linear convolution sum in Eq.(4.1) to the circular convolution sum [357], [401]. The wireless channel is considered to be static for an OFDM symbol-block period. Further, the output of DFT operation corresponding to the *jth* receiver antenna is expressed as

$$\vec{R}_j = \vec{H}_{j,1}\vec{St}_1 + \vec{H}_{j,2}\vec{St}_2 + \vec{W}_j + \vec{Imp}_j \qquad (4.6)$$

where, $\vec{R}_j = \left[R_j\{0\}, R_j\{1\}, ..., R_j\{N-1\} \right]^T$ is the received signal at *jth* receiver antenna, $\vec{H}_{j,i} = diag\left[H_{j,i}\{0\}, H_{j,i}\{1\}, ..., H_{j,i}\{N-1\} \right]_{N\times N}$ denotes the diagonal matrix with elements corresponding to the channel impulse response between the *ith* transmitter antenna and *jth* receiver antenna, $\vec{W}_j = \left[W_j\{0\}, W_j\{1\}, ..., W_j\{N-1\} \right]^T$

and $\vec{Imp}_j = \left[Imp_j\{0\}, Imp_j\{1\}, ..., Imp_j\{N-1\} \right]^T$ indicates the AWGN samples and impulsive noise samples at the *jth* receiver antenna respectively. Using a scheme analogous to Alamouti's received signal combining technique [46] to exploit the space-frequency diversity [73], [100], [143], it can be shown that the input to maximum-likelihood (ML) decoder for symbol-detection is

$$\hat{S}\{2k\} = \sum_{j=1}^{Mrx}\left[H_{j,1}^{*}\{2k\} R_j\{2k\} + H_{j,2}\{2k\} R_j^{*}\{2k+1\}\right] \tag{4.7}$$

$$\hat{S}\{2k+1\} = \sum_{j=1}^{Mrx}\left[H_{j,2}^{*}\{2k+1\} R_j\{2k\} - H_{j,1}\{2k+1\} R_j^{*}\{2k+1\}\right] \tag{4.8}$$

Akin to STBC decoding scheme in [73], [100], [143], [400], it is assumed that channel gain coefficients between two adjacent subchannels in SFBC-OFDM system are approximately equal i.e., $H_{j,i}\{2k+1\} = H_{j,i}\{2k\}$ for $i = 1, 2$. Substitution of this assumption in Eqs.(4.7)–(4.8) results in

$$\begin{aligned}\hat{S}\{2k\} = &\sum_{j=1}^{Mrx}\left(\left|H_{j,1}\{2k\}\right|^2 + \left|H_{j,2}\{2k\}\right|^2\right) S\{2k\} \\ &+ \sum_{j=1}^{Mrx}\left\{ H_{j,1}^{*}\{2k\}\vec{W}Imp_j\{2k\} + H_{j,2}\{2k\}\vec{W}Imp_j^{*}\{2k+1\}\right\}\end{aligned} \tag{4.9}$$

with $\vec{W}Imp_j = \vec{W}_j + \vec{I}mp_j$ (as in Eqs.(4.5)–(4.6)).

$$\begin{aligned}\hat{S}\{2k+1\} = &\sum_{j=1}^{Mrx}\left(\left|H_{j,1}\{2k\}\right|^2 + \left|H_{j,2}\{2k\}\right|^2\right) S\{2k+1\} \\ &+ \sum_{j=1}^{Mrx}\left\{ H_{j,2}^{*}\{2k\}\vec{W}Imp_j\{2k\} - H_{j,1}\{2k\}\vec{W}Imp_j^{*}\{2k+1\}\right\}\end{aligned} \tag{4.10}$$

By utilizing Eqs.(4.9) and (4.10), the benefit of transmitter antenna diversity can be achieved in case of the SFBC–OFDM communication systems, which provides it an edge over the traditional OFDM systems working under identical scenario.

4.3.1 BER Performance of SFBC-OFDM System Using MQAM

Let us consider an SFBC-OFDM system using the M-ary quadrature-amplitude-modulation (MQAM) digital modulation scheme, which is equipped with *Mtx* number of transmitting antennas and *Mrx* number of receiving antennas. With imperfect channel-state-information $\hat{H}$ in a MIMO-OFDM system, the lower bound for the mutual information is reported in [143], [404], [405] as

$$I_L\left(\vec{S};\vec{R}\middle|\hat{H}\right) = \log_2\left[\det\left\{\vec{I}_{NMrx} + \frac{\hat{H}\hat{H}^H}{Mtx}\frac{\hat{\gamma}_s}{1+\hat{\gamma}_s\sigma_\varepsilon^2}\right\}\right] \tag{4.11}$$

$$\text{with } E\left[\left(\vec{H}-\hat{H}\right)\left(\vec{H}-\hat{H}\right)^H \middle/ \hat{H}\right] = \sigma_\varepsilon^2\vec{I}_{NMrx} \tag{4.12}$$

where, $\vec{I}_{NMrx}$ is the $NMrx \times NMrx$ dimensional identity-matrix. For further analysis, the channel estimation error/noise [313] is considered as in Eq.(4.4), which leads to the modification of Eq.(4.6) as

$$\vec{R}_j = \hat{H}_{j,1}\vec{S}t_1 + \hat{H}_{j,2}\vec{S}t_2 + \Delta\vec{H}_{j,1}\vec{S}t_1 + \Delta\vec{H}_{j,2}\vec{S}t_2 + \vec{W}_j + \vec{I}mp_j \text{ with } \vec{H}_{j,i} = \hat{H}_{j,i} + \Delta\vec{H}_{j,i} \quad (4.13)$$

$$\vec{R}_j = \hat{H}_{j,1}\vec{S}t_1 + \hat{H}_{j,2}\vec{S}t_2 + \vec{\eta}_j \quad (4.14)$$

with $\vec{\eta}_j = \Delta\vec{H}_{j,1}\vec{S}t_1 + \Delta\vec{H}_{j,2}\vec{S}t_2 + \vec{W}_j + \vec{I}mp_j = \Delta\vec{H}_{j,1}\vec{S}t_1 + \Delta\vec{H}_{j,2}\vec{S}t_2 + \vec{W}Imp_j$

While executing the decoding operation to detect the information symbols [46], [73], [100], [143], we incorporate the estimated channel-state-information matrix $\hat{H}^H$ (*i.e.,* noisy CSI or imperfect CSI [313], [402]). However for an SFBC-OFDM system, we also need to take into account the code-rate R_c while considering the equivalent scaled noisy channel (similar to the STBC code-rate in [55]) induced by the SFBC for the complex constellation [143], [407]. It follows that

$$\hat{S}\{k\} = \frac{1}{R_c}\sum_{j=1}^{Mrx}\sum_{i=1}^{Mtx}\left|\hat{H}_{j,i}\{k\}\right|^2 S\{k\} + \hat{\eta}\{k\} \quad (4.15)$$

with SNR at the kth subchannel as

$$\gamma_k = \frac{1}{R_c}\sum_{j=1}^{Mrx}\sum_{i=1}^{Mtx}\left|\hat{H}_{j,i}\{k\}\right|^2 \frac{\hat{\gamma}_s}{\left(1+\sigma_\varepsilon^2\hat{\gamma}_s\right)} \quad (4.16)$$

where, $\hat{H}_{j,i}\{k\}$ indicates the estimated channel impulse response between the ith transmitter antenna and jth receiver antenna, the real and imaginary components of the scaled total noise $\hat{\eta}\{k\}$ exhibit $\mathbb{N}\left(mean = 0; variance = \left(\hat{N}_o B_s / 2R_c\right)\left(1+\sigma_\varepsilon^2\hat{\gamma}_s\right)\sum_{j=1}^{Mrx}\sum_{i=1}^{Mtx}\left|\hat{H}_{j,i}\{k\}\right|^2\right)$ [400], [407]. The ML decoder minimizes the following decision metric

$$\left|\hat{S}\{k\} - S\{k\}\right|^2 \text{ for } k = 0,1,2,.....,N-1 \quad (4.17)$$

The total energy of symbols transmitted through all the transmitter antennas can be normalized to Mtx, therefore we can represent the effective/normalized instantaneous SNR corresponding to kth subcarrier/subchannel as

$$\hat{\gamma}_k = \frac{\gamma_k}{Mtx} = \frac{1}{R_c Mtx}\sum_{j=1}^{Mrx}\sum_{i=1}^{Mtx}\left|\hat{H}_{j,i}\{k\}\right|^2 \frac{\hat{\gamma}_s}{\left(1+\sigma_\varepsilon^2\hat{\gamma}_s\right)} \quad (4.18)$$

The effective random capacity [55] associated with kth subcarrier/subchannel can be expressed as

$$C_k = R_c \log_2\left(1+\hat{\gamma}_k\right) \; bps/Hz \quad (4.19)$$

Further, it is considered that M-ary QAM digital modulation technique (along with Gray bit-mapping) is incorporated while assigning β bits/symbol to each subchannel, where the total number of information symbols is $M = 2^{\beta}$ (those information symbols exhibit equal *a priori* probability of occurrence). The instantaneous information symbol-error-rate (SER) [331] associated with *kth* subcarrier/subchannel is represented as

$$SER\{k\} = P_{M_k} = 1-\left(1-P_{\sqrt{M}}\right)^2 \simeq 2P_{\sqrt{M}} \tag{4.20}$$

Here, $P_{\sqrt{M}}$ is the probability of error of a $\sqrt{M}$ -ary PAM with one-half the average power in quadrature signal of the received QAM signal [331], such that

$$P_{\sqrt{M}} = 2\left(1-\frac{1}{\sqrt{M}}\right)Q\left(\sqrt{\frac{3\hat{\gamma}_k}{(M-1)}}\right) \tag{4.21}$$

where, $Q(\hat{t}) = (1/2)erfc\left(\hat{t}/\sqrt{2}\right)$ is the frequently used function to obtain area under the tail of Gaussian probability density function for $\hat{t} \geq 0$, with the complementary error function $erfc(\hat{t}) = \frac{2}{\sqrt{\pi}}\int_{\hat{t}}^{\infty}\exp\left(-\hat{t}^2\right)d\hat{t}$. However, the approximate value of information symbol error rate corresponding to an OFDM symbol-block with N subcarriers is calculated as

$$SER_N = (1/N)\sum_{k=0}^{N-1} SER\{k\} \tag{4.22}$$

where, $SER\{k\}$ is the instantaneous SER of *kth* subchannel in an OFDM information symbol-block. As β bits/symbol are assigned to each subchannel, therefore the approximate value of BER for the underlying MQAM-SFBC-OFDM system (using Eqs.(4.20) and (4.22)) working under the fading conditions is obtained as

$$BER_{MQAM\_N} = (1/N\beta)\sum_{k=0}^{N-1} SER\{k\} = (1/N\beta)\sum_{k=0}^{N-1} P_{M_k} \tag{4.23}$$

Using Eqs.(4.20)–(4.23), it can be demonstrated that

$$BER_{MQAM\_N} \simeq (4/N\beta)\sum_{k=0}^{N-1} Q\left(\sqrt{\frac{3\hat{\gamma}_k}{(M-1)}}\right)\left(1-\frac{1}{\sqrt{M}}\right) \tag{4.24}$$

The above equation can also be represented as

$$BER_{MQAM\_N} = (2/N\beta)\sum_{k=0}^{N-1} erfc\left(\sqrt{\frac{1.5\hat{\gamma}_k}{\left(2^{\beta}-1\right)}}\right)\left(1-\frac{1}{\sqrt{2^{\beta}}}\right) \tag{4.25}$$

Based on Eq.(4.24), the upper bound on BER [331], [384] of MQAM-SFBC-OFDM system working over the frequency-selective fading channels is expressed as

$$BER_{MQAM\_N} < BER_{MQAM}\left(Tight\ Upper\ Bound\right) \simeq \left(4/N\beta\right)\sum_{k=0}^{N-1} Q\left(\sqrt{\frac{3\hat{\gamma}_k}{\left(2^{\beta}-1\right)}}\right) \tag{4.26}$$

$$\text{or } BER_{MQAM\_N} < BER_{MQAM}\left(Tight\ Upper\ Bound\right) \simeq \left(2/N\beta\right)\sum_{k=0}^{N-1} erfc\left(\sqrt{\frac{1.5\hat{\gamma}_k}{\left(2^{\beta}-1\right)}}\right) \tag{4.27}$$

By utilizing curve-fitting (as in [394]), Eq.(4.25) can be further tightly approximated as

$$BER_{MQAM\_N} \approx \left(0.2/N\right)\sum_{k=0}^{N-1} \exp\left(-\frac{1.6\hat{\gamma}_s \sum_{j=1}^{Mrx}\sum_{i=1}^{Mtx}\left|\hat{H}_{j,i}\left\{k\right\}\right|^2}{R_c Mtx\left(2^{\beta}-1\right)\left(1+\sigma_{\varepsilon}^2\hat{\gamma}_s\right)}\right) \tag{4.28}$$

Eventually, average value of BER can be evaluated by using

$$BER_{MQAM\_Avg} = E\left[\, BER_{MQAM\_N}\,\right] \tag{4.29}$$

If the estimated channel tap-coefficients $\hat{H}_{j,i}\left\{k\right\}$ are considered to be independent and identically distributed random variables exhibiting zero-mean and unity variance (Rayleigh distribution [384]), then it can be shown that the closed-form expression [143], [394] for average BER is

$$BER_{MQAM\_Avg} \approx 0.2\left(1+\frac{1.6\hat{\gamma}_s}{R_c Mtx\left(2^{\beta}-1\right)\left(1+\sigma_{\varepsilon}^2\hat{\gamma}_s\right)}\right)^{-MrxMtx} \tag{4.30}$$

where, $\hat{\gamma}_s = E_s/\hat{N}_o = \sigma_s^2/\left(\hat{N}_o B_s\right)$ with $\hat{N}_o = N_o + \mu\sigma_i^2$ in the presence of noisy channel estimates, AWGN and dominating impulsive noise.

4.3.2 BER Performance of SFBC-OFDM System Using MPSK

Akin to aforementioned analysis under impulsive environment, the approximate value of BER for the underlying MPSK-SFBC-OFDM system working under fading conditions is expressed as

$$BER_{MPSK\_N} = \left(2/N\beta\right)\sum_{k=0}^{N-1} Q\left(\sqrt{\frac{2\hat{\gamma}_s \sum_{j=1}^{Mrx}\sum_{i=1}^{Mtx}\left|\hat{H}_{j,i}\left\{k\right\}\right|^2}{R_c Mtx\left(1+\sigma_{\varepsilon}^2\hat{\gamma}_s\right)}}\sin\left(\frac{\pi}{2^{\beta}}\right)\right) \tag{4.31}$$

By utilizing curve-fitting (as in [394]), the above equation can be further tightly approximated as

$$BER_{MPSK\_N} \approx \left(0.2/N\right)\sum_{k=0}^{N-1} \exp\left(-\frac{7\hat{\gamma}_s \sum_{j=1}^{Mrx}\sum_{i=1}^{Mtx}\left|\hat{H}_{j,i}\left\{k\right\}\right|^2}{R_c Mtx\left(2^{1.9\beta}+1\right)\left(1+\sigma_{\varepsilon}^2\hat{\gamma}_s\right)}\right) \tag{4.32}$$

Eventually, the average value of BER can be evaluated by using

$$BER_{MPSK\_Avg} = E\left[BER_{MPSK\_N} \right] \tag{4.33}$$

Similar to the procedure opted for the calculation of BER_{MQAM_Avg} with Rayleigh distributed estimated channel tap-coefficients $\hat{H}_{j,i}\{k\}$ [384], the above equation can be simplified to obtain a closed-form expression [143], [394] for the average BER as

$$BER_{MPSK\_Avg} \approx 0.2\left(1+\frac{7\hat{\gamma}_s}{R_c Mtx\left(2^{1.9\beta}+1\right)\left(1+\sigma_\varepsilon^2\hat{\gamma}_s\right)} \right)^{-MrxMtx} \tag{4.34}$$

Here, the average value of BER for SFBC-OFDM system is undoubtedly dependent on the impulse-noise statistics through the factor $\hat{\gamma}_s = E_s / \hat{N}_o = \sigma_s^2 / \left(\hat{N}_o B_s \right)$.

4.4 Simulation Results and Discussion

We shall investigate the bit error rate performance of space-frequency block-coded OFDM system working over the wireless fading channels under the impulsive environment. In time-domain, the impulse response of the channel between the ith ($i = 1, 2, ..., Mtx$) transmitter antenna and jth receiver antenna ($j = 1, 2, ..., Mrx$) is conventionally [331] represented as

$$h_{j,i}(t) = \sum_{l=0}^{L-1} \alpha_{l;j,i}(t)\delta\left(t - \tau_l(t)\right) \tag{4.35}$$

where, $\alpha_{l;j,i}(t)$ is the channel tap-coefficient, $\tau_l(t)$ is the corresponding time-delay factor of the lth path, and $L = 3$ is the total number of significant resolvable paths (here, the cyclic-prefix length is fixed at $G \geq L-1$ [401]). In case of Rayleigh fading channel, the channel tap-coefficients $\alpha_{l;j,i}(t)$ are considered to be complex Gaussian random variables with zero-mean and variance $\sigma_{hl}^2 = 1/L$ (exhibiting equal power). In the presented research work, each time-delay factor $\tau_l(t)$ is assumed to be the integer multiples of information symbol duration T_s, which is also equal to the sampling interval [331]. It is noteworthy that the tap-coefficients of channel impulse response remain static during each CP-OFDM symbol-block period *i.e.,* for the time-period $T = (G+N)T_s$. For simulation of Rayleigh fading environment, the channel tap-coefficient pertaining to each resolvable path is modelled as an independent stationary ergodic first-order Markov/ autoregressive process (AR1) with correlation coefficient/ fading parameter $\bar{\alpha}_h = J_o(2\pi f_D T)$, which follows that

$$\alpha_{l;j,i}(p) = \bar{\alpha}_h \alpha_{l;j,i}(p-1) + \nu h_{l;j,i}(p) \tag{4.36}$$

where, $\alpha_{l;j,i}(p)$ is the value of channel tap-coefficient in pth CP-OFDM symbol-block period, $J_o(.)$ is the zeroth-order Bessel-function of first-kind, f_D is the maximum value of Doppler-spread/frequency [335], [348], [349], $f_D T = 0.01$ is the fade-rate (i.e., under time-varying channel conditions), and $vh_{l;j,i}$ is the zero-mean stationary ergodic complex process-noise (Gaussian white noise) with variance $\sigma_{vh}^2 = \sigma_{hl}^2 \left\{1 - \left|\bar{\alpha}_h\right|^2\right\}$ [349]. Here, $\alpha_{l;j,i}$ is considered to be a zero-mean and $\sigma_{hl}^2 = 1/L$ variance complex Gaussian process, to maintain the constant signal power constraint (propagating through the resolvable multiple paths of wireless channel).

The number of transmitter antennas is considered to be $Mtx = 2$ and the number of receiver antennas is kept $Mrx = 1$, which leads to $R_c = 1$ by using the technique similar to Alamouti's space-time block-coded scheme [46]. Before transmission, the data bit stream is processed by using an M-ary digital modulator to generate the information symbols (as shown in Fig. 4.1), and the presented research work is carried out by employing the 2-PSK (BPSK), 4-PSK (QPSK), 16-QAM and 64-QAM modulation schemes. However, the value of symbol energy E_s is kept unity for the underlying system. The average number of impulses encountered during an OFDM symbol-block period is considered to be 1 or 3, and we calculate $\mu = N_i / N$ accordingly. The presented results are based on the ensemble average of 250 independent Monte-Carlo simulation trials by utilizing different fading channel realizations, at different values of E_s/N_o, such that

$$Avg\left\{BER\right\}\Big|_{E_s/N_o} = E\left\{BER\right\}\Big|_{E_s/N_o} \simeq \sum_{a=1}^{250} BER(a)\Big|_{E_s/N_o} \Big/ 250 \qquad (4.37)$$

***Case 1*:-** In first case, the variance of channel estimation error is assumed to be zero i.e., $\sigma_\varepsilon^2 = 0$ for perfect CSI at receiver. The number of subcarrirers/subchannels is kept fixed at $N = 128$, which results in $\mu = 1/128 = 0.0078125$ for the average number of impulses in an OFDM symbol-block period $N_i = 1$, and $\mu = 3/128 = 0.023438$ for $N_i = 3$. The effective impulse-noise variance is considered to be $10\log_{10}\sigma_i^2 = -7.5dB$. As occurrence of impulses adversely affects the BER performance of SFBC-OFDM communication systems, therefore $\Delta 0 N_i$ is the loss (dB) in terms of E_s/N_o at a particular value of BER, when N_i average number of impulses are encountered in a single OFDM symbol-block period with respect to the condition when $N_i = 0$. It follows that

$$\Delta 0 N_i = \left\{E_s/N_o \ \ at\ BER(z)\ \ with\ N_i = 0\ \right\} - \left\{E_s/N_o \ \ at\ BER(z)\ \ with\ N_i \neq 0\right\}. \qquad (4.38)$$

At $BER = 0.01$ and 16–QAM digital modulation scheme, the E_s/N_o values are found to be in the range $+18dB\ to\ +20dB$. It can be inferred from the simulation results presented in Fig. 4.3 that the approximate values of $\Delta 0N_i$ are $\Delta 01 = 0.4dB$ and $\Delta 03 = 1.35dB$, for $N_i = 1$ and $N_i = 3$ respectively. Further, the number of subcarriers/subchannels is kept fixed at $N = 512$, which leads to $\mu = 1/512 = 0.0019531$ for the average number of impulses in an OFDM symbol-block period $N_i = 1$, and $\mu = 3/512 = 0.0058594$ for $N_i = 3$. The effective impulse-noise variance is kept same i.e., $10\log_{10}\sigma_i^2 = -7.5dB$. At $BER = 0.01$ and 64–QAM digital modulation scheme, the SNR values are found to be in the range $+24dB\ to\ +26dB$, as shown in Fig. 4.4. The impact of impulse-noise gets alleviated with the increasing number of subcarriers in the same OFDM symbol-block period, which facilitates the usage of higher-order M-ary QAM schemes. It is apparent from the simulation outcomes presented in Fig. 4.4 that the approximate values of $\Delta 0N_i$ are $\Delta 01 = 0.44dB$ and $\Delta 03 = 1.46dB$, for $N_i = 1$ and $N_i = 3$ respectively. It is clear that the loss in terms of E_s/N_o increases at fixed BER, as the occurrence of average number of impulses in a single OFDM symbol-block duration elevates.

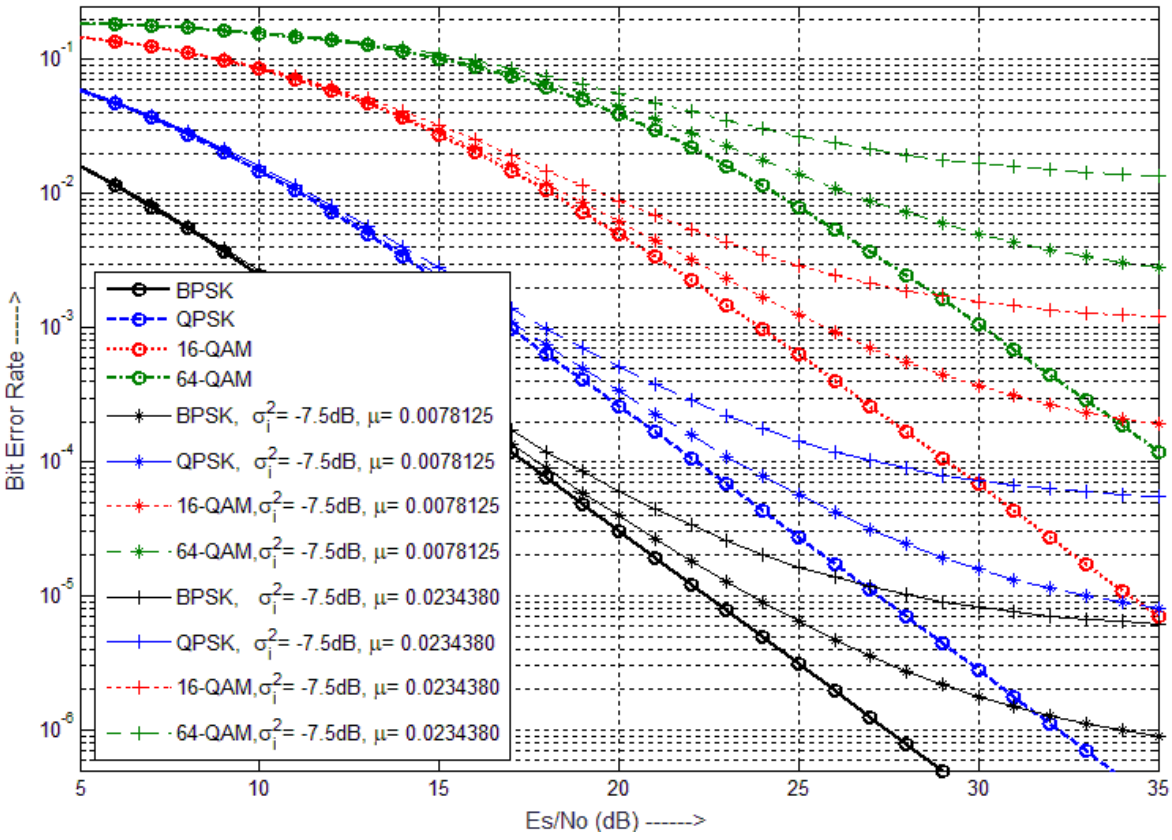

Fig. 4.3: BER vs. $E_s/N_o(dB)$ for $N = 128$ at different values of μ.

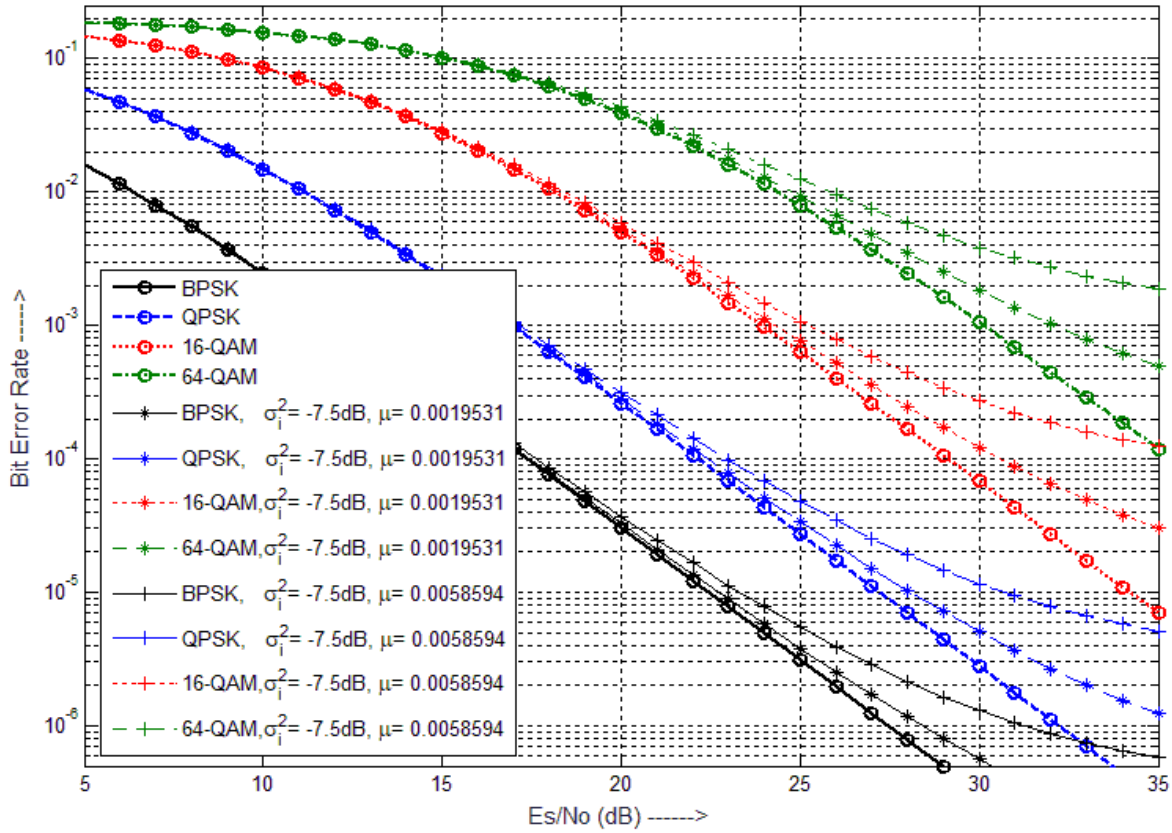

Fig. 4.4: BER vs. $E_s/N_o\,(dB)$ for $N=512$ at different values of μ.

***Case 2*:-** In second case, the variance of channel estimation error is assumed to be non-zero i.e., $\sigma_\varepsilon^2 \neq 0$ for imperfect CSI at receiver. The number of subcarrirers/subchannels is kept fixed at $N=64$, which results in $\mu = 1/64 = 0.015625$ for the average number of impulses in an OFDM symbol-block period $N_i = 1$, and $\mu = 3/64 = 0.046875$ for $N_i = 3$. The effective impulse-noise variance is considered to be $10\log_{10}\sigma_i^2 = -12.5dB$. At $E_s/N_o = +30dB$, $\sigma_\varepsilon^2 = 0.005$ and 16–QAM scheme, the BER values are found to be approximately $BER = 2.0\times10^{-3}$ for $N_i = 0$, $BER = 2.7\times10^{-3}$ for $N_i = 1$ and $BER = 4.0\times10^{-3}$ for $N_i = 3$, as shown in Fig. 4.5.

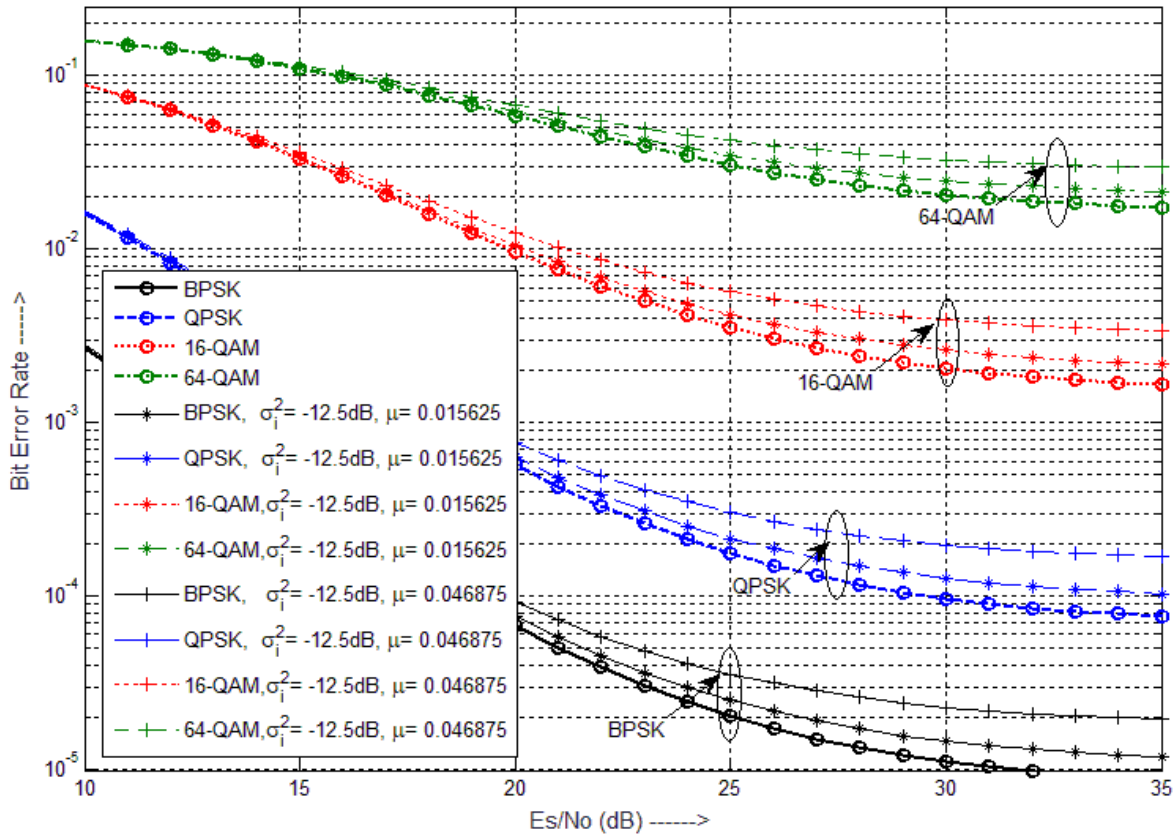

Fig. 4.5: BER vs. $E_s/N_o\,(dB)$ **for** $N=64$ **with imperfect CSI in the presence of impulse-noise.**

Subsequently, the number of subcarriers/subchannels is kept fixed at $N=256$, which leads to $\mu=1/256=0.0039063$ for the average number of impulses in an OFDM symbol-block period $N_i=1$, and $\mu=3/256=0.0117190$ for $N_i=3$. The effective impulse-noise variance is kept same i.e., $10\log_{10}\sigma_i^2=-12.5dB$. At $E_s/N_o=+30dB$, $\sigma_\varepsilon^2=0.005$ and 16–QAM scheme, the BER values are observed to be approximately $BER=2.0\times10^{-3}$ for $N_i=3$, $BER=2.25\times10^{-3}$ for $N_i=1$ and $BER=2.5\times10^{-3}$ for $N_i=3$, as shown in Fig. 4.6. Under similar conditions, the BER rate performance of underlying SFBC-OFDM system improves with the increasing number of subcarriers/subchannels [389] in the same OFDM symbol-block period, even under the availability of imperfect channel estimates at receiver.

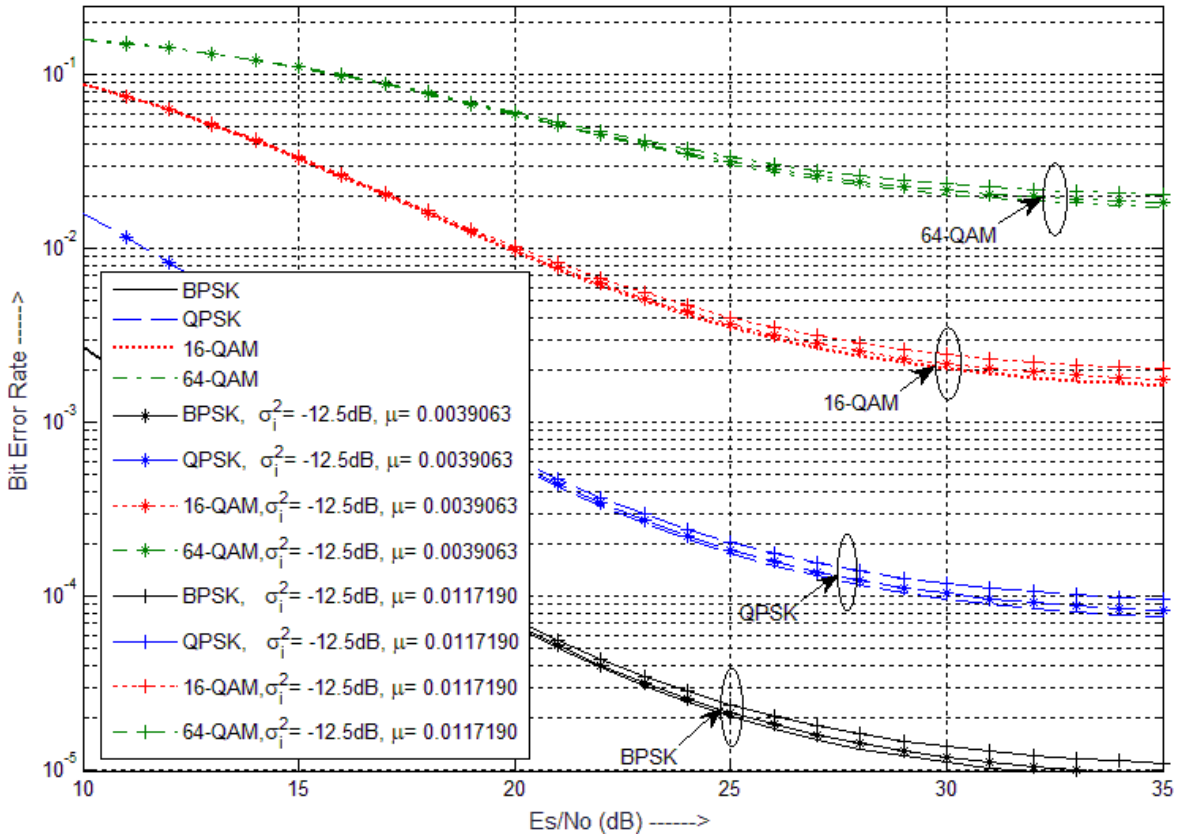

Fig. 4.6: BER vs. $E_s/N_o(dB)$ for $N=256$ with imperfect CSI in the presence of impulse-noise.

***Case 3*:-** In third case, the BER performance of SFBC-OFDM system is investigated at different values of channel estimation error variance, while keeping various attributes set at $E_s/N_o=+35dB$, $10\log_{10}\sigma_i^2=-12.5dB$, $N=128$, $N_i=1$ and $\mu=1/128=0.0078125$. The simulation results depicted for QPSK scheme (with $N_i=1$) in Fig. 4.7 clearly indicate that the approximate values of average bit error rate are observed to be $BER=8.5\times10^{-6}$ for $\sigma_\varepsilon^2=0.001$ and $BER=3.0\times10^{-4}$ for $\sigma_\varepsilon^2=0.01$. However for 16-QAM scheme under similar conditions (with $N_i=1$), the approximate values of average bit error rate are found to be $BER=2.0\times10^{-4}$ for $\sigma_\varepsilon^2=0.001$ and $BER=5.5\times10^{-3}$ for $\sigma_\varepsilon^2=0.01$.

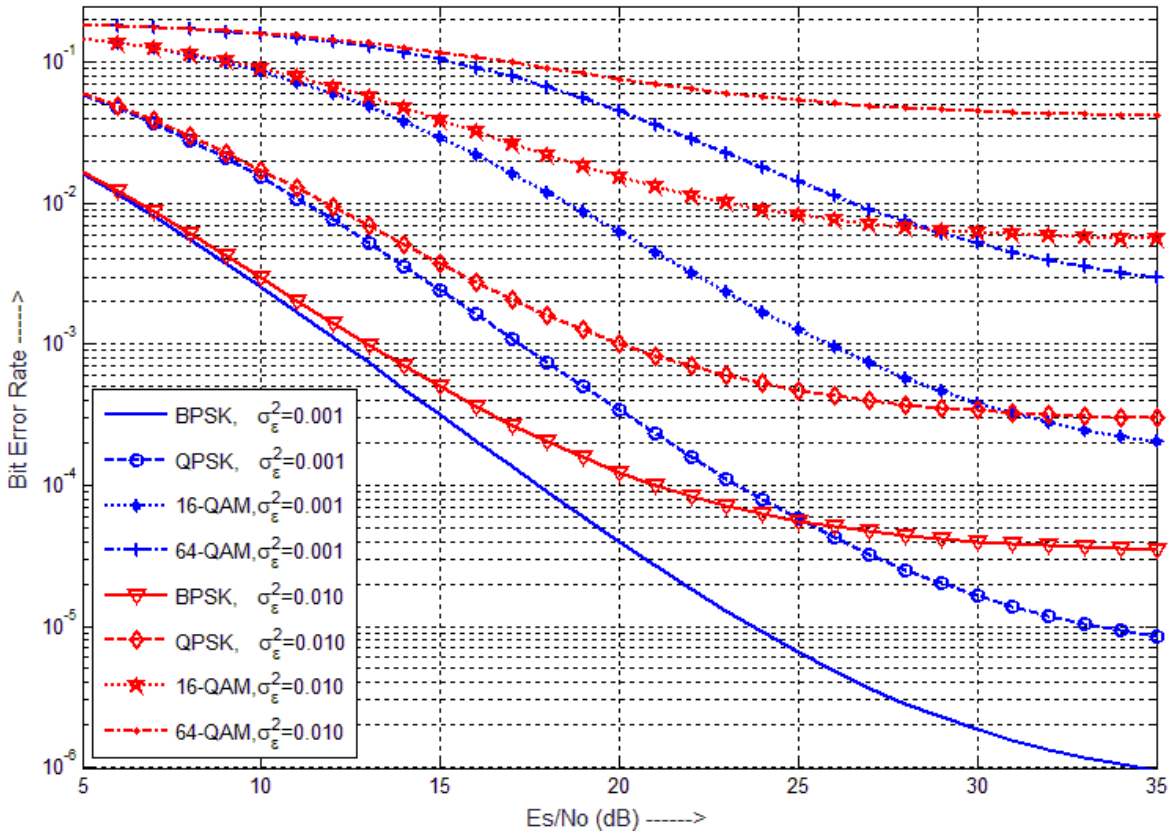

Fig. 4.7: BER vs. $E_s/N_o(dB)$ for $N=128$ at different values of channel estimation error variance.

Next, the number of subcarriers is increased to $N=512$, which results in $\mu=1/512=0.0019531$ for $N_i=1$. The simulation results illustrated for QPSK scheme (with $N_i=1$) in Fig. 4.8 show that the approximate values of average bit error rate are $BER=6.0\times10^{-6}$ for $\sigma_\varepsilon^2=0.001$ and $BER=3.0\times10^{-4}$ for $\sigma_\varepsilon^2=0.01$. However for 16-QAM scheme under similar scenario (with $N_i=1$), the approximate values of average bit error rate are found to be $BER=1.4\times10^{-4}$ for $\sigma_\varepsilon^2=0.001$ and $BER=5.5\times10^{-3}$ for $\sigma_\varepsilon^2=0.01$. It is noteworthy that the BER performance gets deteriorated substantially with the increasing value of the variance of channel estimation error, for both QPSK as well as 16-QAM schemes. The value of average BER is lower in case of QPSK based SFBC-OFDM system, as compared to 16-QAM based system. It is because of the reduced Euclidean distance between the signal constellation points in case of the 16-QAM digital modulation scheme as compared to the QPSK scheme.

However for the lower value of channel estimation error variance σ_ε^2, the increasing number of subcarriers helps in reducing the BER by combating the impulse-noise. It is due to spreading of impulse-noise [389] over more number of subcarriers at the output of DFT operation at receiver

(as shown in Fig. 4.1). But at the higher values of σ_{ε}^2, the BER performance of SFBC-OFDM system gets degraded significantly due to the adverse effects of channel estimation error/noise. Here, the adverse effects of channel estimation errors overwhelm the benefits of higher number of subcarriers, while performing information symbol-detection.

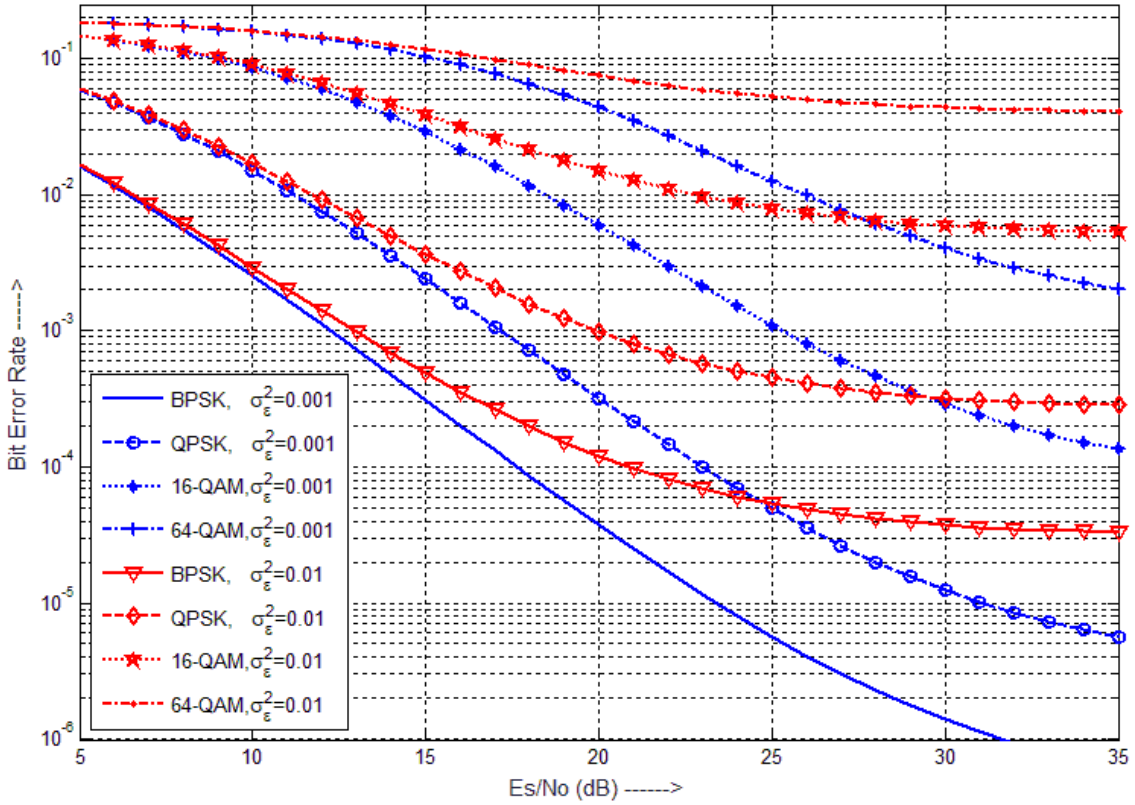

Fig. 4.8: BER vs. $E_s/N_o\,(dB)$ for $N=512$ at different values of channel estimation error variance.

***Case 4*:-** In the fourth case, we shall explore the bit error rate performance of SFBC-OFDM system working over the Nakagami-*m* fading channels under impulsive environment. We therefore focus on the statistics of encountered fading channel and its simulation. In a "brute force method" (computationally complex) for integer and half integer values of m, the square root of a sum of the squares of n zero-mean identically distributed Gaussian random variables is usually incorporated to generate the Nakagami distributed data with $m=n/2$ [395]. In presented research work, we utilize an efficient scheme for generating the correlated Nakagami-*m* fading envelop samples [314], in which the Rayleigh-faded envelop samples (denoted by RV R_{Ray} depending on $J_o(2\pi f_D T)$) with specified autocorrelation and phase properties are involved. To generate the uniform RV samples $u \in [0,\ 1)$ using R_{Ray} [314], the following transformation is employed.

$$u = F_{Ray}\left(r_{Ray}\right) = 1 - \exp\left(-r_{Ray}^2 / 2\sigma_{Ray}^2\right) \tag{4.39}$$

where, σ_{Ray}^2 is the second moment of RV R_{Ray}, and $F_{Ray}\left(r_{Ray}\right)$ is the cumulative-distribution-function (CDF) of a Rayleigh distributed RV [331], [384]. However, the envelop samples i.e., RV R_{Nak} exhibiting Nakagami-*m* distribution are generated by utilizing inverse CDF $F_{Nak}^{-1}(.)$, such that

$$R_{Nak} = F_{Nak}^{-1}(u) = F_{Nak}^{-1}\left(F_{Ray}\left(r_{Ray}\right)\right) \tag{4.40}$$

$$\text{where, } F_{Nak}(q) = \int_0^q \frac{2m^m t^{2m-1}}{\Gamma(m)\Omega^m} \exp\left\{-(m/\Omega)t^2\right\} dt \tag{4.41}$$

in which, m is the parameter that controls the severity level of related amplitude fading, $\Omega = E\left[R_{Nak}^2\right]$, and $\Gamma(.)$ is the gamma function. This Nakagami model reduces to the traditional Rayleigh fading model for $m = 1$. However, $m > 1$ leads to the Nakagami fading less severe than the Rayleigh fading; but, $0.5 \le m < 1$ results in higher Nakagami fading severity level in comparison to the Rayleigh fading level. We utilize Hastings' approach [408] to obtain a precise approximation of $F_{Nak}^{-1}(\rho) \approx G(\rho)$, where

$$G(\rho) = \rho + \left\{\left(a_1\rho + a_2\rho^2 + a_3\rho^3\right) / \left(1 + b_1\rho + b_2\rho^2\right)\right\} \tag{4.42}$$

in which, $\rho = \left(\sqrt{\ln\left(1/(1-u)\right)}\right)^{1/m}$ is an ancillary variable [314]. Here, the coefficients a_1, a_2, a_3, b_1 *and* b_2 are selected to minimize the approximation error $e_\rho = F_{Nak}^{-1}(\rho) - G(\rho)$, which are chosen as per the table given in [409]. However, the uniformly distributed phase is considered to be associated with RV R_{Nak} for simulating the Nakagami-*m* fading channel tap-coefficient values, which is quite motivated by the uniform phase assumption for the Rayleigh fading RVs [331], [384].

For conducting the simulation trials, the value of "*m*" for Nakagami fading channel is set at 0.85 and 0.65, while utilizing the BPSK digital modulation scheme based SFBC-OFDM system, at $E_s / N_o = +30dB$. The variance of channel estimation error is assumed to be $\sigma_\varepsilon^2 = 0.0001$, the effective impulse-noise variance is kept $10\log_{10}\sigma_i^2 = -12.5dB$, and the number of subcarriers/subchannels is kept fixed at $N = 64$, which results in $\mu = 1/64 = 0.015625$ for the average number of impulses in an OFDM symbol-block period $N_i = 1$. For $m = 0.85$, the approximate value of bit error rate (as shown in Fig. 4.9) are $BER = 3.5 \times 10^{-4}$ for $N_i = 0$ and

$BER = 6.5\times10^{-4}$ for $N_i = 1$. However for $m = 0.65$, the approximate value of bit error rate are $BER = 2.5\times10^{-3}$ for $N_i = 0$ and $BER = 4.5\times10^{-3}$ for $N_i = 1$.

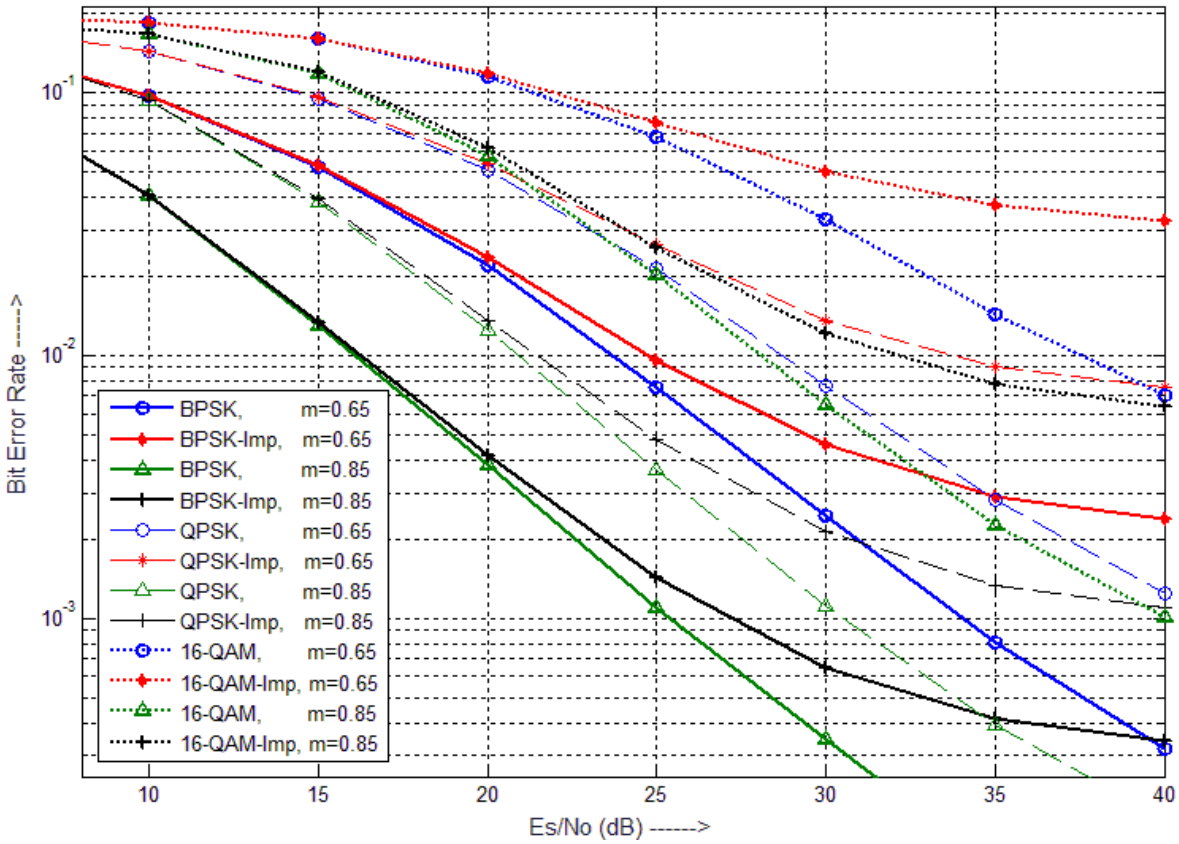

Fig. 4.9: BER vs. $E_s/N_o\,(dB)$ for $N = 64$ at different values of "m" under Nakagami-*m* fading scenario.

Subsequently, the number of subcarriers /subchannels is set at $N = 256$ under similar conditions, which leads to $\mu = 1/256 = 0.0039063$ for the average number of impulses in an OFDM symbol-block period with $N_i = 1$. For $m = 0.85$, the approximate value of bit error rate (as shown in Fig. 4.10) are $BER = 3.5\times10^{-4}$ for $N_i = 0$ and $BER = 4.2\times10^{-4}$ for $N_i = 1$. However for $m = 0.65$, the approximate value of bit error rate are $BER = 2.5\times10^{-3}$ for $N_i = 0$ and $BER = 3.0\times10^{-3}$ for $N_i = 1$. It is inferred from the simulation results presented in Fig. 4.9 and Fig. 4.10 that the value of average BER gets elevated with the alleviating value of "m", due to the boosted severity level of Nakagami fading. In addition, the presence of impulse-noise causes a surge in the value of average BER. However, it is evident that the adverse effects of impulse-noise can be suppressed by increasing the number of subcarriers/subchannels [389].

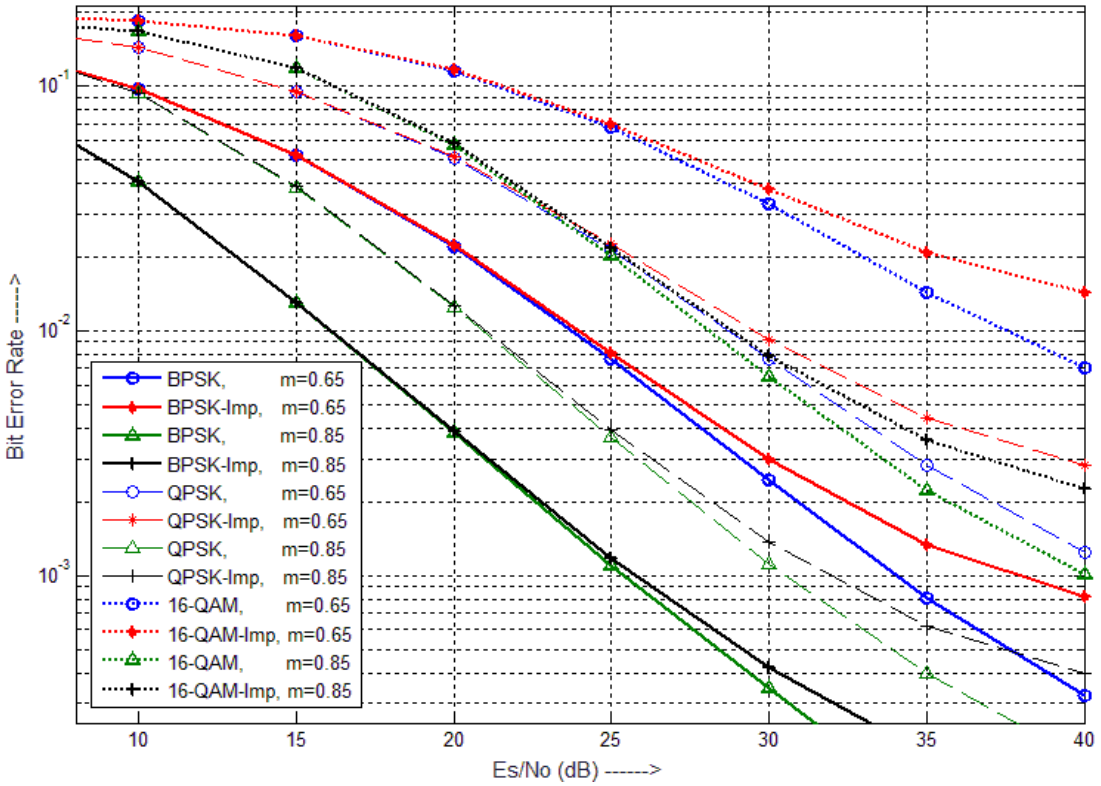

Fig. 4.10: BER vs. $E_s/N_o\,(dB)$ **for** $N=256$ **at different values of "***m***" under Nakagami-*m* fading scenario.**

4.5 Summary of Chapter

In this chapter, we have investigated the impact of impulse-noise on the bit-error-rate performance of the SFBC-OFDM systems, working under the frequency-selective fading environment. Specifically, the effects of imperfect channel-state-information on its BER performance have been observed, when the M-ary PSK and M-ary QAM digital modulation techniques are incorporated in the underlying SFBC-OFDM communication system; as CSI-estimation error cannot be zero in the practical scenario. However, the adverse impact of impulse-noise can be controlled by increasing the number of subcarriers/subchannels in the same fixed OFDM symbol-block period (as a result of the noise-bucket effect). An alternate option to control the adverse effects of impulse-noise is to reduce the modulation order (i.e., reducing the value of M in MPSK and MQAM schemes).

Under severe Nakagami-*m* fading environment, the value of average BER surges up with *m*<1. In addition to this, as the CSI-estimation error variance increases, the average value of BER also gets elevated (as observed through the Monte-Carlo simulation results).

However, the major contribution in this chapter is the description of closed-form expressions for BER performance of the underlying SFBC-OFDM communication systems (under the Rayleigh-fading scenario i.e., a special case of Nakagami-*m* fading) corrupted by the impulse-noise, in the presence of CSI-estimation error.

Future scope includes the incorporation of low-density-parity-check coding scheme, to further reduce the symbol error rate of SFBC-OFDM systems, which may find applications in the latest high data-rate hybrid-free-space-optical/radio-frequency communication schemes using the license free spectrum. Its spectral efficiency can also be enhanced by using the two-way relaying, in cooperative green networks (while exploiting intercell-interference), which can cater services to multiple users. It provides motivation to extend presented research work in the domain of cooperative multiantenna relay networking and its throughput performance analysis in the presence of intercell-interference and Nakagami-*m* fading. But, an accurate knowledge of CSI at the wireless receiver appears as a stringent constraint. Moreover, the impact of impulse-noise on the performance of DVB-T commercial communication systems and underwater acoustic systems can be investigated further. The BER performance analysis of SFBC-OFDM systems in the presence of phase-noise, under the influence of two-wave-with-diffuse-power fading is also under consideration.

CHAPTER 5

ADAPTIVE-SLOPE SQUASHING-FUNCTION BASED ANN FOR CSI-ESTIMATION AND SYMBOL-DETECTION IN SFBC-OFDM SYSTEM

5.1 Introduction

Incorporation of multiple-input-multiple-output (MIMO) scheme in wireless communication systems has resulted in an efficient solution to the ever-increasing demand for high-speed reliable data/information transfer/communication. The usage of orthogonal-frequency-division-multiplexing (OFDM) technique in MIMO systems not only results in an ability to convert the frequency-selective fading channel into flat-fading channel for each subcarrier, but also improves the overall signal-to-noise-ratio (SNR) at receiver [3]. The MIMO-OFDM systems exploit both transmitter-antenna as well as receiver-antenna diversity techniques to enhance the system data/information transmission capacity, at the cost of marginal increase in computational complexity. However, space-time-block-code (STBC) scheme has appeared as an appropriate choice while communicating over the frequency-selective (slow time-varying) channels, as the coding is performed over a few consecutive symbol-periods [392]. But, space-frequency-block-code (SFBC) scheme has found applications in the communication systems working over fast time-varying (flat-fading) channels, as the coding is implemented across few spatially separated antennas and over a few adjacent subcarriers [393]. Since, SFBC-OFDM system maps the codewords across adjacent subcarriers, the channel is considered to be constant during one OFDM symbol-block interval only. Torabi *et al.* have derived closed-form expressions for approximating the bit-error-rate (BER) performance for general SFBC-OFDM systems working over the frequency-selective fading channel in [143], for M-ary quadrature-amplitude-modulation (MQAM) and M-ary phase-shift-keying (MPSK) digital modulation techniques. Therefore, SFBC-OFDM technique has emerged as a potential candidate for 3GPP long-term-evolution (LTE) system [410], LTE-Advanced (LTE-A) system [411] and in supporting technology for the deployment of 5G wireless communication systems [148], by taking into account its various benefits.

However, MIMO-OFDM system requires the knowledge of channel-state-information (CSI) at the receiver to efficiently recover/decode the transmitted information symbols. This necessitates the deployment of channel estimator as an integral part of OFDM based communication system while using transmitter-antenna diversity, as the coding schemes are only capable of achieving near optimal diversity-gain when the receiver has perfect knowledge of CSI in MIMO systems

[272]. Moreover, the signals transmitted simultaneously from different antennas cause interference to each other and pose difficulty in accurate estimation of channel variations. The most common way to get the CSI estimated is the pilot-based scheme, in which the pilot tones are inserted either into all subcarriers of few OFDM symbols (block-type), or into few subcarriers of all OFDM symbols (comb-type). The pilot-based channel estimation scheme utilizes either least-squares (LS) estimator [412], or minimum-mean-square-error (MMSE) estimator [174]. The MMSE estimation leads to better performance than the LS algorithm (with a higher degree of complexity) by utilizing the knowledge of channel correlation statistics (in time- and frequency-domain) and noise variance, in contrast to LS estimator. The complexity can be reduced to certain amount by employing linear-MMSE (LMMSE) channel estimator that utilizes frequency-domain correlation explicitly [158]. The primary disadvantage of pilot-based channel estimation scheme is the alleviated bandwidth requirement. It can be further improved by using bandwidth efficient pilot symbols that estimate the channel impulse response from multiple antennas [272]. An expectation-maximization (EM)-based algorithm for the SFBC-OFDM system was proposed in [413], that employs few pilot symbols to iteratively estimate CSI. In the decision-directed-mode of system model, zero-forcing (ZF) or MMSE based equalizers utilize the already estimated CSI from the previous block (first-stage i.e., channel-estimation stage) to decode the transmitted signals at second-stage/symbol-detection stage. These decoded symbols are then fed back to estimate the CSI at first-stage [307]. Though the decision-directed channel estimation is prone to error propagation, but it precludes the continuous usage of pilot tones and thus improves bandwidth efficiency of overall system [272], at the cost of nominal signal processing delay.

Furthermore, artificial-neural-networks (ANNs) exhibit the universal approximation and learning ability [414], due to which, these can be successfully applied to model the nonlinearities in channel for the effective channel estimation and compensation. The pilot symbols transmitted along with OFDM symbol can be utilized to train ANNs without the knowledge of channel statistics. The one-dimensional and two-dimensional radial-basis-function (RBF) networks have been utilized for the frequency-selective channel estimation in OFDM systems [225]. For MIMO-OFDM systems, a channel estimation technique based on ANN, that trains the network parameters by using the backpropagation (BP) algorithm, outperforms conventional estimation algorithms [230]. For space-time-coded-OFDM systems, it is advantageous to use the feedforward architecture of ANN for better channel estimation [236]. However, the usage of RBF based neural networks for channel estimation in MIMO-OFDM systems may be quite beneficial for Rayleigh fading channels [415]. However, ANNs can be directly implemented for the symbol-detection, without the explicit need for channel estimation, which utilizes deep learning paradigms for signal

detection and equalization [248], [416]. This technique requires a huge amount to data for training, which affects its convergence as well as computational complexity. The receiver needs to employ separate learning modules for the channel estimation and signal detection, at different cascaded stages, to exhibit relatively faster convergence and reduced training overhead. In [247], ComNet has been reported, which is a model-driven deep learning based OFDM receiver that utilizes two separate sub-networks for the channel estimation and symbol-detection. A novel artificial intelligence-aided receiver is suggested for CP-free OFDM system in [417], which includes an LMMSE based channel estimation network followed by the orthogonal-approximate-message-passing algorithm based signal detection network, which can be used for underwater OFDM systems also [418]. This chapter presents a two-stage detection scheme (as shown in Fig. 5.1) at the receiver, in which, CSI is estimated at the first-stage that uses pilot-based LMMSE algorithm for initialization and utilizes ANN for refining the coarse CSI-estimation (i.e., at channel-estimation (CE) stage). At second-stage (i.e., symbol-detection (SD) stage), the transmitted symbols are detected using the estimated CSI by utilizing traditional MMSE criterion, which are fed back to the CE-stage for the decision-directed channel estimation (when pilot symbols are not available, after training-mode).

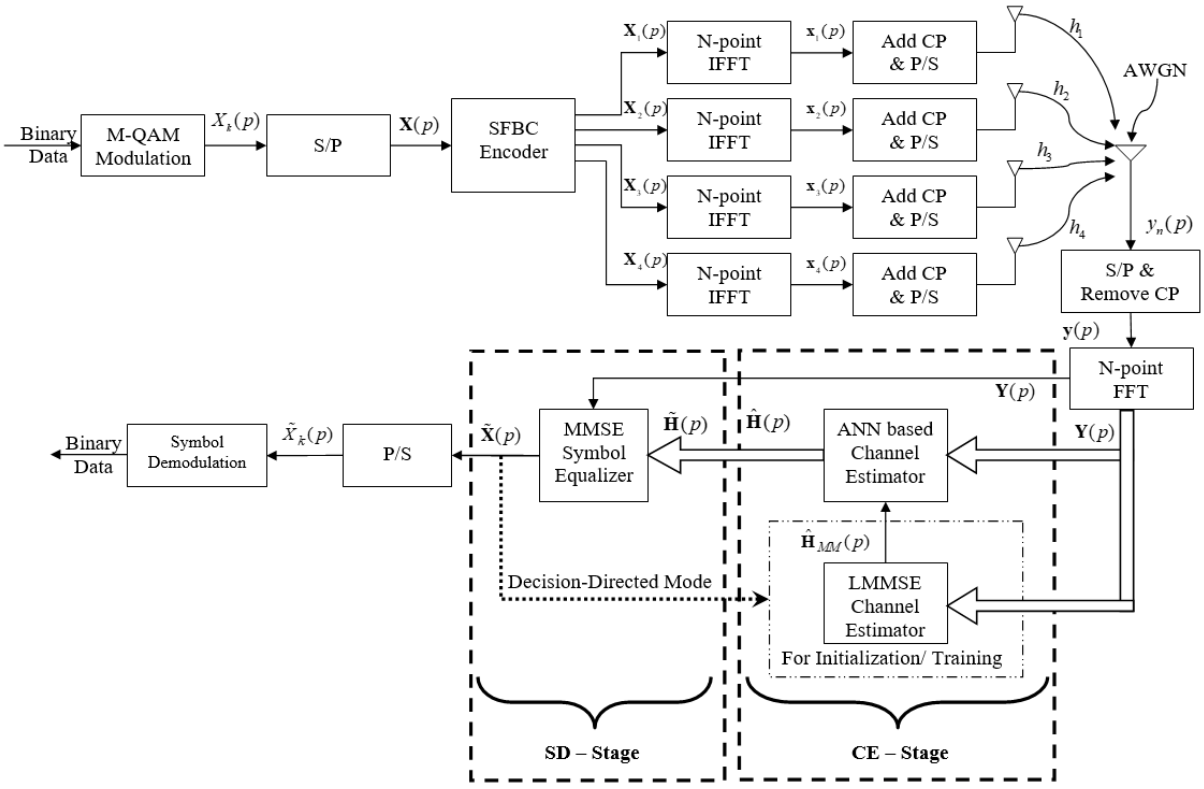

Fig. 5.1: System model for the underlying 4×1 SFBC-OFDM system.

Among various neural network architectures, the most widely used structure is multi-layered perceptron (MLP), because of its simpler implementation, better stability and finite parameterization [419]. The training of MLP is mainly performed using BP algorithm, but its inherent convergence-rate is quite slow [414]. Generally, the learning/approximation capability of ANN is dependent upon the number of hidden layers, number of neurons in each layer, and squashing (activation) function for each neuron [420]. Conventionally used squashing-functions are: the sigmoid function (unipolar/bipolar), linear function, ReLU, and RBF etc., which may be same or different for all layers in neural network. The squashing-function is kept fixed, which is not adaptive to tackle problems under different scenarios, although it plays a critical role in deciding the performance of ANN. In order to reduce the training time and to enhance the convergence-rate under slow time-varying environment, different adaptive squashing-functions have been suggested in the literature [421]-[423], which adaptively adjust the free parameters of the function along with network weights and bias, which leads to reduction in the training time of ANN [424]. Adaptation of a number of free parameters of the squashing-function results in additional computational burden. However, with only one free parameter adaptation/adjustment, BP algorithm is capable of performing better in terms of convergence-rate and training period [425]. Therefore, we propose the utilization of ASF-ANN, which adjusts the slope of squashing-function along with weights and bias in an MLP architecture using BP training algorithm, in the CE-stage of presented 4×1 SFBC-OFDM system.

This chapter is organized as follows. Section 5.2 describes the transceiver paradigm for the underlying 4×1 SFBC-OFDM system with two-stage receiver configuration working under slow time-varying environment (as shown in Fig. 5.1). Subsequently, the channel estimation using ASF-ANN at CE-stage of underlying system is detailed in Section 5.3. Simulation results to depict the efficiency and efficacy of addressed intelligent estimator in terms of mean squared channel estimation error are presented in Section 5.4, which in turn make a significant impact on the SER of underlying system. Finally, summary of the chapter is given in Section 5.5.

5.2 System Paradigm

The transceiver structure of the underlying 4×1 SFBC-OFDM system is illustrated in Fig. 5.1. The binary data stream is first modulated to generate the information symbols using *M*-ary quadrature-amplitude-modulation (MQAM) [347]. These information symbols are converted into blocks of length *N*, as $\mathbf{X}(p)=\left[X_0(p), X_1(p),..., X_{N-1}(p)\right]^T_{N\times1}$, where $[.]^T$ is the matrix transpose operator, and $X_n(p)$ is the *n*-th MQAM symbol of *p*-th block. These symbol-blocks are then

encoded to utilize the space- and frequency-diversity by SFBC encoder, which generates the coded sequence vectors (each of length *N*) for $M_T = 4$ transmitter antennas. The underlying system follows the quasi-orthogonal coding scheme, coined by Jafarkhani *et al*. in [59], as

$$\begin{aligned}
\mathbf{X}_{Tx1}(p) &= \left[+X_0(p), -X_1^*(p), -X_2^*(p), +X_3(p), ..., +X_{N-4}(p), -X_{N-3}^*(p), -X_{N-2}^*(p), +X_{N-1}(p)\right]_{N\times 1}^T \\
\mathbf{X}_{Tx2}(p) &= \left[+X_1(p), +X_0^*(p), -X_3^*(p), -X_2(p), ..., +X_{N-3}(p), +X_{N-4}^*(p), -X_{N-1}^*(p), -X_{N-2}(p)\right]_{N\times 1}^T \\
\mathbf{X}_{Tx3}(p) &= \left[+X_2(p), -X_3^*(p), +X_0^*(p), -X_1(p), ..., +X_{N-2}(p), -X_{N-1}^*(p), +X_{N-4}^*(p), -X_{N-3}(p)\right]_{N\times 1}^T \\
\mathbf{X}_{Tx4}(p) &= \left[+X_3(p), +X_2^*(p), +X_1^*(p), +X_0(p), ..., +X_{N-1}(p), +X_{N-2}^*(p), +X_{N-3}^*(p), +X_{N-4}(p)\right]_{N\times 1}^T
\end{aligned} \tag{5.1}$$

where, $(.)^*$ denotes the complex conjugation operator. Each of these coded sequence vectors are then mapped onto *N* subcarriers via inverse-fast-Fourier-transform (IFFT) to form the transmit vectors, which are then appended with a cyclic-prefix (CP) of length *G* greater than or equal to the maximum delay-spread of channel (to avoid inter-symbol interference) [401]. These vectors/sequences are then transmitted from different antennas simultaneously, which encounter multipath fading wireless channel before reception by the multiple antennas at wireless receiver. The receiver needs to mitigate the deleterious impact of channel distortions/ fading/ interference on the desired information symbol signal through symbol equalization. The encountered wireless fading channel is modelled by assuming it to be a second-order autoregressive (AR2) process. The tap-coefficients of the multipath fading channel, between the *i*-th transmitter and receiver, following AR2 process, are given as [369], [416]

$$h_{i,l}(p) = -K_1 h_{i,l}(p-1) - K_2 h_{i,l}(p-2) + v_{i,l}(p) \tag{5.2}$$

where, $h_{i,l}(p)$ is assumed to possess zero-mean and variance σ_h^2; the scalar coefficients $K_1 = -2r_D \cos\left(\sqrt{2}\pi f_D T\right)$ and $K_2 = r_D^2$ with $r_D = 1 - 2 f_D T$; $f_D T$ is the fade-rate while considering transmission of CP-OFDM symbol-block of duration *T* in the presence of maximum Doppler-spread f_D; $v_{i,l}(p)$ denotes the zero-mean complex Gaussian process-noise with variance σ_v^2; and l denotes the multipath index, where $l = 1, 2, ..., L$ with L as the total number of paths. The channel variations are assumed to be quasi-stationary, which is constant for an OFDM symbol-block of length (*N* + *G*). At receiver, CP is first removed and then *N*-point FFT is performed on the symbol-block of length *N*. Consequently, the received information symbols are expressed as

$$\begin{bmatrix} Y_{4m}(p) \\ Y_{4m+1}(p) \\ Y_{4m+2}(p) \\ Y_{4m+3}(p) \end{bmatrix} = \begin{bmatrix} X_{4m}(p) & X_{4m+1}(p) & X_{4m+2}(p) & X_{4m+3}(p) \\ -X_{4m+1}^*(p) & X_{4m}^*(p) & -X_{4m+3}^*(p) & X_{4m+2}^*(p) \\ -X_{4m+2}^*(p) & -X_{4m+3}^*(p) & X_{4m}^*(p) & X_{4m+1}^*(p) \\ X_{4m+3}(p) & -X_{4m+2}(p) & -X_{4m+1}(p) & X_{4m}(p) \end{bmatrix} \begin{bmatrix} H_{1,4m}(p) \\ H_{2,4m}(p) \\ H_{3,4m}(p) \\ H_{4,4m}(p) \end{bmatrix} + \begin{bmatrix} W_{4m}(p) \\ W_{4m+1}(p) \\ W_{4m+2}(p) \\ W_{4m+3}(p) \end{bmatrix} \tag{5.3}$$

for $m = 0,1,...,(N/4)-1$; where $H_{i,k}(p)$ corresponds to the *k*-th subcarrier FFT of the channel impulse response between *i*-th antenna and receiver, while assuming that channel tap-coefficients are approximately equal for the adjacent subcarriers related to each antenna, i.e., $H_{i,4m}(p) \approx H_{i,4m+1}(p) \approx H_{i,4m+2}(p) \approx H_{i,4m+3}(p)$ [258]. The inevitable frequency-domain additive-white-Gaussian-noise (AWGN) emerging at receiver is indicated as $W_k(p)$ in Eq.(5.3), possesses zero-mean and σ_w^2 variance. Also, the above equation may be re-written in vector/ matrix form as

$$\mathbf{Y}_{4m}(p) = \mathbf{X}_{4m}(p)\mathbf{H}_{4m}(p) + \mathbf{W}_{4m}(p) \tag{5.4}$$

The received symbols are also distorted due to the channel variations along with AWGN. The estimation of CSI is necessary for improved symbol-detection, which can be accomplished by sending the pilot/training symbols and estimating CSI based on the prior knowledge of encountered fading channel (if any) and the assigned training symbols. The LS channel estimation method minimizes the following error function [426]

$$J\left[\hat{\mathbf{H}}_{4m,LS}(p)\right] = \left\|\mathbf{Y}_{4m}(p) - \mathbf{X}_{4m}(p)\hat{\mathbf{H}}_{4m,LS}(p)\right\|^2 \tag{5.5}$$

where, $\hat{\mathbf{H}}_{4m,LS}(p)$ is the LS estimate of fading channel tap-coefficient. The optimum value of $\hat{\mathbf{H}}_{4m,LS}(p)$ can be approximated by minimizing the above-mentioned error function, which is illustrated as

$$\hat{\mathbf{H}}_{4m,LS}(p) = \left(\mathbf{X}_{4m}^H(p)\mathbf{X}_{4m}(p)\right)^{-1}\mathbf{X}_{4m}^H(p)\mathbf{Y}_{4m}(p) \tag{5.6}$$

where, $(.)^H$ is the Hermitian transposition operator. However, based on the results and analysis reported in [426], the LMMSE based channel estimation technique (providing $\hat{\mathbf{H}}_{4m,MM}$ i.e., Eq.(C.12) in Appendix-C) improves the quality of LS estimation process by incorporating the channel statistics to minimize the mean squared error between the actual channel tap-coefficients and estimated channel tap-coefficients [426], which is given as

$$\hat{\mathbf{H}}_{4m,MM}(p) = \mathbf{R}_{HH}\left\{\mathbf{R}_{HH} + \sigma_w^2\left(\mathbf{X}_{4m}^H(p)\mathbf{X}_{4m}(p)\right)^{-1}\right\}^{-1}\hat{\mathbf{H}}_{4m,LS}(p) \tag{5.7}$$

where, $\mathbf{R}_{HH}$ is the auto-correlation matrix of the true channel vector $\mathbf{H}_{4m}(p)$ (detailed derivation, see Appendix-C). As per the scenario addressed in [158], [187], [301], this auto-correlation matrix is considered to be $\mathbf{R}_{HH} = diag\left[(1/L),(1/L),...,(1/L)\right]$ for simulation of presented system.

In order to retrieve transmitted information symbols accurately from the received signal vectors, it is required to compensate the channel impairments through equalization, which necessitates the availability of CSI at receiver. As the perfect knowledge of CSI at receiver is actually an ideal

assumption [331], therefore the ANN based estimation of CSI with high fidelity at the CE-stage (as shown in Fig. 5.1) serves the purpose. For estimation of fading channel frequency response, the received symbols $\mathbf{Y}_{4m}(p)$ are fed to the ASF-ANN based channel estimator to get an estimate of channel tap-coefficients, $\hat{\mathbf{H}}_{4m}(p)$, in the frequency-domain. In case of ideal estimator $\mathbf{H}_{4m}(p) = \hat{\mathbf{H}}_{4m}(p)$ (with zero estimation error), which is not possible in the real-time channel estimation process. The channel estimates for all subcarriers are retained as $\tilde{\mathbf{H}}_{4m}(p) = \hat{\mathbf{H}}_{4m}(p)$, and these are subsequently utilized at SD-stage for the symbol-detection. Using minimum-mean-square-error (MMSE) equalization technique [427], the desired transmitted symbols are approximated as

$$\hat{\mathbf{X}}_{4m}(p) = \left(\tilde{\mathbf{H}}_{4m}^{H}(p)\tilde{\mathbf{H}}_{4m}(p) + \sigma_w^2 \mathbf{I}_4\right)^{-1} \tilde{\mathbf{H}}_{4m}^{H}(p)\tilde{\mathbf{Y}}_{4m}(p) \tag{5.8}$$

where, $\tilde{\mathbf{H}}_{4m}(p) = \begin{bmatrix} \hat{H}_{1,4m}(p) & \hat{H}_{2,4m}(p) & \hat{H}_{3,4m}(p) & \hat{H}_{4,4m}(p) \\ \hat{H}_{2,4m}^{*}(p) & -\hat{H}_{1,4m}^{*}(p) & \hat{H}_{4,4m}^{*}(p) & -\hat{H}_{3,4m}^{*}(p) \\ \hat{H}_{3,4m}^{*}(p) & \hat{H}_{4,4m}^{*}(p) & -\hat{H}_{3,4m}^{*}(p) & -\hat{H}_{4,4m}^{*}(p) \\ \hat{H}_{4,4m}(p) & -\hat{H}_{3,4m}(p) & -\hat{H}_{2,4m}(p) & \hat{H}_{1,4m}(p) \end{bmatrix}$, $\tilde{\mathbf{Y}}_{4m}(p) = \begin{bmatrix} Y_{4m}(p) \\ Y_{4m+1}^{*}(p) \\ Y_{4m+2}^{*}(p) \\ Y_{4m+3}(p) \end{bmatrix}$, and $\mathbf{I}_4$ is 4×4 identity-matrix. Eventually, $\hat{\mathbf{X}}_{4m}(p)$ are used to detect the transmitted information symbols $\mathbf{X}_{4m}(p)$, and which are further demodulated to regenerate the binary data sequence.

5.3 Adaptive-Slope Squashing-Function Based ANN

ANNs are a functional network of the nonlinear units (known as neurons) with interconnections; where each connection has a weight factor, which are adjusted during the training process, to learn about the state of fading channel. In order to perform CSI-estimation in the underlying 4×1 SFBC-OFDM wireless system, an ANN based channel estimation model (as shown in Fig. 5.2) is utilized. The input to this channel estimation module is the complex-valued received symbols $\mathbf{Y}_{4m}(p)$, which are bifurcated into real and imaginary parts, and these are subsequently fed to 4 different ANN blocks utilized to estimate channel tap-coefficients in the frequency-domain $\hat{H}_{i,4m}(p)$, as the ANNs can only process real-valued data. Each ANN block is an MLP structure, with feedforward connection between neurons [414] (as shown in Fig. 5.3), that consists of 8 inputs, 16 neurons in the first hidden-layer, 8 neurons in the second hidden-layer, and 2 neurons in the output-layer. The outputs of every ANN block are combined to form a complex-valued channel estimate $\hat{H}_{i,4m}(p)$, where $i = 1,2,3,4$ and $m = 0,1,...,(N/4)-1$.

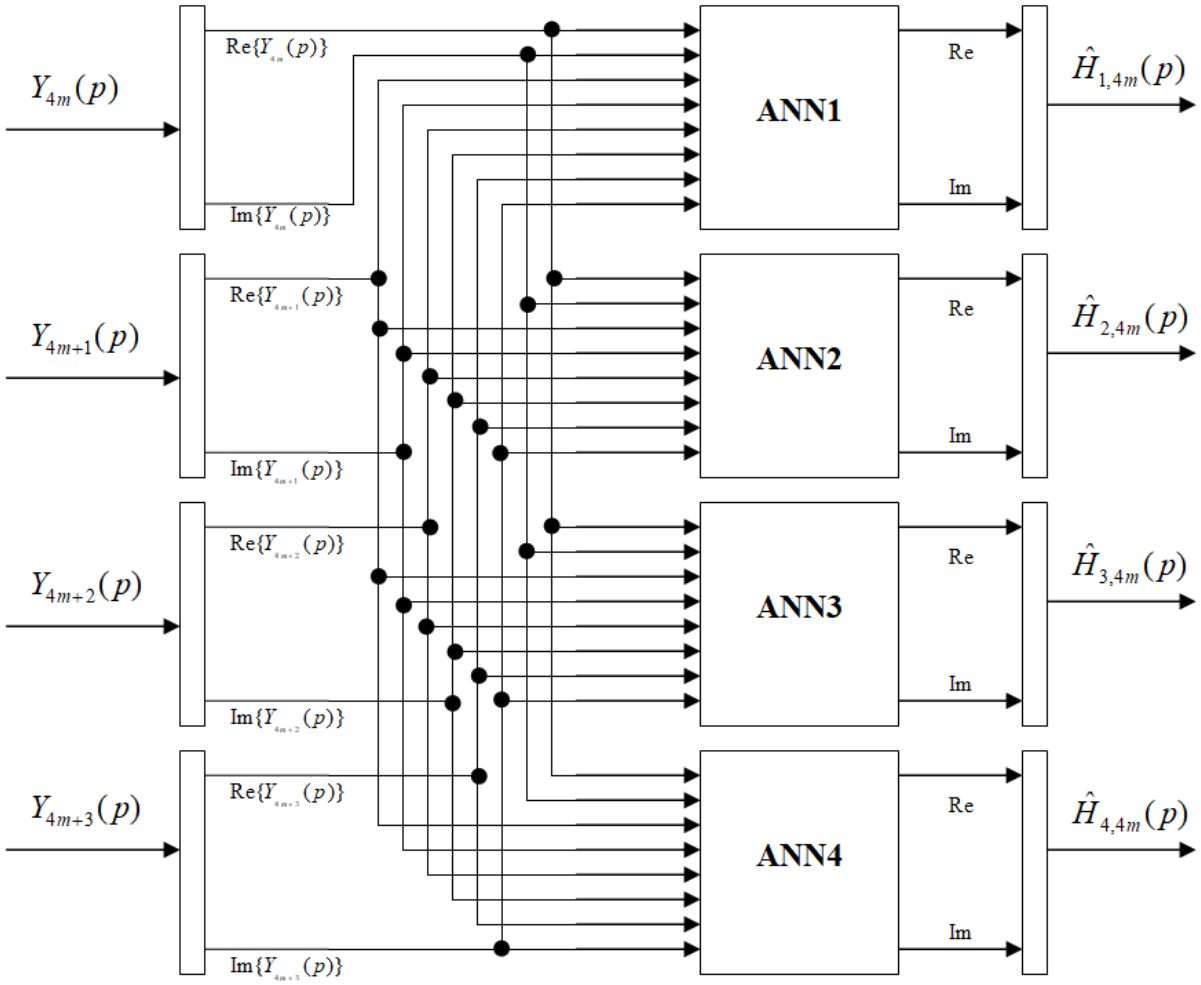

Fig. 5.2: ANN based channel estimation model in 4×1 SFBC-OFDM system [229].

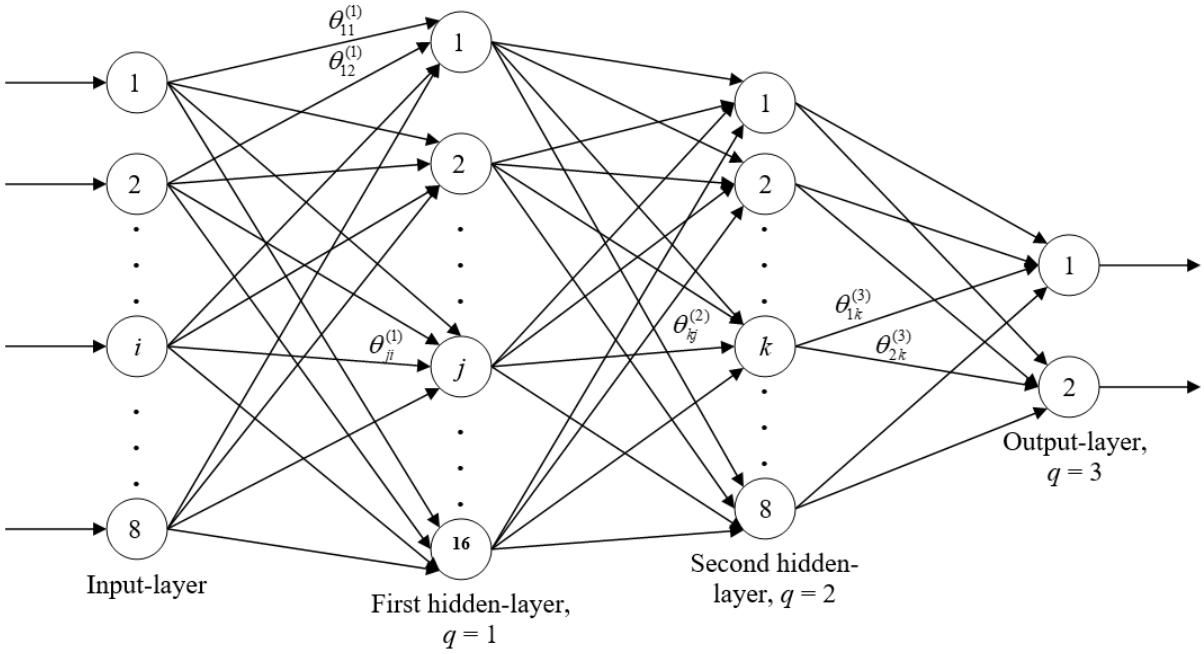

Fig. 5.3: Feedforward MLP structure of ANN for the channel estimation [414].

The real and imaginary components of the received symbol signal vector $\mathbf{Y}_{4m}(p)$ are rearranged in the following vector form, which can be fed into the ANN based channel estimator through 8 nodes of input-layer (i.e., 8 inputs corresponding to 4 received symbols in the frequency-domain) as shown in Fig. 5.3

$$\begin{bmatrix} inp_1(p) \\ inp_2(p) \\ \vdots \\ inp_7(p) \\ inp_8(p) \end{bmatrix} = \begin{bmatrix} \mathrm{Re}\left(Y_{4m}(p)\right) \\ \mathrm{Im}\left(Y_{4m}(p)\right) \\ \vdots \\ \mathrm{Re}\left(Y_{4m+3}(p)\right) \\ \mathrm{Im}\left(Y_{4m+3}(p)\right) \end{bmatrix} \tag{5.9}$$

where, $\mathrm{Re}(t)$ and $\mathrm{Im}(t)$ denote the real and imaginary parts of the complex-valued *t*, respectively. The input-output relationship for the structure demonstrated in Fig. 5.3 are supported by following equations

$$net_j^{(1)} = \sum_{i=1}^{8} \theta_{ji}^{(1)} inp_i(p) + b_j^{(1)} \qquad \text{for } j = 1, 2, ..., 16 \tag{5.10}$$

$$v_j^{(1)} = f\left(net_j^{(1)}\right) = \tanh\left(\alpha_j^{(1)} net_j^{(1)}\right) \tag{5.11}$$

$$net_k^{(2)} = \sum_{j=1}^{16} \theta_{kj}^{(2)} v_j^{(1)} + b_k^{(2)} \qquad \text{for } k = 1, 2, ..., 8 \tag{5.12}$$

$$v_k^{(2)} = f\left(net_k^{(2)}\right) = \tanh\left(\alpha_k^{(2)} net_k^{(2)}\right) \tag{5.13}$$

$$net_o^{(3)} = \sum_{k=1}^{8} \theta_{ok}^{(3)} v_k^{(2)} + b_o^{(3)} \qquad \text{for } o = 1, 2 \tag{5.14}$$

$$v_o^{(3)} = f\left(net_o^{(3)}\right) = \tanh\left(\alpha_o^{(3)} net_o^{(3)}\right) \tag{5.15}$$

where, $\theta_{ji}^{(q)}$ signifies the synaptic-weight of connection between the *j*-th neuron of *q*-th layer with the *i*-th output of previous layer; $net_j^{(q)}$ is the net induced input field of *j*-th neuron in the *q*-th layer by the previous layer neurons; $b_j^{(q)}$ is the bias of the corresponding neuron; $f(.)$ is the nonlinear squashing-function, which is considered here as hyperbolic-tangent function with slope factor $\alpha_j^{(q)}$ [414]. The output of the network is combined to form a complex-valued channel estimate in the frequency-domain with as $\mathrm{Re}\left(\hat{H}_{4m}(p)\right) = v_1^{(3)}$ and $\mathrm{Im}\left(\hat{H}_{4m}(p)\right) = v_2^{(3)}$. In a feedforward MLP architecture, the information flows from input-layer to the output-layer, where the hidden-layer performs nonlinear mappings to tackle the channel variations as well as tracking. Along with weights and bias, the adaptation of squashing-function leads to better convergence speed than the fixed-slope squashing-function based training [428]. In order to enhance the training capability of

BP algorithm, an algorithm that adjusts the slope of squashing-function along with the other network parameters (such as weights and bias) is reported. Since the actual channel impulse response is not available at receiver, the training of ASF-ANN is performed by utilizing the LMMSE based estimated channel frequency response (as mentioned in Eq.(5.7)), which is derived by utilizing pilot information symbol-blocks transmitted in the training phase [247]. The input target-vector sample used for the training of presented ASF-ANN technique using BP algorithm is denoted as $\left\{\mathbf{Y}_{4m}(p), \hat{\mathbf{H}}_{4m,MM}(p)\right\}_{p=1}^{100}$. The error signal generated at each output neuron of each ANN is represented as

$$\begin{aligned} e_1(p) &= \mathrm{Re}\left\{\hat{H}_{4m,MM}(p)\right\} - v_1^{(3)}(p) = \mathrm{Re}\left\{\hat{H}_{4m,MM}(p)\right\} - \mathrm{Re}\left\{\hat{H}_{4m}(p)\right\} \\ e_2(p) &= \mathrm{Im}\left\{\hat{H}_{4m,MM}(p)\right\} - v_2^{(3)}(p) = \mathrm{Im}\left\{\hat{H}_{4m,MM}(p)\right\} - \mathrm{Im}\left\{\hat{H}_{4m}(p)\right\} \end{aligned} \tag{5.16}$$

The total error-energy of network is expressed as the following sum of squared errors at the output (that is differentiable scalar cost function), which is used for updating the network parameters (synaptic-weights, bias, and slope of squashing-function). It follows that

$$\xi(p) = \frac{1}{2}\left[e_1^2(p) + e_2^2(p)\right] \tag{5.17}$$

The learning process of ASF-ANN adjusts the network parameters in such a way that the updated parameters minimize this error-energy $\xi(p)$. In gradient-descent based BP algorithm, ANN parameters are updated by applying a correction, which is proportional to the partial derivative of aforementioned error-energy with respect to the respective network parameter. The adjustments of the network parameters [414] for the next iteration are given as

$$\theta_{ji}^{(q)}(p+1) = \theta_{ji}^{(q)}(p) + \Delta\theta_{ji}^{(q)}(p) = \theta_{ji}^{(q)}(p) - \eta\frac{\partial\xi(p)}{\partial\theta_{ji}^{(q)}(p)} \tag{5.18}$$

$$b_j^{(q)}(p+1) = b_j^{(q)}(p) + \Delta b_j^{(q)}(p) = b_j^{(q)}(p) - \eta\frac{\partial\xi(p)}{\partial b_j^{(q)}(p)} \tag{5.19}$$

with η as the learning-rate of BP algorithm. In addition to the weights as well as bias in ANN, the slope of squashing-function is also considered to be an available parameter that can be adaptively managed to improve the convergence of BP algorithm through the back-propagation of errors into the network. Following the similar methodology as in Eqs.(5.18)–(5.19) [425], the slope can be updated for the next iteration as

$$\alpha_j^{(q)}(p+1) = \alpha_j^{(q)}(p) + \Delta\alpha_j^{(q)}(p) = \alpha_j^{(q)}(p) - \eta\frac{\partial\xi(p)}{\partial\alpha_j^{(q)}(p)} \tag{5.20}$$

For neurons in the output-layer, the partial derivate is calculated by using the chain-rule as

$$\frac{\partial \xi(p)}{\partial \theta_{ok}^{(3)}} = \frac{\partial \xi(p)}{\partial e_o(p)} \frac{\partial e_o(p)}{\partial v_o^{(3)}} \frac{\partial v_o^{(3)}}{\partial net_o^{(3)}} \frac{\partial net_o^{(3)}}{\partial \theta_{ok}^{(3)}}$$

$$= e_o(p)\ (-1)\ \frac{\partial f(net_o^{(3)})}{\partial net_o^{(3)}}\ v_k^{(2)} \tag{5.21}$$

$$= -e_o(p)\ \alpha_o^{(3)} \left(1 - \tanh^2\left(\alpha_o^{(3)} net_o^{(3)}\right)\right)\ v_k^{(2)}$$

$$= -e_o(p)\alpha_o^{(3)} \left(1 - \left(v_o^{(3)}\right)^2\right) v_k^{(2)}$$

The weight update for the output-layer neurons is represented in the following form

$$\Delta \theta_{ok}^{(3)} = -\eta \frac{\partial \xi(p)}{\partial \theta_{ok}^{(3)}} = \eta e_o(p)\alpha_o^{(3)} \left(1 - \left(v_o^{(3)}\right)^2\right) v_k^{(2)} = \eta \delta_o^{(3)} v_k^{(2)} \tag{5.22}$$

where, $\delta_o^{(3)}$ is termed as the local error-gradient for the output-layer neurons, for $o = 1, 2$ and $k = 1, 2, ..., 8$. Similarly, the bias term is updated by using

$$\frac{\partial \xi(p)}{\partial b_o^{(3)}} = \frac{\partial \xi(p)}{\partial e_o(p)} \frac{\partial e_o(p)}{\partial v_o^{(3)}} \frac{\partial v_o^{(3)}}{\partial net_o^{(3)}} \frac{\partial net_o^{(3)}}{\partial b_o^{(3)}}$$

$$= e_o(p)\ (-1)\ \frac{\partial f(net_o^{(3)})}{\partial net_o^{(3)}}\ 1 \tag{5.23}$$

$$= -e_o(p)\alpha_o^{(3)} \left(1 - \left(v_o^{(3)}\right)^2\right)$$

$$\Delta b_o^{(3)} = -\eta \frac{\partial \xi(p)}{\partial b_o^{(3)}} = \eta e_o(p)\alpha_o^{(3)} \left(1 - \left(v_o^{(3)}\right)^2\right) = \eta \delta_o^{(3)} \qquad \text{for } o = 1, 2 \tag{5.24}$$

The slope of squashing-function is also updated by following the same gradient-descent based conditions [425], such that

$$\frac{\partial \xi(p)}{\partial \alpha_o^{(3)}} = \frac{\partial \xi(p)}{\partial e_o(p)} \frac{\partial e_o(p)}{\partial v_o^{(3)}} \frac{\partial v_o^{(3)}}{\partial \alpha_o^{(3)}}$$

$$= e_o(p)\ (-1)\ \frac{\partial f(net_o^{(3)})}{\partial \alpha_o^{(3)}} \tag{5.25}$$

$$= -e_o(p)\left(1 - \tanh^2\left(\alpha_o^{(3)} net_o^{(3)}\right)\right) net_o^{(3)}$$

$$= -e_o(p)\left(1 - \left(v_o^{(3)}\right)^2\right) net_o^{(3)}$$

$$\Delta \alpha_o^{(3)} = -\eta \frac{\partial \xi(p)}{\partial \alpha_o^{(3)}} = \eta e_o(p)\left(1 - \left(v_o^{(3)}\right)^2\right) net_o^{(3)} = \eta \frac{\delta_o^{(3)}}{\alpha_o^{(3)}} net_o^{(3)} \qquad \text{for } o = 1, 2 \tag{5.26}$$

For any hidden-layer, as there are no specific targets for the neurons, the error-signal for this layer has to be determined in terms of the error-signals of the subsequent layer to which the hidden-layer neuron is connected. The partial derivative of the network error-energy with respect to the weights of second hidden-layer neurons is

$$\begin{aligned}\frac{\partial \xi(p)}{\partial \theta_{kj}^{(2)}} &= \frac{\partial \xi(p)}{\partial v_k^{(2)}} \frac{\partial v_k^{(2)}}{\partial net_k^{(2)}} \frac{\partial net_k^{(2)}}{\partial \theta_{kj}^{(2)}} \\ &= \left\{ \sum_{o=1}^{2} e_o(p) \frac{\partial e_o(p)}{\partial net_o^{(3)}} \frac{\partial net_o^{(3)}}{\partial v_k^{(2)}} \right\} \frac{\partial f(net_k^{(2)})}{\partial net_k^{(2)}} v_j^{(1)} \\ &= -\left\{ \sum_{o=1}^{2} e_o(p) \alpha_o^{(3)} \left(1 - \tanh^2\left(\alpha_o^{(3)} net_o^{(3)}\right)\right) \theta_{ok}^{(3)} \right\} \alpha_k^{(2)} \left(1 - \tanh^2\left(\alpha_k^{(2)} net_k^{(2)}\right)\right) v_j^{(1)} \\ &= -\left\{ \sum_{o=1}^{2} \delta_o^{(3)} \theta_{ok}^{(3)} \right\} \alpha_k^{(2)} \left(1 - \left(v_k^{(2)}\right)^2\right) v_j^{(1)}\end{aligned} \tag{5.27}$$

$$\Delta \theta_{kj}^{(2)} = -\eta \frac{\partial \xi(p)}{\partial \theta_{kj}^{(2)}} = \eta \left\{ \sum_{o=1}^{2} \delta_o^{(3)} \theta_{ok}^{(3)} \right\} \alpha_k^{(2)} \left(1 - \left(v_k^{(2)}\right)^2\right) v_j^{(1)} = \eta \delta_k^{(2)} v_j^{(1)} \tag{5.28}$$

for $k = 1, 2, ..., 8$ and $j = 1, 2, ..., 16$. The execution of neural-based channel estimation requires the following critical corrections

$$\Delta b_k^{(2)} = \eta \delta_k^{(2)} \qquad \text{for } k = 1, 2, ..., 8 \tag{5.29}$$

$$\Delta \alpha_k^{(2)} = \eta \frac{\delta_k^{(2)}}{\alpha_k^{(2)}} net_k^{(2)} \qquad \text{for } k = 1, 2, ..., 8 \tag{5.30}$$

$$\Delta \theta_{ji}^{(1)} = \eta \delta_j^{(1)} inp_i(p) \qquad \text{for } j = 1, 2, ..., 16 \text{ and } i = 1, 2, ..., 8 \tag{5.31}$$

$$\Delta b_j^{(1)} = \eta \delta_j^{(1)} \qquad \text{for } j = 1, 2, ..., 16 \tag{5.32}$$

$$\Delta \alpha_j^{(1)} = \eta \frac{\delta_j^{(1)}}{\alpha_j^{(1)}} net_j^{(1)} \qquad \text{for } j = 1, 2, ..., 16 \tag{5.33}$$

where, $\delta_j^{(1)} = \left\{ \sum_{k=1}^{8} \delta_k^{(2)} \theta_{kj}^{(2)} \right\} \alpha_j^{(1)} \left(1 - \left(v_j^{(1)}\right)^2\right)$.

Summary of adaptive-slope squashing-function based ANN training algorithm

The procedure for weight updating/adjustment in the presented ASF-ANN system is summarised as follows:

Step-1: All the weights $\theta_{ji}^{(q)}$ and bias $b_j^{(q)}$ of the network are initialized to small random values, and the slope of squashing-function $\alpha_j^{(q)}$ for each neuron in the network is set to unity.

Step-2: Present an input-target pattern to the network, and calculate the actual output from the network using equations (5.10)–(5.15).

Step-3: Calculate errors of the network as in Eq.(5.16), and evaluate gradients for output and hidden-layers' weight updating from equations (5.21)–(5.33).

Step-4: Adjust the network parameters as per the iterative formulas in equations (5.18)–(5.20).

Step-5: Present another input-target pattern and go back to Step-2, till the maximum epoch count is reached or minimum error value has been achieved [414].

The training pattern is fed to the ASF-ANN cyclically, until all the parameters converge, and the network error function is acceptably low. Though this method is not very different from the conventional BP algorithm, but the slope of squashing-function is made to vary adaptively along with the adaptive tuning of synaptic-weights and other network parameters, which showcases a new approach in the domain of machine-learning using ANNs. It has found application in the CE-stage of the presented 4×1 SFBC-OFDM system, while working under slow time-variant fading environment, which in turn influences the performance of SD-stage in terms of reduced BER, at the cost of a little increase in computational burden. (See Appendix-D to critically observe the impact of squashing-function's slope on ANN based channel estimation in SFBC-OFDM system.)

5.4 Simulation Results

We shall investigate the performance of 4×1 SFBC-OFDM system using ASF-ANN based channel estimator (adaptive-slope squashing-function based approach), which is assumed to be working under the slow time-variant multipath fading environment. The MQAM digital modulation scheme is incorporated in this wireless communication system with $M=4$, while considering $N=64$ number of subcarriers; and length of CP be $G=16$ [174]. The MQAM symbols are QO-coded for 4 transmitter-antennas, as per the spatial-diversity technique suggested by Jafarkhani *et al.* in [59], by using Eq.(5.1). The bandwidth allocated for transmission of SFBC-OFDM information symbol signals is 25 MHz. The duration/period of CP-OFDM symbol-block is fixed at $T=3.2\mu s$, which leads to 0.3125 MHz subcarrier spacing Δf. Based on the power-delay profile calculations [429], the root-mean-squared (rms) delay-spread is considered to be $\tau_{rms}=40ns$ (approximately). As the frequency correlation function is above 0.5 [429], therefore the coherence bandwidth is approximated as $B_{wc}\approx\left(5\tau_{rms}\right)^{-1}=5$ MHz.

The number of significant multipaths contributing in the fading of transmitted signal is found to be $L=5$, as in [174], [331]. Therefore, we utilize 5 tap-coefficients in the tapped-delay-line-filter based multipath fading channel model [331], [380], in which these tap-coefficients are assumed to follow the second-order Markov-process (exhibiting Rayleigh-fading characteristics depending on the fade-rate f_DT). At CE-stage of underlying system (as shown in Fig. 5.1), the multi-layered neural network (as shown in Fig. 5.3) is implemented using 16, 8 and 2 neurons in the first-, second-hidden-layer and output-layer, respectively. The squashing-function in each of

these layers is considered to be the hyperbolic-tangent function with adaptive-slope. The presented results are based on the ensemble-average of 500 independent Monte-Carlo simulation runs, illustrating the mean-squared channel estimation error performance of the ASF-ANN at CE-stage and the average bit-error-rate at SD-stage (using MMSE equalization) for the presented SFBC-OFDM system at different values of SNR as well as fade-rate. We shall compare its performance with the traditional FSF-ANN (fixed-slope squashing-function), direct LS, and direct LMMSE based approaches.

Case 1:- SFBC-OFDM system using LMMSE based training of ASF-ANN

In the first case, ANN based channel estimator (as shown in Fig. 5.2 and Fig. 5.3) is trained using the first 100 SFBC-OFDM symbol-blocks (training samples/ pilot symbols), in which the desired/ target response (Eq.(5.7)) is generated by the LMMSE based channel estimator at CE-stage (as shown in Fig. 5.1). The output of ANN based channel estimator is obtained using Eq.(5.15), which is further used to detect/ demodulate the desired transmitted symbols through MMSE equalization by using Eq.(5.8). Each example/ pattern of the training sample is given to the presented ASF-ANN for tracking the channel variations, which remains same for FSF-ANN. The weights and bias of the ANN are assigned small random non-zero values for initialization, while keeping the slope of squashing-function fixed at unity in the beginning of training. However, the slope of every squashing-function, synaptic-weights and bias terms in ASF-ANN changes as per the procedure discussed in Section 5.3, but the slope remains fixed for FSF-ANN based channel estimator. The learning-rate of the backpropagation algorithm is set at $\eta = 0.1$, for both ASF-ANN and FSF-ANN. At the fade-rate = 0.0001 and SNR = +20dB (as depicted in Fig. 5.4), the ASF-ANN exhibits an MSE of 0.00033 (approximately), but FSF-ANN provides MSE of 0.0006 (approximately) under similar conditions. For comparison, the channel estimation is also performed directly using LS and LMMSE algorithms [174], [247] for same channel attributes. The value of MSE for LS is 0.0014 (approximately), and for LMMSE is 0.00075 (approximately), which is quite higher than the observed values in case of ASF-ANN. It can be inferred from simulation outcomes that ASF-ANN based channel estimation outperforms the other three techniques by providing significantly lower mean-squared channel estimation error at all SNR values.

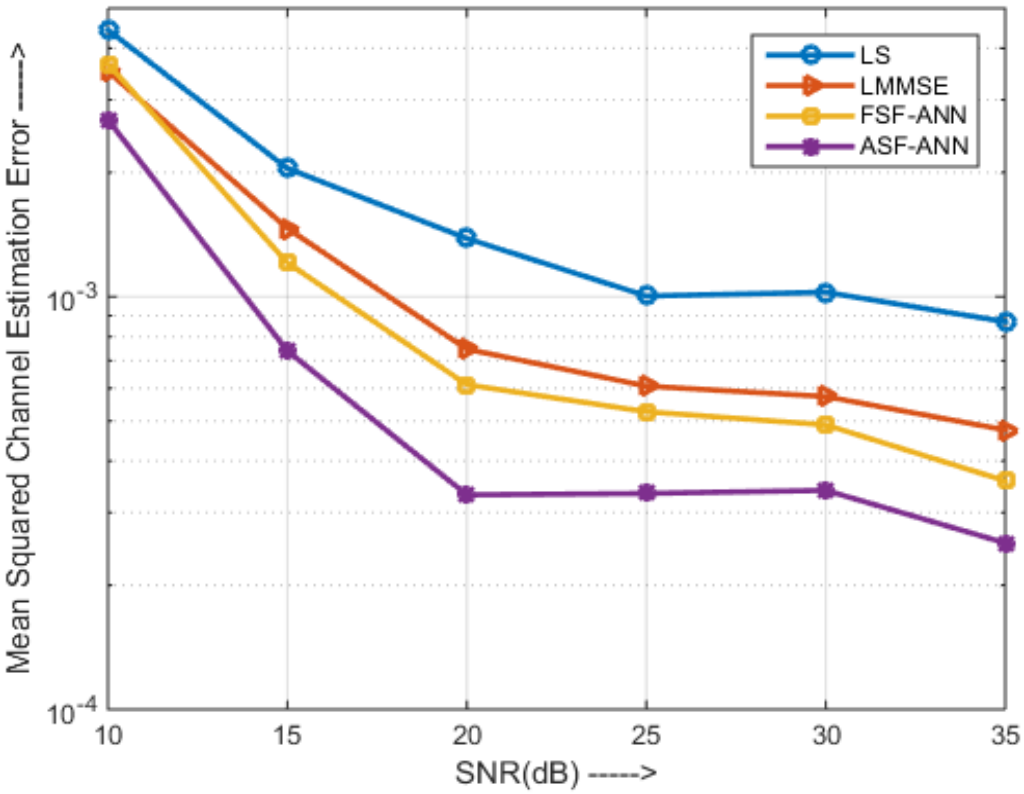

Fig. 5.4: Mean squared channel estimation error comparison at fade-rate = 0.0001 with LMMSE based training.

Fig. 5.5: Bit error rate comparison at fade-rate = 0.0001 with LMMSE based training.

The channel estimation error directly affects the average bit-error-rate performance of underlying 4×1 SFBC-OFDM system [416], [430]. By conducting simulation using Eq.(5.8) for symbol-detection, the average BER is calculated at different SNR values as shown in Fig. 5.5, which is also compared with the case when CSI is assumed to be known at the SD-stage of receiver (indicated as CSI known in Fig. 5.5). At BER = 0.0006, the ASF-ANN channel estimator based approach provides approximately +0.2dB performance advantage in terms of SNR, in comparison to the LS channel estimator based approach. It is apparent from the results in Fig. 5.5 at certain values of SNR that the BER performance of ASF-ANN channel estimator based approach is better than the other three techniques, though the performance advantage is marginal. However, the advantage of ASF-ANN channel estimator based approach comes into picture, when the multipath fading channel is slow time-varying, where the FSF-ANN approach fails to perform well. Therefore, SFBC-OFDM system using LMMSE based training of ASF-ANN is found to be the best choice under slow time-variant fading environment by providing comparatively lower BER.

Further, the performance of presented SFBC-OFDM system is observed under mobile environment, at the different values of fade-rate $f_D T$. Now, the value of SNR is fixed at +15dB. And the fade-rate $f_D T$ is varied from 0.0001 to 0.01, to analyze its impact on the performance of ASF-ANN based channel estimator and average BER. It can be inferred from results demonstrated in Fig. 5.6 that the mean-squared channel estimation error is minimum for the case of ASF-ANN in comparison to FSF-ANN, direct LS, direct LMMSE based approaches. It is noteworthy that ASF-ANN based channel estimator adapts the fading channel environment more efficiently by tracking the channel variations with the help of adaptive-slope hyperbolic-tangent squashing-function [425], [431], [432], at high SNR values. It is evident that this feature is not available in FSF-ANN, which limits its applications. Consequently, the results illustrated in Fig. 5.7 show that the BER performance of SFBC-OFDM system improves due to the usage of ASF-ANN based channel estimator. But, a large performance degradation is observed for ASF-ANN as well as FSF-ANN based approaches, at higher values of fade-rate and lower values of SNR. As the value of fade-rate increases or the value of SNR decreases, the BER of SFBC-OFDM system using ASF-ANN based CE-stage gets elevated sharply, due to the high value of mean-squared channel estimation error.

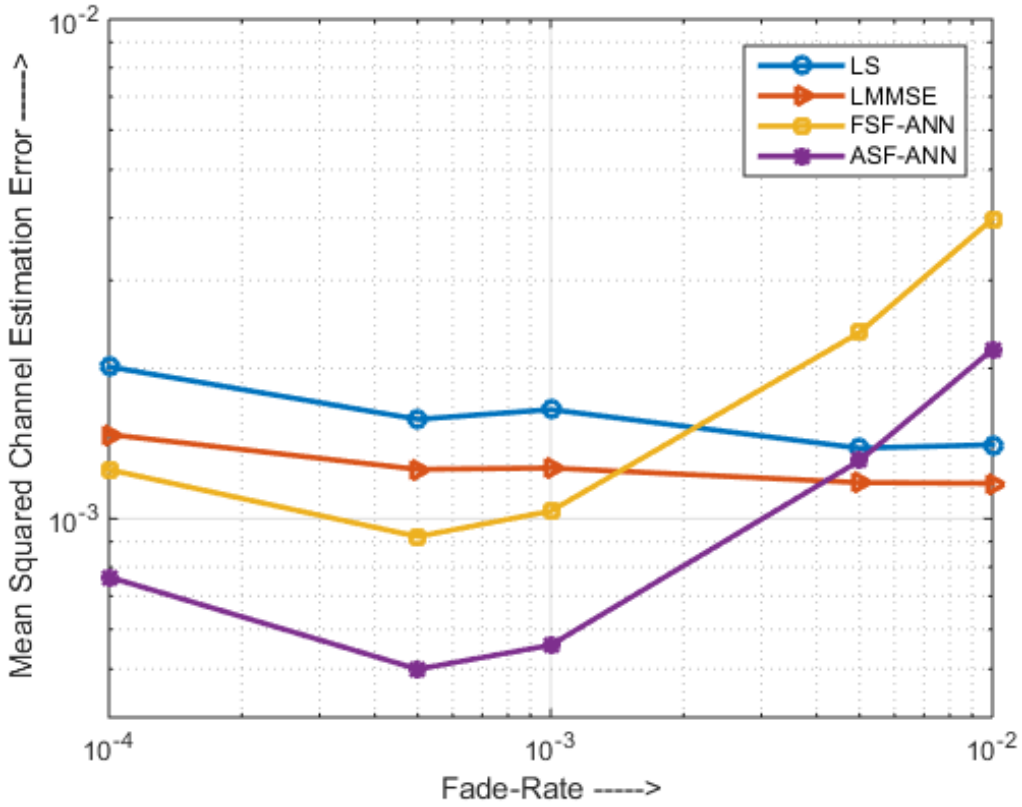

Fig. 5.6: Mean squared channel estimation error comparison at SNR = +15dB.

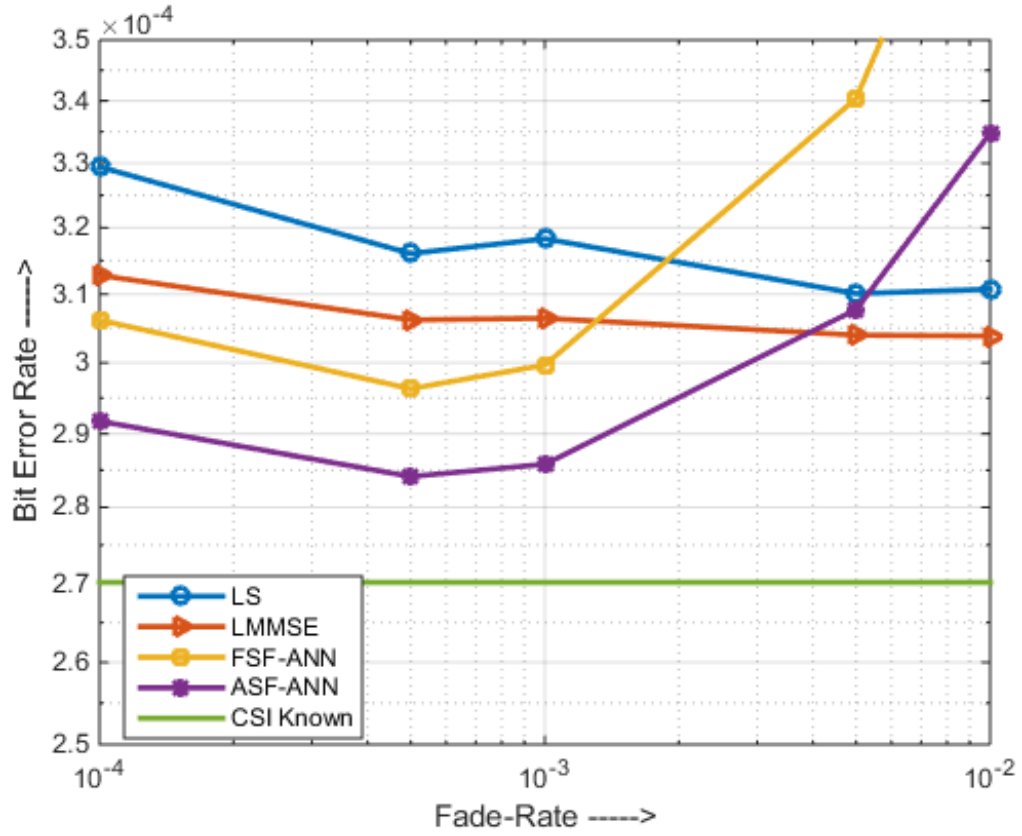

Fig. 5.7: Bit error rate comparison at SNR = +15dB.

<u>Case 2</u>:- SFBC-OFDM system using AR2 model based training of ASF-ANN

In second case, instead of the LMMSE based estimated target channel tap-coefficients (as shown in Fig. 5.1), we now consider availability of the parameters of AR2 based channel model (Eq.(5.2)) at receiver, for the training of ASF-ANN based channel estimator at the CE-stage [247]. The results provided in Fig. 5.8 at $f_D T = 0.0001$ for the different values of SNR clearly indicate that the knowledge of channel model parameters at receiver dramatically improves the channel estimation performance of ASF-ANN as well as FSF-ANN, due to the availability of appropriate target channel tap-coefficients, which improves the training of ANN. Here, the performance difference between ASF-ANN and FSF-ANN at the CE-stage gets reflected under similar conditions, when the multipath fading channel is slowly time-varying. The efficacy of efficient channel estimation through ASF-ANN appears in the results depicted in Fig. 5.9, where the BER performance of SFBC-OFDM system using ASF-ANN at CE-stage supersedes the other three approaches, while using the MMSE based detector at the SD-stage.

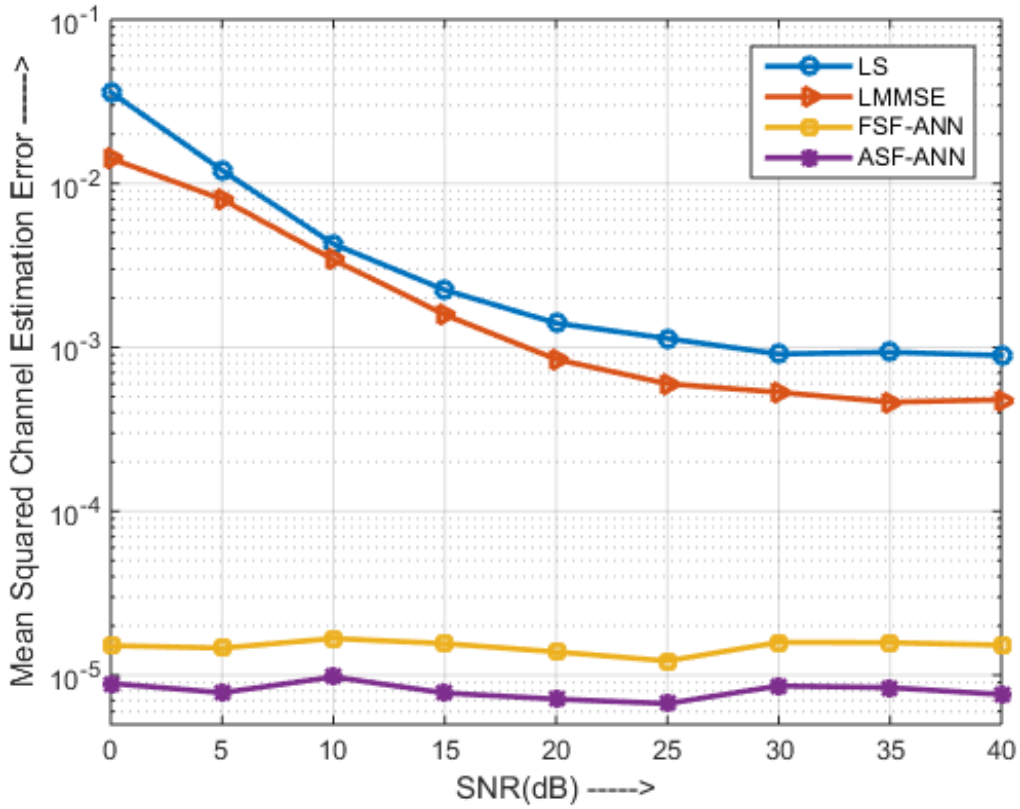

Fig. 5.8: Mean squared channel estimation error comparison at fade-rate = 0.0001 with AR2 channel model based training.

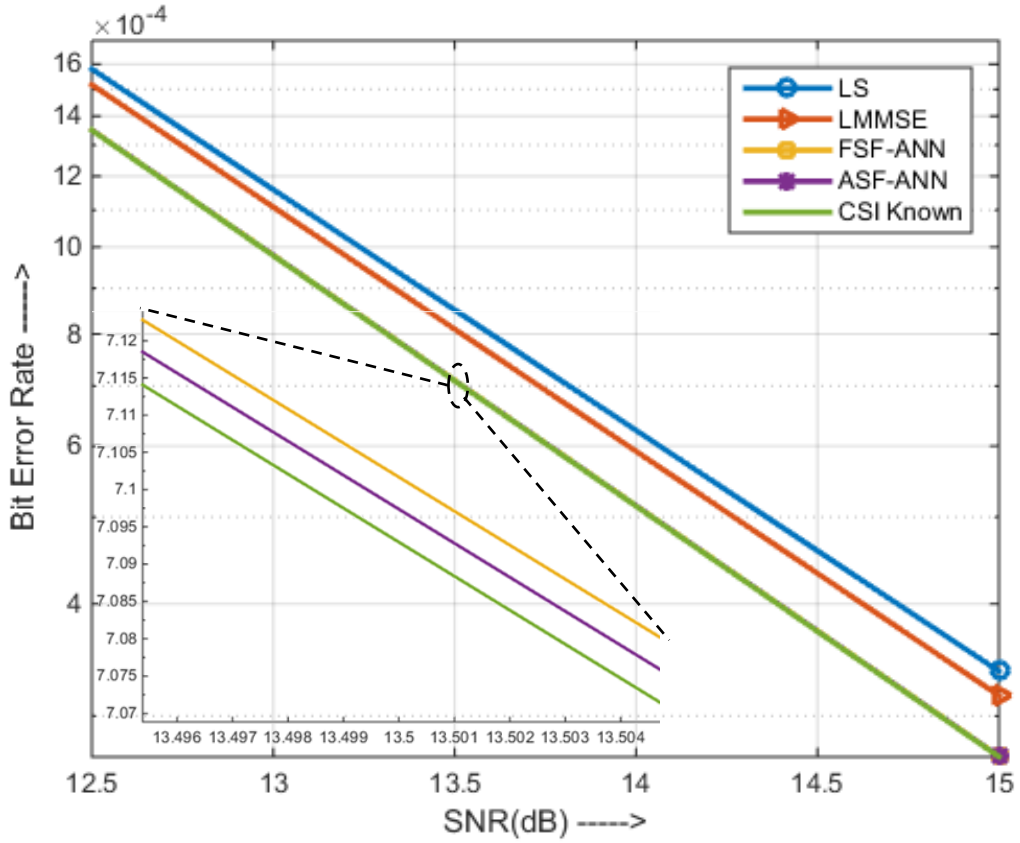

Fig. 5.9: Bit error rate comparison at fade-rate = 0.0001 with AR2 channel model based training.

5.6 Summary of Chapter

In this chapter, we have considered a 4×1 SFBC-OFDM system utilizing an ASF-ANN based channel-estimation stage and an MMSE-equalization based symbol-detection stage for investigation. The CSI estimated at the first-stage has been utilized for OFDM information symbol-detection at the second-stage, while using 64 subcarriers/subchannels in the SFBC-OFDM wireless system. We have mainly focused on the incorporation of ASF-ANN using backpropagation algorithm for the estimation of channel tap-coefficients in frequency-domain. It has been observed that the gradient-descent algorithm based adaptation of the slope of squashing-function boosts the performance of ASF-ANN by providing lower mean squared channel estimation error. Under practical scenario, the usage of LMMSE based estimated CSI (target-vector) for the training of proposed ASF-ANN appears to be an appropriate choice, in the absence of critical information about channel model (i.e., the multipath fading wireless channel encountered in between the transmitter and receiver).

The addressed 4×1 SFBC-OFDM system using ASF-ANN based approach outperforms the traditional direct LS, direct LMMSE and FSF-ANN based strategies by providing lower BER, as a result of efficiently estimated CSI.

Future scope includes the incorporation of latest channel-estimation techniques and efficient signal-detection methods for high-mobility SFBC-OFDM systems under the impulsive environment. The ASF-ANN based channel-estimation approach seems to be the tip of iceberg in the domain of machine learning for 5G communication systems [148].

CHAPTER 6

INTELLIGENCE-BASED CHANNEL-EQUALIZATION FOR 4×1 SFBC-OFDM RECEIVER

6.1 Introduction

The performance of MIMO-OFDM systems has got improved with the usage of coding schemes, such as SFBC [100]. For more than two-transmitters, the coding schemes exhibit either low code-rate or are quasi-orthogonal (QO) with reduced diversity-gain. Prior to detection of the data symbols, the conventional channel estimation techniques utilized in the communication systems are the least-squares (LS) and the minimum-mean-square-error (MMSE). The heuristic approaches for channel estimation and equalization, which employ ANNs, have also been utilized due to their universal approximation and learning ability [414]. As a nonlinear classifier, ANNs can be used to form nonlinear decision boundaries, and these can estimate a nonlinear wireless fading channel for compensation. For MIMO-OFDM systems, the neural-network with feedback is reported for reliable channel estimation by Seyman *et al.* [230], which utilizes the backpropagation (BP) algorithm for network training. For space-time coded OFDM systems, the channel estimation can be performed using a feedforward multilayered perceptron network [236]. But, it is also advantageous to incorporate the ANNs directly for channel-equalization, without the explicit requirement of channel estimation [248], in which, deep neural networks are utilized for signal detection, because of their ability to learn the characteristics of channels without online training.

ANNs can be structured as a feedforward (without feedback), or recurrent (with feedback loop) [414]. The presence of feedback loop in recurrent architectures tends to boost the learning capability of network. The most common learning algorithm is the gradient-descent-with-momentum (GDM), in which, the weight-update is stabilized and accelerated using the influence of previous step on the current update (by minimizing the error between the network outputs and desired response) [414]. As the weight-update is also dependent on the partial derivative of error function w.r.t. weight vector, the resilient-propagation (RProp) algorithm makes the weight-update size vary according to the behavior of partial derivative [433]. Another category of learning algorithms utilizes the standard optimization techniques to minimize the error energy as a function of weights, like the Levenberg-Marquardt (LM) algorithm, which is a modification of Gauss-Newton method for the application of a nonlinear LS algorithm [434].

This chapter addresses an ANN based receiver for the 4×1 SFBC-OFDM system using the backpropagation algorithm for the network training, which directly recovers the transmitted

symbols from the received signal. The conventional matched-filtering (MF) equalization approach, even with a perfectly known channel, introduces interference from the adjacent symbols, because of QO-codes. The feedforward (FFNN) as well as the recurrent (RNN) network architectures are explored as intelligent receivers for the underlying system, while utilizing various learning algorithms for the intended equalization. The bit-error-rate (BER) performance evaluation of the underlying SFBC-OFDM system is also analyzed (through Monte-Carlo simulation) using distinct QO-STBC schemes [435].

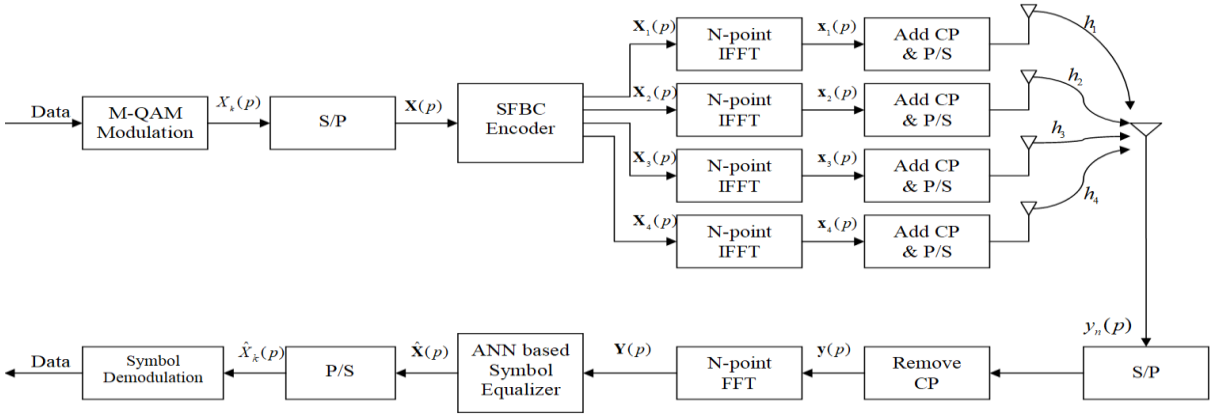

Fig. 6.1: Model for the underlying 4×1 SFBC-OFDM system.

6.2 SFBC-OFDM System Model

In an SFBC-OFDM system (as shown in Fig. 6.1), the serial stream of binary data is taken as an input to the underlying system, and it is first mapped to the M-ary quadrature-amplitude-modulation (M-QAM) to generate information symbols. These symbols are collected in a serial-to-parallel converter to form a symbol vector as: $\mathbf{X}(p) = \left[X_0(p), X_1(p), ..., X_{N-1}(p)\right]^T_{N\times 1}$, where $[.]^T$ is matrix transposition operator, and p is block index. The symbol vector is then fed to an SFBC encoder, which generates the coded sequence vectors (of length N) for each of the M_T number of transmitters, to utilize the space-frequency diversity. The QO-coded sequence vectors, for $M_T = 4$ transmitters [59], are given as

$$\begin{aligned}
\mathbf{X}_1(p) &= \left[.., X_{4m}(p), -X^*_{4m+1}(p), -X^*_{4m+2}(p), X_{4m+3}(p), ..\right]^T_{N\times 1} \\
\mathbf{X}_2(p) &= \left[.., X_{4m+1}(p), X^*_{4m}(p), -X^*_{4m+3}(p), -X_{4m+2}(p), ..\right]^T_{N\times 1} \\
\mathbf{X}_3(p) &= \left[.., X_{4m+2}(p), -X^*_{4m+3}(p), X^*_{4m}(p), -X_{4m+1}(p), ..\right]^T_{N\times 1} \\
\mathbf{X}_4(p) &= \left[.., +X_{4m+3}(p), X^*_{4m+2}(p), +X^*_{4m+1}(p), X_{4m}(p), ..\right]^T_{N\times 1}
\end{aligned} \tag{6.1}$$

for $m = 0,1,...,(N/4)-1$, where, $(.)^*$ denotes the complex conjugation operator. The coded sequence vectors $\mathbf{X}_i(p) = \{X_{i,k}(p)\}_{k=0}^{N-1}$ are then mapped on to the *N*-subcarriers via the inverse-fast-Fourier-transform (IFFT) to form transmit sequences, $\mathbf{x}_i(p) = \left[x_{i,0}(p), x_{i,1}(p), ..., x_{i,N-1}(p)\right]_{N\times 1}^T$; where $x_{i,n}(p) = \left(1/\sqrt{N}\right)\sum_{k=0}^{N-1} X_{i,k}(p)\exp\left(j2\pi kn/N\right)$, for $i = 1,2,3,4$, with $X_{i,k}(p)$ as the k^{th} symbol of p^{th} block of i^{th} transmit sequence, as in Eq.(6.1). Each of $\mathbf{x}_i(p)$ is processed to have a cyclic-prefix (CP) of length *G*, which is larger than the delay-spread of channel *L* (number of multipath) [401]. The transmitted SFBC-OFDM signal encounters the time-varying fading channel, which is assumed to remain static for one CP-OFDM block period. Its tap-coefficients are considered to follow the second-order autoregressive (AR2) process [369], [382], as

$$h_{i,l}(p) = -K_1 h_{i,l}(p-1) - K_2 h_{i,l}(p-2) + v_{i,l}(p) \tag{6.2}$$

where, $h_{i,l}(p)$ is the channel tap-coefficient for the l^{th} path (with $L = 4$) while the transmission of the p^{th} block through i^{th} transmitter, and $v_{i,l}(p)$ is the complex zero-mean white Gaussian-noise. The scalar coefficients are considered to be $K_1 = -2r_D\cos\left(\sqrt{2}\pi f_D T_1\right)$ and $K_2 = r_D^2$ with $r_D = 1 - 2f_D T_1$, f_D is the maximum Doppler-shift, $f_D T_1$ is the fade-rate, $T_1 = (N+G)T_s$ is the CP-OFDM symbol-block period, and T_s is the M-QAM information symbol duration (i.e., equivalent to the sampling period). After removal of CP, the received signal $y_n(p)$ is processed using an *N*-point FFT operator to obtain the symbols as

$$Y_k(p) = \sum_{i=1}^{4} H_{i,k}(p)X_{i,k}(p) + W_k(p) \tag{6.3}$$

where, $H_{i,k}(p)$ for $k = 0,1,...,N-1$ corresponds to FFT of the channel impulse response between the i^{th} transmitter antenna and receiver; $W_k(p)$ is the zero-mean additive-white-Gaussian-noise with variance σ_w^2. When channel gains between adjacent subcarriers are approximately equal, i.e., $H_{i,4m}(p) \approx H_{i,4m+1}(p) \approx H_{i,4m+2}(p) \approx H_{i,4m+3}(p)$ for $i = 1,2,3,4$ [258], the equation (6.3) can be expressed as

$$\begin{bmatrix} Y_{4m}(p) \\ Y_{4m+1}^*(p) \\ Y_{4m+2}^*(p) \\ Y_{4m+3}(p) \end{bmatrix} = \begin{bmatrix} H_{1,4m}(p) & H_{2,4m}(p) & H_{3,4m}(p) & H_{4,4m}(p) \\ H_{2,4m}^*(p) & -H_{1,4m}^*(p) & H_{4,4m}^*(p) & -H_{3,4m}^*(p) \\ H_{3,4m}^*(p) & H_{4,4m}^*(p) & -H_{1,4m}^*(p) & -H_{2,4m}^*(p) \\ H_{4,4m}(p) & -H_{3,4m}(p) & -H_{2,4m}(p) & H_{1,4m}(p) \end{bmatrix} \begin{bmatrix} X_{4m}(p) \\ X_{4m+1}(p) \\ X_{4m+2}(p) \\ X_{4m+3}(p) \end{bmatrix} + \begin{bmatrix} W_{4m}(p) \\ W_{4m+1}^*(p) \\ W_{4m+2}^*(p) \\ W_{4m+3}(p) \end{bmatrix} \tag{6.4}$$

or, equivalently the above equation can be represented in a vector/matrix form as

$$\tilde{\mathbf{Y}}_{4m}(p) = \tilde{\mathbf{H}}_{4m}(p)\tilde{\mathbf{X}}_{4m}(p) + \tilde{\mathbf{W}}_{4m}(p) \tag{6.5}$$

The QO-codes retain full code-rate with reduced diversity-gain. The conventional application of MF for the symbol decoding leads to

$$\begin{aligned}\hat{\mathbf{X}}_{4m}(p) &= \tilde{\mathbf{H}}_{4m}^{H}(p)\tilde{\mathbf{Y}}_{4m}(p) \\ &= \tilde{\mathbf{H}}_{4m}^{H}(p)\tilde{\mathbf{H}}_{4m}(p)\tilde{\mathbf{X}}_{4m}(p) + \tilde{\mathbf{H}}_{4m}^{H}(p)\tilde{\mathbf{W}}_{4m}(p) \\ &= \begin{bmatrix} \gamma & 0 & 0 & \beta \\ 0 & \gamma & -\beta & 0 \\ 0 & -\beta & \gamma & 0 \\ \beta & 0 & 0 & \gamma \end{bmatrix} \tilde{\mathbf{X}}_{4m}(p) + \tilde{\mathbf{H}}_{4m}^{H}(p)\tilde{\mathbf{W}}_{4m}(p)\end{aligned} \tag{6.6}$$

where, $(.)^{H}$ is the Hermitian transpose operator, the parameter $\gamma = \left|H_{1,4m}(p)\right|^2 + \left|H_{2,4m}(p)\right|^2 + \left|H_{3,4m}(p)\right|^2 + \left|H_{4,4m}(p)\right|^2$ depicts diversity-gain, and the interference term is indicated by the parameter $\beta = 2\,\mathrm{Re}\left\{H_{1,4m}^{*}(p)H_{4,4m}(p) - H_{2,4m}^{*}(p)H_{3,4m}(p)\right\}$. The need for appropriate symbol decoding motivates the usage of ANN for intended channel-equalization in the underlying SFBC-OFDM system.

6.3 ANN Based Equalization

ANNs learn about the fading environment by adjusting synaptic weights with the help of training algorithms, in order to provide a desired response for a given stimuli. The network paradigm employed for equalization in the 4×1 SFBC-OFDM system is illustrated in Fig. 6.2, in which, there are 4 independent NNs for recovering the symbols transmitted from each transmitter. During training, the complex-valued received symbols $\tilde{\mathbf{Y}}_{4m}(p)$ are split into real and imaginary parts, and then fed to the input layer of each ANN block, since a neural network efficiently processes only real symbols. Thus, each network has 8 input- and 2 output-nodes (real and imaginary), which are combined to form a complex-valued estimate of the transmitted symbol [229]. The training sample, utilized to train the ANN in a supervised manner, is denoted as $\left\{\tilde{\mathbf{Y}}_{4m}(p), X_{4m}(p)\right\}_{p=1}^{P}$. Considering $\hat{X}_{4m}(p)$ as the symbol produced at output of the ANN, the error signal generated at each output node is

$$\begin{aligned} e_1(p) &= \mathrm{Re}\left\{X_{4m}(p)\right\} - \mathrm{Re}\left\{\hat{X}_{4m}(p)\right\} \\ e_2(p) &= \mathrm{Im}\left\{X_{4m}(p)\right\} - \mathrm{Im}\left\{\hat{X}_{4m}(p)\right\} \end{aligned} \tag{6.7}$$

where, $\mathrm{Re}\{x\}$ and $\mathrm{Im}\{x\}$ indicate the real and imaginary parts of the complex-valued x respectively. Total instantaneous error energy of the network is represented as

$$\xi(p) = 0.5\left[e_1^2(p) + e_2^2(p)\right] \tag{6.8}$$

For batch learning, the synaptic weights of the network are adjusted based on the average error energy over the training sample as

$$\xi_{av} = (1/P)\sum_{p=1}^{P}\xi(p) = (0.5/P)\sum_{p=1}^{P}\left[e_1^2(p) + e_2^2(p)\right] \tag{6.9}$$

where, P is the number of SFBC-OFDM symbol-blocks utilized as the training sample (epoch).

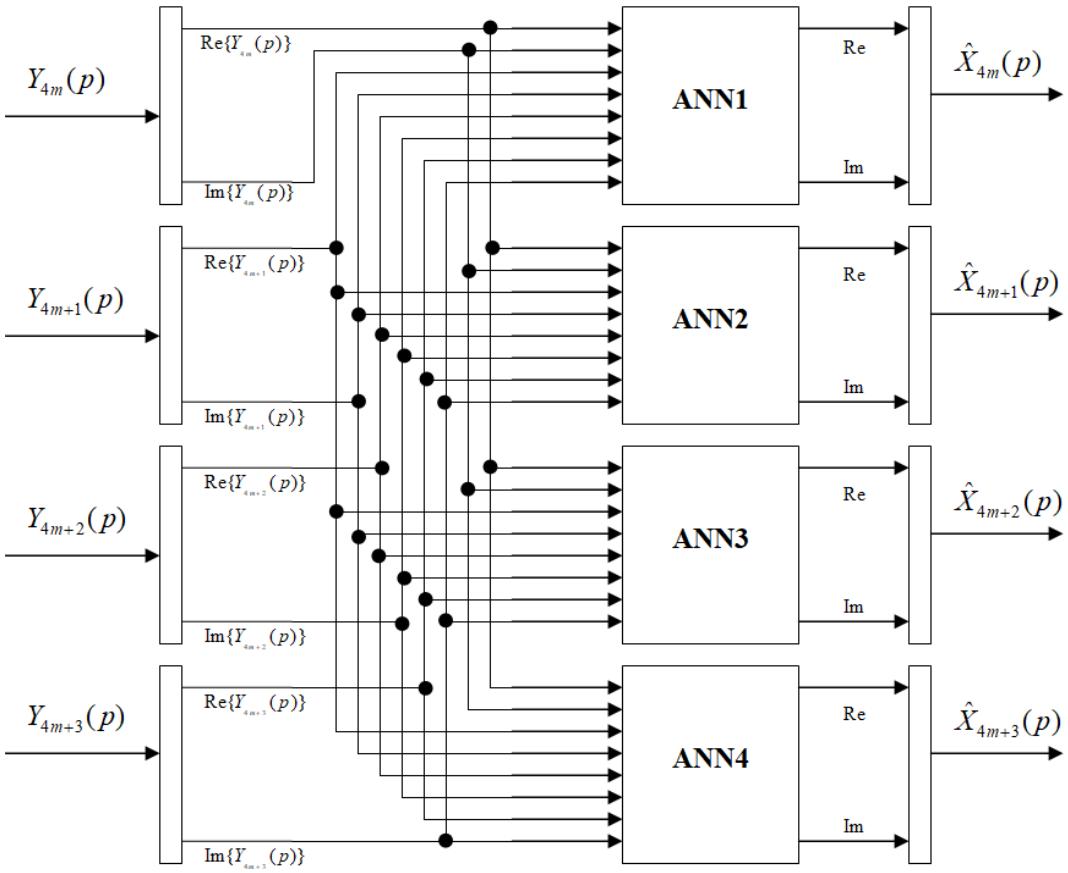

Fig. 6.2: ANN based model for equalization in the 4×1 SFBC-OFDM system [229].

6.3.1 Network Architectures

The FFNN [414] consists of an input layer of 8 nodes, two hidden layers of 16 and 8 nodes respectively, and an output layer of 2 nodes. For the RNN (shown in Fig. 6.3), the number of input and output nodes are same as in FFNN. There is only one hidden layer (of 8 neurons) with a feedback loop. For both hidden layers, the squashing-function is sigmoid with values in the range

–1 to +1 (hyperbolic-tangent function) i.e., $f_{Sig}(r) = \tanh(r)$; and for the output layer, it is the linear function i.e., $f_{Lin}(r) = r$.

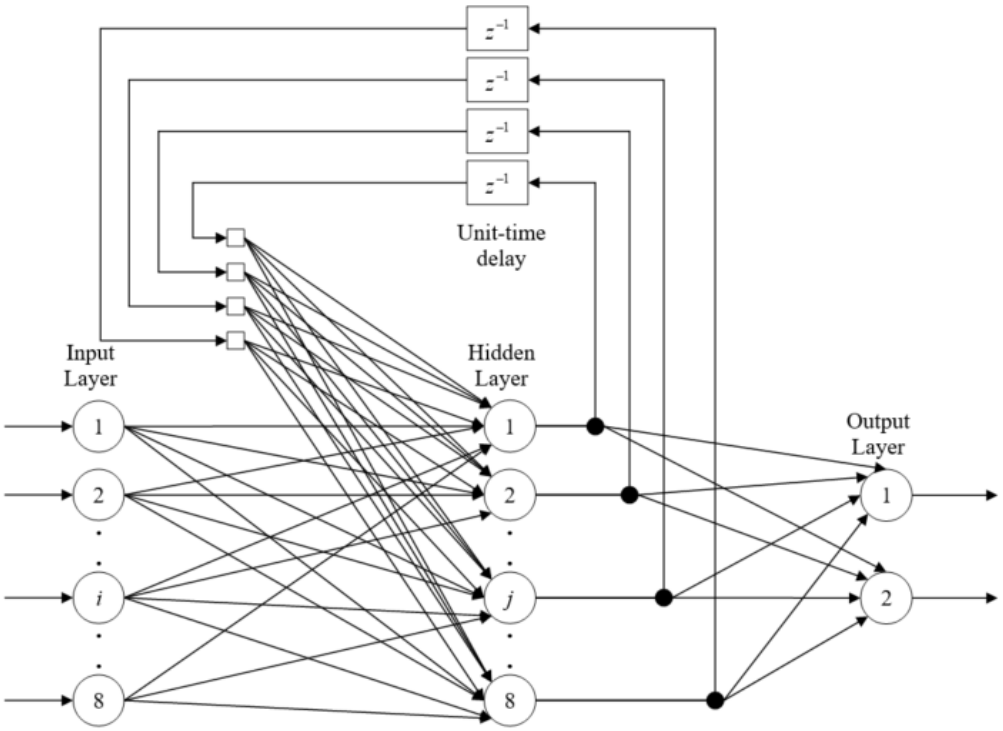

Fig.6.3: RNN architecture [414].

6.3.2 Training Algorithms

ANN models are trained by assuming the SFBC, OFDM modulation and fading channels as black boxes. The BP algorithm [414] adjusts the weight of connection from i^{th} neuron to j^{th} neuron in the q^{th} layer of NN, denoted as $\theta_{ji}^{(q)}$, by applying a correction $\Delta\theta_{ji}^{(q)}$, which is proportional to the partial derivative $\partial\xi_{av} / \partial\theta_{ji}^{(q)}$ in Eq.(6.9). The synaptic weights are updated as

$$\theta_{ji}^{(q)}(n_{ep}+1) = \theta_{ji}^{(q)}(n_{ep}) + \Delta\theta_{ji}^{(q)}(n_{ep}) \tag{6.10}$$

where, n_{ep} is the epoch/iteration index. The performance of the GDM [414], RProp [433] and LM [434] algorithms is compared in terms of the bit-error-rate (BER) of the SFBC-OFDM system. For the appropriate convergence of BP algorithm, the synaptic weight-adjustment/update for GDM algorithm [414] is given as

$$\Delta\theta_{ji}^{(q)}(n_{ep}) = \alpha\Delta\theta_{ji}^{(q)}(n_{ep}-1) + \eta\left(\partial\xi_{av} / \partial\theta_{ji}^{(q)}(n_{ep})\right) \tag{6.11}$$

where, α is a momentum constant, and η is learning-rate, which controls the convergence-rate of algorithm. In order to avoid the problem of update disturbance due to unforeseeable behaviour

of the derivative term in Eq.(6.11), the RProp algorithm changes the weight update size (which will be subtracted/added to the weight based on the sign of partial derivative) [433] as

$$\Delta\theta_{ji}^{(q)}(n_{ep}) = \begin{cases} \eta^{+}\Delta\theta_{ji}^{(q)}(n_{ep}-1) & , \frac{\partial\xi_{av}}{\partial\theta_{ji}^{(q)}}(n_{ep}-1)\frac{\partial\xi_{av}}{\partial\theta_{ji}^{(q)}}(n_{ep}) > 0 \\ \eta^{-}\Delta\theta_{ji}^{(q)}(n_{ep}-1) & , \frac{\partial\xi_{av}}{\partial\theta_{ji}^{(q)}}(n_{ep}-1)\frac{\partial\xi_{av}}{\partial\theta_{ji}^{(q)}}(n_{ep}) < 0 \end{cases} \tag{6.12}$$

where, $0 < \eta^{-} < 1 < \eta^{+}$. If the partial derivative changes signs from one epoch to other, the weight-update size is decreased by η^{-}; otherwise it is increased by η^{+}. The LM algorithm [434] is a batch learning technique that minimizes the average error energy by updating the network weights after every epoch. The weight updating in the NN training using the LM algorithm is

$$\Delta\boldsymbol{\theta}(n_{ep}) = \left[\mathbf{J}^{T}(\boldsymbol{\theta})\mathbf{J}(\boldsymbol{\theta}) + \mu\mathbf{I}\right]^{-1}\mathbf{J}^{T}(\boldsymbol{\theta})\boldsymbol{\xi}(n_{ep}) \tag{6.13}$$

where, $\boldsymbol{\theta} = \left[\theta_{11}^{(1)},...,\theta_{ji}^{(q)},...\right]^{T}$ is the network weight-vector, $\boldsymbol{\xi} = \left[\xi(1),...,\xi(p),...,\xi(P)\right]^{T}$ is the error energy vector, μ is the regularization parameter, $\mathbf{I}$ is the identity-matrix; and $\mathbf{J}(\boldsymbol{\theta})$ is the Jacobian matrix, defined as

$$\mathbf{J}(\boldsymbol{\theta}) = \begin{bmatrix} \partial\xi(1)/\partial\theta_{11}^{(1)} & \cdots & \partial\xi(1)/\partial\theta_{ji}^{(q)} & \cdots \\ \vdots & & \vdots & \\ \partial\xi(P)/\partial\theta_{11}^{(1)} & \cdots & \partial\xi(P)/\partial\theta_{ji}^{(q)} & \cdots \end{bmatrix} \tag{6.14}$$

Once, all the examples of a training sample are fed to the network, the error energy vector and the Jacobian matrix are computed for weight updating. Then, the error energy vector is again computed with recent updated weights. If the resultant new errors are alleviated, then the regularization parameter μ is divided by a factor δ; otherwise vice-versa for next epoch [236], [434].

6.4 Simulation Results

For the Monte-Carlo simulation under various fading scenarios, fade-rates and different values of the signal-to-noise-ratio (SNR), a 4×1 SFBC-OFDM system with 4-QAM scheme, $N = 64$ and $G = 16$ (CP) is considered that corresponds to the work of Ye *et al.* [248]. The QAM symbols are then encoded for 4-transmit antennas using the QO-STBC scheme (as in Eq.(6.1)). The ANN is trained using $P = 50$ SFBC-OFDM symbol-blocks as a training sample (epoch). Each example in a training sample is first fed to the NN for the output and error calculations, which are utilized for weight updating after each epoch (after averaging errors from all examples in an epoch). The received signal and originally transmitted signal for the first 50 SFBC-OFDM blocks are treated

as training data. The input to ANN model is the received signal; and the model is trained to reduce (by iterative process) the difference between the network output and originally transmitted signal [248].

6.4.1 BER Performance of ANN Algorithms at Different Fade-rate and SNR Values

For the GDM algorithm, the learning-rate and momentum constant are considered to be $\eta = 0.1$ and $\alpha = 0.01$, respectively, for both the FFNN and RNN. For the RProp algorithm, the initial learning rate is kept at $\eta = 0.95$ for the FFNN, $\eta = 0.1$ for the RNN, with $\eta^{+} = 1.2$ and $\eta^{-} = 0.5$. The initial value of the regularization parameter in the LM algorithm is set at $\mu = 0.95$ for the FFNN, $\mu = 0.1$ for RNN, and with δ =10. For fade-rate = 0.0001 at SNR = +25dB for FFNN, the BER value in case of the LM algorithm is 0.0017 (as illustrated in Fig. 6.4), which provides approximately +1dB performance advantage over the MF approach under similar conditions. However, the BER = 0.0021 for the RProp and the BER = 0.0035 for the GDM algorithms are observed under the same scenario. For the RNN, the BER values are 0.0010, 0.0013, and 0.0021 for the LM, RProp and GDM algorithms respectively, which is in the close vicinity to BER = 0.001 for the LS algorithm (as shown in Fig. 6.5).

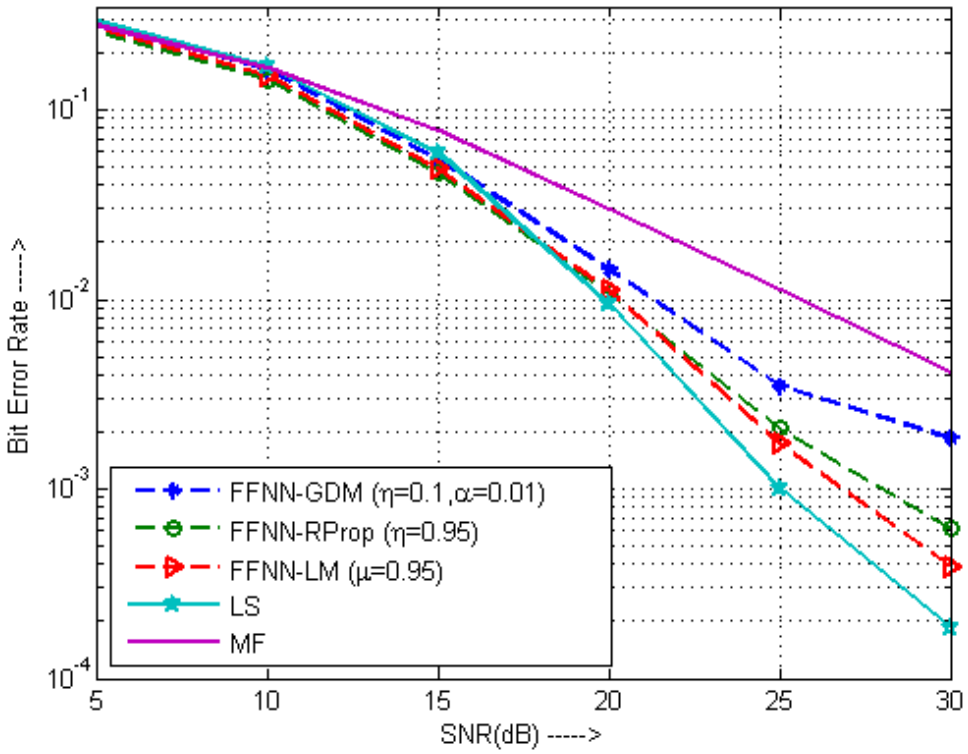

Fig. 6.4: BER vs. SNR for the FFNN at the fade-rate = 0.0001.

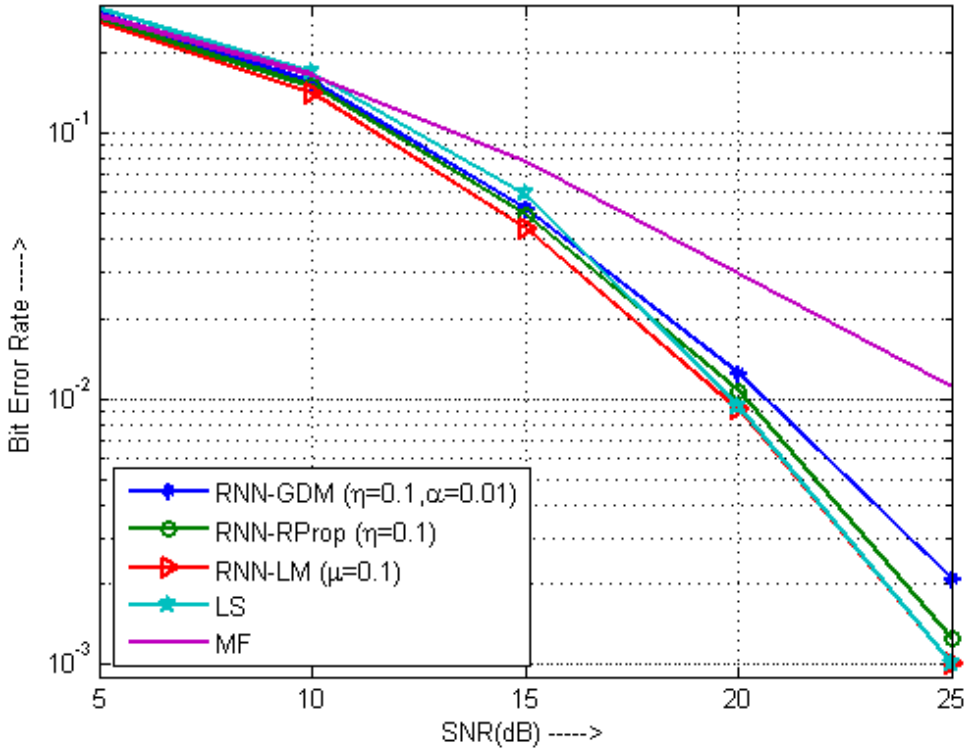

Fig. 6.5: BER vs. SNR for the RNN at the fade-rate = 0.0001.

For the fade-rate =0.001 and BER =0.01 in case of the LM algorithm, its performance advantage in terms of the SNR is approximately 3dB for the FFNN and 4.5dB for the RNN in comparison to the MF approach [258] (as depicted in Fig. 6.6 and Fig. 6.7). The RNN provides better symbol recovery with a SNR advantage of approximately +1dB for LM, 0.5dB for the RProp and 1.75dB for the GDM algorithms, at the BER = 0.01, in comparison to the FFNN. The LS algorithm performs approximately +1dB better than the LM algorithm in the RNN at a fade-rate = 0.001 and BER = 0.01. It is evident from Fig. 6.8 that as the fade-rate elevates, the BER performance gets deteriorated for all the algorithms, but the performance of RNN supersedes FFNN. However, LM algorithm apparently outperforms the RProp as well as the GDM algorithms, by providing a lower BER under similar conditions, such that the $BER(LM) < BER(RProp) < BER(GDM)$. Table 6.1 illustrates the BER performance of various ANN algorithms at different fade-rates for distinct values of SNR.

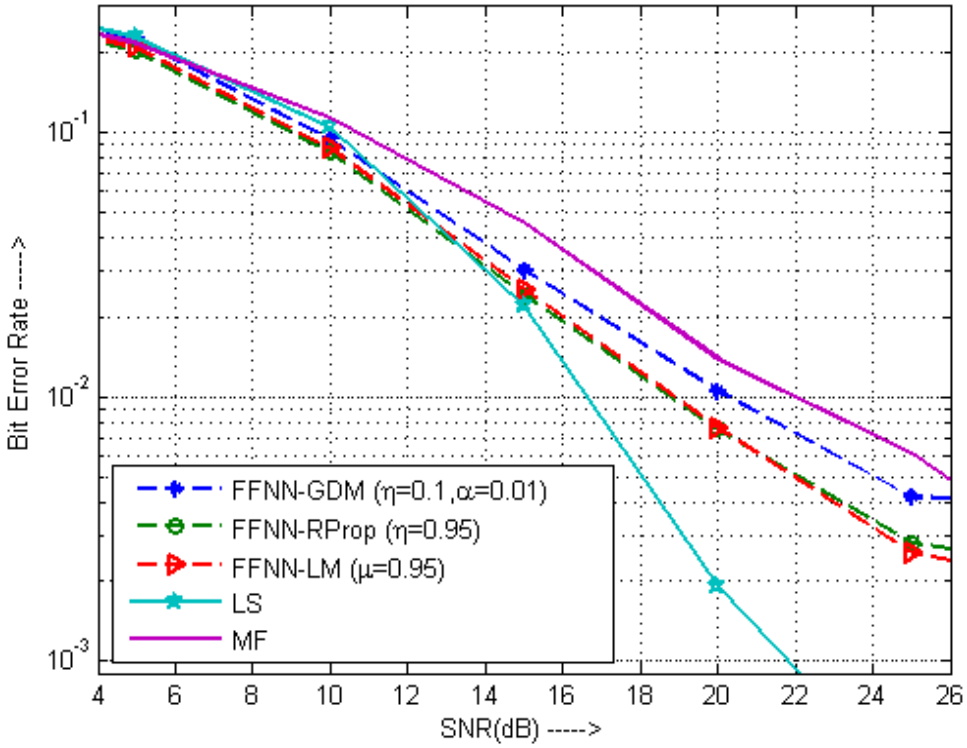

Fig. 6.6: BER vs. SNR for FFNN at the fade-rate = 0.001.

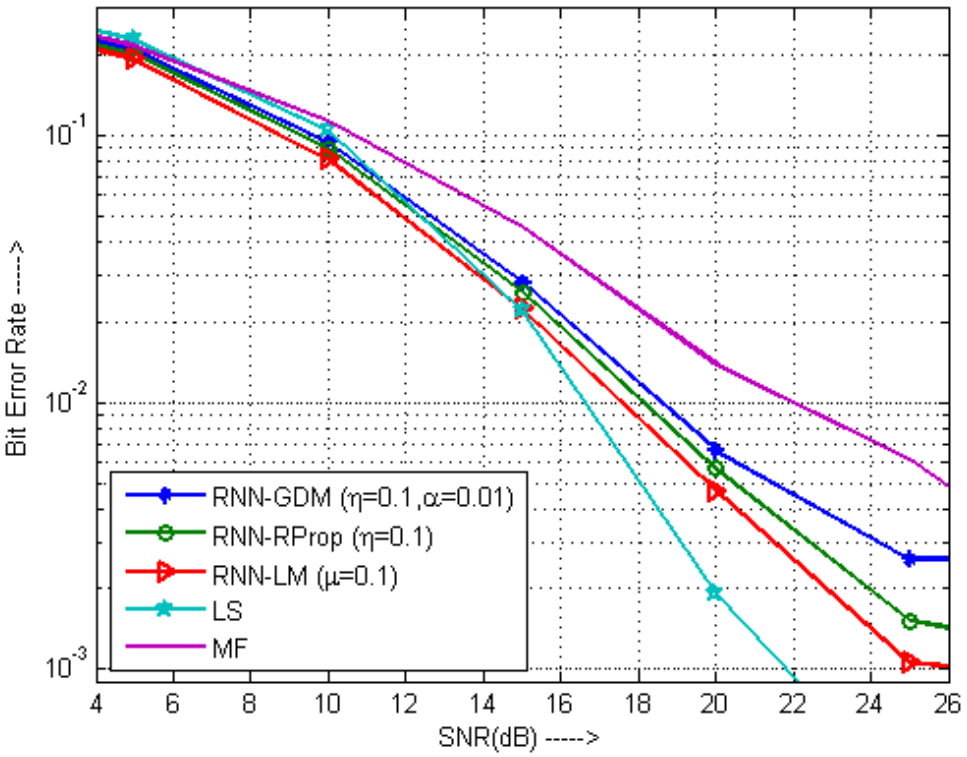

Fig. 6.7: BER vs. SNR for RNN at the fade-rate = 0.001.

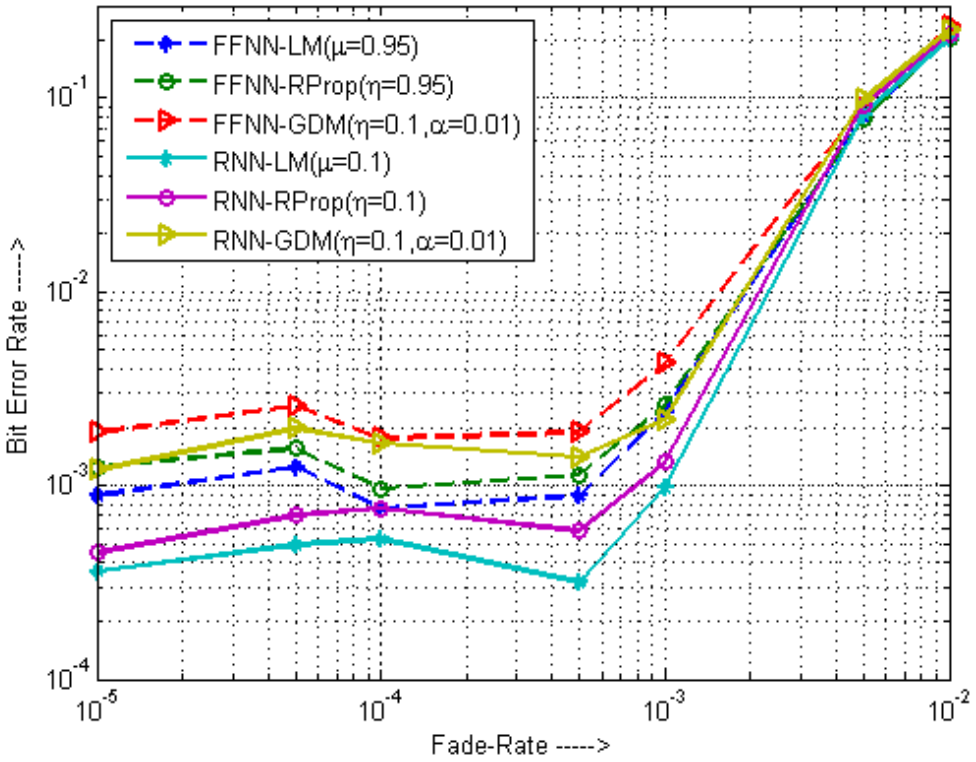

Fig. 6.8: BER vs. fade-rate at the fixed SNR = +27.5dB.

Table 6.1: BER values of different ANN algorithms at distinct values of the fade-rate for the fixed SNR.

Fade-Rate	FFNN-LM		FFNN-RP		FFNN-GDM		RNN-LM		RNN-RP		RNN-GDM	
	BER at fixed SNR		BER at fixed SNR		BER at fixed SNR		BER at fixed SNR		BER at fixed SNR		BER at fixed SNR	
	+27.5 dB	+22.5 dB	+27.5 dB	+22.5 dB	+27.5 dB	+22.5 dB	+27.5 dB	+22.5 dB	+27.5 dB	+22.5 dB	+27.5 dB	+22.5 dB
0.00001	0.00089	0.005	0.00124	0.00576	0.00188	0.00672	0.000359	0.00375	0.000448	0.00449	0.00121	0.00589
0.00005	0.00124	0.0048	0.001548	0.00535	0.002569	0.00583	0.000494	0.00296	0.000705	0.00367	0.00196	0.00507
0.0001	0.00076	0.004	0.000964	0.00455	0.001757	0.0066	0.000528	0.0027	0.000765	0.0036	0.001655	0.005
0.0005	0.00089	0.0013	0.001134	0.001619	0.001886	0.0022	0.000317	0.001264	0.000584	0.00149	0.001401	0.00221
0.001	0.002396	0.003	0.002599	0.003758	0.004237	0.00446	0.000973	0.00263	0.001314	0.0032	0.002184	0.00491
0.005	0.078151	0.0827	0.07728	0.08593	0.090127	0.09634	0.08173	0.0797	0.090985	0.0897	0.098272	0.09602
0.01	0.21099	0.2198	0.20367	0.2195	0.23222	0.2402	0.20323	0.2132	0.21462	0.2237	0.2265	0.2391

6.4.2 BER Performance for Different Quasi-orthogonal Codes

The performance of ANN based equalisation in the SFBC-OFDM system is also analysed using various quasi-orthogonal block-codes, in which, the different distribution of conjugates in the transmission matrix results in distinct positions of the correlated values [435]. In this chapter, different QO-STBC schemes are incorporated in the underlying SFBC-OFDM system under similar conditions. These schemes are the Jafarkhani code [59], the Tirkkonen–Boariu–Hottinen (TBH) code [60], the Jafarkhani with TBH correlated positions code, and the TBH with Jafarkhani correlated positions code [435].

It is quite evident from the results demonstrated in Fig. 6.9 that BER performance of the underlying system is approximately similar for the aforementioned four QO-STBC codes, while using the recurrent neural network architecture with the LM training algorithm for equalization. The results are in close agreement with the observation reported by Su *et al.* [436]. Under the typical channel conditions, the performance of TBH based QO-STBC codes [60] is observed to be deteriorated [435]; but in combination with the OFDM system, their performance improves significantly, as the DFT operation at the receiver in OFDM system randomizes the interference/noise terms [323]. However, QO-STBC based codes pioneered by Jafarkhani [59] always perform well, with or without the OFDM based system configuration, even under the adverse fading environment.

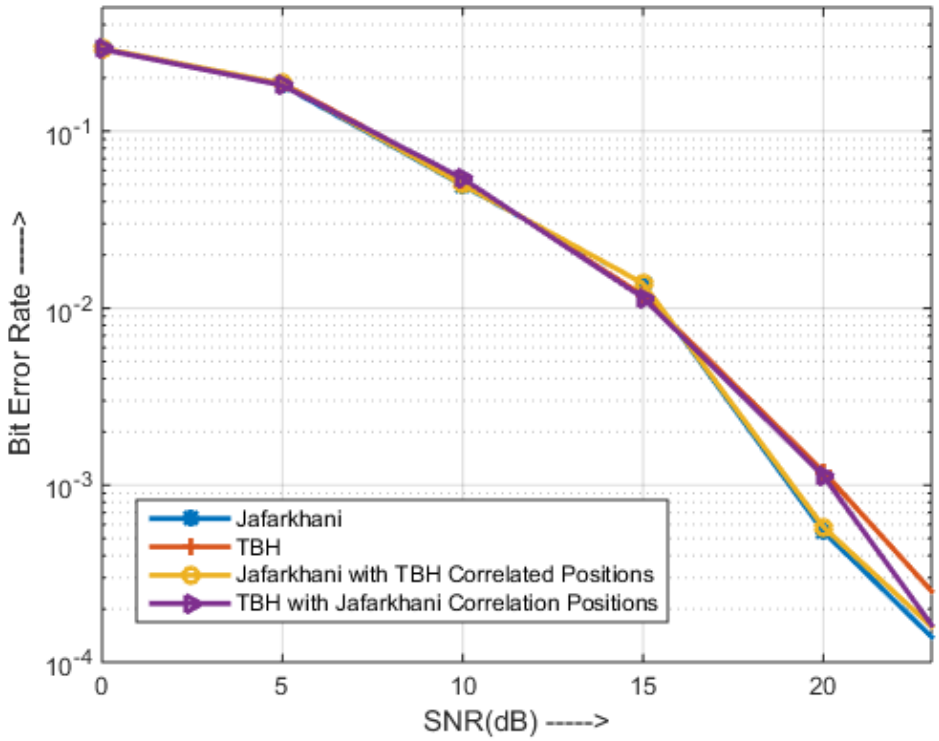

Fig. 6.9: BER for QO-codes at fade-rate = 0.0001.

6.5 Summary of Chapter

In this chapter, we have explored an intelligence-based channel-equalization technique for the 4×1 SFBC-OFDM system, while working under the slow time-variant multipath fading channels. The ANN based strategy precludes the explicit need of channel estimation at the wireless receiver because of its ability to learn the channel characteristics, which enables ANNs to directly recover the transmitted information symbols from the distorted received wireless signals. We have implemented ANN based equalizer by using the feedforward as well as recurrent neural network architectures, which are trained using the error backpropagation algorithms. The major contribution in this chapter is the investigation of three different strategies; namely GDM, RProp, and LM algorithm based approaches. It has been observed that for the 4×1 SFBC-OFDM systems, the recurrent architecture with LM algorithm supersedes all other aforementioned ANN algorithms by providing the lower average bit-error-rate, while using various quasi-orthogonal space-time block-codes.

The future scope includes applications of the presented channel-equalization based intelligent SFBC-OFDM technique in the radio-over-fiber transmission systems using millimeter waves [437], [438], [439] and under various fading scenarios [349], [440], [441].

CHAPTER 7

CONCLUDING REMARKS AND FUTURE SCOPE

With substantial increase in the demand for applications that require high-speed wireless data transmission, the need for development of algorithms/techniques suitable for the wideband systems has become essential. A large number of schemes have been addressed that utilize the combination of MIMO with OFDM. It has enabled an efficient data transfer between the wireless transmitter and receiver, by exploiting its capability to incorporate coding over time-, frequency- as well as spatial-domain. It is quite evident from literature that the STBC-OFDM with orthogonal-codes have relatively lower complexity, that accounts for its simple implementation. However, the quasi-orthogonal STBC-OFDM systems are not able to attain the full multipath diversity as well as high rate simultaneously. On the contrary, the SFBC-OFDM system can achieve relatively higher diversity as well as full-rate, but at the cost of higher computational complexity of the decoder. Also, it has been analyzed that for the channel variations caused due to high mobility of vehicles, the STBC based systems have shown severe degradation in the performance due to time-selectively of fading channel. However, the frequency-selective nature of channel significantly limits the performance of SFBC based systems; which may be mitigated by the usage of a large number of subcarriers. Further, in order to efficiently decode the received data symbols, the knowledge of CSI plays an important role for the coherent detection in spatially-coded OFDM systems. In this research work, we have studied various CSI-estimation/prediction strategies for the spatially-coded OFDM systems, for improvement as per the requirements of its desired features. And, this well approximated CSI is further used for the efficient information symbol-detection under the fading environment. In the following, we summarize the significant observations/outcomes of our study, and also give suggestions for further investigations.

7.1 Concluding Remarks

We have first presented an adaptive orthogonal-frequency-division-multiplexing modulation based wireless communication system, working over the frequency-selective time-varying multipath fading channels, which utilizes a combination of the MKF-GVSS-LMS algorithm based channel estimator and the NVFF-RLS algorithm based channel predictor. However, the long-range-fading-prediction is necessary for the efficient AOFDM wireless system, which makes use of the estimated channel-state-information for the prediction of future CSI. The predicted CSI is eventually used for the adaptive bit-allocation/loading at the transmitter (through the predicted CSI

feedback from the receiver to transmitter). The time-variations in the wireless fast-fading channel response account for the nonstationarity of the received signal, which adversely affects the performance of adaptive channel estimator at the receiver.

In presented research work, the MKF-FSS-LMS algorithm is replaced by the MKF-GVSS-LMS algorithm to generate the accurate channel impulse response estimates with the lower mean-squared-channel-estimation error, when the fade-rate variations are not highly abrupt. The quality of estimated CSI significantly affects the performance of adaptive prediction algorithm at the wireless receiver, therefore the FFF-RLS algorithm is replaced with NVFF-RLS algorithm for the long-range-channel-prediction with lower mean-squared-prediction error, under the time-variant multipath fading channels. The estimation of AR1 parameter (fading parameter) by using the GVSS-LMS algorithm and the prediction of channel tap-coefficients by using the NVFF-RLS algorithm are two major features incorporated in the underlying AOFDM system, which lead to the reliable and appropriate adaptive bit-allocation, resulting in an approach suitable to exploit the potential of an AOFDM system. The simulation outcomes connote that the presented MKF-GVSS-LMS algorithm provides the higher convergence-rate and the lower tracking-error, which ultimately results in the lower SER due to efficient working of the NVFF-RLS algorithm based long-range-channel-predictor, even at the higher fade-rate values under the high SNR conditions.

We have next presented adaptive channel prediction techniques utilizing the cyclic-prefix information in wireless OFDM systems. The appropriate length of CP not only circumvents the problem of ISI, but also precludes the requirement of additional training symbol sequences for the channel estimation/prediction. The Kalman-filtering, RK-LMS, RLS, NVFF-RLS algorithm based adaptive channel predictors have been compared on the basis of convergence-rate and tracking performance in the training-mode and decision-directed-mode. It can be inferred from simulation outcomes that the overall performance of KF is better than other adaptive algorithms. The NVFF-RLS algorithm performs marginally better than the conventional RLS algorithm under static environment, but it outperforms substantially as compared to the RLS algorithm under time-varying channels, as far as the channel tracking is concerned. This is because of lag-misadjustment appeared during the channel tracking in conventional RLS algorithm based channel predictors. Under typical conditions, even the tracking-mode performance of RK-LMS algorithm is comparable to RLS algorithm, which provides an opportunity to reduce the computational burden in OFDM systems.

In decision-directed-mode, the decision feedback errors and channel estimation/prediction errors go hand in hand. Therefore, the tracking performance degradation is observed in case of all the adaptive algorithms due to intricate decision error propagation problem, which adversely

affects the tracking performance of KF. However, simulation results under the time-varying channels elucidate that the performance advantage of KF is slightly better than NVFF-RLS algorithm. It is apparent from simulation results that the NVFF-RLS algorithm provides enhanced channel tracking performance than the traditional RLS algorithm in 2×1 STBC-OFDM system, under time-varying environment, which results in substantial reduction in the symbol error rate in comparison to the conventional OFDM system.

Further, this research work has also addressed the significant impact of impulse-noise on the BER performance of SFBC-OFDM systems, while working under the frequency-selective fading channels. In addition to impulse-noise and AWGN, the imperfect CSI utilized to decode/detect the information symbols also deteriorates the BER performance of SFBC-OFDM systems using the MPSK and MQAM digital modulation techniques. In real-time scenario, the imperfect CSI comes into picture due to the noisy channel estimates at wireless receiver. Therefore, closed-form average BER expressions for the underlying SFBC-OFDM systems under the Rayleigh multipath fading conditions have been presented, which take into account the impulse-noise, AWGN and channel estimation error statistics. These expressions may be utilized to quantify the amount of deterioration in average BER under the influence of impulse-noise as well as imperfect CSI. It may be inferred from the simulation outcomes that the BER performance of SFBC-OFDM system gets substantially degraded, as the average number of impulses per OFDM symbol-block period elevates. However as the channel estimation error variance increases, the average value of BER also gets elevated.

It is evident from results that the increasing number of impulses per OFDM symbol-block period dramatically and drastically boosts the value of BER, which has been controlled by increasing the number of subcarriers/subchannels in the same fixed OFDM symbol-block period, while keeping the total signal transmission power constant. Hence, the noise bucket effect apparently results in the reduction of impulsive energy per subcarrier/subchannel (by enhancing SNR per subchannel), due to the DFT operation (causing the spreading of impulse-noise energy over the increased number of subcarriers) at the wireless receiver. The simulation results for Nakagami-*m* fading channels connote similar observations under similar conditions. But, the average value of BER for the underlying SFBC-OFDM systems has been found to increase with the alleviating value of "*m*" under Nakagami-*m* fading scenario because the severity level of fading surges up. When the value of "*m*" reduces from 0.85 to 0.65 (typical example discussed in Case 4 of Section 4.4), the average BER gets enhanced significantly in the presence of impulse-noise, but the adverse impact of impulse-noise has been reduced appreciably by increasing the value of "*N*" form 64 to 256 in an OFDM symbol-block period.

Also, we have presented a 4×1 SFBC-OFDM system using an ASF-ANN based channel-estimation stage and an MMSE equalization based symbol-detection stage. The pilot-based supervised training of ASF-ANN appears to be an appropriate choice to curb the possibility of divergence of the backpropagation based learning algorithm. The ASF-ANN based channel estimator captures the required knowledge about the multipath fading channel during training-mode, and keeps the knowledge intact under slow time-varying environment. It reduces the frequent usage of periodic pilot-based training sessions, which in turn enhances the bandwidth efficiency. For real-time applications, we have suggested the usage of LMMSE based estimated CSI (target-vector) for the training of ASF-ANN using BP algorithm, because the accurate values of parameters of the AR2 channel model are usually not available at the wireless receiver. The simulation results showcased in the presented research work connote that the ASF-ANN based 4×1 SFBC-OFDM system performs well under the high SNR and low fade-rate conditions, which supersedes the direct LS, direct LMMSE and FSF-ANN based approaches, by providing comparatively lower BER.

Eventually, an ANN based intelligent receiver for a 4×1 SFBC-OFDM system is explored, which detects the transmitted symbols directly from the received signaling waveform under slowly time-varying multipath environment. It precludes the usage of channel estimation. The simulation results connote that the RNN configuration with LM and RProp algorithms has an edge over the FFNN under similar conditions for the different fade-rate and SNR values, in terms of lower BER. The performance of the RNN with GDM algorithm is found to be better than the FFNN with GDM, but its performance is quite inferior to the LM and RProp algorithms. The results for the 4×1 SFBC-OFDM systems manifest that the recurrent architecture with the LM algorithm outperforms all other discussed ANN algorithms by exhibiting comparatively a lower BER. However, some distinct QO-STBC codes may be utilized in the underlying SFBC-OFDM system, but the QO-STBC codes proposed by Jafarkhani [59] undoubtedly appear to be the best choice.

7.2 Suggestions for Further Work

Future scope includes the extension of the presented research work in the domain of 5G wireless communication networks. In some of the communication networks, CP-OFDM can be employed for the downlink services to meet the needs of massive MIMO [442], to provide higher capacity at the higher bandwidths. But, it is not suitable for the uplink under the same scenario in combination with IoT. Here, polynomial-cancellation-coded OFDM has appeared as a potential substitute, that has waveforms, which are well-suited for the usage in 5G networks (due to its accurate localization in time- as well as frequency-domain) [443]. A novel channel-conditional-

recovery-network (which utilizes the output of a channel estimation network) can also be used to recover the transmitted signalling waveform in the OFDM systems [444]. Undoubtedly, a hybrid power-domain NOMA technique [445] utilizing the superposition of conventional-OFDM and index-modulated-OFDM has emerged as an attractive option to boost the capacity of 5G networks [446].When only partial CSI is available at the wireless receiver, the space-time/frequency-line-coded OFDM scheme can be utilized, which exploits CSI at the transmitter to linearly encode successively modulated symbols [447]. Generalized-DFT-spread-OFDM is a good option for 5G communication systems, as it replaces the cyclic-prefix with a sequence exhibiting tunable length. Here, such sequence is part of the IFFT output. In addition to its various benefits, it combats the phase-noise and Doppler-spread based hazards [448].

However, for CSI-estimation in MIMO-OFDM systems for 5G networks, a compressed-sensing-based CE method can be utilized, known as MIMO-linearizing technique [449], [450]. The recurrent neural network can also be used to operate channel predictor (by considering benefits of time-series prediction) in the MIMO-OFDM systems. It can predict future channel-state-information from its previously obtained values at the same subcarrier [451]. However, an intelligence-based receiver can be used in STBC-OFDM systems, which utilizes radial-basis-function neural network in combination with principal-component-analysis approach [452]. Deep-learning based equalization technique can also be employed when the underlying MIMO-OFDM system is working with insufficient CP (i.e., multipath delay-spread exceeds the length of CP) [453]. The concept of adaptive-modulation is introduced to maintain the data-rate and reliability as per the channel conditions. Therefore, the deep neural network based machine learning paradigm for the adaptive-modulation in MIMO-OFDM systems uses training symbols, which are dependent on the extracted features from received signals and assigned labels according to the signal detection [454]. However, the nonlinear power-amplifier and imperfect CSI adversely affect the performance of SFBC-OFDM systems working under the TWDP channel, which need to be tackled to improve the bandwidth efficiency [148]. Moreover in SFBC-OFDM systems, the usage of softsign squashing-function in the ANN-based channel estimation leads to improvement in the symbol-error-rate performance, due to the reduction in channel estimation errors [430]. Even, some other optimization techniques [455], [456] can also be applied to improve the performance of channel estimator/predictor.

A combination of a traditional neural-network [457] and a long-short-term with memory network is also a suitable approach for the learning framework, which can be used for CSI prediction in 5G wireless systems (including the massive MIMO, OFDM and millimetre-wave based techniques) [243]. For 5G V2I networks, the channel prediction algorithm using the channel

modelling approach may be incorporated, which doesn't require pilot-symbols. Here, an adaptive RLS algorithm based CSI prediction approach [401] is utilized to predict one or more future OFDM block channel impulse response coefficients [458]. In the presence of nonlinear distortion arising due to the RF components in transceiver, the deep-echo-state-network based symbol-detection strategy has found application in the intelligence-based 5G MIMO-OFDM systems, which can process the received signal both in spatial- as well as temporal-domain [459]. However, an intelligent receiver based on ANNs (using gradient-descent with momentum or resilient-propagation or Levenberg-Marquardt algorithm [416]) can be a suitable choice for the SFBC-OFDM systems, working under slow time-variant frequency-selective fading channels.

APPENDIX-A

SIMULATION OF BASIS-EXPANSION-MODEL FOR CHANNEL FADING USING AR1-PROCESS

A.1 Introduction

The wireless communication systems encounter multipath Rayleigh fading channels, which are conventionally simulated by using the well-known Jakes' fading model [385]. This fading paradigm evidenced that the autocorrelation of channel tap-coefficients is $R_{hh}(k) = J_0\{2\pi f_D T_s k\}$ [335], where $J_0\{.\}$ is the zeroth-order Bessel-function of the first-kind, f_D is the maximum Doppler frequency, T_s is the sampling interval, k is the discrete-time lag and h is the channel tap-coefficient. In an alternate approach [460], the basis-expansion-model is proposed for the multipath rapidly fading channels, in which the time-varying channel impulse response (that arises due to the Doppler-effects) is expanded over a basis of complex exponentials. The BEM coefficients are considered to be randomly-varying, which follow the normal Gaussian-distribution [334], [460]. However in Kalman-filtering based adaptive channel estimation, the AR1 process is used to characterize the time-variations of the BEM coefficients [461]-[464].

A.2 Basic BEM-AR1 Model

Let us consider the received wireless signal in the discrete-time domain to be

$$y(n) = \sum_{l=0}^{L-1} h(n;l)x(n-l) + \eta(n) \qquad \text{(A.1)}$$

where, $h(n;l) = h(l;n)$ is the l^{th} time-varying channel tap-coefficient at the n^{th} time instant, L is the total number of channel tap-coefficients, x is the transmitted signal, and η is the zero-mean complex white Gaussian-noise with variance σ_η^2. The BEM captures the randomness of fading environment by

$$h(n;l) = \sum_{q=1}^{Q} \bar{h}_q(n;l) b_q(n) \qquad \text{(channel tap-coefficients)} \qquad \text{(A.2)}$$

with $\bar{h}_q(n;l) = c_q(n;l)e^{j\phi_q}$ (uncorrelated BEM coefficients), c_q is amplitude of the q^{th} path, ϕ_q is uniformly distributed RV in the range $[0, 2\pi]$, $b_q(n) = \exp(j\omega_q n)$, $\omega_q = (2\pi f_D)\cos(2\pi q/Q)$, $f_D = v/\lambda$, v is the speed of mobile, and λ is the carrier wavelength. The BEM approximates

Jakes' model for the large values of Q [460] because the envelope of $h(n;l)$ follows Rayleigh probability density function. However in the Kalman-filtering based channel estimation [461] using BEM-AR1 hypothesis, each BEM coefficient is considered to be generated by an independent AR1 process, it follows that

$$\bar{h}_q(n;l) = \alpha_{AR1}\bar{h}_q(n-1;l) + \bar{w}(n;l) \tag{A.3}$$

where, the coefficient $\bar{h}_q(n;l)$ is assumed to possess zero-mean and variance $\sigma^2_{\bar{h}}$, the Markov parameter is given as α_{AR1} in the range $[0,1)$, and $\bar{w}$ is the zero-mean complex Gaussian process-noise with variance $\sigma^2_{\bar{w}}$, which is supposed to be independent and uncorrelated with BEM coefficients. The AR1 process in Eq.(A.3) can be simplified to provide

$$\begin{aligned}\bar{h}_q(n;l) &= \alpha_{AR1}\left\{\alpha_{AR1}\bar{h}_q(n-2;l) + \bar{w}(n-1;l)\right\} + \bar{w}(n;l) \\ &= \alpha^2_{AR1}\bar{h}_q(n-2;l) + \alpha_{AR1}\bar{w}(n-1;l) + \bar{w}(n;l)\end{aligned} \tag{A.4}$$

The above equation can be represented in terms of $\bar{h}_q(n-k;l)$ as

$$\bar{h}_q(n;l) = \alpha^k_{AR1}\bar{h}_q(n-k;l) + \sum_{m=0}^{k-1}\alpha^m_{AR1}\bar{w}(n-m;l) \tag{A.5}$$

The autocorrelation of BEM-AR1 coefficients is given as

$$R_{\bar{h}\bar{h}}(k) = E\left[\bar{h}_q(n;l)\bar{h}^*_q(n-k;l)\right] \tag{A.6}$$

where, $E[.]$ is the expectation/ensemble average operator and $(.)^*$ denotes the complex conjugate operator. For the lag $k=0$, the autocorrelation of BEM coefficients is determined as

$$\begin{aligned}R_{\bar{h}\bar{h}}(0) &= E\left[\bar{h}_q(n;l)\bar{h}_q{}^*(n;l)\right] \\ &= E\left[\left\{\alpha_{AR1}\bar{h}_q(n-1;l) + \bar{w}(n;l)\right\}\left\{\alpha_{AR1}\bar{h}_q(n-1;l) + \bar{w}(n;l)\right\}^*\right] \\ &= \alpha^2_{AR1}R_{\bar{h}\bar{h}}(0) + \sigma^2_{\bar{w}}\end{aligned} \tag{A.7}$$

$$\sigma^2_{\bar{h}} = \alpha^2_{AR1}\sigma^2_{\bar{h}} + \sigma^2_{\bar{w}} \tag{A.8}$$

However for the non-zero lag $k>0$, the autocorrelation of BEM-AR1 coefficients can be calculated by substituting the value of $\bar{h}_q(n;l)$ from equation (A.5) in Eq.(A.6), which leads to

$$R_{\bar{h}\bar{h}}(k) = E\left[\left\{\alpha^k_{AR1}\bar{h}_q(n-k;l) + \sum_{m=0}^{k-1}\alpha^m_{AR1}\bar{w}(n-m;l)\right\}\bar{h}_q{}^*(n-k;l)\right]$$

$$\begin{aligned}R_{\bar{h}\bar{h}}(k) &= \alpha^k_{AR1}E\left[\bar{h}_q(n-k;l)\bar{h}_q{}^*(n-k;l)\right] + \sum_{m=0}^{k-1}\alpha^m_{AR1}E\left[\bar{w}(n-m;l)\bar{h}_q{}^*(n-k;l)\right] \\ &= \alpha^k_{AR1}R_{\bar{h}\bar{h}}(0)\end{aligned} \tag{A.9}$$

Each time-varying BEM-AR1 coefficient exhibits correlation among its successive states. The value of $R_{\bar{h}\bar{h}}(k)$ reduces with the increasing value of lag k because the value of α_{AR1} is usually kept less than unity. At $\alpha_{AR1}=1$, the random-walk model [384] can be used to simulate the nonstationary signals [464], which is not applicable in the presented scenario. However at $\alpha_{AR1}=0$, the BEM-AR1 is equivalent to the conventional basis-expansion-model because the $\bar{h}_q(n;l)=\bar{w}(n;l)=random$. From Eq.(A.1) and Eq.(A.2), the value of $\sigma_{\bar{h}}^2$ is fixed at $1/LQ$ to maintain the constant total signal power constraint. And for conducting simulation, the process-noise statistics are zero-mean and variance $\sigma_{\bar{w}}^2=\left(1-\alpha_{AR1}^2\right)\sigma_{\bar{h}}^2$. Similar, BEM-AR1 channel model is also incorporated in [461] to approximate the multipath channel complex gain within an OFDM symbol, which uses an AR1 model to characterize the variations of BEM coefficients across the OFDM blocks. However, our main focus is on the characterization of BEM-AR1-AR1 channel model in the next section.

A.3 Proposed BEM-AR1-AR1 Model

The finite basis expansions offer well-structured parsimonious modeling, in which the value of Q in Eq.(A.2) is chosen to be high for the accurate approximation of the Jakes' multipath fading channel. In [460], Giannakis *et al.* have considered the conventional BEM coefficients $\bar{h}_q(n;l)$ in Eq.(A.2) to be stochastic in nature. But in the proposed scheme, which is inspired by BEM-AR1 paradigm [461], the BEM-AR1-AR1 coefficients follow

$$\bar{h}_q(n;l)=a_q(n;l)\bar{h}_q(n-1;l)+\bar{w}(n;l) \tag{A.10}$$

Taking into account that BEM-AR1-AR1 coefficients $\bar{h}_q(n;l)$ are samples from time-series with varying spectral properties, it is also natural to consider the Markov parameter $a_q(n;l)$ to be time-dependent, which in turn introduces the nonstationarity [370] in the BEM-AR1-AR1 coefficients

$$a_q(n;l)=\alpha_{AR1-AR1}a_q(n-1;l)+\bar{v}(n;l) \tag{A.11}$$

where, a_q is the time-varying Markov parameter with zero-mean and variance σ_a^2, which follows AR1 model [462]-[464] as expressed in Eq.(A.11) and $\bar{v}$ is the zero-mean complex Gaussian process-noise with variance $\sigma_{\bar{v}}^2$. The BEM-AR1-AR1 model can also be represented in the form

$$\begin{aligned}\bar{h}_q(n;l)&=a_q(n;l)\left\{a_q(n-1;l)\bar{h}_q(n-2;l)+\bar{w}(n-1)\right\}+\bar{w}(n;l)\\&=a_q(n;l)a_q(n-1;l)\bar{h}_q(n-2;l)+a_q(n;l)\bar{w}(n-1;l)+\bar{w}(n;l)\end{aligned} \tag{A.12}$$

The above equation can be represented in terms of $\bar{h}_q(n-k;l)$ as

$$\bar{h}_q(n;l)=\prod_{m=0}^{k-1}a_q(n-m;l)\bar{h}_q(n-k;l)+\sum_{p=1}^{k-1}\left\{\prod_{r=0}^{p-1}a_q(n-r;l)\right\}\bar{w}(n-p;l)+\bar{w}(n;l) \tag{A.13}$$

The autocorrelation of BEM-AR1-AR1 coefficients for the lag $k=0$ is obtained as

$$\begin{aligned}R_{\bar{h}\bar{h}}(0)&=E\left[\bar{h}_q(n;l)\bar{h}_q^*(n;l)\right]\\&=E\left[\left\{a_q(n;l)\bar{h}_q(n-1;l)+\bar{w}(n;l)\right\}\left\{a_q(n;l)\bar{h}_q(n-1;l)+\bar{w}(n;l)\right\}^*\right]\\&=R_{aa}(0)R_{\bar{h}\bar{h}}(0)+\sigma_{\bar{w}}^2\end{aligned} \tag{A.14}$$

in which, $R_{aa}(0)=\alpha_{AR1-AR1}^2R_{aa}(0)+\sigma_{\bar{v}}^2$ is calculated analogous to Eq.(A.7), as $a_q(n)$ is an independent ergodic stationary AR1 process. It follows that

$$\sigma_{\bar{h}}^2=\sigma_a^2\sigma_{\bar{h}}^2+\sigma_{\bar{w}}^2 \tag{A.15}$$

$$\sigma_a^2=\alpha_{AR1-AR1}^2\sigma_a^2+\sigma_{\bar{v}}^2 \tag{A.16}$$

It is also apparent that

$$\sigma_{\bar{v}}^2=\left(1-\alpha_{AR1-AR1}^2\right)\sigma_a^2 \tag{A.17}$$

Using equations (A.14)–(A.17), it can be revealed that

$$\sigma_{\bar{w}}^2=\left(1-\frac{\sigma_{\bar{v}}^2}{1-\alpha_{AR1-AR1}^2}\right)\sigma_{\bar{h}}^2 \tag{A.18}$$

As the value of $\sigma_{\bar{w}}^2$ should always be real and positive, therefore $\frac{\sigma_{\bar{v}}^2}{1-\alpha_{AR1-AR1}^2}\le 1$. It leads to

$$0\le\alpha_{AR1-AR1}\le\sqrt{1-\sigma_{\bar{v}}^2}<1 \tag{A.19}$$

Further, the autocorrelation of coefficients for the non-zero lag values $k>0$ is calculated using Eq.(A.13) as

$$\begin{aligned}R_{\bar{h}\bar{h}}(k)&=E\left[\bar{h}_q(n;l)\bar{h}_q^{\,*}(n-k;l)\right]\\&=E\left[\prod_{m=0}^{k-1}a_q(n-m;l)\left|\bar{h}_q(n-k;l)\right|^2+\left\{\sum_{p=1}^{k-1}\left\{\prod_{r=0}^{p-1}a_q(n-r;l)\right\}\bar{w}(n-p;l)+\bar{w}(n;l)\right\}\bar{h}_q^{\,*}(n-k;l)\right]\end{aligned}$$

$$R_{\bar{h}\bar{h}}(k)=R_{\bar{h}\bar{h}}(0)E\left[\prod_{m=0}^{k-1}a_q(n-m;l)\right] \tag{A.20}$$

On further simplification of above equation, it can be shown that

$$R_{\bar{h}\bar{h}}(k)=\alpha_{AR1-AR1}^kE\left[\left\{a_q(n;l)\right\}^k\right]R_{\bar{h}\bar{h}}(0) \tag{A.21}$$

The term $E\left[\left\{a_q(n;l)\right\}^k\right]$ is the k^{th} moment of time-varying Markov parameter. As compared to the autocorrelation of AR1 process depicted in Eq.(A.9), an extra term corresponding to k^{th}

moment in Eq.(A.21) further alleviates the autocorrelation for the non-zero lag values $k > 0$, since $0 \le \alpha_{AR1-AR1} < 1$. However at $\alpha_{AR1-AR1} = 0$, the time-varying Markov parameter is $a_q(n;l) = \bar{v}(n;l) = random$, which also makes $\bar{h}_q(n;l)$ stochastic in nature. Thus, BEM-AR1-AR1 is approximately equivalent to the conventional basis-expansion-model at $\alpha_{AR1-AR1} = 0$.

A.4 Simulation Results

We shall investigate and compare the presented BEM-AR1-AR1 model with BEM-AR1 [461] and the conventional BEM [460]. It may be inferred from Eq.(A.10) and Eq.(A.11) that each BEM-AR1-AR1 coefficient is characterized as an independent nonstationary process [370], which exhibits high degree of randomness and lower autocorrelation value (Eq.(A.21)) in comparison to the autocorrelation value (Eq.(A.9)) in case of BEM-AR1 coefficients. Therefore, the BEM-AR1-AR1 is expected to perform well at all the values of $\alpha_{AR1-AR1}$, where as the BEM-AR1 is expected to be in close agreement with Jakes' fading model when $\alpha_{AR1} \to 0$, which are verified through computer simulation. The speed of mobile is considered to be $v = 36$ km/hr, the carrier frequency is set to 2.4 GHz, the corresponding maximum Doppler frequency is $f_D = 80$ Hz and the sampling time T_s is 0.0001, which provides fade-rate $f_D T_s = 0.008$. The number of BEM coefficients per channel tap is selected as $Q \ge 2\lceil f_D T_s \rceil$, where $\lceil . \rceil$ is the integer ceiling function [372]. The process-noise variance $\sigma_{\bar{w}}^2$ is obtained using Eq.(A.8) for BEM-AR1 and Eq.(A.18) for BEM-AR1-AR1 respectively. For $Q = 10$ [460], $L = 10$ and $\sigma_{\bar{v}}^2 = 0.01$, the normalized autocorrelation of BEM coefficients in Fig. A.1 manifests that only BEM-AR1 coefficients are relatively more correlated for the Markov parameter $\alpha_{AR1} = 0.9$.

The presented outcomes are based on the ensemble average of 500 independent trials. The normalized autocorrelation of channel tap-coefficients is illustrated in Fig. A.2 and Fig. A.3. The autocorrelation of BEM-AR1-AR1 channel tap-coefficients with $\alpha_{AR1-AR1} = 0.9$ closely match the results obtained for the standard Jakes' model, but the BEM-AR1 channel paradigm fails to perform well at $\alpha_{AR1} = 0.9$, as shown in Fig. A.2. However, the performance is observed to be approximately equivalent for the ideal BEM, BEM-AR1 and BEM-AR1-AR1 for $\alpha_{AR1} = \alpha_{AR1-AR1} = 0.1$, as shown in Fig. A.3.

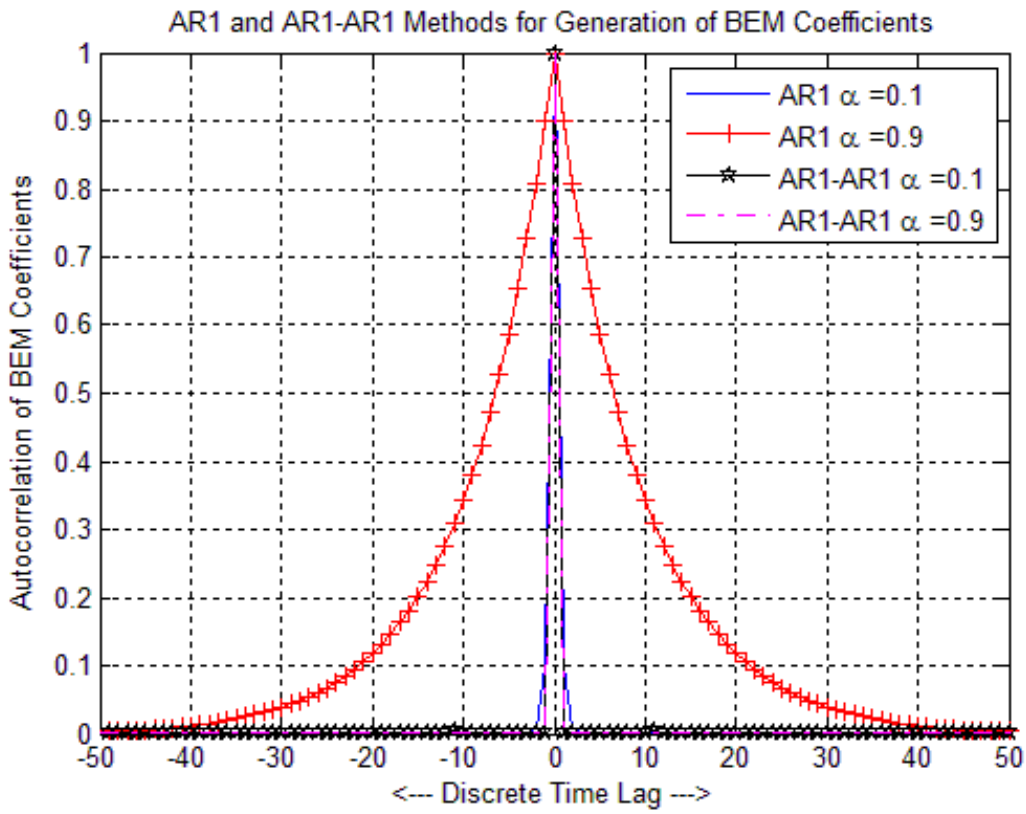

Fig. A.1: Statistical characteristics of BEM coefficients for variable α.

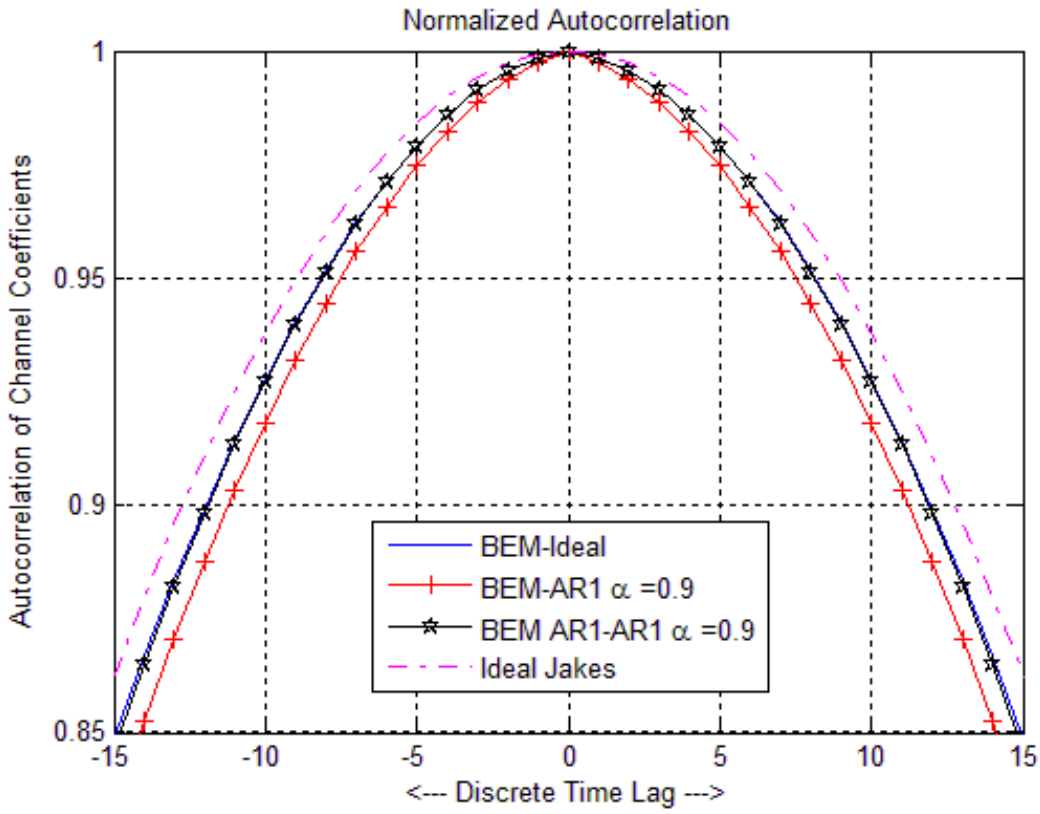

Fig. A.2: Comparison of BEM, BEM-AR1 and BEM-AR1-AR1 ($\alpha = 0.9$).

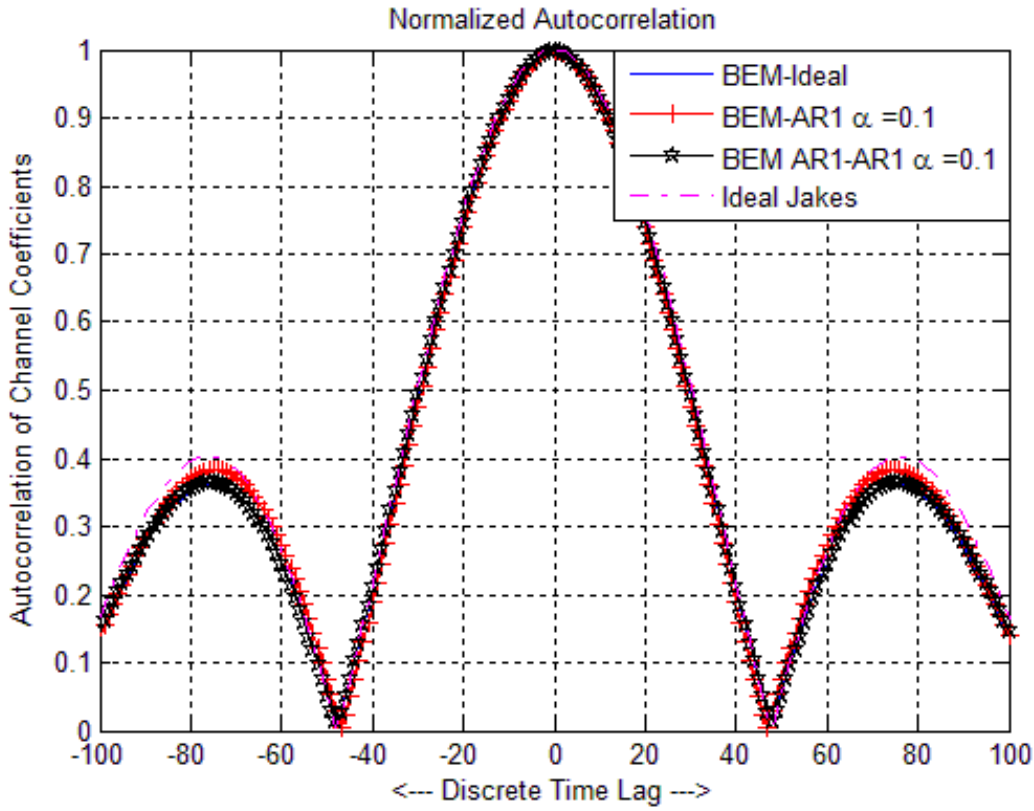

Fig. A.3: Comparison of BEM, BEM-AR1 and BEM-AR1-AR1 ($\alpha = 0.1$).

A.5 Summary

The presented BEM-AR1-AR1 is used to simulate the time-varying Rayleigh multipath fading wireless channel, in which the BEM coefficients are considered to be samples of the time-variant nonstationary-process. The proposed model is a close approximation of Jakes' fading channel model. The simulation results in Fig. A.2 depict that for the large values of α_{AR1}, the BEM-AR1 deviates from the ideal BEM. However, the BEM-AR1-AR1 is found to match with the ideal BEM for low as well as large values of $\alpha_{AR1-AR1}$ in Fig. A.2 and Fig. A.3 because the BEM coefficients are nonstationary and uncorrelated for this case. Moreover, the proposed BEM-AR1-AR1 is suitable for the model-based adaptive algorithms, due to the model-based variations of BEM coefficients.

APPENDIX-B

DERIVATION OF VARIANCE OF NOISE UNDER IMPULSIVE ENVIRONMENT

Using Eq.(4.5), the variance of zero-mean total noise component $\vec{\eta} = \Delta\vec{H}\vec{S} + \vec{W}Imp$ can be obtained as

$$\hat{\sigma}_{\eta}^{2} = \sigma_{\varepsilon}^{2}\sigma_{s}^{2} + \sigma_{W}^{2} + \sigma_{Imp}^{2} \tag{B.1}$$

Substitution of the values of σ_{s}^{2}, σ_{W}^{2} *and* σ_{Imp}^{2} in Eq.(B.1) results in

$$\hat{\sigma}_{\eta}^{2} = \sigma_{\varepsilon}^{2}\left(E_{s}/T_{s}\right) + \left(N_{o}B_{s}\right) + \mu\hat{\sigma}_{i}^{2} \tag{B.2}$$

By considering $B_{s} \simeq 1/T_{s}$, the above equation can be rearranged as

$$\hat{\sigma}_{\eta}^{2} = B_{s}\left\{N_{o} + \mu\left(\hat{\sigma}_{i}^{2}/B_{s}\right) + \sigma_{\varepsilon}^{2}E_{s}\right\} \tag{B.3}$$

Further, it can be shown by denoting $\sigma_{i}^{2} = \hat{\sigma}_{i}^{2}/B_{s}$ and $\hat{N}_{o} = N_{o} + \mu\sigma_{i}^{2}$ that the variance of total noise component may be represented in terms of the symbol energy as

$$\hat{\sigma}_{\eta}^{2} = B_{s}\left\{\hat{N}_{o} + \sigma_{\varepsilon}^{2}E_{s}\right\} = \left(\hat{N}_{o}B_{s}\right)\left\{1 + \sigma_{\varepsilon}^{2}\left(E_{s}/\hat{N}_{o}\right)\right\} \tag{B.4}$$

Therefore, the variance of total complex noise component (exhibiting zero-mean) per unit bandwidth is represented as

$$\sigma_{\eta}^{2} = \hat{\sigma}_{\eta}^{2}/B_{s} = \hat{N}_{o}\left\{1 + \sigma_{\varepsilon}^{2}\left(E_{s}/\hat{N}_{o}\right)\right\} = \hat{N}_{o}\left\{1 + \sigma_{\varepsilon}^{2}\hat{\gamma}_{s}\right\} \tag{B.5}$$

APPENDIX-C

LMMSE BASED CHANNEL ESTIMATION FOR SFBC-OFDM SYSTEM

Let the received symbol vector in underlying SFBC-OFDM system be

$$\mathbf{Y} = \mathbf{HX} + \mathbf{W} \tag{C.1}$$

(subscripts and indices in Eq.(5.4) are not shown for mathematical convenience).

As per conventional LS channel estimation method, the following cost function is minimized to provide optimum LS solution

$$J(\hat{\mathbf{H}}_{LS}) = \left\| \mathbf{Y} - \mathbf{X}\hat{\mathbf{H}}_{LS} \right\|^2 \tag{C.2}$$

where, $\hat{\mathbf{H}}_{LS}$ is the LS estimated channel vector. However, the above function can also be rewritten as

$$J(\hat{\mathbf{H}}_{LS}) = (\mathbf{Y} - \mathbf{X}\hat{\mathbf{H}}_{LS})^H (\mathbf{Y} - \mathbf{X}\hat{\mathbf{H}}_{LS}) = \mathbf{Y}^H\mathbf{Y} - \mathbf{Y}^H\mathbf{X}\hat{\mathbf{H}}_{LS} - \hat{\mathbf{H}}_{LS}^H\mathbf{X}^H\mathbf{Y} + \hat{\mathbf{H}}_{LS}^H\mathbf{X}^H\mathbf{X}\hat{\mathbf{H}}_{LS} \tag{C.3}$$

In order to find the optimum value $\hat{\mathbf{H}}_{LS}$, for which the cost function in Eq.(C.2) gets minimized, the derivative of cost function with respect to the estimated channel vector needs to be calculated and equated to zero. It results in

$$\frac{\partial J(\hat{\mathbf{H}}_{LS})}{\partial \hat{\mathbf{H}}_{LS}} = -2\left(\mathbf{X}^H\mathbf{Y}\right)^* + 2\left(\mathbf{X}^H\mathbf{X}\hat{\mathbf{H}}_{LS}\right)^* = 0 \tag{C.4}$$

where, $(.)^*$ is the complex-conjugation operator. The mathematical simplification of above equation leads to

$$\hat{\mathbf{H}}_{LS} = \left(\mathbf{X}^H\mathbf{X}\right)^{-1}\mathbf{X}^H\mathbf{Y} \tag{C.5}$$

This can also be expressed as

$$\hat{\mathbf{H}}_{LS} = \left(\mathbf{X}^H\mathbf{X}\right)^{-1}\mathbf{X}^H\left[\mathbf{XH} + \mathbf{W}\right] = \mathbf{H} + \left(\mathbf{X}^H\mathbf{X}\right)^{-1}\mathbf{X}^H\mathbf{W} \tag{C.6}$$

As the underlying system utilizes QO-codes, the matrix $\mathbf{X}^H\mathbf{X}$ is not purely diagonal, and therefore it contains some off-diagonal entries as well. Considering the LS estimate in Eq.(C.5), a better linear estimate in terms of weighted LS estimate can be applied by using the LMMSE channel estimation method, as suggested in [426]. This method finds a linear estimate to minimize the following error function

$$J\left(\hat{\mathbf{H}}_{MM}\right) = E\left[\left\|\boldsymbol{\psi}\right\|^2\right] = E\left[\left\|\mathbf{H} - \hat{\mathbf{H}}_{MM}\right\|^2\right] \tag{C.7}$$

where, $\hat{\mathbf{H}}_{MM} = \mathbf{W}_{MM}\hat{\mathbf{H}}_{LS}$ is the LMMSE estimate. As the estimation error $\boldsymbol{\psi}$ is orthogonal to $\hat{\mathbf{H}}_{LS}$, therefore $E\left[\boldsymbol{\psi}\hat{\mathbf{H}}_{LS}^{H}\right] = 0$. It follows that

$$\begin{aligned} E\left[\boldsymbol{\psi}\hat{\mathbf{H}}_{LS}^{H}\right] &= E\left[\left(\mathbf{H} - \hat{\mathbf{H}}_{MM}\right)\hat{\mathbf{H}}_{LS}^{H}\right] \\ &= E\left[\left(\mathbf{H} - \mathbf{W}_{MM}\hat{\mathbf{H}}_{LS}\right)\hat{\mathbf{H}}_{LS}^{H}\right] \\ &= E\left[\mathbf{H}\hat{\mathbf{H}}_{LS}^{H}\right] - \mathbf{W}_{MM}E\left[\hat{\mathbf{H}}_{LS}\hat{\mathbf{H}}_{LS}^{H}\right] \\ &= \mathbf{R}_{\mathbf{H}\hat{\mathbf{H}}_{LS}} - \mathbf{W}_{MM}\mathbf{R}_{\hat{\mathbf{H}}_{LS}\hat{\mathbf{H}}_{LS}} \end{aligned} \quad \text{(C.8)}$$

where, $\mathbf{R}_{\mathbf{H}\hat{\mathbf{H}}_{LS}}$ is the cross-correlation matrix between true-channel vector and LS estimated channel vector, and $\mathbf{R}_{\hat{\mathbf{H}}_{LS}\hat{\mathbf{H}}_{LS}}$ is the auto-correlation matrix of LS estimated channel vector. Further solution of Eq.(C.8) yields

$$\mathbf{W}_{MM} = \mathbf{R}_{\mathbf{H}\hat{\mathbf{H}}_{LS}}\mathbf{R}^{-1}_{\hat{\mathbf{H}}_{LS}\hat{\mathbf{H}}_{LS}} \quad \text{(C.9)}$$

Using Eq.(C.6), it can be shown that the auto-correlation matrix $\mathbf{R}_{\hat{\mathbf{H}}_{LS}\hat{\mathbf{H}}_{LS}}$ is

$$\begin{aligned} \mathbf{R}_{\hat{\mathbf{H}}_{LS}\hat{\mathbf{H}}_{LS}} &= E\left[\hat{\mathbf{H}}_{LS}\hat{\mathbf{H}}_{LS}^{H}\right] \\ &= E\left[\left(\mathbf{H} + \left(\mathbf{X}^{H}\mathbf{X}\right)^{-1}\mathbf{X}^{H}\mathbf{W}\right)\left(\mathbf{H} + \left(\mathbf{X}^{H}\mathbf{X}\right)^{-1}\mathbf{X}^{H}\mathbf{W}\right)^{H}\right] \\ &= E\left[\mathbf{H}\mathbf{H}^{H}\right] + E\left[\left(\mathbf{X}^{H}\mathbf{X}\right)^{-1}\mathbf{W}^{H}\mathbf{W}\right] \\ &= \mathbf{R}_{\mathbf{HH}} + \sigma_{w}^{2}\left(\mathbf{X}^{H}\mathbf{X}\right)^{-1} \end{aligned} \quad \text{(C.10)}$$

However, the cross-correlation matrix $\mathbf{R}_{\mathbf{H}\hat{\mathbf{H}}_{LS}}$ is found to be

$$\begin{aligned} \mathbf{R}_{\mathbf{H}\hat{\mathbf{H}}_{LS}} &= E\left[\mathbf{H}\hat{\mathbf{H}}_{LS}^{H}\right] \\ &= E\left[\mathbf{H}\left(\mathbf{H} + \left(\mathbf{X}^{H}\mathbf{X}\right)^{-1}\mathbf{X}^{H}\mathbf{W}\right)^{H}\right] \\ &= E\left[\mathbf{H}\mathbf{H}^{H}\right] + E\left[\mathbf{H}\mathbf{W}^{H}\mathbf{X}\left(\mathbf{X}\mathbf{X}^{H}\right)^{-1}\right] \\ &\approx \mathbf{R}_{\mathbf{HH}} \end{aligned} \quad \text{(C.11)}$$

Subsequently, the LMMSE channel estimates using equations (C.5), (C.9), (C.10) and (C.11) are expressed as

$$\hat{\mathbf{H}}_{MM} = \mathbf{R}_{\mathbf{HH}}\left\{\mathbf{R}_{\mathbf{HH}} + \sigma_{w}^{2}\left(\mathbf{X}^{H}\mathbf{X}\right)^{-1}\right\}^{-1}\hat{\mathbf{H}}_{LS} \quad \text{(C.12)}$$

$$\hat{\mathbf{H}}_{MM} = \mathbf{R}_{\mathbf{HH}}\left\{\mathbf{R}_{\mathbf{HH}} + \sigma_{w}^{2}\left(\mathbf{X}^{H}\mathbf{X}\right)^{-1}\right\}^{-1}\left(\mathbf{X}^{H}\mathbf{X}\right)^{-1}\mathbf{X}^{H}\mathbf{Y} \quad \text{(C.13)}$$

APPENDIX-D

IMPACT OF SQUASHING-FUNCTION'S SLOPE ON ANN BASED CHANNEL ESTIMATION IN SFBC-OFDM SYSTEM

D.1 Introduction and System Model

The channel-state-information plays an important role in the decoding of information symbols while working over the multipath fading channels using SFBC-OFDM system [324], [465]. ANN based channel estimation [230], [236] has appeared as a promising technique for the underlying 4×1 SFBC-OFDM system [416], in which the received symbol vector in frequency-domain (after the cyclic-prefix removal and FFT operation) is

$$\mathbf{Y}_{4m}(p)=\mathbf{X}_{4m}(p)\mathbf{H}_{4m}(p)+\mathbf{W}_{4m}(p) \tag{D.1}$$

where, $\mathbf{Y}_{4m}(p)=\left[Y_{4m}(p),Y_{4m+1}(p),Y_{4m+2}(p),Y_{4m+3}(p)\right]^T$,

$$\mathbf{X}_{4m}(p)=\begin{bmatrix} X_{4m}(p) & X_{4m+1}(p) & X_{4m+2}(p) & X_{4m+3}(p) \\ -X^*_{4m+1}(p) & X^*_{4m}(p) & -X^*_{4m+3}(p) & X^*_{4m+2}(p) \\ -X^*_{4m+2}(p) & -X^*_{4m+3}(p) & X^*_{4m}(p) & X^*_{4m+1}(p) \\ X_{4m+3}(p) & -X_{4m+2}(p) & -X_{4m+1}(p) & X_{4m}(p) \end{bmatrix},$$

$\mathbf{H}_{4m}(p)=\left[H_{1,4m}(p),H_{2,4m}(p),H_{3,4m}(p),H_{4,4m}(p)\right]^T$, and

$\mathbf{W}_{4m}(p)=\left[W_{4m}(p),W_{4m+1}(p),W_{4m+2}(p),W_{4m+3}(p)\right]^T$ with the assumption of approximately equal channel gains across the 4 adjacent subcarriers. The slowly time-varying multipath fading channel [225] is modelled as a tapped-delay-line-filter in time-domain, in which each tap-coefficient $h_{i,l}(p)$ is assumed to follow a second-order autoregressive process [335] as,

$$h_{i,l}(p)=-K_1h_{i,l}(p-1)-K_2h_{i,l}(p-2)+v_{i,l}(p) \tag{D.2}$$

where, $K_1=-2r_D\cos\left(\sqrt{2}\pi f_DT_1\right)$, $K_2=r_D^2$ with $r_D=1-2f_DT_1$, f_DT_1 is the fade-rate, f_D is the maximum Doppler frequency, T_1 is the OFDM symbol-block period including cyclic-prefix, $v_{i,l}(p)$ denotes the zero-mean Gaussian process with variance σ_v^2 for i^{th} antenna and l^{th} tap-coefficient. Under 4 transmitter-antennas scenario, the ANN based channel estimator [230], [236] consists of 4 different ANN blocks (each having feedforward multi-layered perceptron architecture) for estimating the tap-coefficient $H_{i,4m}(p)$ in frequency-domain. As ANN can only process the real-valued data, the input to each ANN block (termed as intelligent-channel-estimator (ICE)) is bifurcated into real and imaginary parts of the received symbol (as shown in Fig. D.1).

Hence, each ICE block consists of 8 nodes at the input-layer, two hidden-layers with 16 and 8 neurons each, and 2 neurons in the output-layer (motivated by the composite ANN structure proposed in [229]). The two output values from each ICE block are combined to form a single complex-valued estimated channel tap-coefficient. In each neuron, the activation potential/ induced local field is processed through a squashing-function (differentiable) to give output in the range $[-1,+1]$. In order to avoid excessive saturation of the squashing-function, the softsign (SS) function has emerged as an appropriate choice, because its tail is a quadratic polynomial rather than exponential (in case of hyperbolic-tangent function) which approaches its asymptotes in a slow manner [466]. While implementing the back-propagation (BP) algorithm using softsign-function in neurons, the saturation does not occur one layer after the other in a neural network. However, it is faster in the beginning and then gradually slows down (which is quite different from the hyperbolic-tangent function). Commonly used hyperbolic-tangent function (tanh) is $f_{Tanh}(u) = \tanh(\beta u)$ with its first derivative as $f'_{Tanh}(u) = \beta\left(1 - f_{Tanh}(u)\right)\left(1 + f_{Tanh}(u)\right)$. However, softsign-function is expressed as $f_{SS}(u) = \beta u\left[1 + |\beta u|\right]^{-1}$ with its first derivative as $f'_{SS}(u) = \beta\left[1 + |\beta u|\right]^{-2}$ and slope parameter β [467]. SS squashing-function is highly compatible with the BP algorithm, as it does not contain any exponential term, not even in its derivative.

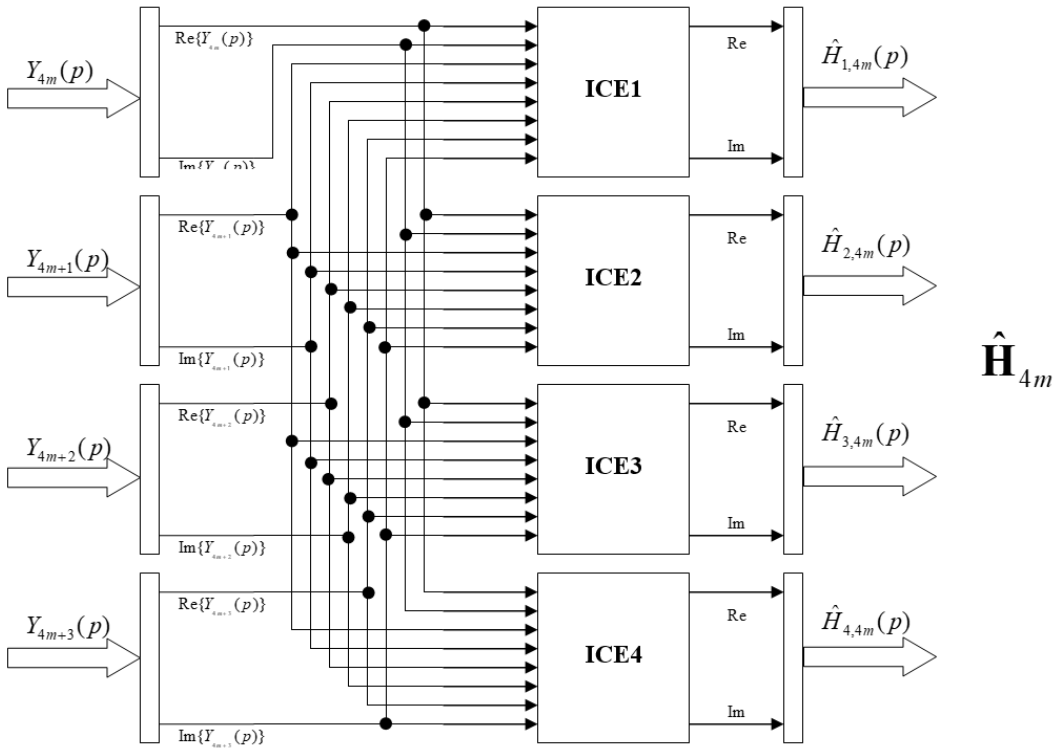

Fig. D.1: Composite ANN structure used for channel estimation in SFBC-OFDM system [229].

D.2 Simulation Results and Discussion

In an SFBC-OFDM system, the number of subcarriers is considered to be 64, in which 4 transmitter-antennas and 1 receiver-antenna are deployed. The number of multipaths for each transmission channel is assumed to be 4. The concerned ANN is trained by sending 100 OFDM pilot symbol-blocks (as demonstrated in Fig. D.1). In low SNR regime and at fade-rate $f_D T_1 = 0.001$, the tanh function based approach deteriorates the performance of channel estimator in comparison to SS, for the specific slope parameters (as depicted in Fig. D.2). The gentle tail of SS function due to the quadratic polynomial based convergence makes it more robust towards the initialization procedure. Large dramatic variations are observed in the performance of channel estimator, when slope parameter β is slightly changed in case of the tanh function. Moreover, the gradient of SS function is larger as compared to the tanh function, which is helpful in getting a better learning signal for weight update while training in the BP algorithm. This also reduces the chances of being caught in a local-minima while searching for the global-minima for better optimization. Under similar conditions at fixed SNR of +25dB, the symbol-error-rate performance (based on Eq.(5.8)) of SFBC-OFDM system is illustrated in Fig. D.3 at the different fade-rate values.

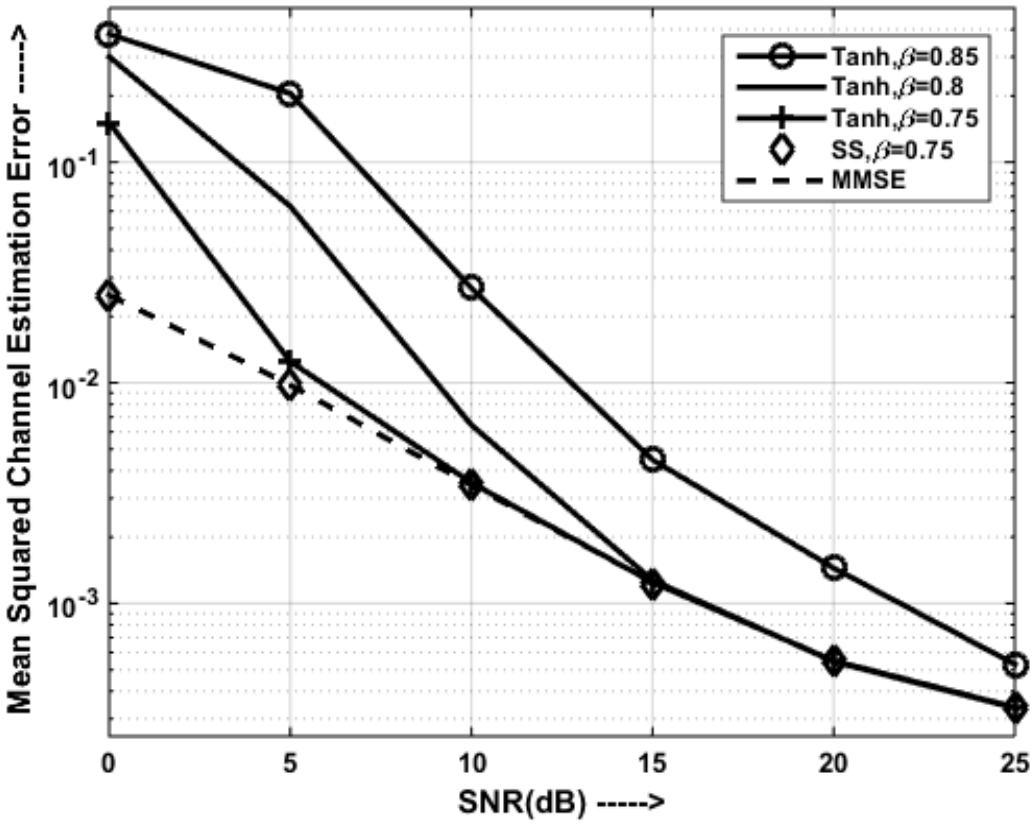

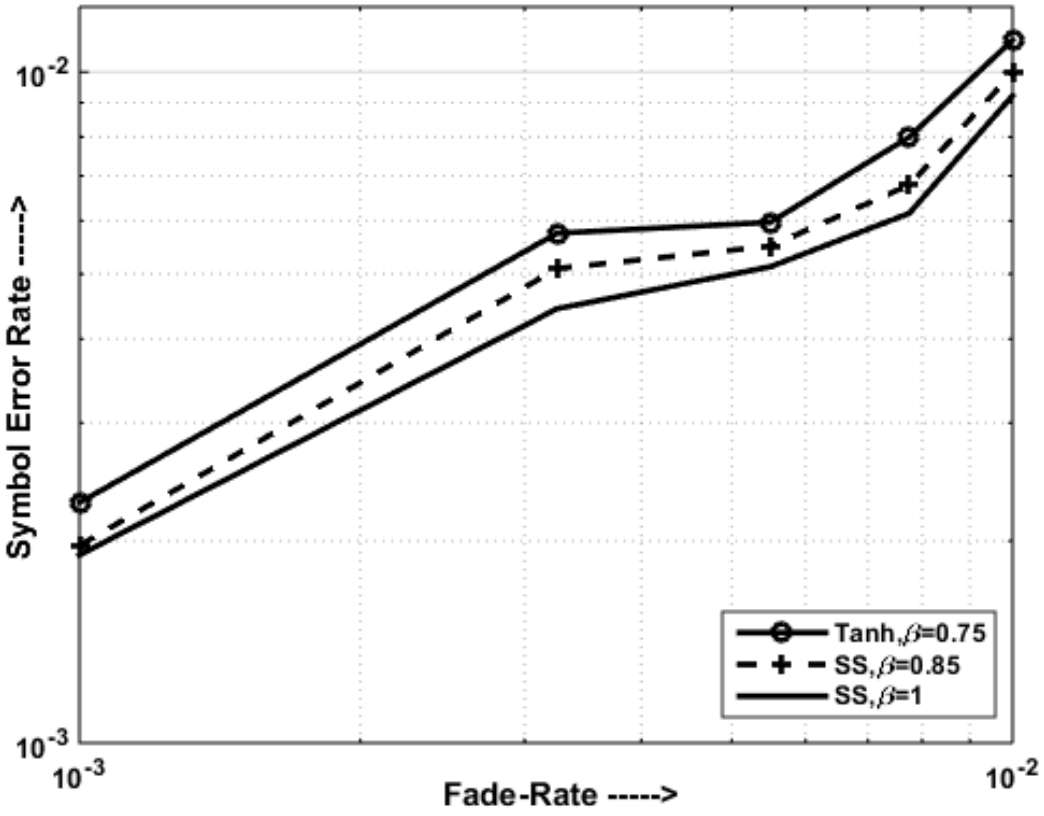

Fig. D.3: SER at different fade-rate values with SNR = +25dB.

D.3 Summary

The usage of softsign squashing-function in an ANN based intelligent channel estimator has been found to exhibit the lower estimation error due to innate polynomial asymptotes, which eventually leads to the lower occurrence of saturation in the hidden-layer neurons (resulting in better gradient propagation). Though the SER of concerned 4×1 SFBC-OFDM systems gets elevated, as the fade-rate increases in all cases, but SS based channel estimation outperforms the tanh based approach for a wide range of signal-to-noise-ratio (SNR) values.

REFERENCES

[1] T. Hwang, C. Yang, G. Wu, S. Li, and G. Y. Li, "OFDM and its wireless applications: A survey," *IEEE Trans. Vehicular Tech.*, vol. 58, no. 4, pp. 1673-1694, May 2009.

[2] G. J. Foschini and M. J. Gans, "On limits of wireless communications in a fading environment when using multiple antennas," *Wireless Pers. Commun.*, vol. 6, no. 3, pp. 311-335, March 1998.

[3] L. J. Cimini, "Analysis and simulation of a digital mobile channel using orthogonal frequency division multiplexing," *IEEE Trans. Commun.*, vol. 33, no. 7, pp. 665-675, July 1985.

[4] S. B. Weinstein, "The history of orthogonal frequency-division multiplexing [History of Communications]," *IEEE Commun. Mag.*, vol. 47, no. 11, pp. 26-35, November 2009.

[5] J. Armstrong, "OFDM for optical communications," *J. Lightw. Technol.*, vol. 27, no. 3, pp. 189-204, February 2009.

[6] M. Engels, *Wireless OFDM Systems: How To Make Them Work?*. Dordrecht: Kluwer Academic Publishers, 2002.

[7] J. A. C. Bingham, "Multicarrier modulation for data transmission: An idea whose time has come," *IEEE Commun. Mag.*, vol. 28, no. 5, pp. 5–14, May 1990.

[8] R. van Nee and R. Prasad, *OFDM for Wireless Multimedia Communications*. Boston: Artech House, 2000.

[9] W. Y. Zou and Y. Wu, "COFDM: An overview," *IEEE Trans. Broadcasting*, vol. 41, no. 1, pp. 1–8, March 1995.

[10] J. H. Stott, "The how and why of COFDM," *EBUTech. Rev.*, pp. 43–50, 1998.

[11] S. Weinstein and P. Ebert, "Data transmission by frequency-division multiplexing using the discrete Fourier transform," *IEEE Trans. Commun. Technol.*, vol. COM-19, no. 5, pp. 628–634, October 1971.

[12] Y. Li and G. L. Stüber, *Orthogonal Frequency Division Multiplexing for Wireless Communications*, US: Springer, 2007.

[13] I. Koffman and V. Roman, "Broadband wireless access solutions based on OFDM access in IEEE 802.16," *IEEE Commun. Mag.*, vol. 40, no. 4, pp. 96–103, April 2002.

[14] I. Barhumi, G. Leus, and M. Moonen, "Optimal training design for MIMO–OFDM systems in mobile wireless channels," *IEEE Trans. Signal Processing*, vol. 51, no. 6, pp. 1615–1624, June 2003.

[15] *IEEE Standard for Local and Metropolitan Area Networks Part 20 Air Interface for Mobile Broadband Wireless Access Systems Supporting Vehicular Mobility - Physical and Media Access Control Layer Specification*, IEEE Standard 802.20, August 2008.

[16] A. Greenspan, M. Klerer, J. Tomcik, R. Canchi, and J. Wilson, "IEEE 802.20: Mobile broadband wireless access for the twenty-first century," *IEEE Commun. Mag.*, vol. 46, no. 7, pp. 56-63, July 2008.

[17] *Air Interface for Fixed and Mobile Broadband Wireless Access Systems*, IEEE P37e/D12, October 2006.

[18] *LTE Physical Layer-General Description*, 3GPP TS36.201, August 2007.

[19] L. Sun, H. Tian, Q. Sun, D. Shen, and P. Zhang, "Traffic allocation scheme with cooperation of WWAN and WPAN," *IEEE Commun. Lett.*, vol. 14, no. 6, pp. 551-553, June 2010.

[20] R. W. Chang, “Synthesis of band-limited orthogonal signals for multichannel data transmission,” *Bell Syst. Tech. J.*, vol. 45, pp. 1775–1797, December 1966.

[21] R. W. Chang, “Orthogonal frequency division multiplexing,” U. S. Patent 3 488 445, January 6, 1970.

[22] B. R. Saltzberg, “Performance of an efficient parallel data transmission system,” *IEEE Trans. Commun. Technol.*, vol. COM-15, no. 6, pp. 805–811, December 1967.

[23] M. L. Doelz, E. T. Heald, and D. L. Martin, “Binary data transmission techniques for linear systems,” *Proc. IRE*, pp. 656–661, May 1957.

[24] B. Hirosaki, “An analysis of automatic equalizers for orthogonally multiplexed QAM systems,” *IEEE Trans. Commun.*, vol. COM-28, no. 1, pp. 73–83, January 1980.

[25] B. Hirosaki, S. Hasegawa, and A. Sabato, “Advanced groupband data modem using orthogonally multiplexed QAM technique,” *IEEE Trans. Commun.*, vol. COM-34, no. 6, pp. 587–592, June 1986.

[26] A. Peled and A. Ruiz, “Frequency domain data transmission using reduced computational complexity algorithms,” *Proc. IEEE Int. Conf. Acoust. Speech Signal Process.*, Denver, Colorado, USA, pp. 964–967, April 1980.

[27] M. S. Zimmerman and A. L. Kirsch, “The AN/GSC-10 (KATHRYN) variable rate data modem for HF radio,” *IEEE Trans. Commun. Technol.*, vol. COM-15, no. 2, pp. 197–205, April 1967.

[28] W. E. Keasler, Jr., “Reliable data communications over the voice bandwidth telephone using orthogonal frequency division multiplexing,” Ph.D. dissertation, Univ. Illinois, Urbana, IL, 1982.

[29] I. Kalet, “The multitone channel,” *IEEE Trans. Commun.*, vol. 37, no. 2, pp. 119–124, February 1989.

[30] T. J. Willink and P. H. Wittke, “Optimization and performance evaluation of multicarrier transmission,” *IEEE Trans. Inf. Theory*, vol. 43, no. 2, pp. 426–440, March 1997.

[31] R. Lassalle and M. Alard, “Principles of modulation and channel coding for digital broadcasting for mobile receivers,” *EBU Tech. Rev.*, pp. 168–190, 1987.

[32] E. F. Casas and C. Leung, “OFDM for data communication over mobile radio FM channels. I. Analysis and experimental results,” *IEEE Trans. Commun.*, vol. 39, no. 5, pp. 783–793, May 1991.

[33] C. E. Shannon, “A mathematical theory of communication,” *Bell Syst. Tech. J.*, vol. 27, pp. 379–423, July 1948.

[34] J. S. Chow, J. C. Tu, and J. M. Cioffi, “A discrete multitone transceiver system for HDSL applications,” *IEEE J. Sel. Areas Commun.*, vol. 9, no. 6, pp. 895–908, August 1991.

[35] P. S. Chow, J. M. Cioffi, and J. A. C. Bingham, “A practical discrete multitone transceiver loading algorithm for data transmission over spectrally shaped channels,” *IEEE Trans. Commun.*, vol. 43, no. 2–4, pp. 773–775, February–April 1995.

[36] L. Hanzo and T. Keller, *OFDM and MC-CDMA: A Primer*. Chichester: John Wiley & Sons, 2007.

[37] S. Shepherd, P. van Eetvelt, C. Wyatt-Millington, and S. Barton, “Simple coding scheme to reduce peak factor in QPSK multicarrier modulation,” *Electron. Lett.*, vol. 31, no. 4, pp. 1131–1132, July 1995.

[38] A. E. Jones, T. A.Wilkinson, and S. K. Barton, "Block coding scheme for reduction of peak to mean envelope power ratio of multicarrier transmission schemes," *Electron. Lett.*, vol. 30, no. 25, pp. 2098–2099, December 1994.

[39] D. Wulich, "Reduction of peak to mean ratio of multicarrier modulation by cyclic coding," *Electron. Lett.*, vol. 32, no. 5, pp. 432–433, February 1996.

[40] D. Wulich, "Peak factor in orthogonal multicarrier modulation with variable levels," *Electron. Lett.*, vol. 32, no. 20, pp. 1859–1861, September 1996.

[41] T. Pollet, M. van Bladel, and M. Moeneclaey, "BER sensitivity of OFDM systems to carrier frequency offset and Wiener phase noise," *IEEE Trans. Commun.*, vol. 43, no. 2/3/4, pp. 191–193, February/March/April 1995.

[42] R. D. Murch and K. B. Letaief, "Antenna systems for broadband wireless access," *IEEE Commun. Mag.*, vol. 40, no. 4, pp. 76–83, April 2002.

[43] N. Al-Dhahir and S. N. Diggavi, "On achievable rates on time-varying frequency-selective channels," *Proc. Conf. Info. Sci. Systems*, Princeton, New Jersey, pp. 860-865, March 2002.

[44] G. J. Foschini, "Layered space–time architecture for wireless communication in a fading environment when using multi-element antennas," *Bell Labs Tech. J.*, vol. 1, no. 2, pp. 41–59, Autumn 1996.

[45] W. Zhang, X. G. Xia, and K. B. Letaief, "Space-time/frequency coding for MIMO-OFDM in next generation broadband wireless systems," *IEEE Wireless Commun.*, vol. 14, no. 3, pp. 32-43, June 2007.

[46] S. M. Alamouti, "A simple transmit diversity technique for wireless communications," *IEEE J. Sel. Areas Commun.*, vol. 16, no. 8, pp. 1451-1458, October 1998.

[47] P. Elia, K. R. Kumar, S. A. Pawar, P. V. Kumar, and H. -F. Lu, "Explicit space–time codes achieving the diversity–multiplexing gain tradeoff," *IEEE Trans. Info. Theory*, vol. 52, no. 9, pp. 3869-3884, September 2006.

[48] H. El Gamal and M. O. Damen, "Universal space-time coding," *IEEE Trans. Info. Theory*, vol. 49, no. 5, pp. 1097-1119, May 2003.

[49] S. N. Diggavi, N. Al-Dhahir, A. Stamoulis, and A. R. Calderbank, "Great expectations: the value of spatial diversity in wireless networks," *Proc. IEEE*, vol. 92, no. 2, pp. 219-270, February 2004.

[50] D. Gesbert, M. Shafi, D. Shiu, P. Smith, and A Naguib, "From theory to practice: An overview of MIMO space-time coded wireless systems," *IEEE J. Sel. Areas Commun.*, vol. 21, no. 3, pp. 281-302, April 2003.

[51] V. Tarokh, H. Jafarkhani, and A. R. Calderbank, "Space-time block codes from orthogonal designs," *IEEE Trans. Info. Theory*, vol. 49, no. 5, pp. 1456-1467, July 1999.

[52] W. Su, X.-G. Xia, and K. J. R. Liu, "A systematic design of high-rate complex orthogonal space-time block codes," *IEEE Commun. Lett.*, vol. 8, no. 6, pp. 380-382, June 2004.

[53] A. V. Geramita and J. M. Geramita, "Complex orthogonal designs," *J. Comb. Theory Ser. A*, vol. 25, no. 3, pp. 211-225, November 1978.

[54] K. Lu, S. Fu, and X.-G. Xia, "Closed-form designs of complex orthogonal space-time block codes of rates (k+1)/(2k) for 2k-1 or 2k transmit antennas," *IEEE Trans. Info. Theory*, vol. 51, no. 12, pp. 4340-4347, December 2005.

[55] S. Sandhu and A. Paulraj, "Space-time block codes: A capacity perspective," *IEEE Commun. Lett.*, vol. 4, no. 12, pp. 384-386, December 2000.

[56] H. Shin and J. H. Lee, "Exact symbol error probability of orthogonal space-time block codes," *Proc. IEEE Global Telecommun. Conf.*, vol. 2, Taipei, Taiwan, pp. 1197-1201, November 2002.

[57] W. Su and X.-G. Xia, "On space-time block codes from complex orthogonal designs," *Wireless Pers. Commun.*, vol. 25, no. 1, pp. 1–26, April 2003.

[58] X.-B. Liang, "Orthogonal designs with maximal rates," *IEEE Trans. Info. Theory*, vol. 49, pp. 2468–2503, October 2003.

[59] H. Jafarkhani, "A quasi-orthogonal space-time block code," *IEEE Trans. Commun.*, vol. 49, no. 1, pp. 1-4, January 2001.

[60] O. Tirkkonen, A. Boariu, and A. Hottinen, "Minimal nonorthogonality rate 1 space-time block code for 3+ Tx antennas," *Proc. IEEE 6th Int. Symp. Spread-Spectrum Techniques Applications*, vol. 2, Parsippany, NJ, USA, pp. 429–432, September 2000.

[61] C. B. Papadias and G. J. Foschini, "Capacity-approaching space-time codes for systems employing four transmitter antennas," *IEEE Trans. Info. Theory*, vol. 49, pp. 726–732, March 2003.

[62] W. Su and X.-G. Xia, "Signal constellations for quasi-orthogonal space-time block codes with full diversity," *IEEE Trans. Info. Theory*, vol. 50, no. 10, pp. 2331-2347, October 2004.

[63] A. Y.-C. Peng, I.-M. Kim, and S. Yousefi, "Low-complexity sphere decoding algorithm for quasi-orthogonal space-time block codes," *IEEE Trans. Commun.*, vol. 54, no. 3, pp. 377-382, March 2006.

[64] J. Leuschner and S. Yousefi, "On the ML decoding of quasi-orthogonal space-time block codes via sphere decoding and exhaustive search," *IEEE Trans. Wireless Commun.*, vol. 7, no. 11, pp. 4088-4093, November 2008.

[65] M.-T. Le, V.-S. Pham, L. Mai, and G. Yoon, "Low-complexity maximum-likelihood decoder for four-transmit-antenna quasi-orthogonal space-time block code," *IEEE Trans. Commun.*, vol. 53, no. 11, pp. 1817-1821, November 2005.

[66] V.-S. Pham, M.-T. Le, L. Mai, and G. Yoon, "Low complexity MMSE-QRD-based ML decoder for quasi-orthogonal STBC scheme in MIMO wireless communications systems with four-transmit antennas," *Proc. 2006 8th Int. Conf. Advanced Commun. Technol.*, Phoenix Park, South Korea, pp. 1937-1939, February 2006.

[67] M. Rupp, C. Mecklenbrauker, and G. Gritsch, "High diversity with simple space time block-codes and linear receivers," *Proc. IEEE Global Telecommun. Conf.*, vol. 1, San Francisco, CA, pp. 302-306, December 2003.

[68] B. Badic, M. Rupp, and H. Weinrichter, "Quasi-orthogonal space-time block codes: approaching optimality," *Proc. 2005 13th European Signal Process. Conf.*, Antalya, Turkey, pp. 1-8, September 2005.

[69] H. Lee, J. Cho, J. Kim, and I. Lee, "An efficient decoding algorithm for STBC with multi-dimensional rotated constellations," *Proc. 2006 IEEE Int. Conf. Commun.*, Istanbul, Turkey, pp. 5558-5563, June 2006.

[70] L. Azzam and E. Ayanoglu, "Maximum likelihood detection of quasi-orthogonal space-time block codes: analysis and simplification," *Proc. 2008 IEEE Int. Conf. Commun.*, Beijing, China, pp. 3948-3954, May 2008.

[71] U. Park, S. Kim, K. Lim, and J. Li, "A novel QO-STBC scheme with linear decoding for three and four transmit antennas," *IEEE Commun. Lett.*, vol. 12, no. 12, pp. 868-870, December 2008.

[72] L.-P. Xiao and X.-X. Dai, "A novel QO-STBC scheme with linear decoding," *The J. China Univ. Posts Telecommun.*, vol. 18, no. 5, pp. 53-57, October 2011.

[73] K. F. Lee and D. B. Williams, "A space-time coded transmitter diversity technique for frequency selective fading channels," *Proc. 2000 IEEE Sensor Array Multichannel Signal Process. Workshop*, Cambridge, MA, USA, pp. 149-152, March 2000.

[74] D. Agarwal, V. Tarokh, A. Naguib, and N. Seshadri, "Space-time coded OFDM for high data-rate wireless communication over wideband channels," *Proc. 48th IEEE Veh. Technol. Conf.*, vol. 3, Ottawa, Ont., pp. 2232-2236, May 1998.

[75] Y. Gong and K. B. Letaief, "Low complexity channel estimation for space-time coded wideband OFDM systems," *IEEE Trans. Wireless Commun.*, vol. 2, no. 5, pp. 876-882, September 2003.

[76] C. B. Papadias and G. J. Foschini, "A space-time coding approach for systems employing four transmit antennas," *Proc. Int. Conf. Acoust. Speech Signal Process.*, vol. 4, Salt Lake City, UT, pp. 2481–2484, May 2001.

[77] V. Tarokh, N. Seshadri, and A. R. Calderbank, "Space-time codes for high data rate wireless communication: Performance criterion and code construction," *IEEE Trans. Info. Theory*, vol. 44, no. 2, pp. 744-765, March 1998.

[78] G. Ganesan and P. Stoica, "Space-time block codes: A maximum SNR approach," *IEEE Trans. Info. Theory*, vol. 47, no. 4, pp. 1650–1656, May 2001.

[79] L. T. Younkins, W. Su, and K. J. R. Liu, "On the robustness of space-time coding techniques based on a general space-time covariance model," *IEEE Trans. Veh. Technol.*, vol. 55, no. 1, pp. 219–233, January 2006.

[80] E. Ko and D. Hong, "A robust transmit diversity for OFDM systems in spatially correlated Rayleigh fading channels," *Proc. IEEE 59th Veh. Technol. Conf.*, vol. 4, Milan, Italy, pp. 1840-1843, May 2004.

[81] E. Ko and D. Hong, "Improved space-time block coding with frequency diversity for OFDM systems," *Proc. IEEE ICC 04*, Paris, France, pp. 3217-3220, June 2004.

[82] J. Kim, R. W. Heath Jr., and E. J. Powers, "Receiver designs for Alamouti coded OFDM systems in fast fading channels," *IEEE Trans. Wireless Commun.*, vol. 4, pp. 550-559, March 2005.

[83] A. Stamoulis, S. N. Diggavi, and N. Al-Dhahir, "Intercarrier interference in MIMO OFDM," *IEEE Trans. Signal Process.*, vol. 50, pp. 2451-2464, October 2002.

[84] H. A. Suraweera and J. Armstrong, "Alamouti coded OFDM in Rayleigh fast fading channels - receiver performance analysis," *Proc. IEEE TENCON 2005*, Melbourne, Qld., pp. 1-5, November 2005.

[85] D.-B. Lin, P.-H. Chiang, and H.-J. Li, "Performance analysis of two-branch transmit diversity block-coded OFDM systems in time-varying multipath Rayleigh-fading channels," *IEEE Trans. Veh. Technol.*, vol. 54, no. 1, pp. 136-148, January 2005.

[86] Y. Li, N. Seshadri, and S. Ariyavisitakul, "Channel estimation for OFDM systems with transmitter diversity in mobile wireless channels," *IEEE J. Sel. Areas Commun.*, vol. 17, no. 3, pp. 461–470, March 1999.

[87] Y. Li, “Simplified channel estimation for OFDM systems with multiple transmit antennas,” *IEEE Trans. Wireless Commun.*, vol. 1, no. 1, pp. 67–75, January 2002.

[88] S. Zhou, B. Muquet, and G. B. Giannakis, “Subspace-based (semi-)blind channel estimation for block precoded space time OFDM,” *IEEE Trans. Signal Process.*, vol. 50, no. 5, pp. 1215–1228, May 2002.

[89] Y. Zeng and T.-S. Ng, “A semi-blind channel estimation method for multiuser multi-antenna OFDM systems,” *IEEE Trans. Signal Process.*, vol. 52, no. 5, pp. 1419–1430, May 2004.

[90] W. H. Gerstacker, F. Obernosterer, R. Schober, A. T. Lehmann, A. Lampe, and P. Gunreben, “Equalization concepts for Alamouti’s space–time block code,” *IEEE Trans. Commun.*, vol. 52, no. 7, pp. 1178–1190, Jul. 2004.

[91] Z. Ding, D. B. Ward, and W. H. Chin, “A general scheme for equalization of space-time block-coded systems with unknown CSI,” *IEEE Trans. Signal Process.*, vol. 54, no. 7, pp. 2737-2746, July 2006.

[92] M. Marey, O. A. Dobre, and R. Inkol, “Novel algorithm for STBC-OFDM identification in cognitive radios,” *Proc. IEEE Int. Conf. Commun.*, Budapest, pp. 2770–2774, June 2013.

[93] M. Marey, O. A. Dobre, and R. Inkol, “Blind STBC identification for multiple-antenna OFDM systems,” *IEEE Trans. Commun.*, vol. 62, pp. 1554–1567, May 2014.

[94] Y. A. Eldemerdash, M. Marey, O. A. Dobre, G. Karagiannidis, and R. Inkol, “Fourth-order statistics for blind classification of spatial multiplexing and Alamouti space–time block code signals,” *IEEE Trans. Commun.*, vol. 61, no. 6, pp. 2420-2431, June 2013.

[95] Y. A. Eldemerdash and O. A. Dobre, “Second-order correlation-based algorithm for STBC-OFDM signal identification,” *Proc. IEEE Int. Conf. Commun.*, London, pp. 4972-4977, June 2015.

[96] E. Karami and O. A. Dobre, “Identification of SM-OFDM and AL-OFDM signals based on their second-order cyclostationarity,” *IEEE Trans. Veh. Technol.*, vol. 64, pp. 942–953, March 2015.

[97] Y. A. Eldemerdash, O. A. Dobre, and M. Öner, “Signal identification for multiple-antenna wireless systems: achievements and challenges,” *IEEE Commun. Surveys Tuts.*, vol. 18, no. 3, pp. 1524-1551, 3rd Quarter 2016.

[98] G. Caire, G. Taricco, and E. Biglieri, “Bit-interleaved coded modulation,” *IEEE Trans. Info. Theory*, vol. 44, no. 3, May 1998, pp. 927–46.

[99] H. Bölcskei and A. J. Paulraj, “Space-frequency coded broadband OFDM systems,” *Proc. IEEE Wireless Commun. Networking Conf.*, Chicago, IL, pp. 1–6, September 2000.

[100] K. F. Lee and D. B. Williams, “A space-frequency transmitter diversity technique for OFDM systems,” *Proc. IEEE Global Commun. Conf.*, vol. 3, San Francisco, USA, pp. 1473–1477, December 2000.

[101] B. Lu and X. Wang, “Space-time code design in OFDM systems,” *Proc. IEEE GLOBECOM*, vol. 2, San Francisco, CA, pp. 1000–1004, November 2000.

[102] H. Bölcskei and A. J. Paulraj, “Space-frequency codes for broadband fading channels,” *Proc. IEEE Int. Symp. Info. Theory*, Washington, DC, pp. 219, June 2001.

[103] W. Su, Z. Safar, M. Olfat, and K. J. R. Liu, “Obtaining full-diversity space-frequency codes from space-time codes via mapping,” *IEEE Trans. Signal Process.*, vol. 51, no. 11, pp. 2905–2916, November 2003.

[104] W. Su, Z. Safar, and K. J. R. Liu, "Full-rate full-diversity space-frequency codes with optimum coding advantage," *IEEE Trans. Info. Theory*, vol. 51, no. 1, pp. 229-249, January 2005.

[105] G. Yu and J. Kang, "Quasi-orthogonal space-frequency block code," *Proc. Int. Symp. Commun. Info. Technol.*, Japan, pp. 979-982, October 2004.

[106] L. Lihua, T. Xiaofeng, Z. Ping, and H. Haas, "A practical space-frequency block coded OFDM scheme for fast fading broadband channels," *Proc. 13th IEEE Int. Symp. Pers. Indoor Mobile Radio Commun.*, vol. 1, Lisboa, Portugal, pp. 212-216, September 2002.

[107] Y. Gong and K. B. Letaief, "An efficient space-frequency coded OFDM system for broadband wireless communications," *IEEE Trans. Commun.*, vol. 51, no. 11, pp. 2019-2029, November 2003.

[108] S. D. Muruganathan and A. B. Sesay, "A computationally efficient QR-successive interference cancellation scheme for simplified receiver implementation in SFBC-OFDM systems," *IEEE Trans. Wireless Commun.*, vol. 6, no. 10, pp. 3641-3647, October 2007.

[109] H. El Gamal and A. R. Hammons Jr., "Method and system for utilizing space-time and space-frequency codes for multi-input multi-output frequency selective fading channels," U. S. Patent 7 010 053 B2, March 7, 2006.

[110] H. El Gamal and A. R. Hammons Jr., "On the design of algebraic space-time codes for MIMO block-fading channels," *IEEE Trans. Inf. Theory.*, vol. 49, no. 1, pp. 151–163, January 2003.

[111] X. Ma and G. B. Giannakis, "Full-diversity full-rate complex-field space-time coding," *IEEE Trans. Signal Process*, vol. 51, pp. 2917–2930, November 2003.

[112] Z. Wang and G. B. Giannakis, "Complex-field coding for OFDM over fading wireless channels," *IEEE Trans. Inf. Theory.*, vol. 49, pp. 707–720, March 2003.

[113] W. Zhang, X.-G. Xia, and P. C. Ching, "High-rate full-diversity space time-frequency codes for broadband MIMO block-fading channels," *IEEE Trans. Commun.*, vol. 55, pp. 25–34, January 2007.

[114] T. Kiran and B. S. Rajan, "A systematic design of high-rate full-diversity space-frequency codes for MIMO-OFDM systems," *Proc. Int. Symp. Info. Theory, ISIT 2005*, Adelaide, SA, pp. 2075-2079, September 2005.

[115] M. R. Bhavani and K. V. S. Hari, "Systematic construction of linear transform based full-diversity, rate-one space-time frequency codes," *IEEE Trans. Signal Process.*, vol. 57, no. 6, pp. 2285–2298, June 2009.

[116] A. Naguib and N. Seshadri, "Combined interference cancellation and ML decoding of space-time block codes," *Proc. Comm. Theory Miniconference*, vol. 2, Anaheim, CA, USA, pp. 7–15, November 1998.

[117] G. G. Raleigh and J. M. Cioffi, "Spatio-temporal coding for wireless communication," *IEEE Trans. Commun.*, vol. 46, no. 3, pp. 357–366, March 1998.

[118] D. J. Love, R. W. Heath, W. Santipach, and M. Honig, "What is the value of limited feedback for MIMO channels?," *IEEE Commun. Mag.*, vol. 42, no. 10, pp. 54–59, October 2004.

[119] A. Naguib, N. Seshadri, and A. Calderbank, "Applications of space-time block codes and interference suppression for high capacity and high data rate wireless systems," *Proc. 32nd*

Asilomar Conf. Signals Systems Computers, vol. 2, Pacific Grove, CA, USA, pp. 1803–1810, November 1998.

[120] A. Calderbank, G. Pottie, and N. Seshadri, "Cochannel interference suppression through time/space diversity," *IEEE Trans. Inform. Theory*, vol. 46, no. 3, pp. 922–932, May 2000.

[121] J. Liu and E. Gunawan, "Exact bit-error rate analysis for the combined system of beamforming and Alamouti's space-time block code," *IEEE Microwave Wireless Compon. Lett.*, vol. 14, no. 8, pp. 398–400, August 2004.

[122] G. Jongren, M. Skoglund, and B. Ottersten, "Combining beamforming and orthogonal space-time block coding," *IEEE Trans. Inform. Theory*, vol. 48, no. 3, pp. 611–627, March 2002.

[123] J. Kim, "Interference suppression for high data rate STBC/SFBC with 1-bit feedback," *IEEE Commun. Lett.*, vol. 13, no. 1, pp. 13-15, January 2009.

[124] Z. Mohammadian, M. Shahabinejad, and S. Talebi, "New full-diversity space-frequency block codes based on the OSTBCs," *IEEE Commun. Lett.*, vol. 16, no. 10, pp. 1620-1623, October 2012.

[125] Z. Liu, X. Ma, and G.B. Giannakis, "Space-time coding and Kalman filtering for diversity transmissions through time-selective fading channels," *IEEE Trans. Commun.*, vol. 50, pp. 183-186, February 2002.

[126] T. A. Tran and A. B. Sesay, "A generalized simplified ML decoder of orthogonal space-time block code for wireless communications over time-selective fading channels," *Proc. IEEE Veh. Technol. Conf.*, Vancouver, Canada, pp. 1911-1915, Fall 2002.

[127] M. Li, X. Zhang, Z. Bu, and W. Zhang, "A concatenated ML decoder for SFBC-OFDM systems in frequency selective fading channels," *Proc. 2005 IEEE 16th Int. Symp. Pers. Indoor Mobile Radio Commun.*, Berlin, pp. 196-200, September 2005.

[128] A. Massaoudi, N. Sellami, N. Masmoudi, and M. Siala, "Study and implementation of an iterative decoder for SFBC-OFDM systems with imperfect channel knowledge," *Proc. 15th IEEE Mediterranean Electrotechnical Conf.*, Valletta, Malta, pp. 570–574, April 2010.

[129] H. Wang, X.-G. Xia, and Q. Yin, "Computationally efficient equalization for asynchronous cooperative communications with multiple frequency offsets," *IEEE Trans. Wireless Commun.*, vol. 8, no. 2, pp. 648–655, February 2009.

[130] V. Tarokh, H. Jafarkhani, and A. R. Calderbank, "Space–time block coding for wireless communications: Performance results," *IEEE J. Sel. Areas Commun.*, vol. 17, no. 3, pp. 451-460, March 1999.

[131] B. Özbek and D. Le Ruyet, "Low complexity ZF receiver for orthogonal SFBC-OFDM in broadband wireless channels," *Electron. Lett.*, vol. 42, no. 8, pp. 479-481, April 2006.

[132] K. Kim and H. Kim, "An ICI suppression scheme based on the correlative coding for Alamouti SFBC-OFDM system with phase noise," *IEEE Trans. Wireless Commun.*, vol. 10, no. 7, pp. 2023-2027, July 2011.

[133] Q. Huang, M. Ghogho, D. Ma, and J. Wei, "Low-complexity data-detection algorithm in cooperative SFBC-OFDM systems with multiple frequency offsets," *IEEE Trans. Veh. Technol.*, vol. 59, no. 9, pp. 4614-4620, November 2010.

[134] M. Gao, Y. Li, O. A. Dobre, and N. Al-Dhahir, "Blind identification of SFBC-OFDM signals using subspace decompositions and random matrix theory," *IEEE Trans. Veh. Technol.*, vol. 67, no. 10, pp. 9619-9630, March 2018.

[135] M. Marey and O. A. Dobre, "Automatic identification of space-frequency block coding for OFDM systems," *IEEE Trans. Wireless Commun.*, vol. 16, no. 1, pp. 117-128, January 2017.

[136] M. Marey, "Integer CFO estimation algorithm for SFBC-OFDM systems," *IEEE Commun. Lett.*, vol. 22, no. 8, pp. 1632-1635, August 2018.

[137] K.-C. Chan, Y.-M. Chen, C.-J. Wu, and C.-P. Li, "Achieving full diversity on a single-carrier distributed QOSFBC transmission scheme utilizing PAPR reduction," *IEEE Trans. Commun.*, vol. 66, no. 4, pp. 1636-1648, April 2018.

[138] W.-W. Hu, W.-J. Huang, Y.-C. Ciou, and C.-P. Li, "Reduction of PAPR without side information for SFBC MIMO-OFDM systems," *IEEE Trans. Broadcast.*, vol. 65, no. 2, pp. 316-325, June 2019.

[139] S.-J. Ku, "Low-complexity PTS-based schemes for PAPR reduction in SFBC MIMO-OFDM systems," *IEEE Trans. Broadcast.*, vol. 60, no. 4, pp. 650-658, December 2014.

[140] J. Han and G. Leus, "Space-time and space-frequency block coded vector OFDM modulation," *IEEE Commun. Lett.*, vol. 21, no. 1, pp. 204-207, January 2017.

[141] F. Delestre and Y. Sun, "Performance of SFBC-OFDM system with pilot aided channel estimation," *Proc. 7th Int. Wireless Commun. Mobile Comput. Conf.*, Istanbul, Turkey, pp. 1423-1428, July 2011.

[142] H. El Gamal, A. R. Hammons, Jr., Y. Liu, M. P. Fitz, and O. Y. Takeshita, "On the design of space-time and space-frequency codes for MIMO frequency-selective fading channels," *IEEE Trans. Inf. Theory*, vol. 49, no. 9, pp. 2277-2292, September 2003.

[143] M. Torabi, S. Aissa, and M. R. Soleymani, "On the BER performance of space-frequency block coded OFDM systems in fading MIMO channels," *IEEE Trans. Wireless Commun.*, vol. 6, no. 4, pp. 1366-1373, April 2007.

[144] D. Singh and H. D. Joshi, "BER performance of SFBC OFDM system over TWDP fading channel," *IEEE Commun. Lett.*, vol. 20, no. 12, pp. 2426-2429, December 2016.

[145] D. Singh and H. D. Joshi, "Performance analysis of SFBC-OFDM system with channel estimation error over generalized fading channels," *Trans. Emerg. Telecommun. Technol.*, vol. 29, no. 3, p. e3293, March 2018.

[146] D. Singh and H. D. Joshi, "Error probability analysis of STBC-OFDM systems with CFO and imperfect CSI over generalized fading channels," *Int. J. Electron. Commun.*, vol. 98, pp. 156-163, January 2018.

[147] C. van den Bos, M. H. L. Ksuwenhoven, and W. A. Serdijn, "Effect of smooth nonlinear distortion on OFDM symbol error rate," *IEEE Trans. Commun.*, vol. 49, no. 9, pp. 1510-1514, September 2001.

[148] Y. Du, J. Liu, and Y. Chen, "Performance analysis of nonlinear SFBC OFDM systems over TWDP fading channel," *IEEE Access*, vol. 7, pp. 101981-101991, July 2019.

[149] H. Arslan and G. E. Bottomley, "Channel estimation in narrowband wireless communication systems," *Wireless Commun. Mobile Comput.*, vol. 1, no. 2, pp. 201–219, April 2001.

[150] M. K. Ozdemir and H. Arslan, "Channel estimation for wireless OFDM systems," *IEEE Commun. Surveys Tuts.*, vol. 9, no. 2, pp. 18-48, Second Quarter 2007.

[151] S. Wu and Y. Bar-Ness, "OFDM channel estimation in the presence of frequency offset and phase noise," *Proc. IEEE Int. Conf. Commun.*, vol. 5, Anchorage, AK, pp. 3366–3370, May 2003.

[152] B. Han *et al.*, "An iterative joint channel estimation and symbol detection algorithm applied in OFDM system with high data to pilot power ratio," *Proc. IEEE Int. Conf. Commun.*, vol. 3, Anchorage, AK, pp. 2076–2080, May 2003.

[153] I. W. Group, "IEEE 802.11 Wireless Local Area Networks," May 2001, [Online]. Available: http://Grouper.IEEE.Org/Groups/802/11.

[154] H. Tang, K. Y. Lau, and R. W. Brodersen, "Interpolation-based maximum likelihood channel estimation using OFDM pilot symbols," *Proc. IEEE Globecom Conf.*, vol. 2, Taipei, Taiwan, pp. 1860–1864, November 2002.

[155] Y. Sun, X. Wang, and K. J. R. Liu, "A joint channel estimation and unequal error protection scheme for video transmission in OFDM systems," *Proc. IEEE Int. Conf. Image Process.*, vol. 1, Rochester, NY, pp. 549–552, September 2002.

[156] M. Bossert, A. Donder, and A. Trushkin, "Channel estimation and equalization in orthogonal frequency division multiplexing systems," *Proc. ITG-Fachberitcht, Mobile Kommunikation*, vol. 1, Neu-Ulm, Germany, pp. 485–492, September 1995.

[157] V. Mignone, A. Morello, and M. Visintin, "Cd3–OFDM: A new channel estimation method to improve the spectrum efficiency in digital terrestrial television systems," *Proc. Int. Broadcasting Convention*, vol. 1, Amsterdam, Netherlands, pp. 122–128, September 1995.

[158] O. Edfors *et al.*, "OFDM channel estimation by singular value decomposition," *IEEE Trans. Commun.*, vol. 46, no. 7, pp. 931–939, July 1998.

[159] Y. Li, J. H. Winters, and N. R. Sollenberger, "MIMO-OFDM for wireless communications: Signal detection with enhanced channel estimation," *IEEE Trans. Commun.*, vol. 50, no. 9, pp. 1471–1477, September 2002.

[160] M. K. Ozdemir, H. Arslan, and E. Arvas, "MIMO–OFDM channel estimation for correlated fading channels," *Proc. IEEE Wireless and Microwave Technol. Conf.*, vol. 1, Clearwater, FL, pp. 1–5, April 2004.

[161] R. Negi and J. Cioffi, "Pilot tone selection for channel estimation in a mobile OFDM system," *IEEE Trans. Consumer Electron.*, vol. 44, no. 3, pp. 1122–1228, August 1998.

[162] B. M. Sadler, R. J. Kozick, and T. Moore, "Bounds on MIMO channel estimation and equalization with side information," *Proc. IEEE Int. Conf. Acoust. Speech Signal Process.*, vol. 4, Salt Lake City, UT, pp. 2145–2148, May 2001.

[163] I. Bradaric and A. P. Petropulu, "Performance of training–based OFDM systems in the presence of time varying frequency–selective channels," *Proc. IEEE Int. Conf. Acoust. Speech Signal Process.*, vol. 4, Montreal, Canada, pp. 737–740, May 2004.

[164] M. Li, J. Tan, and W. Zhang, "A channel estimation method based on frequency–domain pilots and time–domain processing for OFDM systems," *IEEE Trans. Consumer Electron.*, vol. 50, no. 4, pp. 1049–1057, November 2004.

[165] I. Gaspard, “Impact of the channel estimation onto the BER performance of PSAM–OFDM systems in mobile radio channels,” *Proc. IEEE Veh. Technol. Conf.*, vol. 1, Rhodes, Greece, pp. 673–677, May 2001.

[166] R. Chen, C. Hou, and J. Guo, “Symbol timing and channel estimation of IEEE 802.11a based on OFDM,” *Proc. IEEE Canadian Conf. Electron. Comput. Eng.*, vol. 3, Montreal, Canada, pp. 1547–1550, May 2003.

[167] H. Arslan and T. Yucek, “Estimation of frequency selectivity for OFDM based new generation wireless communication systems,” *Proc. World Wireless Congress*, vol. 1, San Francisco, CA, May 2003.

[168] Q. Sun *et al.*, “Estimation of continuous flat fading MIMO channels,” *IEEE Trans. Wireless Commun.*, vol. 1, no. 4, pp. 549–553, October 2002.

[169] J. K. Cavers, “An analysis of pilot symbol assisted modulation for Rayleigh fading channels,” *IEEE Trans. Veh. Technol.*, vol. 40, pp. 686–693, November 1991.

[170] A. Dowler, A. Doufexi, and A. Nix, “Performance evaluation of channel estimation techniques for a mobile fourth generation wide area OFDM system,” *Proc. IEEE Veh. Technol. Conf.*, vol. 4, Vancouver, Canada, pp. 2036–2040, September 2002.

[171] C. Suh, C. S. Hwang, and H. Choi, “Preamble design for channel estimation in MIMO-OFDM systems,” *Proc. IEEE Globecom Conf.*, vol. 1, San Francisco, CA, pp. 317–321, December 2003.

[172] M. J. F. G. Garcia, O. Edfors, and J. M. P. Borrallo, “Joint channel estimation and peak-to-average power reduction in coherent OFDM: A novel approach,” *Proc. IEEE Veh. Technol. Conf.*, vol. 2, Rhodes, Greece, pp. 815–819, May 2001.

[173] W. G. Jeon, K. H. Paik, and Y. S. Cho, “An efficient channel estimation technique for OFDM systems with transmitter diversity,” *Proc. IEEE Int. Symp. Pers. Indoor Mobile Radio Commun.*, vol. 2, London, UK, pp. 1246–1250, September 2000.

[174] J. J. Van de Beek *et al.*, “On channel estimation in OFDM systems,” *Proc. IEEE Veh. Technol. Conf.*, vol. 2, Rosemont, IL, pp. 815–819, July 1995.

[175] O. Edfors *et al.*, “Analysis of DFT-based channel estimators for OFDM,” *Wireless Pers. Commun.*, vol. 12, no. 1, pp. 55–70, January 2000.

[176] M. Morelli and U. Mengali, “A comparison of pilot–aided channel estimation methods for OFDM systems,” *IEEE Trans. Signal Processing*, vol. 49, no. 12, pp. 3065–3073, December 2001.

[177] F. D. Nunes and J. M. N. Leitao, “Nonlinear channel estimation in fading OFDM systems,” *Proc. IEEE Globecom Conf.*, vol. 4, Rio De Janeireo, Brazil, pp. 2157–2161, December 1999.

[178] Z. Yuanjin, “A novel channel estimation and tracking method for wireless OFDM systems based on pilots and Kalman filtering,” *IEEE Trans. Consum. Electron.*, vol. 49, no. 2, pp. 275–83, May 2003.

[179] C. S. Yeh and Y. Lin, “Channel estimation using pilot tones in OFDM systems,” *IEEE Trans. Broadcast.*, vol. 45, no. 4, pp. 400–409, December 1999.

[180] Y. Sun, X. Wang, and K. J. R. Liu, “A joint channel estimation and unequal error protection scheme for image transmission in wireless OFDM systems,” *Proc. IEEE Wksp. Multimedia Signal Process.*, vol. 1, St. Thomas, US Virgin Islands, pp. 380–383, December 2002.

[181] J. Rinne and M. Renfors, “Pilot spacing in orthogonal frequency division multiplexing systems on practical channels,” *IEEE Trans. Consumer Electron.*, vol. 42, no. 3, pp. 959–962, November 1996.

[182] S. Coleri *et al.*, “Channel estimation techniques based on pilot arrangement in OFDM systems,” *IEEE Trans. Broadcast.*, vol. 48, no. 3, pp. 223–229, September 2002.

[183] A. Dowler and A. Nix, “Performance evaluation of channel estimation techniques in a multiple antenna OFDM system,” *Proc. IEEE Veh. Technol. Conf.*, vol. 2, Orlando, FL, pp. 1214–1218, October 2003.

[184] S. G. Kang, Y. M. Ha, and E. K. Joo, “A comparative investigation on channel estimation algorithms for OFDM in mobile communications,” *IEEE Trans. Broadcast.*, vol. 49, no. 2, pp. 142–149, June 2003.

[185] M. X. Chang and Y. T. Su, “Model–based channel estimation for OFDM signals in Rayleigh fading,” *IEEE Trans. Commun.*, vol. 50, no. 4, pp. 540–544, April 2002.

[186] J. J. Van de Beek, “Synchronization and channel estimation in OFDM systems,” Ph.D. Dissertation, Luleå Univ. Technol., Sweden, 1998.

[187] B. Yang, K. B. Letaief, R. S. Cheng, and Z. Cao, “Channel estimation for OFDM transmission in multipath fading channels based on parametric channel modeling,” *IEEE Trans. Commun.*, vol. 49, no. 3, pp. 467–479, March 2001.

[188] S. W. Ellingson, “Detection of tones and pulses using a large, uncalibrated array,” *Proc. IEEE Antennas Propagat. Soc. Conf.*, vol. 4, Columbus, OH, pp. 196–199, June 2003.

[189] I. Tolochko and M. Faulkner, “Real time LMMSE channel estimation for wireless OFDM systems with transmitter diversity,” *Proc. IEEE Veh. Technol. Conf.*, vol. 3, Vancouver, Canada, pp. 1555–1559, September 2002.

[190] M. H. Hsieh and C. H. Wei, “Channel estimation for OFDM systems based on comb-type pilot arrangement in frequency selective fading channels,” *IEEE Trans. Consum. Electron.*, vol. 44, no. 1, pp. 217–225, February 1998.

[191] A. F. Kurpiers, “Improved channel estimation and demodulation for OFDM on HF ionospheric channels,” *Proc. IEE Int. Conf. HF Radio Syst. Techniques*, vol. 1, Guildford, UK, pp. 65–69, July 2000.

[192] H. H. H’mimy, “Channel estimation based on coded pilot for OFDM,” *Proc. IEEE Veh. Technol. Conf.*, vol. 3, Phoenix, AZ, pp. 1375–1379, May 1997.

[193] J. Cho *et al.*, “A novel channel estimation method for OFDM in high–speed mobile system,” *Proc. IEEE Int. Symp. Ind. Electron.*, vol. 1, Pusan, Korea, pp. 571–574, June 2001.

[194] J. Siew *et al.*, “A channel estimation method for MIMO–OFDM systems,” *Proc. London Commun. Symp.*, London, England, pp. 1–4, September 2002.

[195] S. B. Bulumulla, S. A. Kassam, and S. S. Venkatesh, “A systematic approach in detecting OFDM signals in a fading channel,” *IEEE Trans. Commun.*, vol. 48, no. 5, pp. 725–28, May 2000.

[196] Y. Wang *et al.*, “Threshold channel estimation for OFDM in wireless systems,” *Proc. IEEE Veh. Technol. Conf.*, vol. 3, Jeju, Korea, pp. 1586–1589, April 2003.

[197] M. Bossert, A. Donder, and V. Zyablov, “Improved channel estimation with decision feedback for OFDM systems,” *Electron. Lett.*, vol. 34, no. 11, pp. 1064–1065, May 1998.

[198] T. Roman, M. Enescu, and V. Koivunen, “Time-domain method for tracking dispersive channels in MIMO OFDM systems,” *Proc. IEEE Int. Conf. Acoust. Speech Signal Process.*, vol. 4, Hong Kong, China, pp. 393–396, April 2003.

[199] M. Enescu and V. Koivunen, “Estimating the fading coefficient in mobile OFDM systems using state-space model,” *Proc. IEEE Int. Symp. Circuits Systems*, vol. 6, Kobe, Japan, pp. 6094-6097, May 2005.

[200] M. Sternad and D. Aronsson, “Channel estimation and prediction for adaptive OFDM downlinks,” *Proc. IEEE Veh. Technol. Conf.*, vol. 2, Orlando, FL, pp. 1283–1287, October 2003.

[201] X. Zhuang and F. W. Vook, “Iterative channel estimation and decoding for a turbo-coded OFDM system via the EM algorithm,” *Proc. IEEE Int. Conf. Acoust. Speech Signal Process.*, vol. 3, Orlando, FL, pp. 2337–2340, May 2002.

[202] X. Ma, H. Kobayashi, and S. C. Schwartz, “An EM-based estimation of OFDM signals,” *Proc. IEEE Wireless Commun. Networking Conf.*, vol. 1, Orlando, FL, pp. 228–232, March 2002.

[203] E. Jaffrot and M. Siala, “Turbo channel estimation for OFDM systems on highly time and frequency selective channels,” *Proc. IEEE Int. Conf. Acoust. Speech Signal Process.*, vol. 5, Istanbul, Turkey, pp. 2977–2980, June 2000.

[204] J. Yue *et al.*, “Channel estimation and data detection for MIMO–OFDM systems,” *Proc. IEEE GLOBECOM Conf.*, vol. 2, San Francisco, CA, pp. 581–585, December 2003.

[205] J. Cai, X. Shen, and J. W. Mark, “EM channel estimation algorithm for OFDM wireless communication systems,” *Proc. IEEE Int. Symp. Pers. Indoor Mobile Radio Commun.*, vol. 1, Beijing, China, pp. 804–808, September 2003.

[206] S. C. Schwartz, J. Zhang, and D. Gu, “Iterative channel estimation for OFDM with clipping,” *Proc. Int. Symp. Wireless Pers. Multimedia Commun.*, vol. 3, Honolulu, HI, pp. 1304–1308, October 2002.

[207] M. Flament, B. Mielczarek, and A. Svensson, “Joint channel estimation and turbo decoding for OFDM-based systems,” *Proc. Int. Symp. Wireless Pers. Multimedia Commun.*, vol. 3, Honolulu, HI, pp. 1299–1303, October 2002.

[208] K. J. Kim and J. Yue, “Joint channel estimation and data detection algorithms for MIMO-OFDM systems,” *Proc. Asilomar Conf. Signals Syst. Computers*, vol. 2, Monterey, CA, pp. 1857–1861, November 2002.

[209] M. Ito *et al.*, “An OFDM receiver with decision–directed channel estimation for the scattered pilot scheme in fast fading environments,” *Proc. IEEE Veh. Technol. Conf.*, vol. 1, Jeju, Korea, pp. 368–372, April 2003.

[210] M. Munster and L. Hanzo, “RLS-adaptive parallel interference cancellation assisted decision-directed channel estimation for OFDM,” *Proc. IEEE Wireless Commun. Networking Conf.*, vol. 1, New Orleans, LA, pp. 50–54, March 2003.

[211] D. Hu and L. Yang, “Time-varying channel estimation based on pilot tones in OFDM systems,” *Proc. Int. Conf. Neural Networks Signal Process.*, vol. 1, Nanjing, China, pp. 700–703, December 2003.

[212] J. Rinne and M. Renfors, “An equalization method for orthogonal frequency division multiplexing systems in channels with multipath propagation, frequency offset and phase noise,” *Proc. IEEE Globecom Conf.*, vol. 2, London, UK, pp. 1442–1446, November 1996.

[213] H. A. Mahmoud and H. Arslan, "Improved channel estimation in OFDM systems with synchronization errors and back-off," *Proc. IEEE Veh. Technol. Conf.*, Montreal, Quebec, pp. 1-4, September 2006.

[214] W. G. Song and J. T. Lim, "Pilot–symbol aided channel estimation for OFDM with fast fading channels," *IEEE Trans. Broadcast.*, vol. 49, no. 4, pp. 398–402, December 2003.

[215] A. Stamoulis, S. N. Diggavi, and N. Al-Dhahir, "Estimation of fast fading channels in OFDM," *Proc. IEEE Wireless Commun. Networking Conf.*, vol. 1, Orlando, FL, pp. 465–470, March 2002.

[216] J. Cai, X. Shen, and J. W. Mark, "Robust channel estimation for OFDM wireless communication systems — an H∞ approach," *Proc. IEEE Veh. Technol. Conf.*, vol. 4, Vancouver, Canada, pp. 2106–2110, September 2002.

[217] W. Samek, S. Stanczak, and T. Wiegand., "The convergence of machine learning and communications," 2017. [Online]. Available: https://arxiv.org/abs/1708.08299

[218] M. Egmont Petersen, D. D. Ridder, and H. Handels, "Image processing with neural networks-A review," *Pattern Recognit.*, vol. 35, no. 10, pp. 2279-2301, 2002.

[219] A. Cochocki and R. Unbehauen, *Neural Networks for Optimization and Signal Processing*. Hoboken, NJ, USA: Wiley, 1992.

[220] A. Krizhevsky, I. Sutskever, and G. E. Hinton, "ImageNet classification with deep convolutional neural networks," *Commun. ACM*, vol. 60, no. 6, pp. 84-90, June 2017.

[221] S. Li, J. He, Y. Li, and M. U. Rafique, "Distributed recurrent neural networks for cooperative control of manipulators: A game-theoretic perspective," *IEEE Trans. Neural Netw. Learn. Syst.*, vol. 28, no. 2, pp. 415-426, February 2017.

[222] Y. Li, S. Li, and B. Hannaford, "A model based recurrent neural network with randomness for efficient control with applications," *IEEE Trans. Ind. Informat.*, vol. 15, no. 4, pp. 2054-2063, April 2019.

[223] Y. Li, S. Li, D. Caballero, M. Miyasaka, A. Lewis, and B. Hannaford, "Improving control precision and motion adaptiveness for surgical robot with recurrent neural network," *Proc. IEEE/RSJ Int. Conf. Intell. Robots Syst. (IROS)*, Vancouver, BC, Canada, pp. 3538-3543, September 2017.

[224] Y. Li, S. Li, and B. Hannaford, "A novel recurrent neural network for improving redundant manipulator motion planning completeness," *Proc. IEEE Int. Conf. Robot. Autom. (ICRA)*, Brisbane, QLD, Australia, pp. 2956-2961, May 2018.

[225] X. Zhou and X. Wang, "Channel estimation for OFDM systems using adaptive radial basis function networks," *IEEE Trans. Veh. Technol.*, vol. 52, no. 1, pp. 48-59, January 2003.

[226] X. W. He, R. Z. Yang, J. Zhang, and Y. H. Zhang, "An OFDM channel estimation method with radial basis function neural network," *Appl. Mech. Mater.*, vol. 263, pp. 1142-1149, December 2013.

[227] C. Simsir and N. Taspinar, "Channel estimation using radial basis function neural network in OFDM-IDMA system," *Wireless Pers. Commun.*, vol. 85, no. 4, pp. 1883-1893, December 2015.

[228] C. Çifiikli, A. T. Özsahin, and A. Ç. Yapici, "Artificial neural network channel estimation based on Levenberg-Marquardt for OFDM systems," *Wireless Pers. Commun.*, vol. 51, no. 2, pp. 221-229, October 2009.

[229] S. J. Nawaz, S. Mohsin, and A. A. Ikaram, "Neural network based MIMO-OFDM channel equalizer using comb-type pilot arrangement," *Proc. Int. Conf. Future Comput. Commun.*, Kuala Lumpar, Malaysia, pp. 36-41, April 2009.

[230] M. N. Seyman and N. Taspinar, "Channel estimation based on neural network with feedback for MIMO OFDM mobile communication systems," *Intell. Autom. Soft Comput.*, vol. 18, no. 3, pp. 307-316, 2012.

[231] E. Chen, R. Tao, and X. Zhao, "Channel equalization for OFDM system based on the BP neural network," *Proc. 8th Int. Conf. Signal Process.*, vol. 3, Beijing, China, pp. 2253-2256, November 2006.

[232] N. Taspinar and M. N. Seyman, "Back propagation neural network approach for channel estimation in OFDM system," *Proc. IEEE Int. Conf. Wireless Commun. Netw. Inf. Secur. (WCNIS)*, Beijing, China, pp. 265-268, June 2010.

[233] C. H. Cheng, Y.-P. Cheng, Y.-H. Huang, and W.-C. Li, "Using backpropagation neural network for channel estimation and compensation in OFDM systems," *Proc. 7th Int. Conf. Complex, Intell. Softw. Intensive Syst. (CISIS)*, Taichung, Taiwan, pp. 340-345, July 2013.

[234] K. Hiray and K. V. Babu, "A neural network based channel estimation scheme for OFDM system," *Proc. Int. Conf. Commun. Signal Process. (ICCSP)*, Melmaruvathur, India, pp. 0438-0441, April 2016.

[235] L. Zhang and X. Zhang, "MIMO channel estimation and equalization using three-layer neural networks with feedback," *Tsinghua Sci. Technol.*, vol. 12, no. 6, pp. 658-662, 2007.

[236] M. N. Seyman and N. Taspinar, "Channel estimation based on neural network in space time block coded MIMO-OFDM system," *Digit. Signal Process.*, vol. 23, no. 1, pp. 275-280, January 2013.

[237] C. Simsir and N. Taspinar, "Channel estimation using neural network in orthogonal frequency division multiplexing-interleave division multiple access (OFDM-IDMA) system," *Proc. Telecommun. Symp.*, Sao Paulo, Brazil, pp. 1-5, August 2014.

[238] R. Choubey and V. Reddy, "Channel estimation in space time block coded MIMO-OFDM system: A review," *Int. J. Adv. Technol. Eng. Explor.*, vol. 5, no. 38, pp. 17-22, January 2018.

[239] C. H. Cheng, Y. H. Huang, and H. C. Chen, "Channel estimation in OFDM systems using neural network technology combined with a genetic algorithm," *Soft Comput.*, vol. 20, no. 10, pp. 4139-4148, October 2016.

[240] X. Wang, L. Gao, and S. Mao, "BiLoc: Bi-modal deep learning for indoor localization with commodity 5GHz WiFi," *IEEE Access*, vol. 5, pp. 4209-4220, March 2017.

[241] X. Wang, X. Wang, and S. Mao, "Deep convolutional neural networks for indoor localization with CSI images," *IEEE Trans. Netw. Sci. Eng.*, vol. 7, no. 1, pp. 316-327, 1 January-March 2020.

[242] C.-B. Ha and H.-K. Song, "Signal detection scheme based on adaptive ensemble deep learning model," *IEEE Access*, vol. 6, pp. 21342-21349, April 2018.

[243] C. Luo, J. Ji, Q.Wang, X. Chen, and P. Li, "Channel state information prediction for 5G wireless communications: A deep learning approach," *IEEE Trans. Netw. Sci. Eng.*, vol. 7, no. 1, pp. 227-236, 1 January-March 2020.

[244] M. Kim, W. Lee, and D.-H. Cho, "A novel PAPR reduction scheme for OFDM system based on deep learning," *IEEE Commun. Lett.*, vol. 22, no. 3, pp. 510-513, March 2018.

[245] Q. Huang, C. Zhao, M. Jiang, X. Li, and J. Liang. (2018). "Cascadenet: A new deep learning architecture for OFDM detection." [Online]. Available: https://arxiv.org/abs/1812.00023

[246] E. Balevi and J. G. Andrews. (2018). "One-bit OFDM receivers via deep learning." [Online]. Available: https://arxiv.org/abs/1811.00971

[247] X. Gao, S. Jin, C.-K. Wen, and G. Y. Li, "ComNet: Combination of deep learning and expert knowledge in OFDM receivers," *IEEE Commun. Lett.*, vol. 22, no. 12, pp. 2627-2630, December 2018.

[248] H. Ye, G. Y. Li, and B.-H. Juang, "Power of deep learning for channel estimation and signal detection in OFDM systems," *IEEE Wireless Commun. Lett.*, vol. 7, no. 1, pp. 114-117, February 2018.

[249] H. Ye and G. Y. Li, "Initial results on deep learning for joint channel equalization and decoding," *Proc. Veh. Technol. Conf. (VTC-Fall)*, Toronto, ON, pp. 1-5, September 2017.

[250] Y. Zhang, J. Li, Y. Zakharov, D. Sun, and J. Li. (2018). *Underwater acoustic OFDM communications using deep learning* [Online]. Available: https://eprints.soton.ac.uk/426097/1/FCAC_Deeplearning_OFDM_finally.pdf

[251] E. Telatar, "Capacity of multi-antenna Gaussian channels," *Eur. Trans. Telecomm.*, vol. 10, no. 6, pp. 585-595, November-December 1999.

[252] G. G. Raleigh and J. M. Cioffi, "Spatio-temporal coding for wireless communications," *Proc. IEEE Global Telecommun. Conf.*, London, UK, vol. 3, pp. 1809-1814, November 1996.

[253] H. Bolcskei, D. Gesbert and A. J. Paulraj, "On the capacity of OFDM-based spatial multiplexing systems," *IEEE Trans. Commun.*, vol. 50, no. 2, pp. 225-234, February 2002.

[254] N. Seshadri and J. H. Winters, "Two signaling schemes for improving the error performance of frequency-division-duplex (FDD) transmission systems using transmitter antenna diversity," *Proc. IEEE 43rd Veh. Technol. Conf.*, Secaucus, NJ, USA, pp. 508-511, May 1993.

[255] B. C. Banister and J. R. Zeidler, "Tracking performance of the RLS algorithm applied to an antenna array in a realistic fading environment," *IEEE Trans. Signal Process.*, vol. 50, no. 5, pp. 1037-1050, May 2002.

[256] H. Olofsson, M. Almgren, and M. Hook, "Transmitter diversity with antenna hopping for wireless communication systems," *Proc. IEEE 47th Veh. Technol. Conf.*, Phoenix, AZ, USA, pp. 1743-1747, May 1997.

[257] C. Toker, S. Lambotharan, and J. A. Chambers, "Closed loop quasi-orthogonal STBCs and their performance in multipath fading environments and when combined with turbo codes," *IEEE Trans. Wireless Commun.*, vol. 3, pp. 1890-1896, November 2004.

[258] S. Rouquette, S. Merigeault and K. Gosse, "Orthogonal full diversity space-time block coding based on transmit channel state information for 4 Tx antennas," *Proc. IEEE ICC*, vol. 1, New York, USA, pp. 558-562, May 2002.

[259] S. Lambotharan and C. Toker, "Closed-loop space time block coding techniques for OFDM broadband wireless access systems," *IEEE Trans. Consumer Electron.*, vol. 51, no. 3, pp. 765-769, August 2005.

[260] P. S. Henry and B. S. Glance, "A new approach to high-capacity digital mobile Radio," *Bell Syst. Tech. J.*, vol. 60, no. 8, pp. 1891-1904, October 1981.

[261] A. Wittneben, “Basestation modulation diversity for digital simulcast,” *Proc. 41st IEEE Veh. Technol. Conf.,* St. Louis, MO, USA, pp. 848-853, May 1991.

[262] T. Hattori and K. Hirade, “Multi-transmitter simulcast digital signal transmission by using frequency offset strategy in land mobile radio-telephone system,” *IEEE Trans. Veh. Technol.,* vol. VT-27, pp. 231-238, 1978.

[263] J. Lin, J. G. Proakis, Fuyun Ling, and H. Lev-Ari, “Optimal tracking of time-varying channels: A frequency domain approach for known and new algorithms,” *IEEE J. Sel. Areas Commun.,* vol. 13, no. 1, pp. 141-154, January 1995.

[264] S. Song, J.-S. Lim, S. J. Baek, and K.-M. Sung, “Variable forgetting factor linear least squares algorithm for frequency selective fading channel estimation,” *IEEE Trans. Veh. Technol.,* vol. 51, no. 3, pp. 613-616, May 2002.

[265] D. K. Borah and B. T. Hart, “Frequency-selective fading channel estimation with a polynomial time-varying channel model,” *IEEE Trans. Commun.,* vol. 47, no. 6, pp. 862-873, June 1999.

[266] B. Toplis and S. Pasupathy, “Tracking improvements in fast RLS algorithms using a variable forgetting factor,” *IEEE Trans. Acoust. Speech Signal Process.,* vol. 36, no. 2, pp. 206-227, February 1988.

[267] Y. S. Cho, S. B. Kim, and E. J. Powers, “Time-varying spectral estimation using AR models with variable forgetting factors,” *IEEE Trans. Signal Process.,* vol. 39, no. 6, pp. 1422-1426, June 1991.

[268] S. Haykin, *Adaptive Filter Theory.* 4th Edition, New York: Pearson Education, 2002.

[269] L. Chen and B. Chen, “A robust adaptive DFE receiver for DS-CDMA systems under multipath fading channels,” *IEEE Trans. Signal Process.,* vol. 49, no. 7, pp. 1523-1532, July 2001.

[270] J. Armstrong and H. A. Suraweera, “Impulse noise mitigation for OFDM using decision directed noise estimation,” *Proc. IEEE Int. Symp. Spread Spectrum Techniq. Apps.,* Sydney, NSW, Australia, pp. 174-178, September 2004.

[271] Y. Li, “Optimum training sequences for OFDM systems with multiple transmit antennas,” *Proc. IEEE Global Telecommun. Conf.,* San Francisco, Calif, USA, pp. 1478–1482, November 2000.

[272] K. F. Lee and D. B. Williams, “Pilot-symbol-assisted channel estimation for space-time coded OFDM systems,” *EURASIP J. Applied Signal Process.,* vol. 2002, no. 5, pp. 507-516, May 2002.

[273] S. Shahbazpanahi, A. B. Gershman, and J. H. Manton, “Closed-form blind MIMO channel estimation for orthogonal space-time block codes,” *IEEE Trans. Signal Process.,* vol. 53, no. 12, pp. 4506-4517, December 2005.

[274] W.-K. Ma, B.-N. Vo, T. N. Davidson, and P.-C. Ching, “Blind ML detection of orthogonal space-time block codes: efficient high-performance implementations,” *IEEE Trans. Signal Process.,* vol. 54, no. 2, pp. 738-751, February 2006.

[275] N. Ammar and Z. Ding, “Channel identifiability under orthogonal space-time coded modulations without training,” *IEEE Trans. Wireless Commun.,* vol. 5, no. 5, pp. 1003-1013, May 2006.

[276] A. L. Swindlehurst and G. Leus, "Blind and semi-blind equalization for generalized space-time block codes," *IEEE Trans. Signal Process.*, vol. 50, no. 10, pp. 2489-2498, October 2002.

[277] J. Choi, "Equalization and semi-blind channel estimation for space-time block coded signals over a frequency-selective fading channel," *IEEE Trans. Signal Process.*, vol. 52, no. 3, pp. 774-785, March 2004.

[278] Z. Liu, G. B. Giannakis, S. Barbarossa, and A. Scaglione, "Transmit antennae space-time block coding for generalized OFDM in the presence of unknown multipath," *IEEE J. Sel. Areas Commun.*, vol. 19, no. 7, pp. 1352-1364, July 2001.

[279] J. Wu and T. Lee, "Nonredundant precoding-assisted blind channel estimation for single-carrier space–time block-coded transmission with frequency-domain equalization," *IEEE Trans. Signal Process.*, vol. 55, no. 3, pp. 1062-1080, March 2007.

[280] J. Vía, I. Santamaría, J. Pérez and L. Vielva, "A new subspace method for blind estimation of selective MIMO-STBC channels," *Wireless Commun. Mobile Comput.*, vol. 10, no. 11, pp. 1478-1492, 2010.

[281] D. Cabric, "Addressing feasibility of cognitive radios," *IEEE Signal Process. Mag.*, vol. 25, no. 6, pp. 85–93, November 2008.

[282] J. L. Xu, W. Su, and M. Zhou, "Software-defined radio equipped with rapid modulation recognition," *IEEE Trans. Veh. Technol.*, vol. 59, no. 4, pp. 1659–1667, May 2010.

[283] Y. A. Eldemerdash, O. A. Dobre, and B. J. Liao, "Blind identification of SM and Alamouti STBC-OFDM signals," *IEEE Trans. Wireless Commun.*, vol. 14, no. 2, pp. 972-982, February 2015.

[284] R. Parisi, E. D. Di Claudio, G. Orlandi, and B. D. Rao, "Fast adaptive digital equalization by recurrent neural networks," *IEEE Trans. Signal Process.*, vol. 45, no. 11, pp. 2731-2739, November 1997.

[285] E. D. Di Claudio, R. Parisi, and G. Orlandi, "Neural sequence detector for digital equalization," *Proc. 10th European Signal Process. Conf.*, Tampere, pp. 1-4, September 2000.

[286] A. Omri, R. Hamila, M. Hasn, R. Bouallegue, and H. Chamkhia, "Estimation of highly selective channels for downlink LTE MIMO-OFDM system by a robust neural network," *J. Ubiquitous Systems Pervasive Netw.*, vol. 2, no. 1, pp. 31-38, April 2011.

[287] M. N. Seyman and N. Taspinar, "Radial basis function neural networks for channel estimation in MIMO-OFDM systems," *Arab. J. Sci. Eng.*, vol. 38, no. 8, pp. 2173–2178, August 2013.

[288] J. Zhang, Z. He, X. Wang, and Y. Huang, "TSK Fuzzy Approach to Channel Estimation for MIMO-OFDM Systems," *IEEE Signal Process. Lett.*, vol. 14, no. 6, pp. 381-384, June 2007.

[289] H. Dogan, H. A. Cirpan, and E. Panayirci, "Iterative channel estimation and decoding of turbo coded SFBC-OFDM systems," *IEEE Trans. Wireless Commun.*, vol. 6, no. 8, pp. 3090-3101, August 2007.

[290] H. Bolcskei, M. Borgmann, and A. J. Paulraj, "Impact of the propagation environment on the performance of space-frequency coded MIMO-OFDM," *IEEE J. Sel. Areas Commun,*, vol. 21, no. 3, pp. 427-439, April 2003.

[291] M. Torabi and M. R. Soleymani, "Adaptive modulation for OFDM systems using space-frequency block codes," *Proc. 2003 IEEE Wireless Commun. Network.*, New Orleans, LA, USA, pp. 61-65, March 2003.

[292] L. Lihua, G. Zhiheng, T. Xiaofeng, and Z. Ping, "SFBC-AOFDM scheme in fast and frequency selective fading scenarios," *Proc. 14th IEEE Pers. Indoor Mobile Radio Commun.*, Beijing, China, pp. 1949-1953, September 2003.

[293] H. Kanemaru and T. Ohtsuki, "Space-time/space-frequency block coded OFDM with diagonalized maximum likelihood decoder (ST/SF-OFDM with DMLD)," *IEICE Trans. Commun.*, vol. E87-B, no. 7, pp. 2034-2039, July 2004.

[294] S. D. Muruganathan and A. B. Sesay, "Signal detection for orthogonal/quasi-orthogonal space-frequency block coded OFDM transmit diversity schemes," *Proc. 2005 IEEE Military Commun. Conf.*, Atlantic City, NJ, pp. 299-304, October 2005.

[295] T. X. Lai, S. D. Muruganathan, and A. B. Sesay, "Performance analysis and multi-stage iterative receiver design for concatenated space- frequency block coding schemes," *IEEE Trans. Wireless Commun.*, vol. 7, no. 11, pp. 4208-4214, November 2008.

[296] S. Lu, B. Narasimhan, and N. Al-Dhahir, "A novel SFBC-OFDM scheme for doubly selective channels," *IEEE Trans. Veh. Technol.*, vol. 58, no. 5, pp. 2573-2578, June 2009.

[297] H. M. Park, J. S. Han, and H.-J. Choi, "Enhanced detection method for 3GPP LTE QO-SFBC system in frequency selective Rayleigh fading channel environment," *Proc. 4th Int. Conf. Uniquitous Info. Management Commun.*, Suwon, South Korea, pp. 1-5, January 2010.

[298] A. Al-Dweik, F. Kalbat, S. Muhaidat, O. Filio, and S. M. Ali, "Robust MIMO-OFDM system for frequency-selective mobile wireless channels," *IEEE Trans. Veh. Technol.*, vol. 64, no. 5, pp. 1739-1749, May 2015.

[299] S. M. Kay, *Fundamentals of Statistical Signal Processing: Estimation Theory*. vol. 1. Englewood Cliffs, NJ: Prentice–Hall, 1993.

[300] X. Wautelet, C. Herzet, A. Dejonghe, J. Louveaux, and L. Vandendorpe, "Comparison of EM-based algorithms for MIMO channel estimation," *IEEE Trans. Commun.*, vol. 55, no. 1, pp. 216–226, January 2007.

[301] M. Morelli and L. Sanguinetti, "Estimation of channel statistics for iterative detection of OFDM signals," *IEEE Trans. Wireless Commun.*, vol. 4, no. 4, pp. 1360–1365, July 2005.

[302] C. Shin, J. G. Andrews, and E. J. Powers, "An efficient design of doubly selective channel estimation for OFDM systems," *IEEE Trans. Wireless Commun.*, vol. 6, no. 10, pp. 3790–3802, October 2007.

[303] H. A. Cirpan, E. Panayirci, and H. Dogan, "Nondata-aided channel estimation for OFDM systems with space–frequency transmit diversity," *IEEE Trans. Veh. Technol.*, vol. 55, no. 2, pp. 449–457, March 2006.

[304] L. Deneire, P. Vandenameele, L. van der Perre, B. Gyselinckx, and M. Engels, "A low complexity ML channel estimator for OFDM," *Proc. IEEE Int. Conf. Commun.*, Helsinki, Finland, pp. 1461-1465, June 2001.

[305] H. Minn, D. I. Kim, and V. K. Bhargava, "A reduced complexity channel estimation for OFDM systems with transmit diversity in mobile wireless channels," *IEEE Trans. Commun.*, vol. 50, no. 5, pp. 799-807, May 2002.

[306] T. Liu *et al*., "A minimum-complexity high-performance channel estimator for MIMO-OFDM communications," *IEEE Trans. Veh. Technol.*, vol. 59, no. 9, pp. 4634-4639, November 2010.

[307] S. D. Muruganathan and A. B. Sesay, "A low-complexity decision-directed channel-estimation scheme for OFDM systems with space–frequency diversity in doubly selective fading channels," *IEEE Trans. Veh. Technol.*, vol. 58, no. 8, pp. 4277-4291, October 2009.

[308] F. Delestre, G. Owojaiye, and Y. Sun, "Efficient space-frequency block coded pilot-aided channel estimation method for multiple-input-multiple-output orthogonal frequency division multiplexing systems over mobile frequency-selective fading channels," *IET Commun.*, vol. 8, no. 6, pp. 841-851, April 2014.

[309] D. J. Love and R. W. Heath, "Limited feedback unitary precoding for orthogonal space-time block codes," *IEEE Trans. Signal Process.*, vol. 53, no. 1, pp. 64-73, January 2005.

[310] S.-Y. Kung, Y. Wu, and X. Zhang, "Bezout space-time precoders and equalizers for MIMO channels," *IEEE Trans. Signal Processing*, vol. 50, no. 10, pp. 2499–2514, October 2002.

[311] Y. Fu, C. Tellambura, and W. A. Krzymien, "Limited-feedback precoding for closed-loop multiuser MIMO OFDM systems with frequency offsets," *IEEE Trans. Wireless Commun.*, vol. 7, no. 11, pp. 4155-4165, November 2008.

[312] N. M. Eltayeb, S. K. Kassim and J. A. Chambers, "Closed-loop extended orthogonal space frequency block coding techniques for OFDM based broadband wireless access systems," *Proc. 5th Int. Conf. Broadband Commun. Networks Systems*, London, pp. 426-430, September 2008.

[313] S. Ye, R. S. Blum, and L. J. Cimini, "Adaptive OFDM systems with imperfect channel state information," *IEEE Trans. Wireless Commun.*, vol. 5, no. 11, pp. 3255-3265, November 2006.

[314] N. C. Beaulieu and C. Cheng, "Efficient Nakagami-m fading channel Simulation," *IEEE Trans. Veh. Technol.*, vol. 54, no. 2, pp. 413-424, March 2005.

[315] S. R. Sabuj and M. S. Islam, "Performance analysis of SFBC in MIMO-OFDM system over Nakagami-m fading channel," *Proc. 14th Int. Conf. Computer Info. Technol.*, Dhaka, pp. 30-33, December 2011.

[316] S. P. Majumder and M. A. Jumana, "Performance analysis of a space-frequency block coded OFDM wireless communication system with MSK and GMSK modulation," *Proc. Int. Conf. Electrical Engineering Info. Commun. Technol.*, Dhaka, pp. 1-5, April 2014.

[317] U. Raj and V. Bhaskar, "Performance analysis of scheduling schemes for MIMO OSFBC-OFDM system in α-μ fading channel scenarios," *Proc. Int. Conf. Commun. Signal Process.*, Melmaruvathur, India, pp. 144-148, August 2013.

[318] U. Raj and V. Bhaskar, "Performance analysis of SNR based scheduling scheme for MIMO OSFBC-OFDM systems in η–μ fading channels," *Int. J. Wireless Inf. Networks*, vol. 22, pp. 147–156, April 2015.

[319] L. Heng and L. M. A. Jalloul, "Performance of the 3GPP LTE space–frequency block codes in frequency-selective channels with imperfect channel estimation," *IEEE Trans. Veh. Technol.*, vol. 64, no. 5, pp. 1848-1855, May 2015.

[320] S. V. Zhidkov, "Analysis and comparison of several simple impulsive noise mitigation schemes for OFDM receivers," *IEEE Trans. Commun.*, vol. 56, no. 1, pp. 5-9, January 2008.

[321] J. Armstrong, M. Feramez, and H. A. Suraweera, "Optimum noise thresholds in decision directed impulse noise mitigation for OFDM," *Proc. IEEE CSNDSP 2004*, Newcastle, UK, pp. 168-171, July 2004.

[322] H. A. Suraweera, C. Chai, J. Shentu, and J. Armstrong, "Analysis of impulse noise mitigation techniques for digital television systems," *Proc. 8th Int. OFDM Workshop*, Hamburg, Germany, pp. 172-176, September 2003.

[323] A. Grover, D.S. Kapoor, and A.K. Kohli, "Characterisation of impulse noise effects on space-time block-coded orthogonal frequency division multiplexing (OFDM) signal reception," *Int. J. Phys. Sci.*, vol. 7, no. 25, pp. 4003–4011, June 2012.

[324] A. K. Kohli and D. S. Kapoor, "BER performance of SFBC–OFDM systems working over fading channels under impulsive environment," *Arab. J. Sci. Eng.*, vol. 45, no. 3, pp. 1749–1763, March 2020.

[325] Y. Li, L. J. Cimini and N. R. Sollenberger, "Robust channel estimation for OFDM systems with rapid dispersive fading channels," *IEEE Trans. Commun.*, vol. 46, no. 7, pp. 902-915, July 1998.

[326] A. Duel-Hallen, H. Hallen, and Tung-Sheng Yang, "Long range prediction and reduced feedback for mobile radio adaptive OFDM systems," *IEEE Trans. Wireless Commun.*, vol. 5, no. 10, pp. 2723-2733, October 2006.

[327] D. L. Goeckel, "Adaptive coding for time-varying channels using outdated fading estimates," *IEEE Trans. Commun.*, vol. 47, no. 6, pp. 844-855, June 1999.

[328] A. J. Goldsmith and S.-G. Chua, "Variable-rate variable-power MQAM for fading channels," *IEEE Trans. Commun.*, vol. 45, no. 10, pp. 1218-1230, October 1997.

[329] A. J. Goldsmith and S. G. Chua, "Adaptive coded modulation for fading channels," *IEEE Trans. Commun.*, vol. 46, no. 5, pp. 595-602, May 1998.

[330] T. Ue, S. Sampei, N. Morinaga, and K. Hamaguchi, "Symbol rate and modulation level-controlled adaptive modulation/TDMA/TDD system for high-bit-rate wireless data transmission," *IEEE Trans. Veh. Technol.*, vol. 47, no. 4, pp. 1134-1147, November 1998.

[331] J. G. Proakis, *Digital Communications*. 3rd Edition, New York: McGraw-Hill, 1995.

[332] Y.-S. Choi, P. J. Voltz, and F. A. Cassara, "On channel estimation and detection for multicarrier signals in fast and selective Rayleigh fading channels," *IEEE Trans. Commun.*, vol. 49, no. 8, pp. 1375-1387, August 2001.

[333] W. G. Jeon, K. H. Chang, and Y. S. Cho, "An equalization technique for orthogonal frequency-division multiplexing systems in time-variant multipath channels," *IEEE Trans. Commun.*, vol. 47, no. 1, pp. 27-32, January 1999.

[334] M. K. Tsatsanis, G. B. Giannakis, and G. Zhou, "Estimation and equalization of fading channels with random coefficients," *Signal Process.*, vol. 53, no. 2–3, pp. 211-229, September 1996.

[335] A. K. Kohli, "Fading model for antenna array receiver for a ring-type cluster of scatterers," *Int. J. Electronics*, vol. 98, no. 7, pp. 933-940, July 2011.

[336] K.-Y. Han, S.-W. Lee, J.-S. Lim, and K.-M. Sung, "Channel estimation for OFDM with fast fading channels by modified Kalman filter," *IEEE Trans. Consumer Electronics*, vol. 50, no. 2, pp. 443-449, May 2004.

[337] M. K. Khan, R. A. Carrasco, I. J. Wassell, and J. A. Neasham, "Performance comparison of low density parity check codes using square root Kalman equalisation and orthogonal

frequency division multiplexing techniques for broadband fixed wireless access systems," *IET Commun.*, vol. 2, no. 2, pp. 272-283, February 2008.

[338] G. Liu, L. Zeng, H. Li, L. Xu, and Z. Wang, "Adaptive complex interpolator for channel estimation in pilot-aided OFDM system," *J. Commun. Networks*, vol. 15, no. 5, pp. 496-503, October 2013.

[339] T. Ekman and G. Kubin, "Nonlinear prediction of mobile radio channels: measurements and MARS model designs," *Proc. IEEE Int. Conf. Acoust. Speech Signal Process.*, Phoenix, AZ, USA, pp. 2667-2670, March 1999.

[340] J.-K. Hwang and J. H. Winters, "Sinusoidal modeling and prediction of fast fading processes," *Proc. IEEE GLOBECOM 1998*, Sydney, New South Wales, Australia, pp. 892-897, November 1998.

[341] J. B. Andersen, J. Jensen, S. H. Jensen, and F. Frederiksen, "Prediction of future fading based on past measurements," *Proc. IEEE VTS 50th Veh. Technol. Conf.*, Amsterdam, Netherlands, pp. 151-155, September 1999.

[342] R. H. Kwong and E. W. Johnston, "A variable step size LMS algorithm," *IEEE Trans. Signal Process.*, vol. 40, no. 7, pp. 1633-1642, July 1992.

[343] T. Aboulnasr and K. Mayyas, "A robust variable step-size LMS-type algorithm: Analysis and simulations," *IEEE Trans. Signal Process.*, vol. 45, no. 3, pp. 631-639, March 1997.

[344] W.-P. Ang and B. Farhang-Boroujeny, "A new class of gradient adaptive step-size LMS algorithms," *IEEE Trans. Signal Process.*, vol. 49, no. 4, pp. 805-810, April 2001.

[345] A. Rai and A. K. Kohli, "Adaptive polynomial filtering using generalized variable step-size least mean pth power (LMP) algorithm," *Circuits Syst. Signal Process.*, vol. 33, no. 12, pp. 3931-3947, December 2014.

[346] A. K. Kohli and A. Rai, "Numeric variable forgetting factor RLS algorithm for second-order Volterra filtering," *Circuits Syst. Signal Process.*, vol. 32, no. 1, pp. 223-232, February 2013.

[347] R. Ratan, S. Sharma, and A. K. Kohli, "Performance comparison of quadrature amplitude modulation (QAM)-based single-and double-stage digital interpolators," *Int. J. Electron.*, vol. 100, no. 12, pp. 1724-1734, December 2013.

[348] H. S. Wang and P.-C. Chang, "On verifying the first-order Markovian assumption for a Rayleigh fading channel model," *IEEE Trans. Veh. Technol.*, vol. 45, no. 2, pp. 353-357, May 1996.

[349] D. S. Kapoor and A. K. Kohli, "Simulation of basis expansion model for channel fading using AR1 process," *Wireless Pers. Commun.*, vol. 85, no. 3, pp. 791-798, December 2015.

[350] L. L. Scharf, *Statistical Signal Processing: Detection, Estimation and Time-Series Analysis*. Reading: Addison-Wesley, 1991.

[351] A. K. Kohli and S. Garg, "High-rate STBC communication system using imperfect CSI under time-selective flat-fading environment," *Wireless Pers. Commun.*, vol. 99, no. 3, pp. 1231-1245, April 2018.

[352] T.-S. Yang, "Performance analysis of adaptive transmission aided by long range channel prediction for realistic single-and multi-carrier mobile radio channels," Ph.D. Dissertation, North Carolina State Uni., 2004.

[353] A. K. Kohli, A. Rai, and M. K. Patel, "Variable forgetting factor LS algorithm for polynomial channel model," *ISRN Signal Process.*, vol. 2011, no. 915259, pp. 1-4, December 2010.

[354] A. Grover and A. K. Kohli, "Space-time block-coded systems using numeric variable forgetting factor least squares channel estimator," *Int. J. Physical Sciences*, vol. 6, no. 32, pp. 7361-7370, December 2011.

[355] H. K. Garg and A. K. Kohli, "Excision of ocular artifacts from EEG using NVFF-RLS adaptive algorithm," *Circuits Syst. Signal Process.*, vol. 36, no. 1, pp. 404-419, January 2017.

[356] A. Rai and A. K. Kohli, "Volterra filtering scheme using generalized variable step-size NLMS algorithm for nonlinear acoustic echo cancellation," *Acta Acustica united with Acustica*, vol. 101, no. 4, pp. 821-828, July/August 2015.

[357] L. Hanzo, T. Keller, M. Muenster, and B.J. Choi, *OFDM and MC-CDMA for Broadband Multi-User Communications, WLANs and Broadcasting*. New York: Wiley, 2003.

[358] H. Ali, "A cyclic prefix based adaptive channel estimation algorithm for multicarrier systems," *Proc. IEEE Int. Symp. Signal Process. Info. Technol.*, Luxor, Egypt, pp. 215–218, December 2010.

[359] Q. Cheng, "Residue carrier frequency offset estimation using cyclic prefix in OFDM systems," *Proc. TENCON 2009*, Singapore, pp. 1-5, January 2009.

[360] J. Coon, M. Beach, and J. McGeehan, "Optimal training sequences for channel estimation in cyclic-prefix-based single-carrier systems with transmit diversity," *IEEE Signal Process. Lett.*, vol. 11, no. 9, pp. 729-732, September 2004.

[361] T. Kim and I. Eo, "Reliable blind channel estimation scheme based on cross-correlated cyclic prefix for OFDM system," *Proc. 8th Int. Conf. Advanced Commun. Technol.*, Phoenix Park, South Korea, pp. 3–5, February 2006.

[362] P. Ling, W. G. Lim, and H. Ali, "Adaptive channel estimation using least mean squares algorithm for cyclic prefix OFDM systems," *Proc. IEEE 9th Malaysia Int. Conf. Commun.*, Kuala Lumpur, Malaysia, pp. 789–793, December 2009.

[363] M. D. Nisar, W. Utschick, H. Nottensteiner, and T. Hindelang, "On channel estimation and equalization of OFDM systems with insufficient cyclic prefix," *Proc. IEEE 65th Veh. Technol. Conf.*, Dublin, Ireland, pp. 1445–1449, April 2007.

[364] A. A. Quadeer and M. S. Sohail, "Enhanced channel estimation using cyclic prefix in MIMO STBC OFDM systems," *Proc. IEEE Int. Symp. Signal Process. Info. Technol.*, Luxor, Egypt, pp. 277–282, December 2010.

[365] H. Senol, E. Panayirci, and H.V. Poor, "Non data-aided joint channel estimation and equalization for OFDM systems in very rapidly varying mobile channels," *IEEE Trans. Signal Process.*, vol. 60, no. 8, pp. 4236–4253, August 2012.

[366] P. Sudheesh *et al*., "Cyclic prefix assisted sparse channel estimation for OFDM systems," *Proc. Int. Conf. Comput. Commun. Applications*, Tamil Nadu, India, pp. 1–4, February 2012.

[367] A. Visakh and N. Upadhyay, "Channel estimation for OFDM systems using Kalman filter algorithm," *Proc. 1st Int. Conf. Wireless Technol. Humanitarian Relief*, Kerala, India, pp. 49–52, December 2011.

[368] R. A. Ziegler and J. M. Cioffi, "Estimation of time-varying digital radio channel," *IEEE Trans. Veh. Technol.*, vol. 41, no. 2, pp. 134–151, May 1992.

[369] A. K. Kohli and D. K. Mehra, "Tracking of time-varying channels using two-step LMS-type adaptive algorithm," *IEEE Trans. Signal Process.*, vol. 54, no. 7, pp. 2606–2615, July 2006.

[370] B. Widrow, J. M. McCool, M. G. Larimore, and C. R. Johnson, "Stationary and nonstationary learning characteristics of the LMS adaptive filter," *Proc. IEEE*, vol. 64, no. 8, pp. 1151–1162, August 1976.

[371] P. Gupta and D.K. Mehra, "A novel technique for channel estimation and equalization for high mobility OFDM systems," *Wireless Pers. Commun.*, vol. 49, no. 4, pp. 613–631, June 2009.

[372] X. Ma and G. B. Giannakis, "Maximum-diversity transmissions over doubly selective wireless channels," *IEEE Trans. Inf. Theory*, vol. 49, no. 7, pp. 1832–1840 July 2003.

[373] X. Wang and K. J. R. Liu, "Adaptive channel estimation using cyclic prefix in multicarrier modulation system," *IEEE Commun. Lett.*, vol. 3, no. 10, pp. 291–293, October 1999.

[374] X. Wang and K. J. R. Liu, "Performance analysis for adaptive channel estimation exploiting cyclic prefix in multicarrier modulation systems," *IEEE Trans. Commun.*, vol. 51, no. 1, pp. 94–105, January 2003.

[375] P. Hoeher, S. Kaiser, and P. Robertson, "Two-dimensional pilot-symbol aided channel estimation by Wiener filtering," *Proc. Int. Conf. Acoust. Speech Signal Process.*, Munich, Germany, pp. 1845–1848, April 1997.

[376] L. M. Davis, I. B. Collings and R. J. Evans, "Coupled estimators for equalization of fast-fading mobile channels," *IEEE Trans. Commun.*, vol. 46, no. 10, pp. 1262-1265, October 1998.

[377] A. H. Sayed and T. Kailath, "A state-space approach to adaptive RLS filtering," *IEEE Trans. Signal Process. Mag.*, vol. 11, no. 3, pp. 18–60, July 1994.

[378] M. S. Grewal and A. P. Andrew, *Kalman Filtering: Theory and Practice*. Englewood Cliffs: Prentice-Hall, 1993.

[379] A. K. Kohli and D. K. Mehra, "Adaptive multiuser channel estimator using reduced Kalman/LMS algorithm," *Wireless Pers. Commun.*, vol. 46, no. 4, pp. 507–521 September 2008.

[380] A. K. Kohli and D. K. Mehra, "Adaptive DFE multiuser receiver for CDMA systems using two-step LMS type algorithm: An equalization approach," *Wireless Pers. Commun.*, vol. 54, no. 3, pp. 543–558, August 2010.

[381] S. Gazor, "Prediction in LMS-type adaptive algorithms for smoothly time varying environments," *IEEE Trans. Signal Process.*, vol. 47, no. 6, pp. 1735-1739, June 1999.

[382] S. Singh and A.K. Kohli, "Wireless fading paradigm for antenna array receiver for a disk-type cluster of scatterers," *Circuits Syst. Signal Process.*, vol. 33, no. 4, pp. 1231–1244, April 2014.

[383] Y. S. Cho, S. B. Kim, and E. J. Powers, "Time-frequency analysis using AR models with variable forgetting factors," *Proc. Int. Conf. Acoust. Speech Signal Process.*, Albuquerque, NM, USA, pp. 2479-2482, April 1990.

[384] A. Papoulis, *Probability, Random Variables, and Stochastic Processes*. 3rd Edition, New York: McGraw-Hill, 1991.

[385] W.C. Jakes, *Microwave Mobile Communications*. New York: McGraw-Hill, 1994.
[386] G.H. Golub, *Matrix Computations*. Baltimore, US: The Johan Hopkins University Press, 1989.
[387] M. Uysal, N. Al-Dhahir, and C.N. Georghiades, "A space–time block-coded OFDM scheme for unknown frequency-selective fading channels," *IEEE Commun. Lett.*, vol. 5, no. 10, pp. 393–395, October 2001.
[388] A. P. Liavas and P. A. Regalia, "On the numerical stability and accuracy of the conventional recursive least squares algorithm," *IEEE Trans. Signal Process.*, vol. 47, no. 1, pp. 88–96, 1999.
[389] H. A. Suraweera and J. Armstrong, "Noise bucket effect for impulse noise in OFDM," *Electron. Lett.*, vol. 40, no. 18, pp. 1156-1157, September 2004.
[390] J. Lago-Fernandez and J. Salter, "Modelling impulsive interference in DVB-T: statistical analysis, test waveforms and receiver performance," *BBC R&D White Paper* [Online]. Available: https://www.bbc.co.uk/rd/publications/whitepaper080
[391] R. Poole, "DVB-T transmission, reception and measurement," *DTG Monograph*, no. 4, Digital TV Group, 2001.
[392] N. Al-Dhahir, "Single-carrier frequency-domain equalization for space-time block-coded transmissions over frequency-selective fading channels," *IEEE Commun. Lett.*, vol. 5, no. 7, pp. 304-306, July 2001.
[393] J.-H. Jang, H.-C. Won, and G.-H. Im, "Cyclic prefixed single carrier transmission with SFBC over mobile wireless channels," *IEEE Signal Process. Lett.*, vol. 13, no. 5, pp. 261-264, May 2006.
[394] S. T. Chung and A. J. Goldsmith, "Degrees of freedom in adaptive modulation: A unified view," *IEEE Trans. Commun.*, vol. 49, no. 9, pp. 1561-1571, September 2001.
[395] M. Nakagami, "The m-distribution, a general formula of intensity distribution of rapid fading," in *Statistical Methods in Radio Wave Propagation*, W. C. Hoffman, Ed., Los Angeles: Pergamon, 1960, pp. 3-36.
[396] Q. T. Zhang, "Maximal-ratio combining over Nakagami fading channels with an arbitrary branch covariance matrix," *IEEE Trans. Veh. Technol.*, vol. 48, no. 4, pp. 1141-1150, July 1999.
[397] A. Scaglione, S. Barbarossa, and G. B. Giannakis, "Optimal adaptive precoding for frequency-selective Nagakami-m fading channels," *Proc. IEEE VTS Fall VTC2000.*, Boston, MA, USA, pp. 1291-1295, September 2000.
[398] Z. Du, J. Cheng, and N. C. Beaulieu, "Accurate error-rate performance analysis of OFDM on frequency-selective Nakagami-m fading channels," *IEEE Trans. Commun.*, vol. 54, no. 2, pp. 319-328, February 2006.
[399] Z. Kang, K. Yao, and F. Lorenzelli, "Nakagami-m fading modeling in the frequency domain for OFDM system analysis," *IEEE Commun. Lett.*, vol. 7, no. 10, pp. 484-486, October 2003.
[400] M. Torabi, "Adaptive modulation for space–frequency block coded OFDM systems," *AEU Int. J. Electron. Commun.*, vol. 62, no. 7, pp. 521-533, August 2008.
[401] A. K. Kohli and D. S. Kapoor, "Adaptive filtering techniques using cyclic prefix in OFDM systems for multipath fading channel prediction," *Circuits Syst. Signal Process.*, vol. 35, no. 10, pp. 3595-3618, October 2016.

[402] A. Bansal and A. K. Kohli, "Suppression of impulsive noise in OFDM system using imperfect channel state information," *Optik*, vol. 127, no. 4, pp. 2111-2115, February 2016.
[403] S. Sehrawat and A. K. Kohli, "Optimized mitigation of impulsive noise in OFDM system using CSI," *Optik*, vol. 127, no. 20, pp. 9627-9634, October 2016.
[404] T. Yoo and A. Goldsmith, "Capacity of fading MIMO channels with channel estimation error," *Proc. 2004 IEEE Int. Conf. Commun.*, vol. 2, Paris, France, pp. 808-813, June 2004.
[405] M. Torabi, M. R. Soleymani, and S. Aissa, "On the performance of MIMO-OFDM systems with imperfect channel information," *Proc. 2005 Int. Conf. Wireless Networks Commun. Mobile Comput.*, Maui, HI, pp. 600-605, June 2005.
[406] M. Ghosh, "Analysis of the effect of impulse noise on multicarrier and single carrier QAM systems," *IEEE Trans. Commun.*, vol. 44, no. 2, pp. 145-147, February 1996.
[407] W. L., H. Zhang, and T. A. Gulliver, "Capacity and error probability analysis of orthogonal space-time block codes over correlated Nakagami fading channels," *IEEE Trans. Wireless Commun.*, vol. 5, no. 9, pp. 2408-2412, September 2006.
[408] C. Hastings, *Approximations for Digital Computers.* New Jersey: Princeton, 1955.
[409] C. Cheng, "A Nakagami-m fading channel simulator," M.Sc. Thesis, Dept. Electrical Comp. Eng., Queen's Univ., Kingston, Ontario, Canada, 2000.
[410] A. Jemmali, M. Torabi, and J. Conan, "Performance analysis of MIMO schemes in 3GPP long term evolution system," *Wireless Pers. Commun.*, vol. 82, no. 2, pp. 1107-1125, May 2015.
[411] S. S. Ali, D. Castanheira, A. Alsohaily, E. S. Sousa, A. Silva, and A. Gameiro, "Joint space-frequency block codes and signal alignment for heterogeneous networks," *IEEE Access*, vol. 6, pp. 71099-71109, November 2018
[412] T. L. Marzetta, "Noncooperative cellular wireless with unlimited numbers of base station antennas," *IEEE Trans. Wireless Commun.*, vol. 9, no. 11, pp. 3590-3600, November 2010.
[413] X. Ma, H. Kobayashi, and S. C. Schwartz, "An EM-based channel estimation algorithm for space-time and space-frequency block coded OFDM," *Proc. IEEE Int. Conf. Acoust. Speech Signal Process.*, Hong Kong, China, pp. IV-389-392, April 2003.
[414] S. Haykin, *Neural Networks and Learning Machines*. New Jersey: Prentice-Hall, 2009.
[415] T. Cui and C. Tellambura, "Channel estimation for OFDM systems based on adaptive radial basis function networks," *Proc. IEEE 60th Veh. Technol. Conf.*, vol. 1, Los Angeles, CA, pp. 608-611, September 2004.
[416] D. S. Kapoor and A. K. Kohli, "Intelligence-based channel equalization for 4x1 SFBC-OFDM receiver," *Intell. Autom. Soft Comput.*, vol. 26, no. 3, pp. 439-446, July 2020.
[417] J. Zhang, C. Wen, S. Jin, and G. Y. Li, "Artificial intelligence-aided receiver for a CP-free OFDM system: Design, simulation, and experimental test," *IEEE Access*, vol. 7, pp. 58901-58914, May 2019.
[418] J. Zhang, Y. Cao, G. Han, and X. Fu, "Deep neural network-based underwater OFDM receiver," *IET Commun.*, vol. 13, no. 13, pp. 1998-2002, September 2019.
[419] K. Burse, R. N. Yadav, and S. C. Shrivastava, "Channel equalization using neural networks: A review," *IEEE Trans. Systems Man Cybernetics Part C*, vol. 40, no. 3, pp. 352-357, May 2010.

[420] S. Xu and Ming Zhang, "Justification of a neuron-adaptive activation function," *Proc. IEEE-INNS-ENNS Int. Joint Conf. Neural Netw.*, vol. 3, Como, Italy, pp. 465-470, July 2000.

[421] T. I. Liu and K. S. Anantharaman, "On-line sensing of drill wear using neural network approach," *Proc. IEEE Int. Conf. Neural Netw.*, vol. 2, San Francisco, CA, USA, pp. 690–694, April 1993.

[422] L. Vecci, F. Piazza, and A. Uncini, "Learning and approximation capabilities of adaptive spline activation function neural networks," *Neural Netw.*, vol. 11, no. 2, pp. 259–270, March 1998.

[423] C.-C. Yu, Y.-C. Tang, and B.-D. Liu, "An adaptive activation function for multilayer feedforward neural networks," *Proc. IEEE Region 10 Conf. Computers Commun. Control Power Engg.*, vol. 1, pp. 645–650, October 2002.

[424] G. Thimm, P. Moerland, and E. Fiesler, "The interchangeability of learning rate and gain in backpropagation neural networks," *Neural Comput.*, vol. 8, no. 2, pp. 451–460, February 1996.

[425] Z. Zerdoumi, D. Chikouche, and D. Benatia, "Multilayer perceptron based equalizer with an improved back propagation algorithm for nonlinear channels," *Int. J. Mob. Comput. Multimed. Commun.*, vol. 7, no. 3, pp. 16–31, July 2016.

[426] Y. S. Cho, J. Kim, W. Y. Yang, and C. G. Kang, *MIMO-OFDM Wireless Communications with MATLAB*. Chichester, UK: John Wiley & Sons Ltd., 2010.

[427] E. Eraslan, B. Daneshrad, and C. Lou, "Performance indicator for MIMO MMSE receivers in the presence of channel estimation error," *IEEE Wireless Commun. Lett.*, vol. 2, no. 2, pp. 211-214, April 2013.

[428] P. Chandra and Y. Singh, "An activation function adapting training algorithm for sigmoidal feedforward networks," *Neurocomput.*, vol. 61, no. C, pp. 429–437, October 2004.

[429] T. Rappaport, *Wireless Communications: Principles and Practice*, 2nd Edition. USA: Prentice Hall PTR, 2001.

[430] D. S. Kapoor and A. K. Kohli, "Impact of squashing function's slope on ANN based channel estimation in SFBC-OFDM system," *Proc. 12th Int. Conf. Comput. Intell. Commun. Netw.*, Bhimtal, India, pp. 258-260, September 2020.

[431] C.-T. Chen and W.-D. Chang, "A feedforward neural network with function shape autotuning," *Neural Netw.*, vol. 9, no. 4, pp. 627–641, June 1996.

[432] Z. Zerdoumi, D. Chicouche, and D. Benatia, "Neural networks based equalizer for signal restoration in digital communication channels," *Int. Lett. Chem. Phys. Astron.*, vol. 55, pp. 187–200, July 2015.

[433] M. Riedmiller and H. Braun, "A direct adaptive method for faster backpropagation learning: The RPROP algorithm," *Proc. IEEE Int. Conf. Neural Netw.*, vol. 1, San Francisco, CA, USA, pp. 586-591, April 1993.

[434] M. T. Hagan and M. B. Menhaj, "Training feedforward networks with the Marquardt algorithm," *IEEE Trans. Neural Netw.*, vol. 5, no. 6, pp. 989-993, November 1994.

[435] J. Hou, M. H. Lee, and J. Y. Park, "Matrices analysis of quasi-orthogonal space-time block codes," *IEEE Commun. Lett.*, vol. 7, no. 8, pp. 385-387, August 2003.

[436] W. Su and X.-G. Xia, "Quasi-orthogonal space-time block codes with full diversity," *Proc. IEEE Global Telecommun. Conf.*, vol. 2, Taipei, Taiwan, pp. 1098-1102, November 2002.

[437] U. Habib *et al*., "Performance improvement for OFDM-RoF transported 60 GHz system using spatial diversity and multiplexing," *Proc. IEEE Int. Conf. Commun. Workshops*, Paris, France, pp. 211-216, May 2017.

[438] S. Liu *et al*., "A multilevel artificial neural network nonlinear equalizer for millimeter-wave mobile fronthaul systems," *J. Lightwave Technol.*, vol. 35, no. 20, pp. 4406-4417, October 2017.

[439] M. Zhu, L. Zhang, J. Wang, L. Cheng, C. Liu, and G. Chang, "Radio-over-fiber access architecture for integrated broadband wireless services," *J. Lightwave Technol.*, vol. 31, no. 23, pp. 3614-3620, December 2013.

[440] D. S. Kapoor and A. K. Kohli, "Channel estimation and long-range prediction of fast fading channels for adaptive OFDM system," *Int. J. Electron.*, vol. 105, no. 9, pp. 1451-1466, September 2018.

[441] A. K. Kohli and G. S. Lamba, "Impact of phase noise on single-tap equalization for fast–OFDM signals under generic linear fading channels," *Optik*, vol. 169, pp. 382-391, September 2019.

[442] T. Kaur, B. S. Dhaliwal, and S. S Gill, "Performance evaluation of MIMO systems with varying number of transmitting antennas," *Int. J. Innovative Research Electrical Electron. Instrumentation Control Engg.*, vol. 1, no. 2, pp. 38-40, May 2013.

[443] G. Kongara, C. He, L. Yang, and J. Armstrong, "A comparison of CP-OFDM, PCC-OFDM and UFMC for 5G uplink communications," *IEEE Access*, vol. 7, pp. 157574-157594, October 2019.

[444] X. Yi and C. Zhong, "Deep learning for joint channel estimation and signal detection in OFDM systems," *IEEE Commun. Lett.*, Early Access, August 2020.

[445] S. Vidal-Beltrán, J.L. López-Bonilla, F. Martínez-Piñón, and R. Cuenca-Álvarez, "Impact of condition number on total sum rate for NOMA systems," *Electron. Lett.*, vol. 56, no. 20, pp. 1091-1093, September 2020.

[446] A. Tusha, S. Doğan, and H. Arslan, "A hybrid downlink NOMA with OFDM and OFDM-IM for beyond 5G wireless networks," *IEEE Signal Process. Lett.*, vol. 27, pp. 491-495, March 2020.

[447] C. Wu, Y. Xiao, Y. L. Guan, J. Wang, X. Li, and P. Yang, "Space-time/frequency line coded OFDM: System design and practical implementation," *IEEE Access*, vol. 7, pp. 151915-151928, October 2019.

[448] G. Berardinelli, K. I. Pedersen, T. B. Sorensen, and P. Mogensen, "Generalized DFT-spread-OFDM as 5G waveform," *IEEE Commun. Mag.*, vol. 54, no. 11, pp. 99-105, November 2016.

[449] V. Vahidi and E. Saberinia, "MIMO–OFDM communication systems for traffic data transmission in 5G drone small cells," *IET Commun.*, vol. 13, no. 20, pp. 3565-3574, December 2019.

[450] F. Wan, W. Zhu, and M. N. S. Swamy, "Semiblind sparse channel estimation for MIMO-OFDM systems," *IEEE Trans. Veh. Technol.*, vol. 60, no. 6, pp. 2569-2582, July 2011.

[451] W. Jiang and H. D. Schotten, "Neural network-based fading channel prediction: A comprehensive overview," *IEEE Access*, vol. 7, pp. 118112-118124, September 2019.

[452] H. Wang and J. Li, "An intelligent receiver for space time block coded OFDM system," *Proc. 2016 First IEEE Int. Conf. Computer Commun. Internet*, Wuhan, China, pp. 535-538, October 2016.

[453] Y. Sun, C. Wang, H. Cai, C. Zhao, Y. Wu, and Y. Chen, "Deep learning based equalizer for MIMO-OFDM systems with insufficient cyclic prefix," *arXiv*, vol. 2007, no. 11757, pp. 1-5, July 2020.

[454] C. Ha, Y. You, and H. Song, "Machine learning model for adaptive modulation of multi-stream in MIMO-OFDM system," *IEEE Access*, vol. 7, pp. 5141-5152, January 2019.

[455] N. Gowtham and S. Shankar, "PI tuning of shunt active filter using GA and PSO algorithm," *Proc. 2016 2nd Int. Conf. Advances Electrical Electron. Info. Commun. Bio-Informatics*, Chennai, India, pp. 207-213, February 2016.

[456] A. Kaushik, S. Indu, and D. Gupta, "A grey wolf optimization approach for improving the performance of wireless sensor networks," *Wireless Pers. Commun.*, vol. 106**,** no. 3, pp. 1429-1449, June 2019.

[457] W. L. Woo and S. S. Dlay, "Neural network approach to blind signal separation of mono-nonlinearly mixed sources," *IEEE Trans. Circuits Syst. I, Reg. Papers*, vol. 52, no. 6, pp. 1236-1247, June 2005.

[458] T. E. Bogale, X. Wang, and L. B. Le, "Adaptive channel prediction, beamforming and scheduling design for 5G V2I network: Analytical and machine learning approaches," *IEEE Trans. Veh. Technol.*, vol. 69, no. 5, pp. 5055-5067, May 2020.

[459] K. Bai, Y. Yi, Z. Zhou, S. Jere, and L. Liu, "Moving toward intelligence: Detecting symbols on 5G systems through deep echo state network," *IEEE J. Emerging Sel. Topics Circuits Systems*, vol. 10, no. 2, pp. 253-263, June 2020.

[460] G. B. Giannakis and C. Tepedelenlioglu, "Basis expansion models and diversity techniques for blind identification and equalization of time-varying channels," *Proc. IEEE*, vol. 86, no. 10, pp. 1969-1986, October 1998.

[461] E. P. Simon and M. A. Khalighi, "Iterative soft-Kalman channel estimation for fast time-varying MIMO-OFDM channels," *IEEE Wireless Commun. Lett.*, vol. 2, no. 6, pp. 599-602, December 2013.

[462] H. K. Garg and A. K. Kohli, "EEG spike detection technique using output correlation method: A Kalman filtering approach," *Circuits Syst. Signal Process.*, vol. 34, no. 8, pp. 2643–2665, August 2015.

[463] V.P. Oikonomou, A.T. Tzallas, and D.I. Fotiadis, "A Kalman filter based methodology for EEG spike enhancement," *Computer Meth. Programs Biomedicine*, vol. 85, no. 2, pp. 101-108, February 2007.

[464] M. Arnold, X. H. R. Milner, H. Witte, R. Bauer, and C. Braun, "Adaptive AR modeling of nonstationary time series by means of Kalman filtering," *IEEE Trans. Biomedical Eng.*, vol. 45, no. 5, pp. 553-562, May 1998.

[465] F. Fazel and H. Jafarkhani, "Quasi-orthogonal space-frequency and space-time-frequency block codes for MIMO OFDM channels," *IEEE Trans. Wireless Commun.*, vol. 7, no. 1, pp. 184–192, January 2008.

[466] X. Glorot and Y. Bengio, "Understanding the difficulty of training deep feedforward neural networks," *Proc. 13th Int. Conf. Artificial Intell. Stats.*, vol. 9, Sardinia, Italy, pp. 249–256, May 2010.

[467] D. L. Elliott, “A better activation function for artificial neural networks,” Inst. Systems Research, Univ. Maryland, College Park, MD, Tech. Rep. TR 93-8, January 1993.